



**Politecnico  
di Torino**

**ScuDo**  
Scuola di Dottorato ~ Doctoral School  
WHAT YOU ARE, TAKES YOU FAR

Doctoral Dissertation  
Doctoral Program in Energy Engineering (34<sup>th</sup> Cycle)

# **Flexibility of multi-energy systems: the role of Power-to-Gas and Power-to-Heat at the district level**

By

**Gabriele Fambri**

\*\*\*\*\*

**Supervisor**

Prof. Marco Badami

**Doctoral Examination Committee:**

Prof. Carlo Carcasci, Referee, Università degli Studi di Firenze.


Prof. Michela Vellini, Referee, Università degli Studi di Roma Tor Vergata.

Politecnico di Torino

June 28, 2022

## Declaration

I hereby declare that, the contents and organization of this dissertation constitute my own original work and does not compromise in any way the rights of third parties, including those relating to the security of personal data.



.....  
Gabriele Fambri  
Turin, June 28, 2022

\* This dissertation is presented in partial fulfillment of the requirements for **Ph.D. degree** in the Graduate School of Politecnico di Torino (ScuDo).



# Summary

The European Union established the goal of carbon neutrality by mid-century. The utilization of renewable energy sources will be pivotal for such a decarbonization process. However, renewable generation is not dispatchable, and an increasing share of these sources may lead to problems for the electricity system. This brings about the need to invest in flexible resources capable of handling the generation of renewable sources, so that the delicate balance between electricity generation and demand could be maintained. Flexibility may be defined as the capacity of a system to modify its energy generation/consumption profile. The quest for new forms of flexibility is a paramount challenge for the next decades of research. Such new sources of flexibility may be found, if researchers consider the energy system from a holistic point of view, rather than as a system that only includes the electricity sector. In these scenarios, energy conversion technologies may be used to connect different energy sectors, therefore increasing the flexibility of the whole system.

The study of multi-energy systems requires a number of different competences from different backgrounds. The use of conversion devices that exploit different commodities calls for the modeling of several different energy conversion technologies and different network infrastructures. The current thesis aimed to investigate the extent to which multi-energy systems could be efficient flexibility sources. In the research to be presented in this thesis, a co-simulation platform was developed in order to facilitate the simulation of such complex scenarios. In the co-simulation architecture, each component of the multi-energy system was simulated in a different module. This allowed the research groups involved to develop the different models separately. Some of these modules were developed within the work of this thesis, whereas some others were developed through the collaboration with other research groups. Importantly though, the various models were connected to the co-simulation platform and were made to communicate with each other through the mutual exchange of input and output data.

The co-simulation tool was used within the work of this thesis for the realization of four different multi-energy system case studies.

The first case study was developed to analyze the flexibility resulting from the coupling of the electricity sector to the gas sector. Power-to-Gas technology allowed electricity to be converted into synthetic natural gas, which could be directly injected into the gas network. Results showed the effectiveness of the flexibility enabled by the Power-to-Gas technology to mitigate the problems of

over-generation of renewable sources. However, this solution turned out to be not convenient from an economic point of view, due to high investment costs.

In the second case study, the same multi-energy system scenario was used for another type of analysis. The impact of different simulation approaches was analyzed thanks to the property of the co-simulation platform to plug and play different modules. The results obtained with the use of more simplified models (for the simulation of the electricity and gas networks, and the Power-to-Gas system) were compared with the results obtained with the detailed models of these components. The analysis showed that in some circumstances, the use of simplified models could lead to an underestimation of the flexibility that could be obtained with the Power-to-Gas technology.

The third multi-energy system case study investigated the utilization of large-scale heat pumps for the connection of the electricity sector and the district heating sector. The heat pumps were used to provide heat to district heating and, at the same time, flexibility to the electricity sector. Results showed that, thanks to their high heat production efficiency, the utilization of heat pumps was advantageous, even when their flexibility was not exploited. The flexible utilization of these plants could bring significant benefits from both an energy and economic point of view.

The fourth case study analyzed the flexibility enabled by heat pumps directly installed in buildings. The mass and thermal inertia of buildings could be exploited to flexibly modulate the use of heating systems. The heat pump technology allowed the flexibility of the building's thermal sector to be used within the electricity sector. This flexibility was used to optimize the energy and economic flows of an energy community. Results demonstrated that the exploitation of this kind of flexibility did indeed allow the self-consumption of the energy community to be increased significantly, also leading to a benefit from an economic point of view.

# Acknowledgements

First of all, I would like to thank my PhD. supervisor Prof. Marco Badami who has supported me in the last five years by offering me a position in his research group. He has always been available to share his knowledge with me and, most importantly, he taught me the approach to scientific research. His support was fundamental for the development of this thesis. I would also like to thank Prof. Henrik Lund from Aalborg University (Denmark) and the whole research group for hosting me and sharing their knowledge with me during the final period of my PhD. I would also like to mention my colleagues and friends at the Politecnico di Torino, in particular Paolo, Valeria, Marco, Giovanna and Cesar with whom I shared many good moments. I thank them for their friendship and the interesting technical discussions I had with each of them.

Finally, a dutiful thanks to all my friends and family who have supported me over the years.



# Contents

<b>List of Tables.....</b>	<b>vi</b>
<b>List of Figures .....</b>	<b>viii</b>
<b>List of Abbreviations.....</b>	<b>xiv</b>
<b>List of Symbols .....</b>	<b>xvii</b>
<b>Chapter 1.....</b>	<b>1</b>
Introduction .....	1
1.1 Greenhouse gas emissions and global warming .....	1
1.2 Role of renewable energy sources .....	4
1.3 Future energy scenarios in Italy: the Snam and Terna report.....	7
1.3.1 Evolution of the Italian electricity sector.....	8
1.3.2 Evolution of the Italian gas sector .....	10
1.4 Objectives of the thesis.....	13
1.4.1 Motivation.....	13
1.4.2 Solution for flexibility analyzed in this thesis .....	15
1.4.3 Solution for flexibility not included in this thesis .....	18
1.5 Manuscript contents.....	19
<b>Chapter 2.....</b>	<b>21</b>
Methods .....	21
2.1 Flexibility calculation in multi-energy systems.....	21



---

2.2 The energy networks and the energy conversion technologies models .....	25
2.2.1 Electricity network detailed model .....	27
2.2.2 Electricity network simplified model .....	29
2.2.3 Gas network detailed model .....	30
2.2.4 Gas network simplified model.....	35
2.2.5 District heating network and centralized Power-to-Heat model .....	35
2.2.6 Power-to-Gas detailed model .....	40
2.2.7 Power-to-Gas simplified model.....	42
2.2.8 Building and localized Power-to-Heat model.....	44
2.2.9 Electric Battery model .....	47
2.2.10 Controller.....	49
2.3 Multi-energy system co-simulation tool.....	50
2.3.1 The co-simulation .....	50
2.3.2 The communication between modules .....	52
2.3.3 The modules of the multi-energy system co-simulation tool .....	53
2.3.4 The time-synchronizer module .....	54
<b>Chapter 3.....</b>	<b>56</b>
Case-study 1 – Techno-economic analysis of Power-to-Gas plants in a gas and electricity distribution network system.....	56
3.1 Introduction .....	57
3.1.1 State of the art.....	57
3.1.2 Scientific contribution .....	58
3.2 Scenario description and techno-economic parameters.....	59
3.2.1 Electricity system.....	59

---

---

3.2.2	Gas system .....	60
3.2.3	Power-to-Gas systems .....	62
3.2.4	Scenario energy demand and production.....	64
3.2.5	Economic analysis .....	65
3.3	Mathematical approach and solution strategy .....	68
3.3.1	Co-simulation architecture.....	68
3.3.2	Simulation control algorithm.....	70
3.4	Results and discussion.....	72
3.4.1	Energy impact of Power-to-Gas on the electricity and gas networks in winter and summer seasons .....	72
3.4.2	Economic results.....	78
3.5	Conclusions .....	82
<b>Chapter 4</b>	<b>.....</b>	<b>85</b>
	Case-study 2 – Power-to-Gas plants in gas and electricity distribution network system: a comparison between modeling approaches .....	85
4.1	Introduction .....	86
4.1.1	Scientific contribution .....	86
4.2	The multi-energy system scenario.....	89
4.3	Mathematical approach and solution strategy .....	90
4.3.1	Analyzed modeling approaches.....	90
4.3.2	Co-simulation architecture.....	93
4.4	Results and discussion.....	95
4.4.1	Value of electricity network modeling .....	95
4.4.2	Value of gas network modeling.....	100
4.4.3	Value of P2G modeling .....	102
4.5	Conclusions .....	105

---

<b>Chapter 5.....</b>	<b>108</b>
Case-study 3 – Techno-economic analysis of centralized Power-to-Heat plants in a district heating and electricity distribution network system .....	108
5.1 Introduction .....	109
5.1.1 State of the art.....	109
5.1.2 Scientific contribution .....	110
5.2 Scenario description and techno-economic parameters.....	111
5.2.1 District heating system .....	111
5.2.2 Electricity system.....	112
5.2.3 Centralized Power-to-Heat systems.....	113
5.2.4 Scenario energy demand and production.....	113
5.2.5 Economic analysis .....	115
5.3 Mathematical approach and solution strategy .....	117
5.3.1 Co-simulation architecture.....	117
5.3.2 Simulation control algorithm.....	119
5.4 Results and discussion .....	122
5.4.1 Energy flows between the electricity and district heating energy sectors .....	122
5.4.2 Economic results.....	128
5.5 Conclusions .....	130
<b>Chapter 6.....</b>	<b>132</b>
Case-study 4 – Techno-economic analysis of localized Power-to-Heat plants in an energy community.....	132
6.1 Introduction .....	132
6.1.1 State of the art.....	132

---

---

6.1.2	Scientific contribution .....	134
6.2	Scenario description and techno-economic parameters.....	134
6.2.1	Type of buildings and localized Power-to-Heat systems ...	136
6.2.2	Scenario energy demand, energy production and storage capacity .....	136
6.3	Economic analysis .....	139
6.3.1	Flexible assets cost assumptions.....	139
6.3.2	Energy Community costs and incentives.....	140
6.3.3	Net Present Value .....	141
6.4	Mathematical approach and solution strategy .....	143
6.4.1	Co-simulation architecture.....	143
6.4.2	Simulation control algorithms .....	146
6.5	Results and discussion.....	146
6.5.1	The Virtual Energy Storage effect.....	146
6.5.2	Virtual Energy Storage versus electric batteries.....	149
6.5.3	Self-consumption and Self-sufficiency: sensitivity analysis of the RES penetration.....	153
6.5.4	Economic results.....	155
6.6	Conclusions .....	158
<b>Chapter 7</b>	<b>.....</b>	<b>161</b>
	Conclusions .....	161
7.1	General conclusions.....	161
7.2	Outlook.....	163
7.3	Publications .....	165
<b>References</b>	<b>.....</b>	<b>167</b>

---

# List of Tables

Table 1-1. Italian annual gas demand (2018-2021). .....	10
Table 1-2. Italian biomethane production (2030 and 2040). .....	11
Table 1-3. Italian hydrogen demand (2030 and 2040). .....	12
Table 2-1. List of the models used in this thesis.....	27
Table 2-2. Models involved in the simulation of the various case studies. ....	54
Table 3-1. Non-exhaustive overview of gas network literature models characteristics. ....	62
Table 3-2. Technical parameters of the P2G plants.....	63
Table 3-3. Network connections to the P2G plants. ....	64
Table 3-4. Electricity demand, gas demand and RES installations. ....	64
Table 3-5. Specific investment cost, specific fixed O&M cost and lifetime of the components of the P2G plant. ....	66
Table 3-6. Economic assumptions for the considered P2G. ....	66
Table 3-7. Models involved in the co-simulation loop.....	69
Table 3-8. Results pertaining the electricity network.....	74
Table 3-9. Results pertaining the gas network.....	75
Table 3-10. P2G results. ....	79
Table 3-11. Levelized cost of SNG. ....	79
Table 4-1. Overview of previous studies on P2G in a distribution network scenario and the modeling assumptions. ....	88

---

Table 4-2. Models involved in the co-simulation loop.....	94
Table 4-3. List of simulations. ....	95
Table 4-4. P2G plant results. ....	98
Table 4-5. Gas network results. ....	98
Table 4-6. Electricity network results.....	99
Table 5-1. Multi-energy system parameters. ....	115
Table 5-2. Flexibility incentives and energy costs ....	115
Table 5-3. CP2H plant cost assumptions. ....	116
Table 5-4. Models involved in the co-simulation loop.....	118
Table 5-5. Annual energy flows of the district heating network. ....	126
Table 5-6. Annual energy flows of the electricity network. ....	127
Table 5-7. Annual energy flows of CP2H. ....	129
Table 6-1. Scenario parameters. ....	137
Table 6-2. The main economic parameters of the electric battery plant.....	139
Table 6-3. Economic parameters. ....	140
Table 6-4. Models involved in the co-simulation loop.....	145
Table 6-5. RES over-generation and over-generation absorption as a function of the external temperature. ....	153
Table 6-6. Annual energy flow of the energy community for the three cases (BC, VES and EB) as a function of different RES penetration scenarios. ....	154
Table 6-7. Annual cash flows of the energy community for the three cases (BC, VES and EB) under/as a function of different RES penetration scenarios. ....	156

# List of Figures

Figure 1-1. (a) Change in global surface temperature (decadal average) as reconstructed (1-2000) and observed (1850-2020). (b) Change in global surface temperature (annual average) as observed and simulated using human & natural and only natural factors (both 1850-2020) [1].....	1
Figure 1-2. IPCC future scenarios of CO <sub>2</sub> emissions (a) and their impact on global warming (b) [1]. .....	2
Figure 1-3. Changes in annual surface temperature over the World [1].....	3
Figure 1-4. Greenhouse gas emission intensity for electricity production of EU. ....	5
Figure 1-5. EU electricity generation from renewable energy and fossil fuels. ....	5
Figure 1-6. European countries' and World's energy mix for electricity generation. ....	6
Figure 1-7. PV and WT installation data from [29], [30] and [31]. ....	6
Figure 1-8. Snam-Terna intermediate 2030-2040 steps to net zero emission.....	8
Figure 1-9. Italian electricity demand (years 2019, 2030 and 2040).....	8
Figure 1-10. Italian production of renewable energy sources (2019, 2030 and 2040). ....	9
Figure 1-11. Italian thermoelectric production (2019, 2030 and 2040). ....	10
Figure 1-12. Natural gas (NG) penetration in the Italian gas demand (2019, 2030 and 204). ....	11

---

Figure 1-13. Italian natural gas (NG), biomethane and hydrogen demand (2019, 2030 and 2040). .....	13
Figure 1-14. P2G energy sector coupling. ....	16
Figure 1-15. CP2H energy sector coupling. ....	17
Figure 1-16. LP2H energy sector coupling.....	18
Figure 2-1. Multi-energy system scheme: electricity, heat and gas integration.....	22
Figure 2-2. Modified power node model scheme. ....	23
Figure 2-3. Gas flows within the gas distribution network: winter case. The network’s gas demand is mainly met through withdrawals from the high-pressure network. ....	33
Figure 2-4. Gas flows within the gas distribution network: summer case. The network’s gas demand is mainly met through the SNG produced by the P2G plant. Note that for the sake of clarity, a different scale was used than in Figure 2-3.....	34
Figure 2-5. Relative error of the pressure in the network pipes. The red curve shows the deviation of the pipe with worst performance. The dashed black curve shows the average error of all pipes. Both lines pertain to the day that yielded the highest deviations. ....	34
Figure 2-6. CP2H baseload definition. ....	39
Figure 2-7. Control algorithm of the methanation units. ....	42
Figure 2-8. Building circuit–equivalent thermal resistor-capacitor (3R2C) model.....	44
Figure 2-9. Conceptual architecture of the information exchange during simulation. ....	50
Figure 2-10. MQTT publish/subscribe messaging. ....	53
Figure 2-11. Modules of the multi-energy system co-simulation tool. ....	53
Figure 3-1. Schema of the analyzed multi-energy system.....	59
Figure 3-2. Topology of the electricity network.....	60
Figure 3-3. Topology of the gas network. ....	61



---

Figure 3-4. Scheme of P2G system. ....	63
Figure 3-5. Duration curves of RES generation, electricity demand and natural gas. ....	65
Figure 3-6. Monthly RES generation, monthly electricity and monthly gas demands.....	65
Figure 3-7. Sequence of interactions among co-simulation modules.....	70
Figure 3-8. Control algorithm of the i-th electrolyzer. ....	71
Figure 3-9. Control algorithm of the methanation units. ....	72
Figure 3-10. Balance of transformers of the electricity network in winter. ...	73
Figure 3-11. Balance of the gas network for the winter .....	74
Figure 3-12. Gas network pressure for the winter. ....	74
Figure 3-13. Balance of the electricity network transformers for the summer. ....	76
Figure 3-14. Balance of the gas network for the summer.....	76
Figure 3-15. Gas network pressure (b) for the summer.....	77
Figure 3-16. Status of the methanation units: 1 hot standby, 2 Reactor balancing phase, 3 up and running. ....	77
Figure 3-17. Pressure of the hydrogen buffers. ....	78
Figure 3-18. Levelized cost of SNG as a function of the flexibility provision price and the resulting electricity surplus price considering the investment cost for year 2030 (yellow area) and 2050 (green area). The figure also reports the values of the levelized cost of SNG reported in other publications: a [133], b [141], c [150], d [153], and e [154]. ....	80
Figure 3-19. Impact of oxygen and heat utilization for P2G#1 (a), P2G#2 (b) and P2G#3 (c).....	82
Figure 4-1. Schema of the analyzed multi-energy system.....	89
Figure 4-2. Scheme of the electricity network detailed model (multi-nodal model).....	91

---

---

Figure 4-3. Schema of the electricity network simplified model (single node model).....	91
Figure 4-4. Scheme of the gas network detailed model (multi-nodal model).....	92
Figure 4-5. Schema of the gas network simplified model (single node model).....	92
Figure 4-6. Scheme of the detailed P2G model (multi-components model). .....	93
Figure 4-7. Scheme of the P2G simplified model (lumped parameters model).....	93
Figure 4-8. Sequence of interactions among co-simulation modules (with detailed and simplified models). ....	94
Figure 4-9. Electricity balance referring to the whole grid (winter day): (a) Reference simulation and (b) EN simplified simulation. ....	96
Figure 4-10. Electricity balance on HV/MV transformers (winter day): (a) Reference simulation and (b) EN simplified simulation. ....	97
Figure 4-11. Gas network balance (winter day): (a) Reference simulation and (b) simplified GN simulation.....	100
Figure 4-12. Gas network's balance and pressure (summer day): (a) Reference simulation and (b) simplified GN simulation. ....	101
Figure 4-13. HV/MV transformers' balance (summer day): (a) Reference simulation and (b) simplified GN simulation.....	102
Figure 4-14. Gas network balance (Mid-season day): (a) Reference simulation and (b) simplified P2G simulation. ....	103
Figure 4-15. Gas network pressure (summer day): (a) Reference simulation and (b) simplified P2G simulation. ....	104
Figure 4-16. HV/MV transformers' balance and hydrogen buffer's SoC: (a) Reference simulation and (b) simplified P2G simulation.....	105
Figure 5-1. Schema of the analyzed multi-energy system.....	111
Figure 5-2. Multi-energy system scenario. ....	112

---

Figure 5-3. Yearly heat demand, electricity (EL) demand, RES generation and RES over-generation (Over-gen.).....	113
Figure 5-4. Duration curve of heat demand, electricity (EL) demand and RES generation. TR#1 and DH SN#1 (a), TR#2 and DH SN#2 (b), TR#3 and DH SN#3 (c).....	114
Figure 5-5. Sequence of interactions among co-simulation modules.....	119
Figure 5-6. The $i$ -th CP2H baseload control algorithm. Optimization of DH heat flows .....	120
Figure 5-7. Flexibility exploitation control algorithm of the $i$ -th CP2H unit for RPF absorption. ....	121
Figure 5-8. Energy flows in each DH subnetwork (a) and in each transformer (b). Base case. Details of a day with a high DH heat demand (February). ....	123
Figure 5-9. Energy flows in each DH subnetwork (a) and in each transformer (b). Optimized case. Details of a day with a high DH heat demand (February). ....	123
Figure 5-10. Energy flows in each DH subnetwork (a) and in each transformer (b). Base case. Details of a day with a low DH heat demand (September). ....	125
Figure 5-11. Energy flows in each DH subnetwork (a) and in each transformer (b). Optimized case. Details of a day with a low DH heat demand (September). ....	125
Figure 5-12. Net Present Value (a) and Simple Pay Back (b) of the three CP2H plants for the base case and for the optimized case. ....	130
Figure 6-1. Schema of the analyzed multi-energy systems: Base case (a), VES case (b) and EB case (c). The flexibility assets have been highlighted in yellow.....	135
Figure 6-2. Annual profile of the external temperature [193]. ....	136
Figure 6-3. Annual profile of LP2H devices' electricity consumption. ....	138
Figure 6-4. Annual profile of the passive electricity load. ....	138
Figure 6-5. Annual profile of the PV production [193].....	138

---

Figure 6-6. Load duration curve of PV generation, LP2H electricity consumption and passive load.....	138
Figure 6-7. Electricity flows in the energy community.....	141
Figure 6-8. Sequence of interactions among co-simulation modules (VES case).....	144
Figure 6-9. Sequence of interactions among co-simulation modules (EB case).....	145
Figure 6-10. Energy community's electricity balance: base case (a) versus LP2H optimized load case (b). Details pertaining to 20 <sup>th</sup> April.....	147
Figure 6-11. LP2H electricity load in Base case and VES case. ....	148
Figure 6-12. The Virtual Energy Storage (VES) effect (a). VES electricity charge and discharge (b). Details pertaining to 20 <sup>th</sup> April. ....	149
Figure 6-13. Electricity balance of the energy community for the EB case (a). EB electricity charge and discharge (b). Details pertaining to 20 <sup>th</sup> April. ....	150
Figure 6-14. Electricity balance of the energy community for different seasons: VES case. ....	151
Figure 6-15. Electricity balance of the energy community for different seasons: EB case.....	152
Figure 6-16. Energy accumulated and released by VES and EB throughout the year divided by the average daily temperature.....	152
Figure 6-17. Self-sufficiency (a) and self-consumption (b) of the energy community as a function of the RES installed power. ....	155
Figure 6-18. Energy community incomes derived from the use of flexible assets as a function of RES penetration (a). Flexible assets Net Present Value as a function of RES penetration (b).....	157
Figure 6-19. Energy community incomes derived from the use as a function of RES penetration and EB capacity (a). Net Present Value as a function of RES penetration and EB capacity (b). ....	158

# List of Abbreviations

	Definition
<hr/>	
BC	Base Case
BFS	Backward Forward Sweep
BOS	Balance of System
CAPEX	Capital Expenditure
CCUS	Carbon Capture, Utilization & Storage
CH <sub>4</sub>	Methane
CO <sub>2</sub>	Carbon dioxide
CoP	Conference of the Parties
COP	Coefficient Of Performance
CP2H	Centralized Power-to-Heat
DH	District Heating
DR	Discount Rate
DSO	Distribution System Operator
DTW	Dynamic Time Warping
EB	Electric Battery

EC	Energy Community
EN	Electricity Network
EPA	Environmental Protection Agency
G2P	Gas-to-Power
GN	Gas Network
H <sub>2</sub>	Hydrogen
HP	Heat Pump
HV	High Voltage
IPCC	Intergovernmental Panel on Climate Change
LC <sub>SNG</sub>	Levelized Cost of SNG
LHV	Lower Heating Value
LP2H	Localized Power-to-Heat
MES	Multi-Energy System
MQTT	Message Queuing Telemetry Transport
MV	Medium Voltage
N <sub>2</sub> O	Nitrous oxide
NG	Natural Gas
NPV	Net Present Value
O&M	Operation and Maintenance
O <sub>2</sub>	Oxygen
OPEX	Operation Expenditure

P2G	Power-to-Gas
P2H	Power-to-Heat
P2H <sub>2</sub>	Power-to-Hydrogen
P2H2P	Power-to-Hydrogen-to-Power
P2X	Power-to-X
PEM	Polymer Electrolyte Membrane electrolyzer
PV	Photovoltaic
RES	Renewable Energy Sources
RPF	Reverse Power Flow
SN	DH Sub-Network
SNG	Synthetic Natural Gas
SoC	State of Charge
SPB	Simple Payback
STP	Standard Temperature and Pressure
TES	Thermal Energy Storage
TR	Transformer
TSO	Transmission System Operator
Time-Sync	Time-Synchronizer
UNFCCC	United Nations Framework Convention on Climate Change
VES	Virtual Energy Storage
WT	Wind Turbines

# List of Symbols

## Variables

	Definition	Unit
$\mathbf{A}$	Incidence matrix	[-]
$c$	Specific cost	[€/unit]
$\mathcal{C}$	Thermal capacitance	[kJ/K]
$C\_rate$	Battery C-rate	[h <sup>-1</sup> ]
$Cap$	Storage capacity	[MWh]
$CAPEX$	Capital expenditure	[€]
$CF$	Cash flow	[€]
$COP$	Coefficient of performance	[-]
$Cost$	Cost	[€]
$c_p$	Specific heat	[kJ/kg/K]
$D$	Pipe diameter	[mm]
$DR$	Discount rate	[-]
$E$	Energy	[MWh]
$\dot{E}$	Energy flow	[MW]



---

$g$	Electric generation	[MW <sub>e</sub> ]
$\mathbf{g}$	Vector containing known terms in the energy equation	[kW]
$G$	Water mass flow rate	[kg/s]
$\mathbf{G}$	Matrix of the water mass flows	[kg/s]
$HP_{NG}$	Natural gas withdrawn from the transmission network	[kg/s]
$HV_{el}$	Electricity withdrawn from the transmission network	[MW <sub>e</sub> ]
$\underline{i}$	Electric current	[A]
$\underline{\mathbf{i}}_B$	Vector of line currents	[A]
$\underline{\mathbf{i}}_N$	Vector of nodal currents	[A]
$\mathbf{K}$	Stiffness matrix	[kW/K]
$l$	Storage energy loss	[MW]
$L$	Pipi length	[m]
$LC_{SNG}$	Levelized cost of synthetic natural gas	[€/MWh]
$LT$	Lifetime	[years]
$\dot{m}$	Gas mass flow rate	[kg/s]
$\mathbf{M}$	Mass matrix	[kg]
$NPV$	Net present value	[€]
$OPEX$	Fixed operational expenditure	[€]
$p$	Pressure	[bar]
$\bar{p}$	Mean pressure	[bar]

---

---

$P$	Electric active power	[MW <sub>e</sub> ]
$P_n$	Nominal power	[MW]
$r$	Specific revenue	[€/unit]
$R$	Specific gas constant	[J/kg/K]
$\mathcal{R}$	Thermal resistance	[K/kW]
$Rev$	Revenue	[€]
$\underline{s}$	Vector of electric power	[kVA]
$SoC$	State of Charge	[-]
$SPB$	Simple payback	[years]
$T$	Temperature	[K]
$\mathbf{T}$	Vector containing the temperatures	[K]
$\dot{\mathbf{T}}$	Vector containing the time derivative of the temperatures	[K/s]
$u$	Electricity load	[MW <sub>e</sub> ]
$U$	Heat exchange coefficient	[kW/K]
$\underline{v}$	voltage	[kV]
$\underline{\mathbf{v}}$	Vector of voltages	[kV]
$V$	Volume	[m <sup>3</sup> ]
$\underline{y}_C$	Vector of load admittances	[S]
$\underline{\mathbf{Z}}_B$	Matrix of branch impedances	[Ω]
$\Gamma$	Inverse of the node-to-branch incidence matrix	[-]

---

---

$\eta$	Efficiency	[-]
$\lambda$	battery self discharge rate	[-]
$\xi$	Exported/imported energy flow in the power node	[MW]
$\pi$	Power flexibility	[MW]
$\rho$	Density	[kg/m <sup>3</sup> ]
$\Phi$	Heat flow	[MW <sub>th</sub> ]
$\omega$	Unserviced load / enforced energy loss caused by the power node	[MW]

## Indices, subscripts and superscripts

	Definition
0	Baseload
–	Downwards
+	Upwards
<i>aux</i>	Auxiliary systems
<i>av</i>	Logarithmic average
B	Number of branches
<i>D</i>	Design condition
<i>el</i>	Electricity
<i>ev</i>	Evaporator
<i>ext</i>	External
<i>flex</i>	Flexibility

$gr$	Ground
$i$	Generic component
$in$	Internal
$inj$	Injection
$j$	Generic iteration step
$k$	Generic time step
$K$	Number of time steps
$m$	Generic node
$max$	Maximum
$min$	Minimum
$M_n$	Number of nodes adjacent to node $n$
$n$	Generic node
$N$	Number of nodes
$n - m$	Branch joining node $n$ and node $m$
$\mathcal{N}_m$	Number of nodes adjacent to node $m$
$pass$	Passive load
$rep$	Replacement
$sc$	Self-consumption
$sol$	Solar
$wit$	Withdrawal
$y$	Generic year
$\vartheta$	Generic integration procedure step



# Chapter 1

## Introduction

### 1.1 Greenhouse gas emissions and global warming

In 2021, the Intergovernmental Panel on Climate Change's (IPCC) last report ("Climate Change 2021: The Physical Science Basis") warned that in 2020, the atmospheric concentration of greenhouse gasses, such as carbon dioxide (CO<sub>2</sub>), methane (CH<sub>4</sub>) and nitrous oxide (N<sub>2</sub>O), increased compared to the eighteenth-century's values by about 47%, 156%, and 23%, respectively [1]. An average increase of about 3.5% compared to the values recorded in 2011 [2]. It is now well established that global warming is closely and positively correlated with the increase of greenhouse gasses in the atmosphere. In the last decade (2011-2020), the global surface temperature was 1.09°C higher than during the preindustrial era [1] (see Figure 1-1).

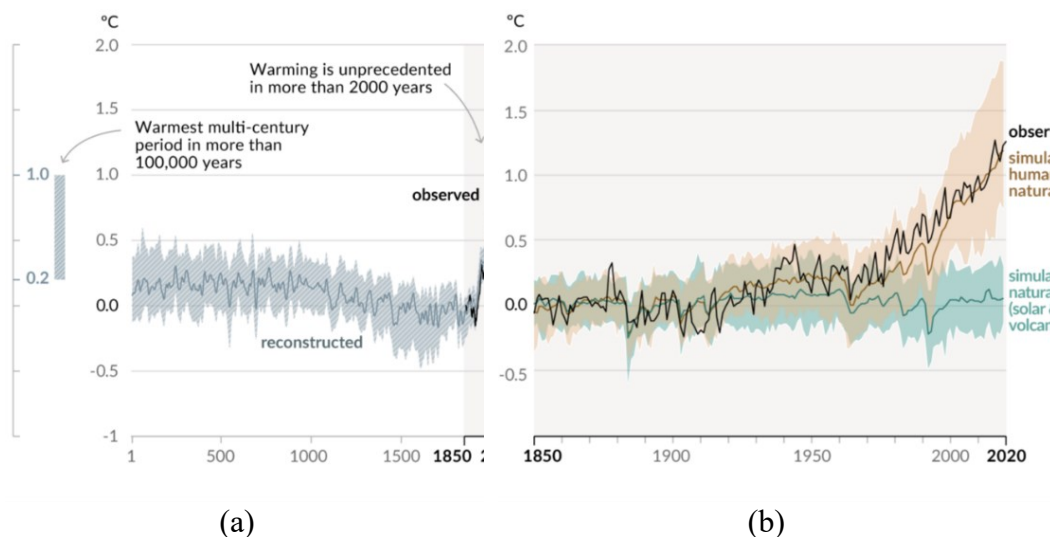


Figure 1-1. (a) Change in global surface temperature (decadal average) as reconstructed (1-2000) and observed (1850-2020). (b) Change in global surface temperature (annual average) as observed and simulated using human & natural and only natural factors (both 1850-2020) [1].

Five greenhouse gasses emission scenarios (see Figure 1-2a) and their expected impact on global warming (see Figure 1-2b) have been defined by IPCC. Two scenarios present high and very high greenhouse gasses emissions (SSP3-7.0 and SSP5-8.5, respectively). A Third, intermediate scenario (SSP2-4.5) shows a slight increase in greenhouse gas production, followed by a steady decrease in the second half of the century. Finally, the last two scenarios illustrate/predict an immediate block in the growth of emissions, followed by a substantial decline, up to a negative production (thanks to carbon capture technologies) from the second half of the century (SSP1-1.9 and SSP1-2.6).

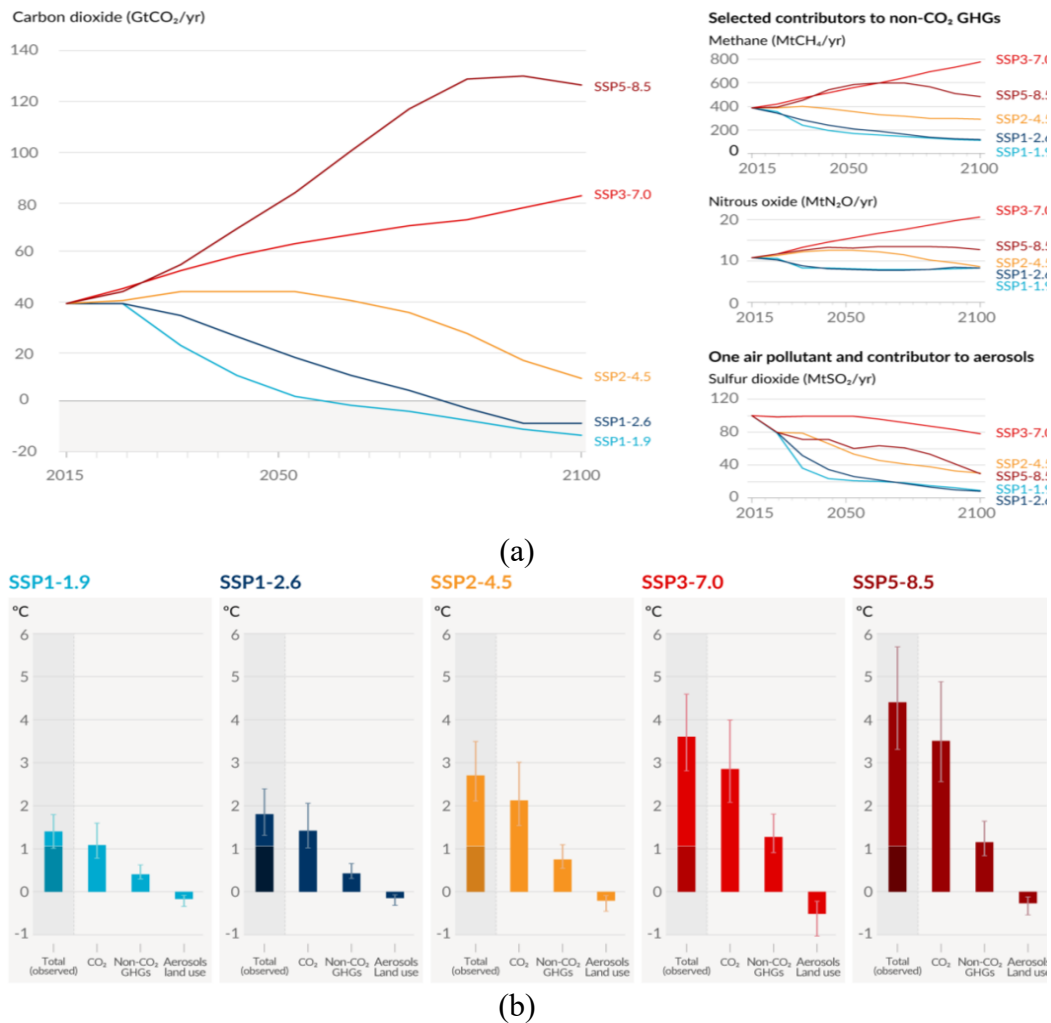


Figure 1-2. IPCC future scenarios of CO<sub>2</sub> emissions (a) and their impact on global warming (b) [1].

Only in the most optimistic scenarios (SSP1-1.9 and SSP1-2.6), the global increase of the surface temperature will remain under 2°C. However, it should be noted that Figure 1-2 shows global warming's average values. The actual rises in local temperature could reach much more marked deviations, even in the more optimistic scenarios (see Figure 1-3).

This dangerous trend could lead to permanent upheaves, such as more frequent and intense thunderstorms [3], intensification of rainfall extremes [4], acidification of oceans [5], sea level rise [6], glaciers and sea ice melting [7],[8], with consequences on both the planet flora and fauna [9], as well as on human society.[10],[11],[12].

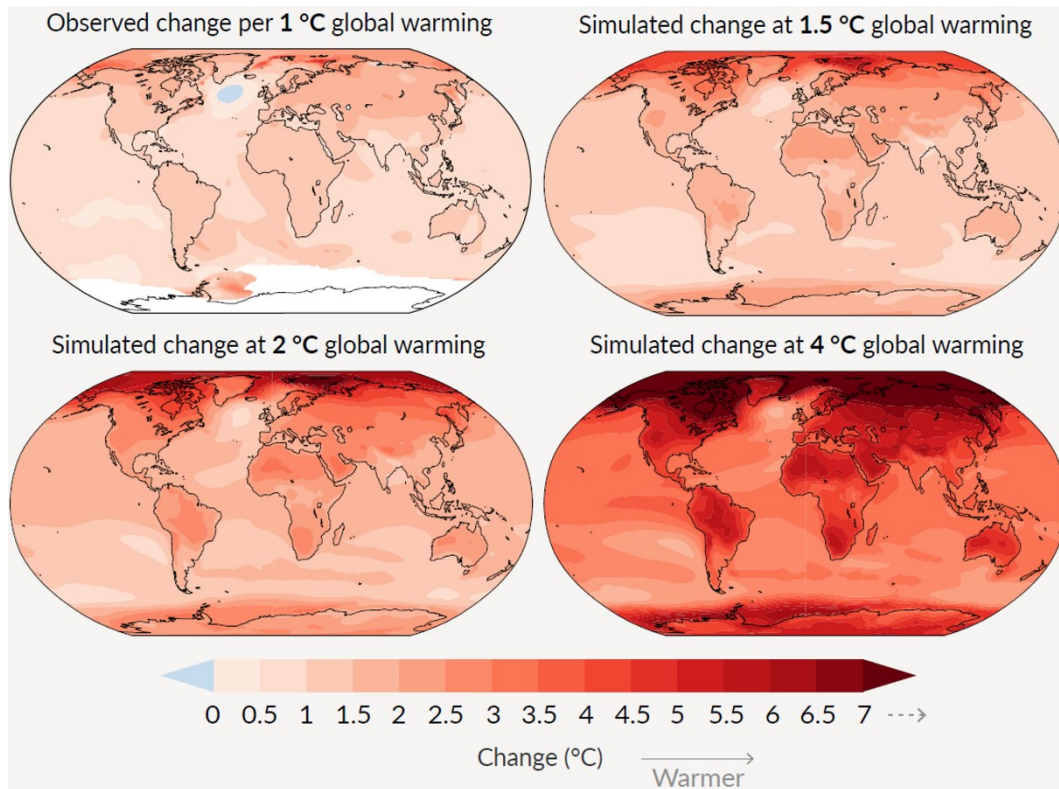


Figure 1-3. Changes in annual surface temperature over the World [1].

To tackle climate change many states have implemented environmental policies in the last decades. In 1995, the United Nations Framework Convention on Climate Change (UNFCCC) began to be enforced. The UNFCCC nowadays consists of 197 parties, including all the member states of the United Nation [13], and its main goal is to prevent the anthropogenic impact on the climate's system. Since 1995, the UNFCCC parties have therefore been meeting every year in the so-called Conference of the Parties (CoP), in order to assess progress and define future agreements for dealing with climate change. In CoP3 (1997), the state parties signed the Kyoto Protocol, which set greenhouse gasses reduction targets for 37 industrialized countries and economies in transition. Specifically, the actors involved agreed to reduce by 5% the emissions compared to 1990 levels [14]. In the Copenhagen Accord [15], signed during CoP15 in 2009, the goal of limiting global warming to 2°C was first introduced. In the Paris Agreement (CoP21, 2015), the state parties confirmed the need to limit global warming to 2°C and declared the intention to reduce it below 1.5°C [16].



In order to fulfill the goals set in the UNFCCC, in 2011, the European Commission defined the Energy Roadmap 2050 [17]. The document defined an emission reduction target between 80% and 95% for 2050. Importantly, 80% of such reduction was set to be obtained without resorting to the use of international credits for CO<sub>2</sub> emissions.

In 2016, the European Commission published the “Clean Energy for all Europeans” package, which introduced new targets to be obtained by 2030: reducing the greenhouse gas emissions by 40% compared to 1990 levels, reaching 32% of renewable energy penetration in the EU’s energy mix and increasing the energy efficiency by at least 32.5% in comparison with the 2016 levels [18]. In 2019, the European Parliament and the European Council redefined UE’S long-term goals by planning to achieve climate neutrality by 2050 [19]. The following year, the European Commission recognized that the medium-term goals set in 2016 would not be sufficient to meet the new, more ambitious goals for 2050 [20]. In 2021, new objectives were therefore defined for 2030, including a decrease of total emissions by 55% compared to 1990 and a higher (from 32% to 40%) minimum target for the penetration of renewables in the EU energy mix [21].

## **1.2 Role of renewable energy sources**

Nowadays, the electricity sector is one of the largest emitters of greenhouse gasses. For instance, the Environmental Protection Agency (EPA) reported that in 2019, about 25% of the GHG emissions in the US were generated for the production of electricity [22]. The intensity of the green gasses emissions for electricity generation was defined by the EPA as the ratio of CO<sub>2</sub> equivalent emission over the electricity production. In the EU, the emission intensity for electricity generation in 2019 was about 50% lower than in 1990 (see Figure 1-4). From 1990 to 2010, this trend was mainly supported by both the increasing efficiency of the power plants and the utilization of less impacting fuels (such as natural gas). From 2010 to 2019, the decrease was mainly driven by the transition from fossil fuels to Renewable Energy Sources (RES) [23]. In European countries, the RES energy generation passed from 129 TWh in 2010 to 212 TWh in 2020, with an increase of 62%, thus exceeding the electricity produced by fossil fuel for the second year [24] (see Figure 1-5). This was largely due to two factors: greenhouse gasses emission reduction targets and RES’s cost decrease. For instance, since 2010, the costs of offshore wind turbine decreased by 29%, those of onshore wind turbines by 39% and those of solar photovoltaic by 82% [25]).

In 2020, the share of RES for electricity generation amounted to nearly 40%: 13% from hydroelectric sources, 15% from wind sources, 5% from solar sources and 6% from other renewable sources. This was, and is, considerably above the world’s average, which remains at around 30% (see Figure 1-6) [26]. It is worth noting that these values refer to the renewable penetration in the electricity sector only; they do not refer to the percentage of renewables in the entire European energy

mix, which includes other sectors, such as the transport sector, where the penetration of renewables is much lower. Eurostat reports that in 2019, the percentage of renewable penetration in the European energy mix was around 15% [27], still far from the targets set for 2030.

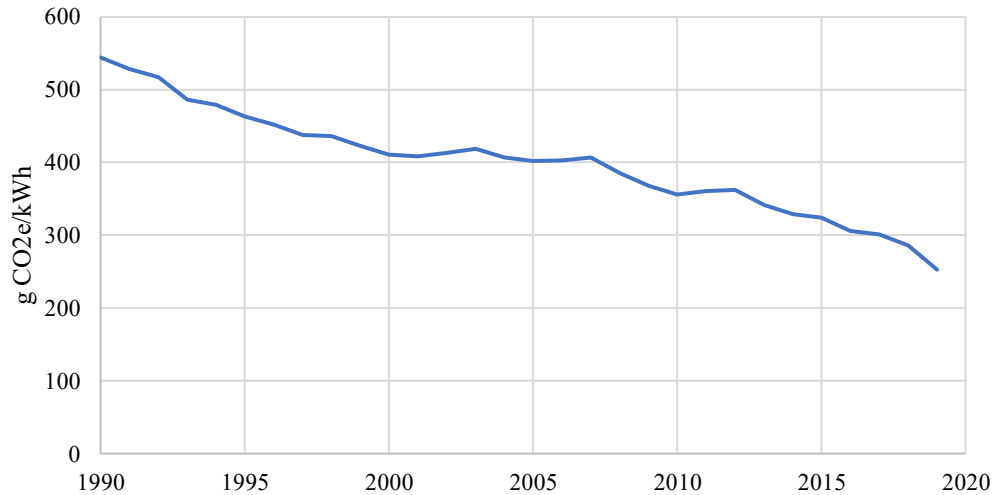


Figure 1-4. Greenhouse gas emission intensity for electricity production of EU.

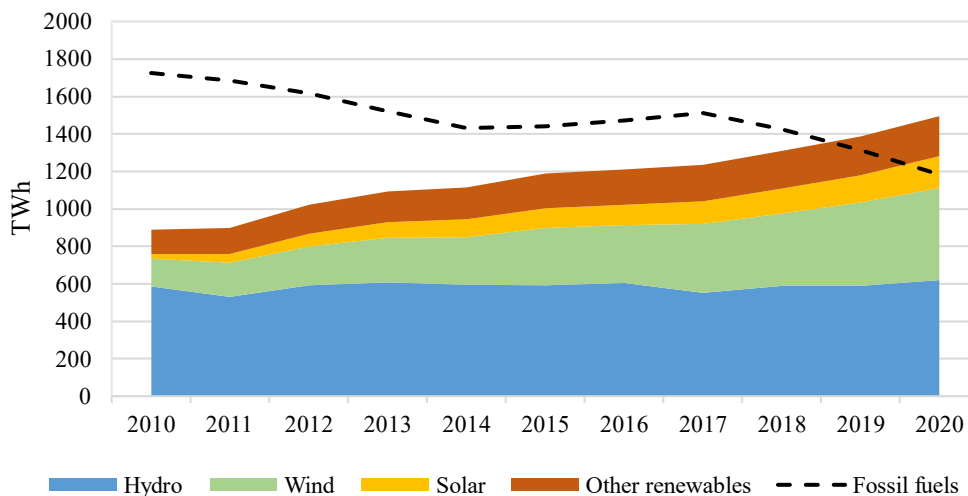


Figure 1-5. EU electricity generation from renewable energy and fossil fuels.

In the next decade (2021-2030), there will therefore be a significant increase in the installed capacity of RES, mainly regarding photovoltaic and wind power, rather than hydropower. As for the latter, the exploitation of hydropower's untapped potentials is extremely challenging. Indeed, even though it is a well-established technology for which many countries would have sites that could be used to host new hydroelectric plants, there still are socio-environmental constraints that still hinder its full development. Nonetheless, both an update of existing hydroelectric

plants through equipment renewals and the construction of new pumping plants will strongly increase [28]. As for photovoltaics, it is expected that in order to reach the 2030 objectives, the photovoltaic capacity of Europe and the United Kingdom, now at about 150 GW, should rise between 455 and 605 GW, depending on the strategic political scenario [29], with a growth of 12-15% only in the three-year period 2020-2023. The installed power of wind turbines, which in Europe is currently around 200 GW, will increase by about 60% in 2030, reaching a total capacity of between 260 and 375 GW [30] [31] (see Figure 1-7).

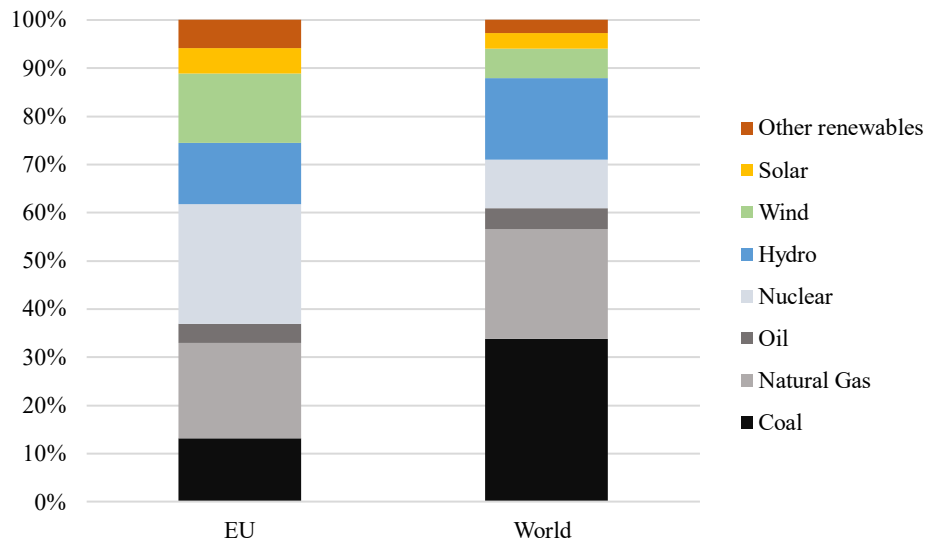


Figure 1-6. European countries' and World's energy mix for electricity generation.

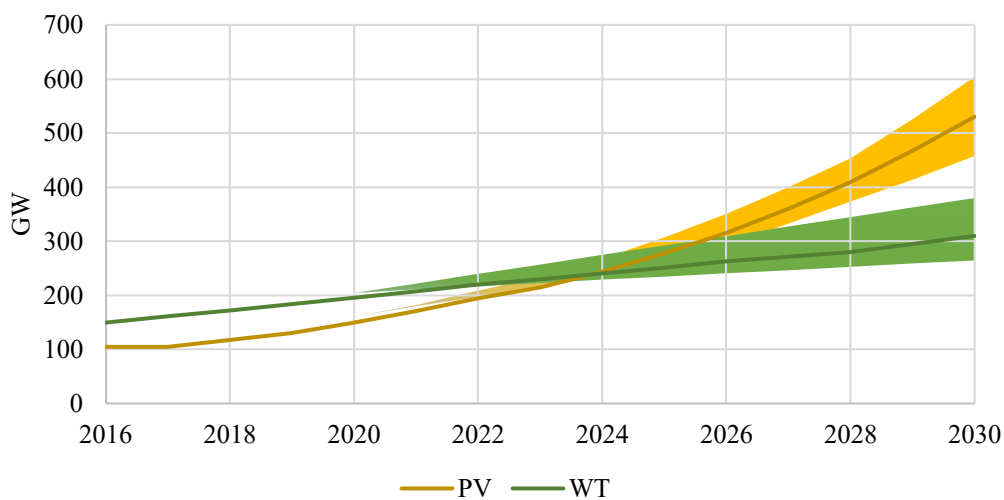


Figure 1-7. PV and WT installation data from [29], [30] and [31].

---

### 1.3 Future energy scenarios in Italy: the Snam and Terna report

In August 2022, the Italian gas Transmission System Operator (TSO) Snam and the Italian electricity TSO Terna published an updated report on the Italian energy scenarios for the next decades [32]. The document aimed to outline the path towards the European target of zero CO<sub>2</sub> emissions by 2050.

As discussed in the previous sections, energy transition is one of the most important European goals. For instance, in Italy, the National Recovery and Resilience Plan (PNRR) allocated nearly 40 billion euros to improve energy efficiency, accelerate the penetration of the electricity vector and booster the use of renewable electricity and green gasses. It is important to point out that the energy crisis triggered by Russia's invasion of Ukraine has highlighted the importance of the evolution of the future energy system and its resilience.

In this context, in order to eliminate CO<sub>2</sub> emissions at the national level, Snam and Terna have planned intermediate steps with specific targets set for 2030 and 2040. More specifically, the plan Fit-For-55 (FF55), which was designed in line with European targets, aims to reduce of 55% CO<sub>2</sub> emissions by 2030. This target will be achieved through the penetration of electricity in strategic sectors (e.g., heating and transport), supported by a strong penetration of renewable electricity sources, which will represent up to 65% of the national electricity demand. As for the gas sector, increased use of biomethane and green hydrogen is expected to meet 11% of national demand. The deployment of Carbon Capture, Utilization & Storage (CCUS) technologies is also foreseen to contribute to the decarbonization of "hard to abate" sectors.

The FF55 scenario for 2030 paves the way for two possible pathways for 2040: the so-called Distributed Energy Italia (DE-IT) scenario and the Global Ambition Italia (GA-IT) scenario. Both scenarios present intermediate targets to be met by 2040, in order to reach net zero emissions by 2050. Although the two scenarios present significant similarities, they differ in the degree of penetration of various decarbonization solutions.

The GA-IT scenario aims to meet the 2040 targets through to an increase of renewable electricity sources (photovoltaic and wind), making energy use more efficient in various sectors. Non-programmable renewable generation will be supported by flexible thermoelectric power plants, whose environmental impact will be contained by the use of green fuels and the deployment of CCUS systems. The DE-IT scenario envisions a greater use of renewable electricity sources, supported by energy storage and energy conversion technologies, so that overproduction during peaks of renewable energy generation could be offset. CCUS technologies are also expected to be deployed in this scenario, but mainly in "hard-to-abate" sectors.

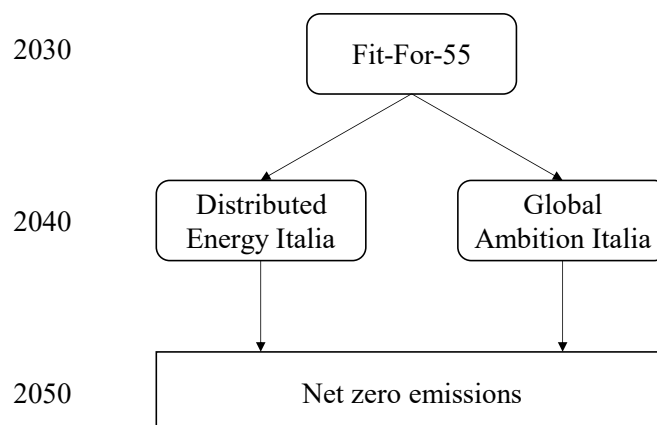


Figure 1-8. Snam-Terna intermediate 2030-2040 steps to net zero emission.

### 1.3.1 Evolution of the Italian electricity sector

#### Electricity demand

Energy consumption efficiency is expected to improve in the coming decades. However, due to the electrification of some energy sectors, Italy's electricity demand is expected to increase. Indeed, according to the FF55 scenarios of both Snam and Terna, Italy's electricity demand will increase by almost 15% in 2030. The current demand of 320 TWh (data refer to consumption in 2019) will increase to almost 370 TWh in 2030, due to the envisaged electrification of the transport and heating sectors. This trend is predicted to continue in the following decade. The GA-IT scenario predicts that electricity demand will increase by 8% compared to 2030, reaching almost 400 TWh. The DE-IT scenario, which is characterized by a higher penetration of the electricity carrier in both the transport and heating sectors, predicts that electricity demand will rise up to about 420 TWh, almost 15% more than in 2030 (see Figure 1-9).

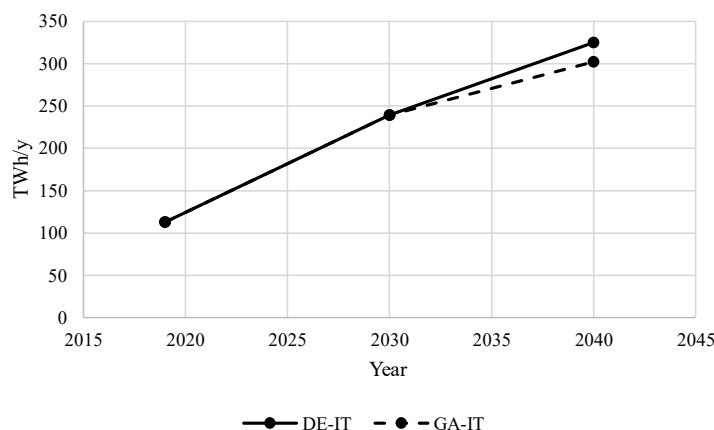


Figure 1-9. Italian electricity demand (years 2019, 2030 and 2040).

## Renewable energy sources

Nowadays, 40% of renewable energy in Italy is produced by hydropower (46 TWh out of 112 TWh). The exploitation of hydro-resources has however reached a saturation level. Hence, even though a 10% increase in the use of this form of energy is expected in the coming years, it will not be enough to meet the targets for the next decades. Total renewable generation is expected to reach 239 TWh in 2030, which will cover 65% of the electricity demand. This target will be achieved through the installation of more than 100 GW of new solar and wind power plants: +12 GW of small-scale PV, +42 GW of large-scale PV, +7 GW of onshore wind, and +9 GW of offshore wind. Small-scale PV will be more concentrated in the northern regions, whereas large-scale PV and wind turbine plants will increase more in the southern part of the country, which is characterized by greater development potentials in terms of full-load hours and areas suitable for new installations. A similar trend will continue until 2040, when renewable resource production will reach 325 TWh in the DE-IT scenario and 302 TWh in the GA-IT scenario (see Figure 1-10).

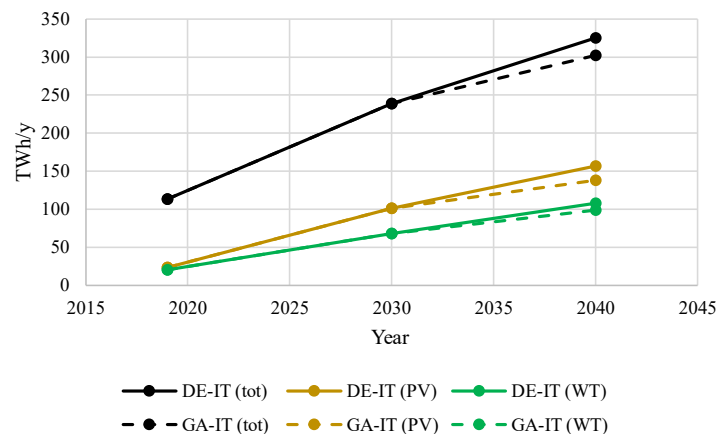


Figure 1-10. Italian production of renewable energy sources (2019, 2030 and 2040).

## Thermoelectric production

In 2019, gas supplied about 80% of the thermoelectric sector's needs. Coal-fired power plants are expected to be completely retired by 2030. Electricity generation from gas is scheduled to decrease from 138 TWh in 2019 to 75 TWh in 2030, a decrease of about 46%. Gas will be used to cover 94% of thermoelectric production (estimated at 80 TWh). The decrease in gas production will regard not only plants that exclusively produce electricity, but also those with cogeneration units. In 2040, a further decrease in the use of thermoelectric generation is expected. The DE-IT scenario envisions the generation of 49 TWh, of which 46 TWh generated by gas-fired power plants. As for the GA-IT scenario, an even greater use of this technology would be adopted, with 50 TWh out of 53 TWh of thermoelectric generation produced by gas-fired power plants (see Figure 1-11).

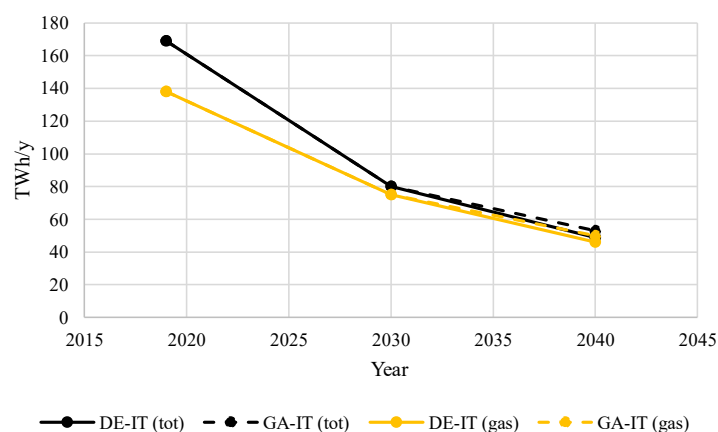


Figure 1-11. Italian thermoelectric production (2019, 2030 and 2040).

## 1.3.2 Evolution of the Italian gas sector

### The gas demand

Table 1-1 shows the annual gas demand: the values given in the table include natural gas, as well as other fuels, such as biogas and hydrogen (the latter two energy sources are discussed in the following sections).

In 2021, gas demand was 810 TWh, slightly higher than in the previous years. This increase was caused by two factors. On the one hand, a colder winter season pushed up consumption by the civil sector for heating purposes. On the other, the tertiary sector returned to pre-Covid pandemic (2020) consumption levels. Currently, the civil sector is responsible for about 40% of Gas consumption (mainly for heating purposes). An identical proportion (40%) is used for electricity and heat generation. Most the remaining gas consumption (about 15%) is attributable to the industrial sector.

Table 1-1. Italian annual gas demand (2018-2021).

	2019 [TWh]	2021 [TWh]	2030 [TWh]	2040 DE-IT [TWh]	2040 GA-IT [TWh]
Civil sector	299	320	240	170	191
Industries	110	114	118	96	110
Transport sector	15	15	67	72	99
Electricity and heat production	329	331	231	177	182
Others	34	31	47	47	47
Total	789	810	700	561	629

Nowadays, gas demand is almost entirely covered by Natural Gas (NG). In 2021, only 0.2% of gas consumption came from biomethane. To meet decarbonization targets, part of the gas demand currently met by NG will be replaced by other green gasses, such as biomethane and hydrogen. However, in 2030, 88% of gas demand will still be met by NG. A higher penetration of green gasses is expected in 2040, and the share of NG will further decrease between 67% and 47%, depending on the specific scenario (see Figure 1-12).

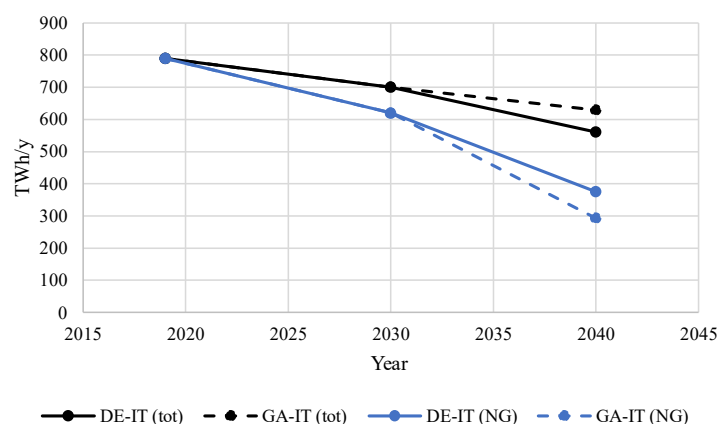


Figure 1-12. Natural gas (NG) penetration in the Italian gas demand (2019, 2030 and 2040).

## Biomethane

Biomethane production was 1.7 TWh in 2021. In 2030, production of this fuel is planned to increase to 57 TWh, almost evenly distributed among the civil, industrial, transport, and power and heat generation sectors (see Table 1-2).

The two scenarios for 2040 (DE-IT and GA-IT) foresee that the production of biomethane will reach 109 TWh, which is considered the maximum value that Italy can sustain.

Table 1-2. Italian biomethane production (2030 and 2040).

	2030 [TWh]	2040 DE-IT [TWh]	2040 GA-IT [TWh]
Civil sector	17	50	43
Industries	11	14	11
Transport sector	16	17	31
Electricity and heat production	15	29	24
Others	0	0	0
Total	57	109	109



In 2040, the greater use of biomethane is expected in the civil sector (50 TWh and 43 TWh for the DE-IT and the GA-IT scenarios, respectively). The latter scenario foresees a greater use in the transport sector (31 TWh compared to the 17 TWh of the scenario DE-IT), due to a lower use of electric mobility. Instead, the DE-IT scenario foresees a greater use of biomethane for the decarbonization of the industrial sectors and the electricity and heat production.

## Hydrogen

The demand for hydrogen in 2030 is forecasted to correspond to 23 TWh, half of which is for direct use: 10 TWh in the transport sector (mainly heavy transport) and 2 TWh in the industrial sector. About 12 TWh are destined for indirect use of this resource (e.g., for the production of synthetic fuels).

Regarding the demand for hydrogen in 2040, the two scenarios foresee different situations. According to the DE-IT scenario, hydrogen demand will be of 77 TWh, whereas the GA-IT scenario assumes that this energy vector will be more widely used until an annual demand of 127 TWh is reached. In the latter scenario, the demand for hydrogen will be mainly concentrated in the transport sector as a carbon-free alternative for heavy and long-distance transport. In the industrial sector, hydrogen will replace natural gas. In the civil sector, hydrogen will be employed as an alternative to electric heat pumps, especially in the GA-IT scenario, which is characterized by a lower electrification of heating consumption. As for indirect uses, hydrogen will be used for the production of synthetic fuels (see Table 1-3).

Figure 1-13 compares the Italian demand for natural gas, biomethane and hydrogen. It can be seen that, despite a gradual decrease in the use of natural gas and a gradual increase in the use of biomethane and hydrogen, natural gas remains predominant compared to the other two types of fuels.

*Table 1-3. Italian hydrogen demand (2030 and 2040).*

	2030 [TWh]	2040 DE-IT [TWh]	2040 GA-IT [TWh]
Civil sector	0	3	19
Industries	2	19	40
Transport sector	10	38	51
Electricity and heat production	0	0	0
Others	12	17	17
Total	23	77	127

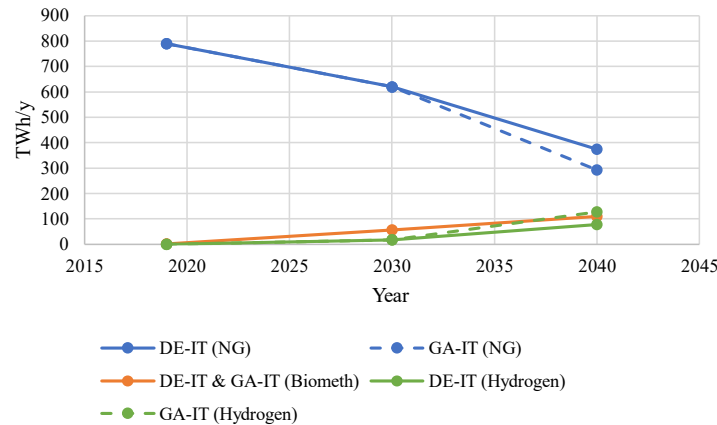


Figure 1-13. Italian natural gas (NG), biomethane and hydrogen demand (2019, 2030 and 2040).

## 1.4 Objectives of the thesis

### 1.4.1 Motivation

#### Needs of flexibility at the distribution level

A pivotal condition for the operation in the electricity energy system is the contemporaneity of energy production and its consumption. That is, in order to preserve the operation condition of the electricity system, the electricity must be generated in the instant it is consumed. This brings about the need to keep electricity generation and consumption in constant balance. [33]. The electricity system was designed to bring the electricity produced by the power plants to the consumers through transmission and distribution networks characterized by a top-down unidirectional power flow. The increasing penetration of distributed generation of renewables is changing this paradigm; the traditional case of a completely passive distribution network, in which only passive users are connected, is moving towards an active network with increasing energy production at the distribution level [34]. The intrinsic high volatility, intermittency and non-dispatchability nature of renewable sources makes it challenging to constantly maintain energy consumption and energy production well balanced [35]. Indeed, sudden variations and over-generations of renewable energy generation could cause problems to the electricity system, such as voltage and current operational constraint violations or reverse power flow (RPF). To avoid these problems, the current practice consists in curtailing the renewable over-generation [36]. However, this practice is disadvantageous from both an environmental point of view, as it is a waste of clean energy, and an economic point of view. As for the economic perspective, a case in point is that of Germany, where a special curtailment remuneration has been implemented in which RES plant operators are reimbursed for the curtailed electricity. In 2015, 472 million euros were spent to repay the 4.72 TWh of curtailment [37].

The role of distributed resources, connected to the distribution system, is gaining increasing importance for the control and regulation of power systems. In fact, their increasing penetration calls for their participation in both the energy and ancillary service markets; in the latter case to support the proper operation of electrical systems. In this context, the European Union has recently opened new perspectives for all distributed resources, by fostering their participation, as aggregated sources, in the ancillary service market [38]. In the future, as concluded in the SmartNet project [39], this kind of flexibility service could also be used by Distribution System Operators (DSOs) to balance their distribution networks. The presence of multi-energy infrastructures (such as gas and electricity networks) in the same district may help handle RES over-generation at a distribution level, by reducing the effects witnessed for the transmission system, and actively support the regulation of the overall electricity system.

### **The flexibility enabled by multi-energy systems**

The installation of pure electric storage technologies, such as electric batteries [40], pumped hydro storage [41] and compressed-air energy storage [42] can partially provide the required flexibility. Indeed, these technologies make it possible to absorb excessive renewable energy production and release the accumulated energy when necessary. However, electricity storages are characterized by a very high investment cost. Furthermore, the optimal solution cannot be found by considering only a single part of the overall energy system (see [43]). To tackle this problem more efficiently, the paradigms of the management of the overall energy system would need to be reviewed within a more holistic approach, one that would take into account all the possible interactions and synergies among all the energy sectors. This approach would allow new and non-negligible sources of flexibility to emerge [44], [45]. Moreover, in parallel with the increase in RES penetration, it is expected that certain important energy-intensive sectors will move towards more sustainable systems powered by electricity. While these new electrical loads may aggravate the grid imbalances, they would nonetheless increase the interconnection between these energy-intensive sectors and the electricity system in an integrated multi-energy system (MES) [46]. The MES consists in the integration and coordination of different energy sectors and networks, such as electricity, heat, gas and transportation [47]. As also reported in [48], the MES will have a fundamental role in the decarbonization of the whole energy system. In fact, other non-electrical energy sectors are usually more flexible than the power sector, because they do not require an instantaneous balance between demand and generation. For instance, the linepack flexibility of the gas network [49], the thermal inertia of the district heating network (DH) [50] or the thermal inertia of buildings [51], all allow a temporal mismatch between energy generation and energy demand. When these non-electrical sectors are powered (or partially powered) using technologies that convert electricity into other forms of energy (Power to X, P2X), the electricity sector and these other more flexible

---

energy sectors are connected. In this way, the flexibility of the non-electric sectors could be exploited to improve the exploitation of renewable energies [52].

### 1.4.2 Solution for flexibility analyzed in this thesis

The research presented in this thesis analyzed the flexibility that some energy conversion technologies would allow in a district context, so that the penetration of RES at the distribution level could be improved. More specifically, various simulation models were used to investigate the extent to which local penetration of RES could be improved by a flexibly energy system that uses energy conversion technologies to connect existing energy infrastructures to the electricity distribution system. To analyze the feasibility of these flexible solutions, analyses were performed for each solution, from both technical and economic perspectives. The flexible solutions analyzed in this thesis are presented below.

#### Coupling electricity and gas sector through Power-to-Gas

One of the most frequently discussed P2X technologies is the so-called Power-to-Gas (P2G) technology. The term P2G can be used to indicate both Power-to-Hydrogen (P2H<sub>2</sub>) and Power-to-Methane technologies. In the former case, electricity is used to produce hydrogen as the final product. In the latter, the production chain also includes a methanation unit, which transforms hydrogen into Synthetic Natural Gas, SNG. Consequently, Power-to-Hydrogen technology is arguably more efficient than Power-to-Methane, as the latter requires an additional conversion step. However, Power-to-Methane presents many advantages over Power-to-Hydrogen: *a*) SNG's volume energy density ( $> 1000 \text{ kWh/Sm}^3$ ) is much higher than that of hydrogen ( $270 \text{ kWh/Sm}^3$ ) [53]; *b*) SNG can be injected into the existing gas infrastructure, as opposed to hydrogen that can only be injected at low concentrations, due to hydrogen embrittlement, which can create cracks in iron and steel pipes [54]; *c*) hydrogen has a higher risk of ignition than SNG, thus making it less safe for domestic utilization [54].

This thesis focused only on Power-to-Methane. P2G will be henceforth used to indicate the Power-to-Methane technology. The main advantages of using P2G and P2H<sub>2</sub> technologies can be summarized in the following three points:

- they can be used to offer flexibility to a power system. Indeed, a system that exploits P2G and P2H<sub>2</sub> technologies can modulate its consumption over a wide range of operation points and quickly change them in a flexible way. This is because the electrolyzer, especially Polymer Electrolyte Membrane (PEM) electrolyzers, can produce fast responses to the variation of its setpoint;
- they produce synthetic fuels. These fuels, if produced from renewable sources, can be used to decarbonize some final-use sectors, whose electrification could be less straightforward;

- they can be used as part of an energy storage system, as they allow the electricity produced from renewable sources to be stored as chemical energy, which in turn can be converted into electricity.

A P2G plant is mainly composed of two components: an electrolyzer and a methanation unit. The former consumes electricity energy to electrolyze pure water and produce hydrogen. In the methanation unit, the produced hydrogen exothermically reacts with carbon dioxide to produce methane, which is also called Synthetic Natural Gas (SNG). Thanks to these energy conversion processes, P2G technology can be used to connect the electricity network with the gas network, thus coupling the two energy sectors (see Figure 1-14).

As will be discussed more in detail in the following chapters, thanks to these features, P2G technology has been analyzed in the literature in different contexts. However, the role and the impact of the P2G technology at the distribution level has been analyzed only in a few studies. This thesis aimed to fill this gap by analyzing from a techno-economic point of view how the P2G flexibility could be exploited at a distribution level.

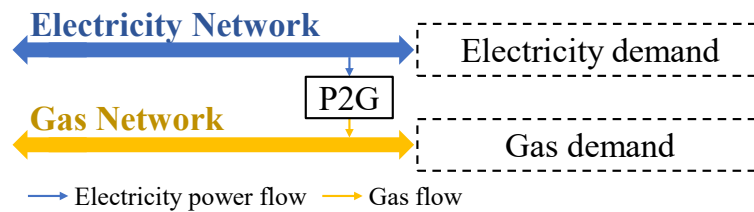


Figure 1-14. P2G energy sector coupling.

### Coupling electricity and district heating sector through Power-to-Heat

The term Power-to-Heat technology (P2H) refers to all those technologies for the conversion of electricity into heat (heat pumps, electric resistant heating systems, etc.). Power-to-Heat (P2H) technologies have existed as commercial products for decades. Their good dynamic characteristics, associated with a source of thermal inertia, guarantee an effective way to manage the intermittency of RES, thus bringing additional flexibility to the system.

Large scale P2H plants can be used to provide heat in District Heating (DH) networks. In this thesis, this type of application will be called centralized P2H (CP2H). CP2H allows the DH sector and the electricity sector to be connected (see Figure 1-15). The interaction between the two infrastructures is made through large-scale heat pumps, which allow efficient conversion of electricity in thermal energy. CP2H plants can be coupled with large-scale thermal storages that can be employed to face the DH heat peak demand and, at the same time, operate the CP2H in a more flexible manner.

This thesis analyzes this type of flexibility used to improve RES dispatching at the distribution level. LP2H plants are evaluated from a techno-economic point of view by considering two different control strategies.

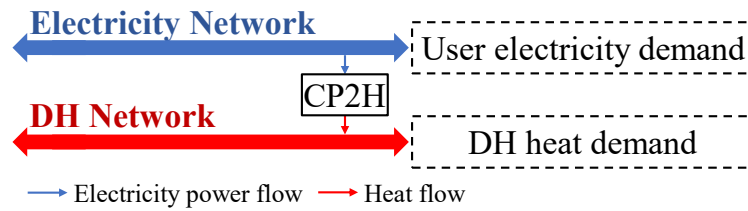


Figure 1-15. CP2H energy sector coupling.

### Coupling electricity and building heating sector through Power-to-Heat

In this thesis, the term Localized P2H (LP2H) will be used to refer to a small scale P2H plant installed directly inside a building to satisfy its thermal demand. The current European decarbonization policies are encouraging countries to electrify their building heating sectors [55]. If buildings are equipped with standalone electrical heating devices (i.e., Localized Power-to-Heat, LP2H), such as electric resistance heaters or heat pumps, the inherent flexibility of this sector can be released and used in the electricity sector [56]. Normally, the heating systems of buildings do not work at their nominal capacity, as they are designed to provide heat to the building in the most extreme conditions. However, when these conditions do not occur, they work at a lower load. For this reason, the design of LP2H systems inherently offers available capacity to be used flexibly. At the same time, the European directives, which are in line with the Nearly Zero-Energy Building (NZEB) target [57], are promoting the efficiency of buildings. These new NZEB-principled buildings permit a higher flexibility of LPH2 devices, as they are characterized by a high thermal insulation that allows them to maintain their heat with low thermal energy losses [58]. The electricity consumption of LP2H devices can therefore be modulated with a certain degree of flexibility since, due to the thermal inertia of the building thermal mass, the thermal response of the buildings is not immediate. Moreover, the indoor temperature setpoint of buildings could be flexibly regulated over a pre-arranged range (that would not violate the internal thermal comfort), so that the electricity consumption of the LP2H devices could be further regulated. Thanks to the connection of the electricity sector and the building heating sector, the flexibility of the building's heat demand could be exploited within the electricity sector (see Figure 1-16).

This thesis analyzed how the flexibility of these localized devices could be exploited to maximize the local self-consumption of renewable resources. This solution was analyzed in an energy community context from both an energy and an economic point of view.

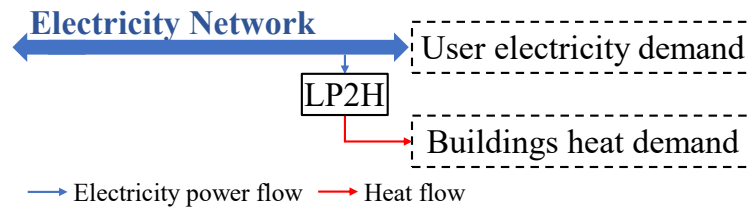


Figure 1-16. LP2H energy sector coupling.

### 1.4.3 Solution for flexibility not included in this thesis

This thesis analyzed the use of P2G and P2H technologies. However, there are other technologies that are worth mentioning, as they have flexibility potentials that could also be exploited at the district level. The analysis of these technological solutions will find place in future developments of this thesis. Indeed, a modification of the simulation tool for the analysis of multi-energy systems is planned, in order to integrate new energy sectors in the simulation (see Chapter 7).

The main technologies that have not been addressed in this thesis are briefly presented below.

#### Power-to-Hydrogen

As introduced in Section 1.3.2, the use of the hydrogen vector is expected to play a very important role in the decarbonization of different energy sectors (especially from 2030 onwards). P2H<sub>2</sub> technology allows the production of hydrogen from the electrolysis of water by consuming electricity. The load of this type of plant can be changed in a very short time (4 minutes from start up to nominal load [59]) and can therefore be used to follow the production of variable RES [59], [60], [61], [62]. The hydrogen produced can be used on-site to produce electricity. This solution is known in the literature as Power-to-Hydrogen-to-Power (P2H2P) and has been analyzed mainly in off-grid contexts to provide electricity when renewable energy sources are not available [63], [64]. Alternatively, hydrogen can be used locally to produce synthetic fuels through dedicated power-to-fuel routes [65].

The produced hydrogen can also be transported and stored to be used for decarbonization of various energy-intensive sectors (transport [66], industry [67], civil [68]). There are several solutions for hydrogen transportation and distribution. P2H<sub>2</sub> systems could be coupled with hydrogen pressurization or cryogenic liquefaction systems for distribution in dedicated tanks. However, this solution comes with some drawbacks, such as the energy cost of hydrogen pressurization/liquefaction. The hydrogen produced by P2H<sub>2</sub> plants could be injected into dedicated pipelines. However, today there are no hydrogen transport and distribution networks. Several studies have investigated the possibility of using the existing natural gas pipeline infrastructure. However, the gas grid is not built to

transport hydrogen. It would therefore be necessary to ensure that the hydrogen content in the pipelines would not exceed a certain limit. In general, a limit of 10% is considered sufficient to ensure a lower risk of ignition [69] and leakage [70], as well as hydrogen embrittlement cracks [71].

### **Electric vehicle charging station**

The transition to electric mobility is a fundamental pathway for the decarbonization of the transport sector [72]. To encourage this transition, several governments provide incentives, such as subsidies and financing, for the purchase of electric vehicles [73]. The transition to electric mobility is expected to have two main consequences. On the one hand, it will lead to an increase in the peak and variability of electricity demand, which will affect the electricity system [74], [75]. On the other hand, it will allow the exploitation of new forms of flexibility [76]. Indeed, the use of electric vehicles has inherent flexibility potentials. For instance, the battery in electric cars could be used as temporary electricity storage when the vehicle is not in use. While a single electric vehicle can only provide limited storage capacity, smart control of a portfolio of electric vehicles' batteries connected to the grid can provide significant distributed flexibility.

With smart control, the charging of electric vehicles could be concentrated during RES production periods. Conversely, during times of excess electricity demand, energy could be drawn from the batteries to balance the electricity demand. However, this flexible vehicle charging management will have to ensure that the vehicles are charged (or have reached a specified minimum state of charge) at the end of the specified time [77]. Since the flexibility of electric vehicles depends on the number of vehicles connected to the grid, the availability of this flexible resource is stochastic and varies significantly, depending on the different times of the day.

Extensive research has been conducted in the literature, and various tools have been developed for the analysis of the flexibility enabled by electric vehicles' charging stations. [78]. In particular, the utilization of such a flexibility has been analyzed in order to investigate the extent to which it could improve RES penetration in the national electricity system [79], [80], increase the RES self-consumption at the local level [81], [82], provide services for the electricity system (e.g. frequency regulation) [83], and smooth the electricity demand curves [84].

## **1.5 Manuscript contents**

The remainder of this manuscript is structured as follows.

**Chapter 2** introduces the different technologies and infrastructures that compose the multi-energy systems analyzed in this thesis. It also describes how energy conversion technologies act as a bridge to transfer the inherent flexibility of non-electrical sectors within the electricity system. The chapter defines how flexibility has been calculated and how it is exploited to improve the energy flows



of the electricity network. The mathematical models used for the simulation of energy conversion technologies and network infrastructures are described in the chapter. Moreover, the chapter introduces the simulation tool created for the analysis of these kinds of scenarios: a co-simulation platform designed for the simulation of multi-energy systems.

**Chapter 3** presents the first case study: the analysis of P2G technology applied to a district scenario. Thanks to the co-simulation tool, it was possible to integrate complex models in the same co-simulation platform: a medium-voltage electricity distribution network model, a medium pressure gas distribution network model and a P2G model, which took into account the intermediate conversion processes that take place within P2G plants. The study evaluated the impact of P2G plants on the electricity and gas distribution system and the levelized cost of SNG.

The analysis presented in **Chapter 4**, the second case study, is a further development of case study 1. The aim of this study was to analyze the impact of different simplified modeling approaches (for the simulation of the electricity network, the gas network model and the P2G plant) and to understand whether, and under which conditions, the simplifications could lead to acceptable results.

In **Chapter 5**, the third case study analyzes the use of CP2H plants as flexible connections between the electricity grid and district heating. This energy conversion technology had a twofold purpose: to produce heat for the district heating and provide flexibility to the electricity network that could be used to optimize the dispatch of RES generation. Different configurations and control strategies were analyzed. The use of CP2H technology in a distribution network context was finally evaluated from an economic point of view by calculating the Net Present Value and Simple Payback of the investment.

In **Chapter 6** the fourth case study is presented. This case study analyzed the flexibility enabled by LP2H technology in an energy community context. This flexible solution was compared with the more conventional flexible solution of electric battery. The two solutions were evaluated from technical and economic points of view. It was evaluated how these two technologies could influence the self-sufficiency and self-consumption of the energy community and how this could affect the economic flow of the energy community.

Finally, in **Chapter 7** the main conclusions of this thesis and possible future developments are outlined.

# Chapter 2

## Methods

This chapter describes the various mathematical models of energy conversion technologies and energy infrastructures of multi-energy systems. The chapter describes how the flexibility enabled by energy conversion technologies is transferred from the non-electric sectors to the electricity sector and how such flexibility is calculated. Finally, the chapter describes the simulation tool used to analyze the different case studies.

### 2.1 Flexibility calculation in multi-energy systems

This thesis mainly focuses on the following energy conversion technologies: Power-to-Gas (P2G), centralized Power-to-Heat (CP2H) and localized Power-to-Heat (LP2H). These energy conversion technologies enable the creation of a connection point between non-electric energy sectors and the electricity sector. Specifically, P2G technology connects the gas network to the electricity network. CP2H technology creates a connection between district heating (DH) and the electricity network. Finally, LP2H technology connects the building heating sector (more precisely, the buildings that are not connected to the district heating network) to the electricity network. These connection points allow a better use of RES. Thanks to these technologies, the energy generated by RES can also be used in the non-electric sectors (in the case studies analyzed in this thesis, in the gas sector and in district and building heating). A schema of a possible multi-energy system is shown in Figure 2-1.

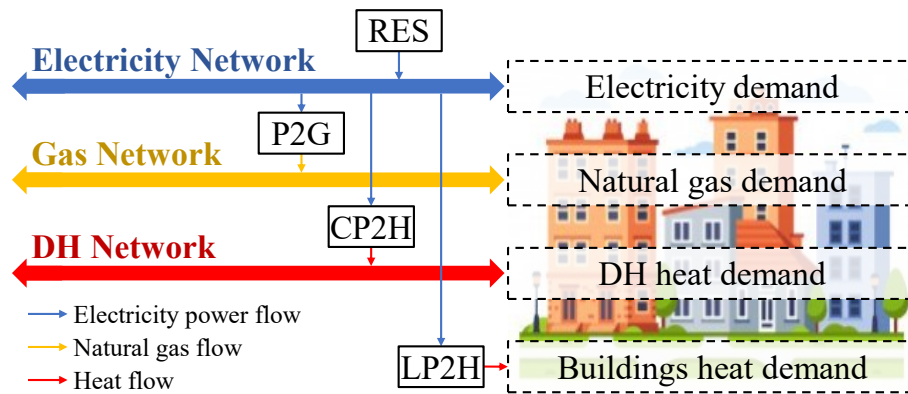


Figure 2-1. Multi-energy system scheme: electricity, heat and gas integration.

Flexibility may be defined as the capability of a system to modify its electricity generation/consumption profile in order to offer ancillary services to the grid. It is possible to define upward and downward flexibility [85]. In this thesis, upward flexibility is defined as the capability of a system to increase its energy consumption or reduce its production. Upward flexibility may be required when the RES generation exceeds the total load and there is a need to balance the energy in the network in order to maintain grid stability; for example by converting or storing excess RES energy. Downward flexibility is the capacity of a system to decrease the total energy consumption in the system itself, or to increase the total energy production [86]. Downward flexibility may be required when the RES production is lower than the total load or during a critical peak pricing event.

In an energy system scenario, flexibility can be provided by different technologies, for example:

- pure load units can provide upward and downward flexibility by increasing or decreasing their electric load [87];
- energy storage systems can offer upward flexibility by absorbing energy from the grid or downward flexibility by releasing stored energy [88];
- energy conversion units (P2G, P2H) can offer both upward and downward flexibility by modifying their operational set-points [89];
- generation units can increase or decrease the power introduced into the network, thus offering both upward and downward flexibility [90];
- the RES could also provide downward flexibility by modulating the power production (e.g., RES generation curtailment) [91],[92].

The Power Node approach, proposed in reference [93], was adopted to calculate and evaluate the available flexibility. The advantage of this method is that it can be used to define the flexibility of any power system with the same mathematical equations. Figure 2-2 reports all the possible power exchanges between the electric grid and a general device. The same notations could be adopted for power

generation plants, power conversion units (P2G, P2H), electric storages, and pure load units.

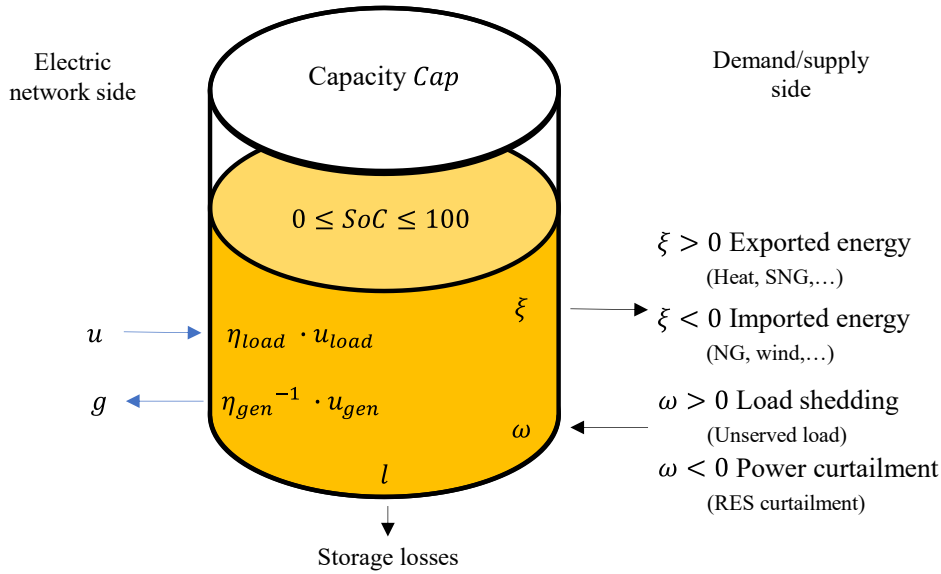


Figure 2-2. Modified power node model scheme.

In Figure 2-2, notations and formulas have to be interpreted as follows:

- $Cap \geq 0$  [MWh] is the internal storage capacity ( $C = 0$ , for a non-buffered unit);
- $0 \leq SoC \leq 1$  [-] is the normalized State of Charge;
- $u \geq 0$  [MW] is the electric consumption of the device and  $\eta_{load}$  is the charging/conversion efficiency;
- $g \geq 0$  [MW] is the electric generation of the device, and  $\eta_{gen}$  is its efficiency;
- $\xi$  [MW] is the energy flow that exits the system ( $\xi > 0$  e.g., Synthetic Natural Gas SNG, heat), or the energy flow that enters into the system ( $\xi < 0$ , e.g., Natural Gas NG, wind energy) by the device;
- $\omega$  [MW] represents an unserved load ( $\omega > 0$ , e.g., demand curtailment), or an enforced energy loss ( $\omega < 0$ , e.g., RES curtailment);
- $l \geq 0$  [MW] is the storage energy loss.

The general Power Node equation is:

$$Cap \cdot \dot{SoC} = \eta_{load} \cdot u - \eta_{gen}^{-1} \cdot g - \xi + \omega - l \quad (2.1)$$

Generally, each term in the above equation may be either controllable or non-controllable.  $l$ ,  $\eta_{load}$  and  $\eta_{gen}$  may be fixed or state-dependent (e.g.,  $l = f(SoC)$ ).

The electricity load/generator of the device is constrained as:

$$0 \leq u^{min} \leq u \leq u^{max} \quad (2.2)$$

$$0 \leq g^{min} \leq g \leq g^{max} \quad (2.3)$$

$$\dot{u}^{min} \leq \dot{u} \leq \dot{u}^{max} \quad (2.4)$$

$$\dot{g}^{min} \leq \dot{g} \leq \dot{g}^{max} \quad (2.5)$$

Eq. (2.2) represents the maximum and minimum power load, whereas Eq. (2.3) represents the maximum and minimum power generation. Both values are normally defined on the basis of the nominal power and the minimum working power. Eqs. (2.4) and (2.5) pertain to the restriction due to the ramp rate capacity of the device. More details on Power Node modeling are reported in references [93],[94].

If a general P2X energy conversion device is considered as an example, the Power Node equation for the  $k$  simulation time step can be written as:

$$u_{P2X}(k) = \frac{(\xi_{P2X}(k) + Cap \cdot \dot{SoC}_{P2X}(k) + l_{P2X}(k))}{\eta_{P2X}} \quad (2.6)$$

where  $Cap$  is the internal energy storage capacity (e.g., a heat storage of a P2H),  $\dot{SoC}_{P2X}$  is its normalized State of Charge and  $l_{P2X}$  is its energy loss.  $\xi_{P2X}$  is the X energy vector provided externally and  $\eta_{P2X}$  is the efficiency of the P2X process. The unit can modify its electric load,  $u_{P2X}$ , by modifying the internal storage SoC and/or the energy exported outside the plant.

For a load unit, the available flexibility can be defined as:

$$\pi_{P2X}(k) = u_{P2X}^{feasible}(k) - u_{P2X}^0(k) = \frac{(\xi_{P2X}^{feasible}(k) + Cap \cdot \dot{SoC}_{P2X}^{feasible}(k) + v_{P2X}(k))}{\eta_{P2X}} - u_{P2X}^0(k) \quad (2.7)$$

where  $u_{P2X}^{feasible}$  is the electric load of the unit in one of the possible working conditions and  $u_{P2X}^0$  is the unit electricity baseload.  $\xi_{P2X}^{feasible}$  is the amount of X energy that may be exported outside the plant without violating the external constraints (e.g., the district heating or gas grid capacity). It is possible to define  $\xi_{P2X}^{max} \geq 0$  and  $\xi_{P2X}^{min} \geq 0$  as the maximum and minimum flows of an energy vector X that may be exported, respectively.  $Cap \cdot \dot{SoC}_{P2X}^{feasible}$  may be positive or negative, and is bound by a maximum  $Cap \cdot \dot{SoC}_{P2X}^{max} \geq 0$  and a minimum  $Cap \cdot \dot{SoC}_{P2X}^{min} \leq 0$ , depending on the buffer's condition (e.g., when the buffer reaches full charge,  $Cap \cdot \dot{SoC}_{P2X}^{max} = 0$ ).

The electric load of the unit is bound by the following constraints:

$$0 \leq u_{P2X}^{min} \leq u_{P2X}^{feasible}(k) \leq u_{P2X}^{max} \quad (2.8)$$

$$\dot{u}_{P2X}^{min} \leq \dot{u}_{P2X}^{feasible}(k) \leq \dot{u}_{P2X}^{max} \quad (2.9)$$

By combining Eqs. (2.7), (2.8), and (2.9) it is possible to define the positive and negative power capacity flexibility ( $\pi^+$ ,  $\pi^-$ ):

$$\pi_{P2X}^+(k) = \min \left\{ \frac{(\xi_{P2X}^{max}(k) + C \cdot S \dot{C}_{P2X}^{max}(k) + v_{P2X}(k))}{\eta_{P2X}}, u_{P2X}^{max}, u_{P2X}^0(k) + \dot{u}_{P2X}^{max} \Delta k \right\} - u_{P2X}^0(k) \quad (2.10)$$

$$\pi_{P2X}^-(k) = \max \left\{ \frac{(\xi_{P2X}^{min}(k) + C \cdot S \dot{C}_{P2X}^{min}(k) + v_{P2X}(k))}{\eta_{P2X}}, u_{P2X}^{min}, u_{P2X}^0(k) + \dot{u}_{P2X}^{min} \Delta k \right\} - u_{P2X}^0(k) \quad (2.11)$$

The terms  $\frac{(\xi_{P2X}^{min}(k) + C \cdot S \dot{C}_{P2X}^{min}(k) + v_{P2X}(k))}{\eta_{P2X}}$  and  $\frac{(\xi_{P2X}^{max}(k) + C \cdot S \dot{C}_{P2X}^{max}(k) + v_{P2X}(k))}{\eta_{P2X}}$  represent the storage and the external constraints at simulation step  $k$ . The limitation, due to minimum and maximum power loads, is defined by  $u_{P2X}^{min}$  and  $u_{P2X}^{max}$ , respectively. The terms  $u_{P2X}^0(k) + \dot{u}_{P2X}^{min} \Delta k$  and  $u_{P2X}^0(k) + \dot{u}_{P2X}^{max} \Delta k$  guarantee that the power increase/decrease during discretization interval  $\Delta k$  does not exceed the ramp rate constraints.

## 2.2 The energy networks and the energy conversion technologies models

This section describes all the models used for the simulation of multi-energy systems presented in the following chapters. Specifically, the mathematical models of the energy conversion technologies, the models of the energy networks and the model for the control of the flexible resources. One last component should also be mentioned, the time-synchronizer (Time-Sync), which is neither a physical component of the multi-energy system, nor a control logic. This last component was created to orchestrate the simulation and is to be presented in Section 2.3.4.

For the analysis presented in Chapter 4, two different mathematical models were used for some components of the multi-energy system: a more detailed one (these types of models are called "*detailed*" models) and a less detailed one (these types of models are called "*simplified*" models).

Thanks to the co-simulation method presented in Section 2.3, the models integrated in the simulation tool developed in this thesis could be developed in different types of programming languages. In this thesis, different modules developed in MATLAB, Simulink, Python and RT-Lab were merged.

The models were:

- The controller model;
- the time-synchronizer (Time-Sync) model;
- The electricity network detailed model;
- The electricity network simplified model;
- The gas network detailed model;
- The gas network simplified model;

- The district Heating (DH) Network and centralized Power-to-Heat (CP2H) model;
- The building and localized Power-to-Heat (LP2H) model;
- The Power-to-Gas (P2G) detailed model;
- The Power-to-Gas (P2G) simplified model;
- The Electricity Battery (EB) model.

All models are reported and summarized in Table 2-1.

Thanks to the features of the co-simulation approach, it was possible to integrate models developed in collaboration with other research groups into those developed within the current research. The former models are henceforth referred to as "*externally developed models*". My contribution to the realization of the externally developed models did not concern the realization of the mathematical model, but, rather, the aspects listed/summarized below:

*Electricity network detailed model:*

- collaboration in the creation of the communication modules required to integrate the model into the co-simulation platform;
- collaboration in defining inputs and outputs of the model;
- collaboration in the model verification tests.

*DH network and CP2H model:*

- creation of the communication modules required for integration into the co-simulation platform;
- definition of the model inputs/outputs;
- tests to verify the model.

*Building and LP2H model:*

- collaboration on model verification tests;
- collaboration on definition of inputs and outputs of the model.

*P2G detailed model:*

- creation of the communication modules required for integration into the co-simulation platform;
- collaboration in defining the inputs and outputs of the model;
- tests to verify the model.

Table 2-1. List of the models used in this thesis.

<i>Internally developed models</i>		
<b>Model</b>	<b>Programming language</b>	<b>Developed in collaboration with:</b>
Controller	MATLAB	–
Time-Sync	Simulink	–
Electricity network (simplified)	MATLAB	–
Gas network (detailed)	MATLAB	–
Gas network (simplified)	MATLAB	–
P2G (simplified)	MATLAB	–
EB	MATLAB	–
<i>Externally developed models</i>		
Electricity network (detailed)	RT-Lab	DENERG (IT)
DH Network and CP2H	MATLAB	DENERG (IT)
Building and LP2H	Python	HYPERTECH (GR)
P2G (detailed)	MATLAB	VTT (FI)

### 2.2.1 Electricity network detailed model

The electricity network detailed model was realized by Cesar Diaz-Londono and Andrea Mazza from Politecnico di Torino (Turin, Italy). The model was used for the simulation of case study 1 (see Chapter 3), case study 2 (see Chapter 4) and case study 3 (see Chapter 5).

The detailed electrical network model simulates the physical behavior of a medium voltage (MV) distribution network. The model takes into account the electricity flow in each branch, the voltage at each node and the withdrawals and injections of electricity at each node. Furthermore, the model takes into account the distribution network topology and the energy flows exchanged with the high voltage (HV) transmission grid through the transformers (TR) that connect the transmission system and the distribution system. The model is thus able to evaluate the local unbalances caused by overproduction of RES that can affect the distribution network. The power flow calculation was solved with the equivalent single-phase Backward Forward Sweep (BFS) algorithm [95] for radial networks (the number of nodes,  $N$ , is equal to the number of branches,  $B$ ). The BFS is a static method that calculates the steady state of the network. The power flow is calculated at each time step. In the case studies analyzed in this thesis, the time step is 15 minutes. The equations are solved in an iterative process until convergence is



achieved. The model calculates the current in the branches and the nodal voltages for each time step,  $k$ , as:

$$\underline{\mathbf{i}}_B^{(j)}(k) = \mathbf{\Gamma}^T \cdot \underline{\mathbf{i}}_N^{(j)}(k) = \mathbf{\Gamma}^T \cdot \left[ \underline{\mathbf{y}}_C \circ \underline{\mathbf{v}}^{(j-1)}(k) + \underline{\mathbf{s}}(k)^* \oslash (\underline{\mathbf{v}}^{(j-1)}(k))^* \right] \quad (2.12)$$

$$\underline{\mathbf{v}}^{(j)}(k) = \underline{\mathbf{v}}_{\text{slack}}(k) - \mathbf{\Gamma} \cdot \underline{\mathbf{Z}}_B \cdot \underline{\mathbf{i}}_B^{(j)}(k) \quad (2.13)$$

where:

- $\underline{\mathbf{i}}_B^{(j)}(k)$  [A] represents the vector that contains the complex currents at time step  $k$ , calculated during the backward phase of the BFS method, at the  $j$ -th iteration;
- $\underline{\mathbf{v}}^{(j)}(k)$  [kV] indicates the vector that contains the complex voltages at time step  $k$ , evaluated during the forward phase of the BFS method, at the  $j$ -th iteration;
- $\underline{\mathbf{i}}_N^{(j)}(k)$  [A] is the vector of the load nodes complex currents, at time step  $k$  and at the  $j$ -th iteration;
- The inverse of the node-to-branch incidence matrix is the  $\mathbf{\Gamma}$  [-] matrix. This matrix provides topological information about the network;
- The load admittances and the network admittances are included in the  $\underline{\mathbf{y}}_C$  [S] vector;
- $\underline{\mathbf{v}}^{(j-1)}(k)$  [kV] is the vector that contains the complex voltages at time step  $t$ , evaluated during the forward phase of the BFS method, at the iteration  $k - 1$ ;
- $\underline{\mathbf{s}}(k)$  [kVA] is the net load vector of the constant power, which can be seen as the difference between absorbed and injected power. A positive sign of the real (imaginary) part implies an absorption of active (reactive) power from the grid. Conversely, a negative sign indicates an injection of active (reactive) power into the grid. This representation is employed any time the power value at time step  $k$  is basically independent of the value of the node voltage at time  $k$ ;
- $\underline{\mathbf{v}}_{\text{slack}}(k)$  [kV] is the vector that contains the slack node voltage at time step  $k$ ;
- $\underline{\mathbf{Z}}_B$  [-] is a diagonal matrix that collects the values of the branch impedances.

Moreover, the mathematical operators  $\circ$  and  $\oslash$  are the Hadamard product and division, respectively. The symbol  $*$  indicates the conjugate operation.

At each step  $k$ , the electrical network model also calculates, the RPF in each transformer of the network as:

$$P_{TR\#i}(k) = \text{real}(\underline{\mathbf{v}}_{\text{slack}}(k) \cdot \underline{\mathbf{i}}_{TR\#i}^*(k)) \cdot 10^3 \quad (2.14)$$

$$RPF_{TR\#i}(k) = \begin{cases} -P_{TR\#i}(k), & \text{if } P_{TR\#i}(k) < 0 \\ 0, & \text{otherwise} \end{cases} \quad (2.15)$$

where:

- $RPF_{TR\#i}(k)$  [ $MW_e$ ] is the RPF of the  $i$ -th transformer at time step  $k$ .
- $P_{TR\#i}(k)$  [ $MW_e$ ] is the electrical energy flow that passes through the  $i$ -th transformer at time step  $k$ ;
- $v_{slack}(k)$  [kV] represents the slack voltage value at time step  $k$ ;
- $i_{TR\#i}(k)$  [A] is the current that passes through the  $i$ -th transformer at time step  $k$ .

More details on the electricity grid model are reported in [96].

## 2.2.2 Electricity network simplified model

The electricity network simplified model was realized within the work of this thesis. This model was used for the simulation of case study 2 (see Chapter 4) and case study 4 (see Chapter 6).

In the simplified electricity network model, instead of simulating the whole distribution electricity network, as in the detailed model, the electricity network is simplified by considering that all the loads and distributed generations are concentrated in a single node. The model is static and, at each simulation time step, calculates the balance of the loads and generations of the distribution network. The network Reverse Power Flow (RPF) is calculated as the positive difference between the sum of the distributed generation in the network and the sum of all the network loads. If the network's distributed generation is lower than the network's energy demand, the difference is assumed to be provided by the HV network:

$$RPF(k) = \begin{cases} \sum_{n=1}^N g_n(k) - u_n(k), & \text{if } \sum_{n=1}^N g_n(k) - u_n(k) > 0 \\ 0, & \text{otherwise} \end{cases} \quad (2.16)$$

$$HV_{el}(k) = \begin{cases} \sum_{n=1}^N u_n(k) - g_n(k), & \text{if } \sum_{n=1}^N u_n(k) - g_n(k) > 0 \\ 0, & \text{otherwise} \end{cases} \quad (2.17)$$

where:

- $RPF(k)$  [ $MW_e$ ] is the network RPF at time step  $k$ ;
- $HV_{el}(k)$  [ $MW_e$ ] is the electricity withdrawn from the HV network at time step  $k$ ;
- $g_n(k)$  [ $MW_e$ ] is the electricity generation at node  $n$  at time step  $k$ ;
- $u_n(k)$  [ $MW_e$ ] is the electricity load at node  $n$  at time step  $k$ .

The model does not take into account the network topology, nor the different connection points with the transmission network (i.e., the HV/MV transformers). For this reason, the simplified model is not able to evaluate the local unbalances that may occur within the distribution network.

### 2.2.3 Gas network detailed model

The gas network detailed model was realized within the work of this thesis. This model was used for the simulation of case study 1 (see Chapter 3) and case study 2 (see Chapter 4).

The gas network detailed model is a dynamic model that simulates the physical behavior of a medium pressure gas distribution network. The model takes into account the gas flow in each pipe and the pressure at each node of the network. The model is based on the (inverted) Renouard's equation for a medium pressure pipeline [97]<sup>1</sup>, the equation of state for ideal gases and the continuity equation. The mass flow between two nodes ( $n$  and  $m$ ) is determined from the difference in their pressure through the Renouard relation. The gas flow between node  $m$  and node  $n$  is positive, if the pressure at node  $m$  is higher than that of node  $n$ . Conversely, it is negative (i.e., it is flowing in the opposite direction), if the pressure at node  $m$  is lower than that of node  $n$ . Hence, the model is bi-directional. The pressure of each node is calculated using the equation of state as a function of the mass that exists at the node. The gas mass at the node is given by the continuity equation, which considers the gas injections and withdrawals, as well as the gas flows that go from that node to the adjacent ones. The model solves the equations dynamically with integration step  $d\vartheta$ , which was adjusted to make the model achieve convergence and depended on the network topology. The smaller the network pipelines, the smaller the time discretization necessary to achieve convergence. In the case studies considered in this thesis, a temporal discretization of the order of 1 second was applied. The gas withdrawal and injection flows into the network were considered constant in each simulation time step (15 minutes).

$$\dot{m}_{n-m}^{(\vartheta)}(k) = \left| \frac{p_m^{(\vartheta-1)^2}(k) - p_n^{(\vartheta-1)^2}(k)}{25.24 \cdot L_{n-m} \cdot D_{n-m}^{-4.82}} \right|^{\frac{1}{1.82}} \cdot \frac{\rho_{NG}}{3600} \cdot \text{sgn}(p_m^{(\vartheta-1)}(k) - p_n^{(\vartheta-1)}(k)) \quad (2.18)$$

$$\frac{dp_n^{(\vartheta)}(k)}{d\vartheta} = \frac{p_n^{(\vartheta)}(k) - p_n^{(\vartheta-1)}(k)}{d\vartheta} = \frac{R_{NG} \cdot T}{V_n} \cdot \dot{m}_n^{(\vartheta)}(k) \cdot 10^5 \quad (2.19)$$

$$\dot{m}_n^{(\vartheta)}(k) = \dot{m}_{inj,n}(k) - \dot{m}_{wit,n}(k) + \sum_{m=1}^{M_n} \dot{m}_{n-m}^{(\vartheta)}(k) \quad (2.20)$$

<sup>1</sup> Renouard's equation was inverted to isolate the gas flow between two nodes (see Eq. 2.18).

where:

- $\dot{m}_{n-m}^{(\vartheta)}(k)$  [kg/s] is the natural gas flow inside pipe  $n - m$  at time step  $k$  and the iteration of the integration procedure  $\vartheta$  (the subscript  $m$  represents a generic node of the nodes adjacent to node  $n$ );
- $p_n^{(\vartheta-1)}(k)$  [bar] and  $p_m^{(\vartheta-1)}(k)$  [bar] are the pressures of nodes  $n$  and  $m$ , respectively, at time step  $k$  and at the iteration of the integration procedure  $\vartheta - 1$ ;
- $L_{n-m}$  [m] is the length of pipe  $n - m$ ;
- $D_{n-m}$  [mm] is the diameter of pipe  $n - m$ ;
- $\rho_{NG}$  [kg/Sm<sup>3</sup>] is the natural gas density under standard conditions;
- $p_n^{(\vartheta)}(k)$  [bar] is the pressures in nodes  $n$  at time step  $k$  and the iteration of the integration procedure  $\vartheta$ ;
- $d\vartheta$  [s] is the integration step;
- $R_{NG}$  [J/kg/K] is the specific gas constant of natural gas;
- $T$  [K] is the temperature of natural gas;
- $V_n$  is the volume of the node  $n$ ;
- $\dot{m}_n^{(\vartheta)}(k)$  [kg/s] is the mass variation at node  $n$  at time step  $k$  and the iteration of the integration procedure  $\vartheta$ ;
- $\dot{m}_{inj,n}(k)$  [kg/s] and  $\dot{m}_{wit,n}(k)$  [kg/s] are the gas injection and withdrawal at node  $n$ , respectively, at time step  $k$ ;
- $M_n$  [-] is the number of nodes adjacent to node  $n$ .

The node's volume is assumed to be equal to half the sum of the volumes of all the pipes connected to the node:

$$V_n = \frac{\sum_{n=1}^{M_n} \left( \frac{D_{n-m}}{1000 \cdot 2} \right)^2 \cdot \pi \cdot L_{n-m}}{2} \quad (2.21)$$

By combining Eqs. (2.18), (2.19) and (2.20)), it is possible to define the evolution of the pressure of each network's node  $n$  as a function of the gas inputs and withdrawals of that specific node  $n$  and the pressure values of the adjacent nodes:

$$p_n^{(\vartheta)}(k) = p_n^{(\vartheta-1)}(k) + d\vartheta \cdot \frac{R_{NG} \cdot T}{V_n} \cdot \left\{ \begin{aligned} &\dot{m}_{inj,n}(k) - \dot{m}_{wit,n}(k) \\ &+ \sum_{i=1}^{M_n} \left[ \left| \frac{p_m^{(\vartheta-1)^2}(k) - p_n^{(\vartheta-1)^2}(k)}{25.24 \cdot L_{n-m} \cdot D_{n-m}^{-4.82}} \right|^{\frac{1}{1.82}} \cdot \frac{\rho_{NG}}{3600} \cdot \text{sgn}(p_n^{(\vartheta-1)}(k) - p_m^{(\vartheta-1)}(k)) \right] \end{aligned} \right\} \quad (2.22)$$

As a boundary condition, the model assumes that the pressure at the city-gate (node 0) is constant. Gas can flow through the city-gate from the high-pressure network to the medium-pressure network, but not vice versa. If the pressure at node 1 is lower than the city-gate's pressure, natural gas flows from the city-gate (coming from the transmission network) to node 1. If the pressure at node 1 is higher than that at the city-gate pressure, the gas flow between node 1 and the city-gate is 0:

$$HP_{NG}^{(\vartheta)}(k) = \dot{m}_{0-1}^{(\vartheta)}(k) = \begin{cases} \left( \frac{p_0^{(\vartheta-1)}(k)^2 - p_1^{(\vartheta-1)}(k)^2}{25.24 \cdot L_{0-1} \cdot D_{0-1}^{-4.82}} \right)^{\frac{1}{1.82}} \cdot \rho_{NG}, & \text{if } p_0^{(\vartheta-1)}(k) - p_1^{(\vartheta-1)}(k) > 0 \\ 0, & \text{otherwise} \end{cases} \quad (2.23)$$

where  $HP_{NG}^{(\vartheta)}(k)$  [kg/s] is the NG withdrawn from the high-pressure transmission network during time step  $k$  at the iteration of the integration procedure  $\vartheta$ .

At each time step, the gas network model calculates the maximum amount of SNG that can be stored in the network. The total amount of SNG that the network can accept is equal to the of gas withdrawals plus the amount of gas that can be accumulated as a result of the linepack effect: i.e., the quantity of gas which, if injected, would bring the network's pressure to exceed the maximum pressure allowed. The total amount of SNG that can be injected at generic time step  $k$  is defined as:

$$E_{SNG}^{max}(k) = \left[ \left( \sum_{n=1}^N \dot{m}_{wit,n}(k) \right) + \frac{(p_{max} - \bar{p}(k)) \cdot 10^5 \cdot V_{GN}}{R_{NG} \cdot T \cdot \tau} \right] \cdot LHV_{SNG} \quad (2.24)$$

where:

- $E_{SNG}^{max}(k)$  [MW<sub>th</sub>] is maximum amount of SNG that the network can host at time step  $k$ ;
- $N$  is the number of nodes of the network;
- $p_{max}$  [bar] is the maximum allowed pressure in the network;
- $\bar{p}(k)$  [bar] is the mean pressure in the network at time step  $k$ ;
- $V_{GN}$  [m<sup>3</sup>] is the total volume of the gas network;
- $\tau$  [h] is the time step duration;
- $LHV_{SNG}$  [MWh<sub>th</sub>/kg] is the lower heating value of the SNG, assumed to be equal to 0.0139 MWh<sub>th</sub>/kg;

As an example, the gas flows of a 69-node network with three P2G plants connected to three network nodes have been reported. Figure 2-3 and Figure 2-4

show the gas flows on each pipe of the network in two different working conditions. Figure 2-3 shows the flows in a typical winter operating condition: the P2G plants supply only a limited part of the total gas demand. Most of the gas consumed is withdrawn from the high-pressure network through the city-gate.

Figure 2-4 shows a summer case with low gas demand. Here, all the gas demand of the network is satisfied by the P2G plant injections (in this case there is no gas withdrawal from the high-pressure network).

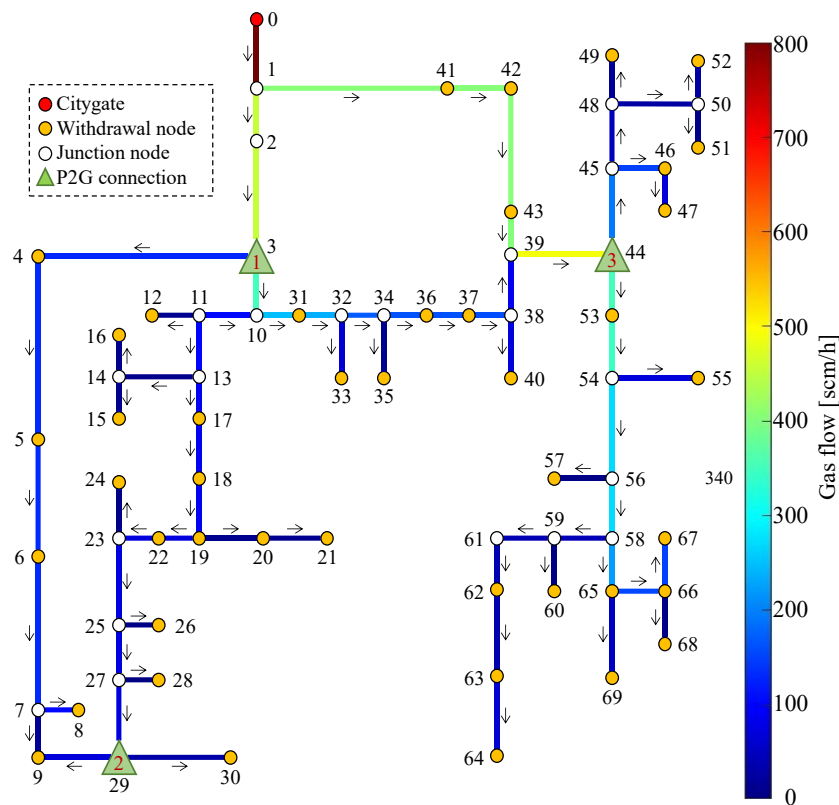


Figure 2-3. Gas flows within the gas distribution network: winter case. The network's gas demand is mainly met through withdrawals from the high-pressure network.

It can be noted that in the two different cases, the flows inside some pipes have opposite directions. For instance, in the flows from node 11 to node 29 of the winter case (a), the gas withdrawn from the high-pressure network goes down to the lower part of the network. Conversely, in the summer case (b), the gas produced by the P2G 2 plant rises in the opposite direction to meet the gas demand of the upper part of the network. In the summer case, the accumulation of gas within the network can be observed. For instance, in node 7 (which is a junction node) the mass balance of the input and output flows is higher than 0, due to gas accumulation in this part of the network.

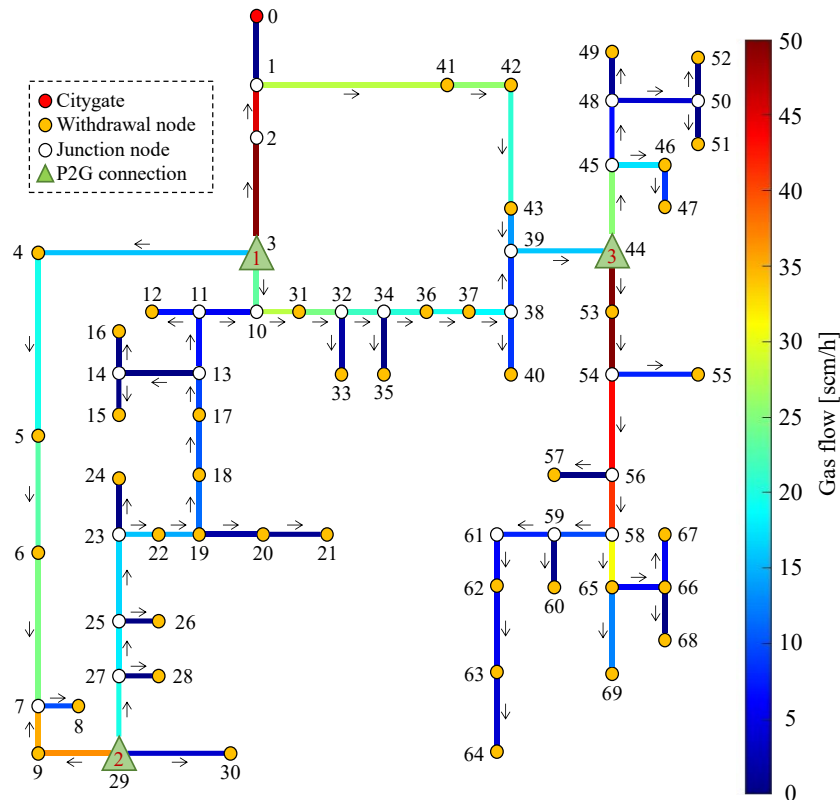


Figure 2-4. Gas flows within the gas distribution network: summer case. The network's gas demand is mainly met through the SNG produced by the P2G plant. Note that for the sake of clarity, a different scale was used than in Figure 2-3.

In order to validate the model, results were compared with those obtained with the steady state and multi-component thermal-fluid-dynamic model presented by Cavana and Leone [98]. Their model is non-isothermal and considers NG as a gaseous hydrocarbon mixture. The comparison was made on a 78 node 4th species network, according to the Italian DM 24/ 11/1984 classification [99]. The relative error on the node's pressure always resulted lower than 2% at each time step (see Figure 2-5).

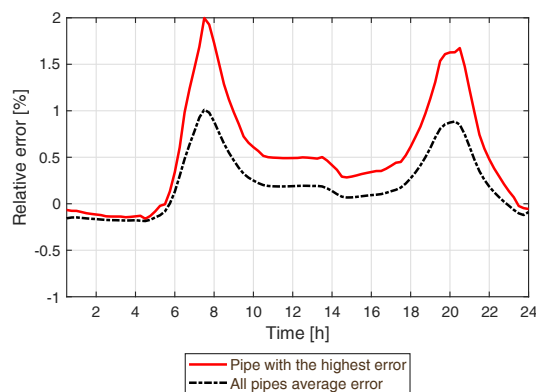


Figure 2-5. Relative error of the pressure in the network pipes. The red curve shows the deviation of the pipe with worst performance. The dashed black curve shows the average error of all pipes. Both lines pertain to the day that yielded the highest deviations.

### 2.2.4 Gas network simplified model

The gas network simplified model was realized within the work of this thesis. This model was used for the simulation of case study case study 2 (see Chapter 4).

The model calculates the steady state energy balance of the medium-pressure distribution network without taking into account either the evolution of the pressure in the network nodes or the gas flow in each network pipe. All the users' gas withdrawals and SNG injections are considered to happen at the same point. If the gas demand is higher than the SNG injection, the difference is taken from the HP network:

$$HP_{NG}(k) = \begin{cases} \sum_{n=1}^N \dot{m}_{wit,n}(k) - \dot{m}_{inj,n}(k), & \text{if } \sum_{m=1}^N \dot{m}_{wit,n}(k) - \dot{m}_{inj,n}(k) > 0 \\ 0, & \text{otherwise} \end{cases} \quad (2.25)$$

The model cannot take into account the linepack effect. Consequently, the maximum SNG that can be injected at time step  $k$  ( $E_{SNG}^{max}(k)$  [MW<sub>th</sub>]) is equal to the network's gas demand:

$$E_{SNG}^{max}(k) = \sum_{m=1}^M \dot{m}_{wit,m}(k) \cdot LHV_{SNG} \quad (2.26)$$

### 2.2.5 District heating network and centralized Power-to-Heat model

The District Heating (DH) network and centralized Power-to-Heat (CP2H) model was realized by Vittorio Verda and Elisa Guelpa from Politecnico di Torino (Turin, Italy). This model was used for the simulation of case study 3 (see Chapter 5).

This module simulates two different physical units (e.g., the DH network and the CP2H plants). The model's developers preferred to integrate the two components into a single module. Such a methodological choice, one the hand, makes the modeling of the system easier and allows the interactions between these two components to be simulated in more detail. On the other hand, it makes the structure of the co-simulation tool less flexible. With this approach it is not possible to integrate a different CP2H model with the current DH model, nor, vice versa, integrate a new DH model with the current CP2H model.

A physical model of the network was used to evaluate the temperature within the DH pipelines in order to accurately estimate the impact of CP2H on DH. This allowed the contribution of the thermal losses and thermal transients to be taken into account. The model includes mass and energy conservation equations for each



junction and each pipe of the network, respectively. These equations were validated in [100]. The model is one-dimensional for each pipe, since the heat propagation follows the main direction of the water flow. A graph approach was used to describe the connection between pipes and junctions. According to this approach, they were considered as branches and nodes. Such an approach is commonly adopted for the description of the topology of a DH network. Specifically, the connection between nodes and branches is described using the incidence matrix ( $\mathbf{A}$ ), which has the same number of rows as the number of nodes ( $N$ ), and the same number of columns as the number of branches ( $B$ ). A general element,  $A_{ij}$ , is equal to 1, or -1, depending on whether the node represents the inlet or outlet of the branch, and 0 if the node is not connected to the branch. This approach allows matrix equations to be written for the entire network. In generic step of the integration procedure  $\vartheta$  in a generic simulation time step  $k$ , the mass conservation equations written for the nodes and for the entire network are defined as:

$$\sum_{m=1}^{M_n} G_{n-m}^{(\vartheta)}(k) = 0 \quad (2.27)$$

$$\mathbf{A} \cdot \mathbf{G}_{B,k}^{(\vartheta)} + \mathbf{G}_{\text{ext}N,k}^{(\vartheta)} = 0 \quad (2.28)$$

Where:

- $M_n$  [-] is the number of nodes adjacent to node  $n$ ;
- $G_{n-m}^{(\vartheta)}(k)$  [kg/s] is the mass flow in the branch  $n - m$  which connect node  $n$  and the adjacent node  $m$ ;
- $\mathbf{G}_{B,k}^{(\vartheta)}$  [kg/s] represents the matrix of the mass flows in the branches;
- $\mathbf{G}_{\text{ext}N,k}^{(\vartheta)}$  [kg/s] is the matrix containing the mass flow exchanged between the nodes of the network and the external environment.

The energy conservation in a generic node  $n$  is the fined by Eq 2.29.

$$\rho \cdot c_p \cdot \frac{\partial T_n^{(\vartheta)}(k)}{\partial t} \cdot V_n + \sum_{m=1}^{M_n} c_p \cdot G_{n-m}^{(\vartheta)}(k) \cdot T_{n-m}^{(\vartheta)}(k) = U_{\text{tot}} \cdot (T_n^{(\vartheta)}(k) - T_{gr}) \quad (2.29)$$

where:

- $\rho$  [kg/m<sup>3</sup>] is the water's density;
- $c_p$  [kJ/kg/K] is the water's specific heat;
- $\frac{\partial T_n^{(\vartheta)}(k)}{\partial t}$  [K/s] indicates the derivative of water's temperature at node  $n$ ;
- $V_n$  is the volume of the node  $n$ ;
- $T_{n-m}^{(\vartheta)}(k)$  [k] is the water temperature in the branch  $n - m$ ;

- $U_{tot}$  [kW/K] global heat exchange coefficient between the water in the network pipe and the ground;
- $T_{gr}$  [K] is the ground's temperature.

Adopting an Upwind scheme this can be written in matrix form for all nodes:

$$\mathbf{M}_N \cdot \dot{\mathbf{T}}_{N,k}^{(\vartheta)} + \mathbf{K}_N \cdot \mathbf{T}_{N,k}^{(\vartheta)} = \mathbf{g}_N \quad (2.30)$$

Where:

- $\mathbf{M}_N$  [kJ/K] represents the nodal mass matrix, which includes the terms multiplied for the temperature derivative.
- $\dot{\mathbf{T}}_{N,k}^{(\vartheta)}$  [K/s] is the vector containing the time derivative of the temperature of the nodes;
- $\mathbf{K}_N$  [kW/K] represents the stiffness matrix of the network nodes, which includes the terms multiplied for the temperature,
- $\mathbf{T}_{N,k}^{(\vartheta)}$  [K] indicates the vector containing the temperatures of the nodes;
- $\mathbf{g}_N$  [kW] is the vector containing known terms in the energy equation.

The model incorporates a Thermal Energy Storage (TES) model. The TES is connected to the supply network. In particular, the TES is used to provide heat during the morning peak demand. During the night, the mass flow circulating in the system is low due to the limited heat demand of the district heating users; in some parts of the network (especially in some distribution networks), the water does not circulate. For this reason, the temperature in the network (and in the buildings and heating devices) decreases due to heat losses. In the morning, when users request heat from the network, in addition to providing heat to the users, the central system must also provide the heat needed to bring the grid temperature back to operating temperature. This results in a peak in district heating demand between 5:00 and 7:00. By using the heat storage, the peak demand of the central plant can be reduced.

Further details on the DH model are provided in [100].

The CP2H configuration is used to increase the return temperature up to the supply value. The efficiency of CP2H is closely related to the temperature of both the heated water and the source side. The CP2H energy conversion process is operated by large-scale geothermal HP plants, which exploit the higher temperature of the groundwater to achieve a higher performance.

The heat produced by the CP2H ( $\Phi_{CP2H}$ ) depends on the COP, which in turn depends on the temperature of the water entering the CP2H plant,  $T_{CP2H,in}$ , of the temperature of the water exiting the plant,  $T_{CP2H,out}$ , and of the temperature of the source adopted at the evaporator side,  $T_{CP2H,ev}$ .

$$\Phi_{CP2H}(k) = f(COP_{CP2H}(k)) = f(T_{CP2H,in}(k), T_{CP2H,out}(k), T_{CP2H,ev}) \quad (2.31)$$

In the specific considered case,  $T_{CP2H,in}$  corresponds to the return temperature of the DH and  $T_{CP2H,ev}$  is the temperature of the groundwater, which can be considered equal to 15°C.

In order to take the characteristics of the device into account, as well as the operating conditions, the COP was estimated adopting the performance of the device in the design condition (taken from the catalogue) and using the Carnot coefficient to simulate performance under real operating conditions.

$$COP_{CP2H}(k) = \epsilon * \frac{T_{CP2H,av}(k)}{T_{CP2H,av}(k) - T_{CP2H,ev}} \quad (2.32)$$

Where:

- $T_{CP2H,av}(k)$  [K] is the logarithmic mean temperature of the water processed in the CP2H plant;
- $\epsilon$  is the ration among the performance of the CP2H plant under the design conditions ( $r$ ) and the Carnot COP under the same conditions ( $COP_{CarnotD}$ ).

$$\epsilon = \frac{EER_D}{COP_{CarnotD}} \quad (2.33)$$

Because of the implicit relationship between the temperature at the exit of the HP,  $T_{CP2H,out}$ , and the exchanged heat flux,  $\Phi_{CP2H}$  (see Eq. 2.31 and Eq. 2.34), an iterative approach was used with the aim of evaluating  $T_{CP2H,out}$  and  $\Phi_{CP2H}$ , given  $T_{CP2H,in}$ ,  $T_{CP2H,ev}$ ,  $r$ ,  $c_p$  and the water flow the flow of water passing through the heat pump  $G_{P2H}$ .

$$T_{CP2H,out}(k) = T_{CP2H,in}(k) + \frac{\Phi_{CP2H}(k)}{G_{CP2H}(k) \cdot c_p} \quad (2.34)$$

The outlet temperature of the CP2H systems is not sufficient to power the DH. For this reason, the production of these plants must always be supported by the high temperature heat generated by the central terminal plant. In this model the CP2H systems are used to supply as much heat as possible to the DH users. During the night, the heat generated by the CP2H is also used to charge the thermal storages. The heat injected into the storages is regulated to charge the storages in a linear manner during the accumulation period. During the day, the CP2H system is turned off to allow the storage to discharge the accumulated heat until the thermal storage is completely empty. The baseload of the  $i$ -th CP2H is defined at each simulation step ( $k$ ) according to the flow diagram shown in Figure 2-6.

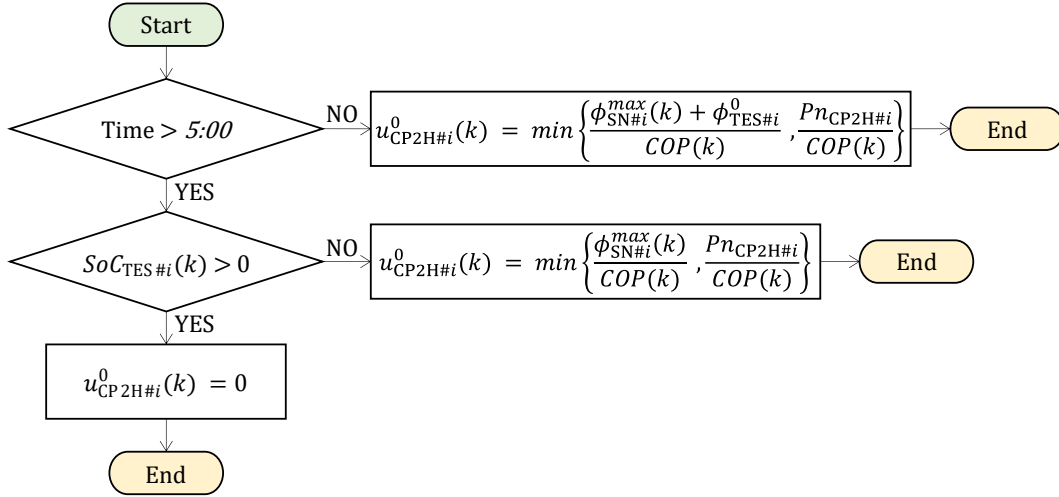


Figure 2-6. CP2H baseload definition.

Where:

- $\Phi_{SN\#i}^{max}(k)$  [MWh<sub>th</sub>] is the maximum heat power that the  $i$ -th CP2H plant can inject into the  $i$ -th SN at step  $k$ ;
- $\Phi_{TES\#i}^0(k)$  [MWh<sub>th</sub>] is the heat that the  $i$ -th CP2H must provide to the  $i$ -th TES to store heat during the charging period and linearly reach the maximum charge at the end of the accumulation period;
- $Pn_{CP2H\#i}$  [MWh<sub>th</sub>] is the nominal heat power of the  $i$ -th CP2H plant;
- $SoC_{TES\#i}(k)$  [-] is the State of Charge (SoC) of the  $i$ -th TES at step  $k$ .

Downward flexibility is defined as the maximum allowable downward deviation from the baseload. Since we consider a time interval of 15 minutes, the electricity consumption of the CP2H systems can always be brought to 0. Therefore, the downward flexibility is always equal to the baseload:

$$\pi_{CP2H\#i}^- = u_{CP2H\#i}^0(k) \quad (2.35)$$

Upward flexibility is defined as the difference between the electrical load of the plant when it works to deliver the maximum amount of heat that can be stored in the DH sector (considering the accumulation in storage) and the baseload:

$$\pi_{CP2H\#i}^+ = \min \left\{ \frac{\Phi_{SN\#i}^{max}(k) + \Phi_{TES\#i}^{max}(k)}{COP(k)}, \frac{Pn_{CP2H\#i}}{COP(k)} \right\} - u_{CP2H\#i}^0(k) \quad (2.36)$$

where  $\Phi_{TES\#i}^{max}(k)$  [MWh<sub>th</sub>] is the maximum heat power that the  $i$ -th CP2H can inject into the  $i$ -th thermal storage system.

## 2.2.6 Power-to-Gas detailed model

The Power-to-Gas detailed model was realized in collaboration with Robert Weiss and Teemu Sihvonen from the VTT Technical Research Centre of Finland (Espoo, Finland). This model was used for the simulation of case studies 1 and 2 (see Chapter 3 and Chapter 4, respectively).

The PEM electrolyzer model is based on a non-linear experimental-based operating curve [101], which is the hydrogen output in relation to the electrical power input. The model combines power-to-hydrogen conversion efficiency in the stack, the transformer and rectifier efficiencies, as well as the balance-of-plant power consumption [102].

$$\dot{E}_{\text{H}_2}(k) = -\frac{0.24}{Pn_{\text{PEM}}} \cdot Pn_{\text{PEM}}(k)^2 + u_{\text{PEM}}(k) - 0.055 \cdot Pn_{\text{PEM}} \quad (2.37)$$

Where:

- $\dot{E}_{\text{H}_2}(k)$  [ $\text{MW}_{\text{th}}$ ] is the hydrogen output power (defined considering its highest heating value, that is,  $12.75 \text{ MJ/Nm}^3$ ) at time step  $k$ ;
- $Pn_{\text{PEM}}$  [ $\text{MW}_e$ ] is the electric nominal capacity of the PEM electrolyzer;
- $u_{\text{PEM}}(k)$  [ $\text{MW}_e$ ] is the electric input of the PEM electrolyzer at time step  $k$ .

The produced hydrogen is accumulated inside the buffer. If the buffer reaches the maximum operating pressure (30 bar), the accumulation of hydrogen should be stopped. The minimum pressure of the storage is 7.2 bar. The pressure of the hydrogen buffer is calculated as a function of the mass of hydrogen accumulated in the buffer, according to the equation of ideal gases. The state of charge of the storage is defined as a function of the pressure attested in the storage unit and the maximum and minimum pressure limits:

$$SoC_{\text{buffer}}(k) = \frac{p_{\text{buffer}}(k) - p_{\text{buffer}}^{\min}}{p_{\text{buffer}}^{\max} - p_{\text{buffer}}^{\min}} \quad (2.38)$$

where:

- $SoC_{\text{buffer}}(k)$  [-] is the state of charge of the hydrogen buffer at time step  $k$ ;
- $p_{\text{buffer}}(k)$  [bar] is the pressure of the hydrogen buffer at time step  $k$ ;
- $p_{\text{buffer}}^{\min}$  [bar] is the minimum pressure of the hydrogen buffer;
- $p_{\text{buffer}}^{\max}$  [bar] is the minimum and the maximum pressure of the hydrogen buffer.

The methanation reactor model considered in this study simulates the operation of a catalytic methanation unit. The methanation unit model is a surrogate model

that was derived from the simulation data extracted from a high-fidelity model [103], [104] based on Apros® dynamic process simulator [105]. The surrogate model was fitted using a lasso regression analysis method, performed using the Alamo (Automatic Learning of Algebraic MOdels) tool [106]. Using data from the Apros® dynamic model, Almo found a linear relation between the hydrogen input power and the SNG power output ( $SNG_{th}$ ):

$$\dot{E}_{SNG}(k) = a_1 \cdot \dot{E}_{H_2}(k) - a_0 \quad (2.39)$$

where:

- $\dot{E}_{SNG}(k)$  [MW<sub>th</sub>] is the Synthetic Natural Gas output power at time step  $k$ ;
- $a_1$  and  $a_0$  [-] are the coefficients of the surrogate model, which depend on the size of the methanation reactor.

Further details on the P2G detailed model can be found in [107].

In this thesis, the P2G units are only used to absorb the over-generation from RES. Therefore, under normal conditions, the P2G unit remains in standby; the baseload of the system ( $u_{P2G}^0$ ) corresponds to the consumption of the auxiliary systems ( $u_{aux}$ ) necessary to keep the system in standby:

$$u_{P2G}^0(k) = u_{aux} \quad (2.40)$$

For this unit, the baseload corresponds to the minimum electrical consumption of the system. The system is not able to operate with a lower electrical consumption, the downward flexibility is therefore always equal to 0:

$$\pi_{P2G}^-(k) = 0 \quad (2.41)$$

The model simulated the interaction among the three main components of the P2G plant: the Polymer Electrolyte Membrane (PEM) electrolyzer, the hydrogen buffer and the methanation reactor. The hydrogen buffer allows a decoupling to be made between the electrolyzer and the methanation unit. The produced hydrogen is accumulated in the buffer, so that the electrolyzer can work, even though, at that moment, the methanation unit does not use the produced hydrogen. Similarly, the methanation unit can operate independently by using the hydrogen previously produced by the electrolyzer that is stored in the buffer.

For this reason, the upward flexibility of the system depends solely on the technical characteristics of the electrolyzer and the state of charge of the hydrogen accumulator:

$$\pi_{P2G}^+(k) = f(Pn_{PEM}, SoC_{buffer}(k)) \quad (2.42)$$

Where  $Pn_{PEM}$  [MW<sub>e</sub>] is the nominal capacity of the electrolyzer.

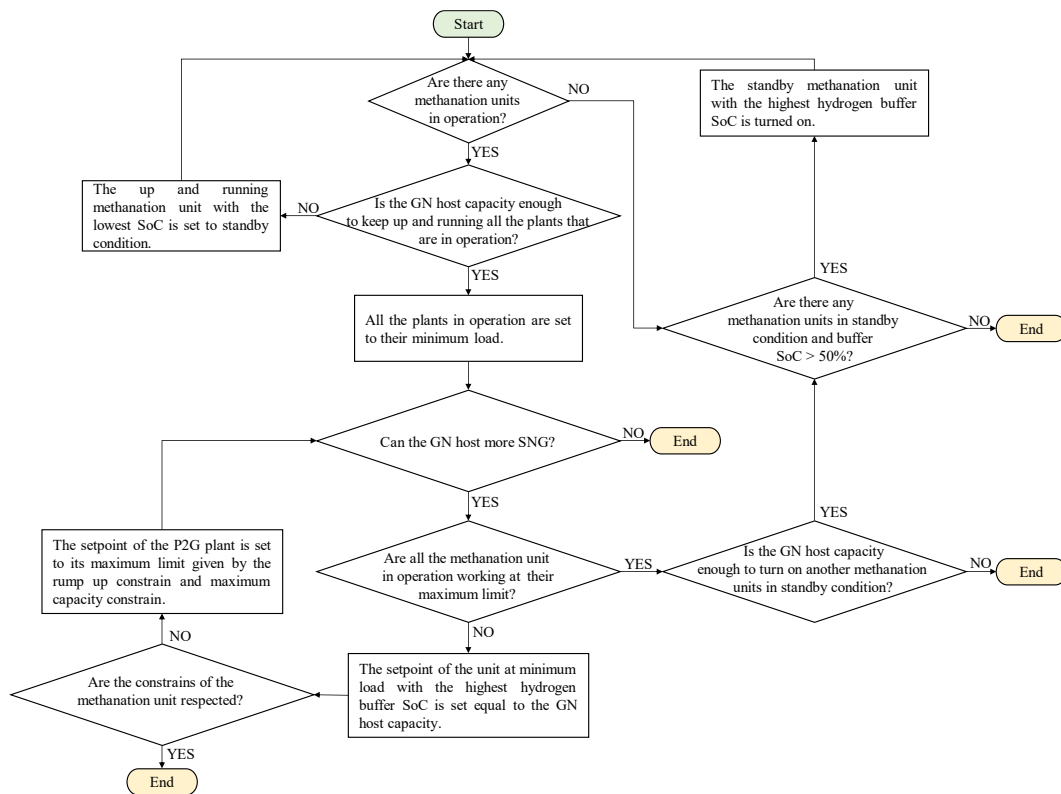


Figure 2-7. Control algorithm of the methanation units.

The use of the methanation unit is regulated by an internal controller as a function of the state of charge of the hydrogen buffer and the availability of the gas network to receive SNG. The methanation unit is turned on when the hydrogen buffer reaches a predefined SoC (in the analyzed cases 0.5). If the gas network does not constrain the production of SNG, the methanation unit produces SNG until the buffer is emptied. The model also considers the maximum upward and downward ramp rate constraints and the minimum load of the unit (50% of its nominal capacity).

If more than one P2G is connected to the same gas network, the maximum quantity of SNG that can be injected into the network is divided among the various P2G systems. When such restrictions, the internal control algorithm favors the use of systems that are in up and running mode. Figure 2-7 shows the algorithm for controlling the methanation units for the general case of several plants connected to the same gas network.

## 2.2.7 Power-to-Gas simplified model

The Power-to-Gas simplified model was realized within the work of this thesis. This model was used for the simulation of case study 1 (see Chapter 3) and case study 2 (see Chapter 4).

The P2G simplified model does not consider the interaction between the main components of the plant. The model considers that the electricity consumed by the plant is directly converted into SNG with a fixed conversion efficiency:

$$\dot{E}_{SNG}(k) = \eta_{P2G} \cdot u_{P2G}(k) \quad (2.43)$$

where:

- $\dot{E}_{SNG}(k)$  [MW<sub>th</sub>] is the Synthetic Natural Gas production at time step  $k$ ;
- $\eta_{P2G}$  [-] is the efficiency of the entire energy conversion process;
- $u_{P2G}(k)$  [MW<sub>e</sub>] is the electricity consumption of the plant at time step  $k$  which also contains the consumption of the auxiliary components ( $u_{aux}$ ). The latter is assumed to be equal to 1% of the nominal electrical load of the plant.

For the sake of consistency,  $\eta_{P2G}$  was set equal to the average efficiencies over the full year, as simulated by the detailed model.

At each time step  $k$ , the model calculates the baseload and upward and downward flexibility of the P2G unit. In the case studies presented in this thesis, P2G technology is only used to absorb the over-generations of renewables. When this condition does not occur, the P2G system is kept in standby. The baseload of the system is therefore defined as the electricity consumption needed to keep the system in standby:

$$u_{P2G}^0(k) = u_{aux} \quad (2.44)$$

The upward flexibility is defined as the difference between the maximum power consumption of the system and the baseload. The maximum power consumption of the system is limited by both the nominal power of the system and the maximum quantity that can be injected in the gas network:

$$\pi_{P2G}^+(k) = \min \left\{ Pn_{P2G}, \frac{E_{SNG}^{max}}{\tau \cdot \eta_{P2G}} \right\} + u_{aux} - u_{P2G}^0(k) \quad (2.45)$$

Where:

- $Pn_{P2G}$  [MW<sub>e</sub>] is the nominal power of the plant;
- $SNG_{max}$  [MWh<sub>th</sub>] is the maximum SNG that can be injected in the energy sink at time step  $k$ . This parameter is calculated by the gas network model. If there is more than one P2G system connected to the gas network, the maximum amount of injectable SNG is equally divided among the various units;
- $\tau$  [h] is the time step duration.



Since the baseload corresponds to the working conditions with the minimum electricity consumption of the plant, the downward flexibility is always equal to 0:

$$\pi_{P2G}^-(k) = 0 \quad (2.46)$$

## 2.2.8 Building and localized Power-to-Heat model

The building and localized Power-to-Heat model was realized by Dimosthenis Tsagkrasoulis and Vasiliki Katsiki from Hypertech SA (Chalandri, Greece). This model was used for the simulation of case study 4 (see Chapter 6).

The building module utilizes a second-order thermal resistor-capacitor (3R2C) equivalent model (see Figure 2-8). It models the thermal resistance between all the sets of indoor, envelope and external temperatures, as well as the thermal capacitance of the indoor area and the building's envelope. The resulting state space model captures the dynamic thermal behavior of a building. LP2H and solar irradiance are considered as only heat sources.

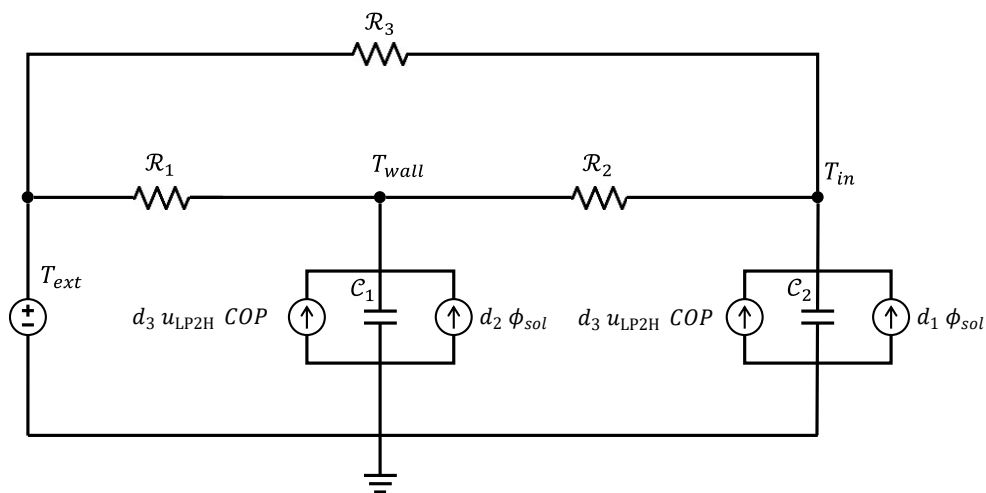


Figure 2-8. Building circuit-equivalent thermal resistor-capacitor (3R2C) model.

Where:

- $T_{in}$  [K] is the building's indoor temperature;
- $T_{wall}$  [K] is the temperature of the building's walls;
- $T_{ext}$  [K] is the external temperature;
- $\phi_{sol}$  [kW] represents the solar gains;
- $u_{LP2H}$  [kW] is the electricity consumption of the LP2H unit;
- $COP$  [-] is the coefficient of performance of the LP2H unit;
- $C_1$  [kJ/K] is the thermal capacitance of the walls' thermal node;
- $C_2$  [kJ/K] is the thermal capacitance of the indoor air's thermal node;

- $\mathcal{R}_1$ , [K/kW] is the thermal resistance between the external air node, the thermal node and the walls' thermal node;
- $\mathcal{R}_2$  [K/kW] is the thermal resistance between the walls' thermal node and the indoor air's thermal node;
- $\mathcal{R}_3$ , [K/kW] is the thermal resistance between the external air node thermal node and indoor air's thermal node;
- $d_1$  [-] is the fraction of solar heat that heats the indoor air thermal node;
- $d_2$  [-] is the fraction of solar heat that heats the walls' thermal node ( $d_1 + d_2 = 1$ );
- $d_3$  [-] is the fraction of LP2H heat that heats the indoor air thermal node;
- $d_4$  [-] is the fraction of LP2H heat that heats the walls thermal node ( $d_3 + d_4 = 1$ ).

The analytical equation of the 3R2C circuit is:

$$\begin{bmatrix} T_{in}(k) \\ T_{wall}(k) \end{bmatrix} = e^{A\tau} \begin{bmatrix} T_{in}(k-1) \\ T_{wall}(k-1) \end{bmatrix} + A^{-1}[e^{A\tau} - I] \cdot B \cdot \begin{bmatrix} T_{ext}(k-1) \\ \phi_{sol}(k-1) \\ u_{LP2H}(k-1) \end{bmatrix} \quad (2.47)$$

Where  $\tau$  [h] is the duration of the time step and the matrixes **A**, **B** and **I** are:

$$A = \begin{bmatrix} -\frac{1}{\mathcal{R}_2 \cdot C_2} - \frac{1}{\mathcal{R}_3 \cdot C_2} & \frac{1}{\mathcal{R}_2 \cdot C_2} \\ \frac{1}{\mathcal{R}_2 \cdot C_1} & -\frac{1}{\mathcal{R}_1 \cdot C_1} - \frac{1}{\mathcal{R}_2 \cdot C_1} \end{bmatrix} \quad (2.48)$$

$$B = \begin{bmatrix} \frac{1}{\mathcal{R}_2 \cdot C_2} & \frac{d_1}{C_2} & \frac{d_3 \cdot COP}{C_2} \\ \frac{1}{\mathcal{R}_1 \cdot C_1} & \frac{d_2}{C_1} & \frac{d_4 \cdot COP}{C_1} \end{bmatrix} \quad (2.49)$$

$$I = \begin{bmatrix} 1 & 0 \\ 0 & 1 \end{bmatrix} \quad (2.50)$$

Using a Maximum Likelihood identification process, the thermal parameters of the state space model ( $R_1, R_2, R_3, C_1, C_2, COP, d_1, d_2, d_3, d_4$ ) were estimated via monitored data regarding the environmental conditions, solar irradiance, indoor temperature and electricity consumption. To this end, real data were collected from residential dwellings in the St. Julien-Mont-Denis (France) municipality during a calibration phase.

The building's heating system consists of geothermal heat pumps (i.e., the LP2H device). These dwellings were equipped with a smart metering and environmental monitoring infrastructure, as well as a real-time communication system/gateway, which made data collection possible. Indoor temperature and LP2H electricity consumption data were available at a time granularity of one minute, while the external environmental conditions were recorded every hour and

interpolated to extract values every quarter of an hour. The time step for the discretization of the thermal model (and subsequently of the optimization method) was 15 minutes. The identification of the parameters of the thermal model was made by fitting the state space models to data recorded over periods of approximately two months. The prediction capabilities of the trained models were then evaluated by simulating the indoor temperature and the LP2H electricity consumption for the subsequent day (96 intervals). Results were then compared with the readings shown on the sensors. In order to perform the comparison, the true and predicted timeseries were aligned using the dynamic time warping algorithm. The error was then computed as the cumulative absolute difference between the values at all the time steps. The validation error in the experiments ranged between 15% and 20% for this 96-step (1 day) prediction evaluation process. When considering only a single step prediction (15 minutes), the errors were significantly lower, with an average error of approximately 5%.

The flexibility of the LP2H system was determined by the range of acceptable temperature conditions of the building. The electrical consumption of the LP2H device could be changed, as long as the internal temperature remained within the limits of thermal comfort. The limits of the acceptable conditions were selected on the basis of the recorded indoor temperature and heating consumption data from the pilot dwellings. Whenever an activation/deactivation of a heating device was observed (based on the consumption data), the internal temperature of the building was flagged at the time of the activation/deactivation as either a low or high temperature limit. The accumulation of these values for each dwelling provided an average low limit, an average high limit, and the associated standard deviations for both metrics. These values were used to estimate the thermal comfort limits. The mean limit value over the examined dwellings were considered as the setpoint of the baseline temperature. The low/upper limits were reduced/increased for the alternative conditions by one standard deviation of the respective metric. Assuming a gaussian distribution of the values (as suggested by the recorded data), a temperature that is one standard deviation below the low limit or one standard deviation above the high limit was considered to be acceptable approximately 70% of the times by the occupant. The building's baseline setpoint resulted to be 20.5°C and the maximum acceptable temperature deviation was found to be equal to  $\pm 2.5^\circ\text{C}$ .

The model incorporated a model predictive control optimization process to forecast the baseline, the minimum and the maximum electricity that could be absorbed by the LP2H units. These calculations were performed at each simulation time step  $k$ . The following measures/values were used as input into the optimization process:

- the baseline internal temperature setpoint ( $T^0$ );
- the minimum and maximum acceptable internal temperature ( $T^{min}$  and  $T^{max}$ , respectively);

- the external temperature and irradiance ( $T_{ext}$  and  $\phi_{sol}$ , respectively);
- the internal temperature at the previous time step ( $T_{in}$ ).

Three distinct optimizations were performed: one using the baseline temperature setpoint, and two others using the minimum and maximum temperature limits. The combined output consists of three electricity power consumption values: the LP2H baseline ( $u_{LP2H}^0$ ) value, the LP2H minimum load ( $u_{LP2H}^-$ ) and the LP2H maximum consumption ( $u_{LP2H}^+$ ).

$$u_{LP2H}^0(k) = f(T^0, T_{ext}(k), \phi_{sol}(k), T_{in}(k-1)) \quad (2.51)$$

$$u_{LP2H}^-(k) = f(T^{max}, T_{ext}(k), \phi_{sol}(k), T_{in}(k-1)) \quad (2.52)$$

$$u_{LP2H}^+(k) = f(T^{min}, T_{ext}(k), \phi_{sol}(k), T_{in}(k-1)) \quad (2.53)$$

The difference between the baseline and the maximum possible consumption was the upward flexibility available for the next step.

$$\pi_{LP2H}^+(k) = u_{LP2H}^+(k) - u_{LP2H}^0(k) \quad (2.54)$$

The difference between the baseline and the minimum possible consumption was the baseline downward flexibility for the next step.

$$\pi_{LP2H}^-(k) = u_{LP2H}^0(k) - u_{LP2H}^-(k) \quad (2.55)$$

The exact mathematical details of the process can be found in [108].

## 2.2.9 Electric Battery model

The Lithium-ion Electric Battery (EB) model was realized within the work of this thesis. This model was used for the simulation of case study case study 4 (see Chapter 6).

The electric battery is modeled as an energy accumulator whose state of charge varies according to the energy it absorbs or releases.

$$SoC_{EB}(k) = SoC_{EB}(k-1) \cdot (1 - \lambda_{EB}) + \frac{u_{EB}(k) \cdot \tau \cdot \eta_{EB,ch}}{Cap_{EB}} - \frac{g_{EB}(k) \cdot \tau \cdot \eta_{EB,dc}}{Cap_{EB}} \quad (2.56)$$

Where:

- $SoC_{EB}(k)$  [-] is the state of charge of the electric battery at time step  $k$ ;
- $\lambda_{EB}$  [-] is the self-discharge rate of the battery (0.05/month [109]);
- $u_{EB}(k)$  [ $kW_e$ ] is the battery's electricity absorption at time step  $k$ ;
- $g_{EB}(k)$  [ $kW_e$ ] is the battery's electricity generation at time step  $k$ ;

- $\tau$  [h] is the time step's duration;
- $\eta_{EB,ch}$  [-] is the storage charging efficiency of the battery ( $\eta_{EB,ch} = 0.95$  [109]);
- $Cap_{EB}$  [kWh<sub>e</sub>] is the storage capacity of the battery;
- $\eta_{EB,ds}$  [-] is the storage discharging efficiency of the battery ( $\eta_{EB,ds} = 0.95$  [109]).

At each time step  $k$  of duration  $\tau$ , the model calculates the upward ( $\pi_{EB}^+(k)$ ) and downward ( $\pi_{EB}^-(k)$ ) flexibility, which are defined as the EB maximum input and output power, respectively:

$$\pi_{EB}^+(k) = \min\{u_{EB}^{max}, Cap_{EB} \cdot (SoC_{EB}^{max} - SoC_{EB}(k-1)) \cdot \tau\} \quad (2.57)$$

$$\pi_{EB}^-(k) = \max\{g_{EB}^{max}, Cap_{EB} \cdot (SoC_{EB}(k-1) - SoC_{EB}^{min}) \cdot \tau\} \quad (2.58)$$

Where:

- $u_{EB}^{max}$  [kW] is the maximum electricity power absorption of the electricity battery;
- $SoC_{EB}^{max}$  [-] is the maximum state of charge of the battery ( $SoC_{EB}^{max} = 1$  [109]);
- $g_{EB}^{max}$  [kW] is the maximum electricity power generation of the electricity battery;
- $SoC_{EB}^{min}$  [-] is the minimum state of charge of the battery ( $SoC_{EB}^{min} = 0.2$  [109]);

The parameter  $C\_rate$  defines the correlation between the maximum input and output power of the battery and the battery capacity:

$$\frac{u_{EB}^{max}}{Cap_{EB}} = \frac{g_{EB}^{max}}{Cap_{EB}} = C\_rate \quad (2.59)$$

The  $C\_rate$  is assumed to be equal to  $0.25 \text{ h}^{-1}$ .

The base working condition of the battery is when it does not generate or absorb electricity energy. The base load of this unit is therefore always equal to zero:

$$u_{EB}^0(k) = 0 \quad (2.60)$$

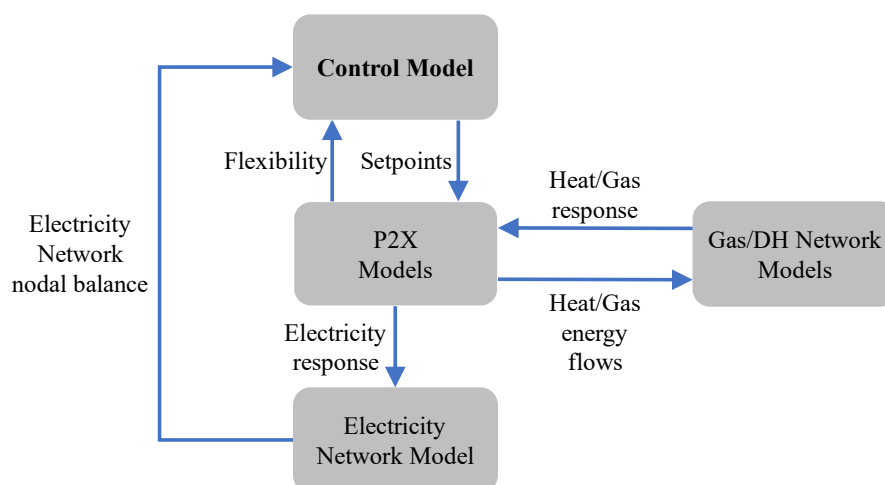
### 2.2.10 Controller

In a multi-energy system, the various energy sectors are linked through energy conversion technologies. This allows the flexibility of these sectors to be transferred within the electricity sector. The control logic used in this thesis for the simulation of multi-energy scenarios is represented in Figure 2-9.

The flexibility of energy conversion technologies is calculated by the corresponding model, according to the demand and energy flows of the non-electric energy sectors. For instance, the flexibility of the CP2H system connected to the DH is calculated according to the characteristics of the CP2H system itself and the heat flows that occur in the DH. How flexibility for energy conversion technologies is calculated is shown in 2.1. At time step  $k$ , the control module receives the flexibility of the energy conversion systems and the nodal production and consumption of the electricity network, defined by the electricity network model in the previous step ( $k - 1$ ). Based on this data, the controller defines the operating setpoints of the energy conversion technologies. In the case studies analyzed in this thesis, the control module exploits the flexibility of the flexible units to increase the match between RES production and electricity consumption. The energy conversion models receive the setpoints defined by the controller and the necessary data from the models of the non-electrical sectors for the simulation of the time step  $k$ .

The output of the conversion models contains the energy consumption / production (of electricity, heat, gas), which will be sent to the models of the corresponding energy network, and the new flexibility of the plants that will be used by the controller for defining the setpoints for step  $k + 1$ .

The energy network models receive the energy consumption and production values and, on the basis of these inputs, they simulate the energy flows of the various networks for the time step  $k$ . The electricity network model also outputs the electricity production and consumption value of the network for step  $k + 1$  that will be used by the controller in the following time step.



---

*Figure 2-9. Conceptual architecture of the information exchange during simulation.*

## **2.3 Multi-energy system co-simulation tool**

A co-simulation tool was created in order to integrate in a single simulation platform all the different models of the multi-energy system components.

### **2.3.1 The co-simulation**

Multi-energy systems with a high penetration of renewables are complex, dynamic systems whose working conditions are constantly influenced by multiple variables. In such systems, the electricity system interacts with the other energy sectors through energy conversion technologies. In the current research, simulation is used to investigate and test multi-energy systems. Due to the integration of different sectors, the simulation of multi-energy systems presents many challenges. Difficulties mainly arise from two aspects. Firstly, the different energy systems that are integrated into the multi-energy system have different dynamics. This makes it difficult to precisely simulate each component in a single simulator. Secondly, it is rare for a single research group to have sufficient specialist knowledge of all those aspects that a multi-energy system must consider (e.g., electricity network, gas network, district heating grid, energy production and conversion, storage systems, energy market, communication devices). In order to overcome such difficulties, researchers developed a particular simulation methodology, in which multiple simulators are interconnected and coordinated. Each simulator considers a particular aspect of the multi-energy system (e.g. the district heating sector) and communicates with the other simulators throughout the simulation process. This practice is referred to as co-simulation.

### **Advantages and disadvantages of the co-simulation approach**

In co-simulation, the general mathematical problem is decoupled into several distributed modules, so that each module performs the modeling of a single problem separately from the remaining modules. The different modules are equivalent to black boxes, which exchange input-output data with each other, without needing to know the internal modeling of the other modules.

A co-simulation approach presents the following advantages:

- it increases the flexibility and maintainability of the simulation tool, as each module can easily be modified or replaced in a plug and play fashion [110].
- The co-simulation architecture increases the scalability of the simulator, as new modules can be easily integrated [111].
- A co-simulation architecture can be realized using different program languages and different simulation system tools [112]. This allows the developers to choose the tool they deem most suitable.

- A simulation approach allows the integration of different models, ensuring a correct handling of the intellectual properties of each module[112]. This is because each module interacts with the others like a black box and can also be physically separate from the other modules.
- The communication signals exchanged during the co-simulation can easily be redirected to a real device, thus enabling hardware-in-the-loop simulations (as opposed to redirecting it to a software module, as done in the framework of this thesis). In the same way, the tool can also receive real-time data from the real world and send demand response control signals to the connected devices [113].
- In a future smart grid system, all the connected smart devices will communicate in a coordinated communication network. The co-simulation approach allows researchers to simulate the communication networks as if it were happening in a real smart grid system [114].

Nevertheless, there are some drawbacks that stem from using a co-simulation methodology:

- The simulation architecture is more complex. For instance, as reported in [115]), the main challenge in creating a co-simulation platform consists in connecting and managing the synchronization of the data exchanged between the different simulators of the platform.
- The different modules are not actually fully integrated, as they are not part of a single computational program. In fact, the different components of the system exchange certain information at a certain time step. Hence, if one user wanted to change the type of data that models exchange or the frequency of the data exchange, s/he would need to modify the co-simulation platform.
- Since in the co-simulation approach, the simulation is run on separate computers/machines, a user may not have multiple computers on which to run the different models. It would still be possible to run all the modules on a single simulator. However, this would mean that multiple computational programs should be opened at the same time (one for each module involved in the simulation), making the simulation computationally expensive.
- If a third-party model located on a remote computer were connected to the co-simulation platform, it would not be possible to change the internal simulation of modules produced by third parties without the support of the module's owners.

### **Literature review on co-simulation**

A case in point is represented by [116], which performed complex simulations by using a co-simulation model, in order to integrate different interdisciplinary domains. In [117], the co-simulation approach was chosen because its flexibility



and scalability to investigate the effect of different controllers on the same scenario, in order to analyze a multi-energy system at the urban scale. The methodology thus allowed the researchers to examine the complex dynamics of the different components and the different control strategies, in a heuristic and unified manner. The work presented in [118] developed a distributed co-simulation platform with multiple models to assess and evaluate generic services in smart networks. The proposed platform had a high flexibility of use, as it integrated different software simulation environments, real-time simulations (enabling actual hardware simulation in the loop), and different communication protocols. In [119], the co-simulation approach was used to study the interactions between the power system and the communication network. More specifically, the communication structure implemented in the co-simulation architecture allowed researchers to study the impact of different control strategies on the network in case of failures or cyber-attacks.

### **2.3.2 The communication between modules**

In the co-simulations architecture utilized in this thesis, the Message Queuing Telemetry Transport (MQTT) protocol was used, in order to enable communication between modules during the co-simulation process. An MQTT architecture is based on three different entities (see Figure 2-10):

- the client publisher, whose role is to send messages;
- the client subscriber, which receives the messages sent by the publisher;
- the broker that bridges all the messages sent from the client publishers to all the client subscribers.

An indefinite number of client publishers and client subscribers can coexist in the communication architecture. In general, a client can be both a publisher and a subscriber. In the latter case the client both sends and receives messages. In the co-simulation architecture analyzed in this thesis, all modules are both publishers and subscribers. The MQTT protocol organizes the messages exchanged through the use of topics. When a publishing client sends a message, it must define the topic to which its message belongs. The broker receives the message and publishes it inside the defined topic. If the topic already existed, the broker replaces the message that was saved inside the topic with the new one. If the topic is new, the broker creates a new topic and saves the message received. The client subscriber must subscribe to the topics about which it wants to receive messages. When a message is posted on a topic, the broker sends the message to all the clients that have subscribed to that topic. In this way, in order to communicate, each client only needs to know the specific topics about which it must send messages to the broker and the topics to which it must subscribe. It is not necessarily that a client know which clients sent the messages or which other clients received them.

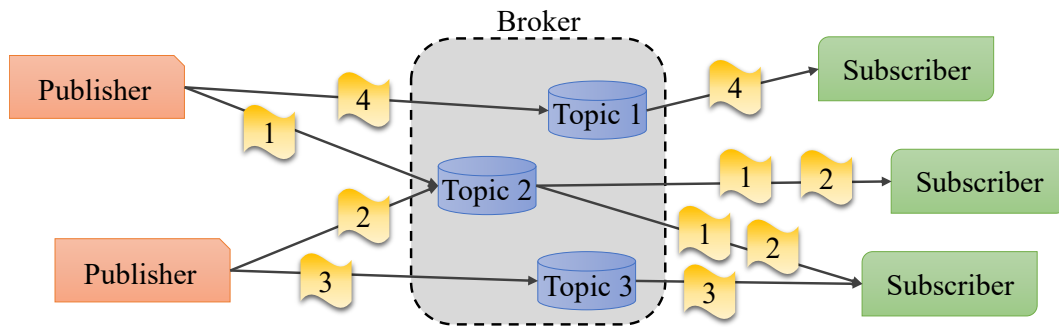


Figure 2-10. MQTT publish/subscribe messaging.

### 2.3.3 The modules of the multi-energy system co-simulation tool

In the co-simulation approach, the different components of the multi-energy system are grouped into separate modules placed in remote dedicated computers (see Figure 2-11). In addition to the physical components represented in Figure 2-1, Figure 2-11 also shows the control module and the time-synchronizer (Time-Sync) module. The functionality of the Time-Sync module will be described in Section 2.3.4.

The various modules contain the mathematical models that simulate the behavior of the physical components. The co-simulation process evolves with discretized time steps; at each time step, each module receives the input data and simulates the physical component for which it is responsible. When a component ends the simulation of the time step, it sends the output data externally and waits for the new input data for the simulation of the next step.

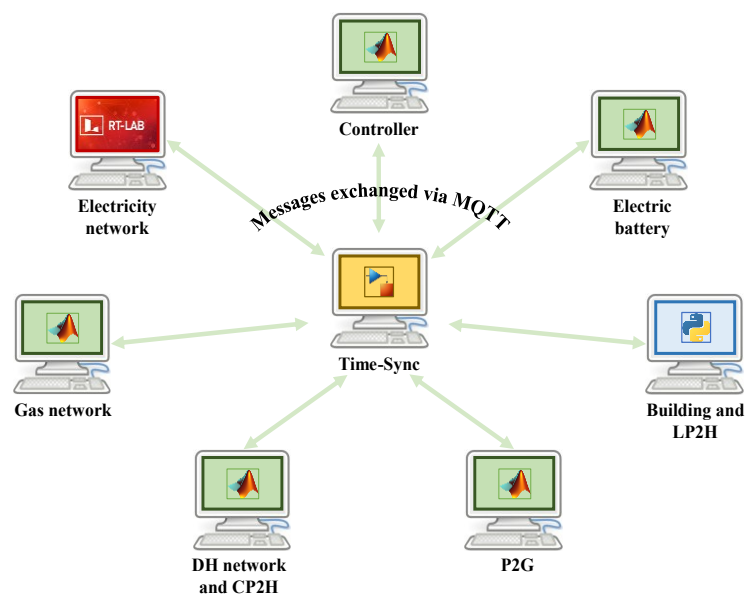


Figure 2-11. Modules of the multi-energy system co-simulation tool.

The different modules were used to simulate four case studies which will be presented in Chapter 3, Chapter 4, Chapter 5 and Chapter 6, respectively. The models involved for each case study are summarized in Table 2-2.

Table 2-2. Models involved in the simulation of the various case studies.

Model	Case study 1	Case study 2	Case study 3	Case study 4
Controller	X	X	X	X
Time-Sync	X	X	X	X
Electricity network (detailed)	X	X	X	
Electricity network (simplified)		X		X
Gas network (detailed)	X	X		
Gas network (simplified)		X		
DH network and CP2H			X	
P2G (detailed)	X	X		
P2G (simplified)		X		
Building and LP2H				X
Electric battery				X

### 2.3.4 The time-synchronizer module

The time-synchronizer (Time-Sync) module is the engine of the co-simulation process. This module does not simulate any physical component of the multi-energy system, nor does it manage operating logics concerning the energy system. The purpose of this module is to coordinate the co-simulation process between the various modules. The roles of this module are:

- To receive all the output data generated by the other modules at each simulation step.
- To send the input data necessary for the simulation to the various modules. The input data a specific module needs can come from any of the modules involved in the simulation. It is the task of Time-Sync to collect the necessary input data, prepare it in the right format and send it to the right modules. For instance, the module that simulates the electricity network receives as input the electricity consumption of all the plants that are connected to the electricity network. If in the analyzed scenario there are LP2H plants and an EB plant, the input message that reaches the electricity network module will be composed of data coming from the LP2H module and the EB module. In addition, if a module does not have an internal

memory (i.e., if it is unable to save data between the simulation of one step and the other), Time-Sync also acts as a data memory. To give a concrete example, let us consider a DH model with thermal storage. At a generic time-step  $k$ , the model outputs the state of charge of the storage (determined on the basis of the heat flows that occurred in the DH). At time step  $k + 1$ , the DH model receives as input this value of state of charge, which will be used as the starting state of charge value for the simulation of the heat flows of the DH of time step  $k + 1$ .

- To synchronize the simulation of all modules involved in the co-simulation. The Time-Sync guarantees that the different modules are activated in the correct order. The simulation of the various modules takes place sequentially: at each step the various modules are simulated one at a time. In theory, the simulation of modules A and B could be carried out in parallel if the two modules did not need to exchange information between them, directly or indirectly. Two modules exchange information directly, when module A receives messages from module B and/or vice versa. Two models exchange information indirectly when data “a”, generated by module A, goes to module C and is used to generate data c, which is then input for module B. However, this type of optimization has not been implemented in this thesis. With the right sequence, Time-Sync triggers the simulation of the various modules by sending them the input data.
- To save the simulation data. The Time-Sync receives all the output data of each module. The data is saved within the Time-Sync to analyze the scenario after the simulation.

The co-simulation architecture, coordinated by the Time-Sync module, depends on the type(s) and number of modules involved in the co-simulation. The co-simulation architecture set up for the simulation of each of the case studies analyzed will be presented in the next chapters.

## **Chapter 3**

# **Case-study 1 – Techno-economic analysis of Power-to-Gas plants in a gas and electricity distribution network system**

Chapter 3 analyzes how the Power-to-Gas technology could be used at the distribution network level (both gas and electricity) to optimize the use of Renewable Energy Sources. The Power-to-Gas technology makes a connection between electricity and gas energy sectors, thus creating new flexible synergies within the multi-energy system. Results pertaining to this research showed that the storage capacity of the medium pressure gas network was insufficient for seasonal gas storage. Nonetheless, the storage capacity of the gas network was sufficient to allow the intra-daily gas storage, allowing the Power-to-Gas plants to operate flexibly for the absorption of over-generations of Renewable Energy Sources. This solution was evaluated from an economic point of view through the calculation of the levelized cost of Synthetic Natural Gas for cost scenarios of the years 2030 and 2050. This cost-evaluation also considered different assumptions about the putative economic contributions obtainable through incentives aimed at encouraging the development of flexible systems. The results showed that levelized cost of Synthetic Natural Gas may vary from 47 to 395 €/MWh, depending on the different configurations. Hence, only in the best-case scenario is the cost of Synthetic Natural Gas comparable to that of natural gas.

## 3.1 Introduction

### 3.1.1 State of the art

The utilization of Power-to-Gas (P2G) plants connected to transmission networks has been widely studied. The potential of P2G was evaluated in [120] for a regional scenario in Germany. The size of the considered P2G plants was optimized in order to minimize the levelized cost of electricity. In [121] it was shown how an industrial P2G plant connected to the transmission grid could optimally operate simultaneously in both wholesale energy and ancillary service markets. A dimension optimization in [122] showed how a P2G plant could operate on energy and ancillary service markets, while absorbing contracted local wind and solar power to avoid reverse power flow. The research in [123] showed that, thanks to the use of distributed resources, including P2G, it was possible to reduce renewable energy curtailment and, at the same time, increase social welfare. In [124] it was shown how it would be possible to reach a cost-efficient fully (100%) decarbonized large city system for a by means of wind and solar power, insofar as either city level P2G solutions or multiple reinforcement of the transmission power grid were adopted. In [125], a gas transmission system was used to store the surplus generation of Renewable Energy Sources (RES). The role of the P2G technology in a near zero-carbon footprint European scenario for the year 2050 was analyzed in [53].

However, as was also concluded in [34],[126],[127], only a few studies have focused on the integration of P2G with the distribution system. The presence of just a few studies about the integration of P2G with the distribution system may partially be explained by the fact that this technology has only begun to be explored, which makes it difficult to design models of an entire P2G chain that would be suitable for its integration with network calculations. In [128], the authors investigated the possibility of absorbing the excess energy of RES in the distribution network for a region in Southern Germany using hundreds of small-scale P2G installations (300-700 kW electrolyzers). The voltage control of a power distribution network was analyzed in [129] using an On-Load Tap Changer and an alkaline Power-to-Hydrogen (P2H<sub>2</sub>). The same P2H<sub>2</sub> was also used in [130] to analyze the optimum size and allocation of a plant, in order to reduce the impact of an increasing RES installation on the distribution network. The coupling of electricity and gas distribution networks through P2H<sub>2</sub> technology was analyzed in [131] and [132]; these articles analyzed how the technology affected the quality of the gas in the distribution network. In [126], the installation of an electrolyzer in an electricity distribution network was evaluated for the absorption of the excess production of RES, in comparison to a network expansion solution. In [102] the interaction between the gas network and the local distribution networks for electricity and district heating were analyzed for a small town to show how to reach a 100% wind and solar power based urban electricity and heating system in cold climate regions,

enabled by the gas grid and P2G. In [133], a techno-economic analysis of a P2G plant was carried out considering different configurations. The optimal P2G capacity was defined, and P2G was also analyzed considering the integration of electrochemical storage, so that the continuous operation of the plant could be improved. In [127],[134], the authors focused on the utilization of P2G and Gas-to-Power (G2P) technologies for voltage regulation in the distribution network. A new algorithm for real time scheduling was presented. P2G plants connected to the distribution network were analyzed in [135] using a real time simulation platform. In the analyzed scenario, the P2G systems operated to absorb local RES over-generation. In [34], the authors analyzed the benefits of a P2G plant in a distribution network with high-RES penetration and presented a novel model of a P2G plant based on real data.

### **3.1.2 Scientific contribution**

In this study, the interaction between the electricity network, the gas network and the P2G components was analyzed by modeling the interactions of the different components of the multi-energy system. In order to create a critical case study, a scenario with a high RES generation and a highly seasonally -influenced gas demand was considered. The scenario was characterized by periods of high RES over-generation and low gas demand. In this context, P2G plants were used to absorb RES over-generation by absorbing surplus electricity from the distribution network and by injecting Synthetic Natural Gas (SNG) into the gas distribution network. It was analyzed how, in order to reach the optimal condition of the overall multi-energy system, the different P2G plants needed to be coordinated not only by just considering the power sector alone. To make the study more generalizable, a typical urban medium pressure gas network used in the Italian gas system was considered. Moreover, the analyzed electricity distribution network presented several Medium Voltage (MV) feeders connected to the High Voltage (HV) system through three HV/MV transformers. This allowed us to analyze the positive impact of P2G plants, both at the local level (i.e., by improving the operation of the distribution system) and at the point of common coupling between distribution system and transmission system. For this reason, the conclusions drawn in this study would arguably be suitable for distribution systems with more complex interface topologies. In the analyzed scenario, the only flexible resources installed were the P2G plants. Technologies such as electric batteries or gas storage could offer further flexibility to the system. However, they were not considered in this study, so that the impact of flexibility of P2G systems could be more clearly singled out. The scenario was also analyzed from an economic point of view by calculating the Levelized Cost of SNG ( $LC_{SNG}$ ) for each P2G plant.

## 3.2 Scenario description and techno-economic parameters

The analyzed multi-energy system includes both electricity and gas distribution networks, coupled through the utilization of P2G technologies (see Figure 3-1). The district gas and electricity scenario has been developed and simulated for one year with a time resolution of 15 minutes. The P2G plants are used to mitigate the energy unbalances caused by RES connected to the distribution electricity network. Thanks to an energy conversion process, P2G plants make it possible to exploit the flexibility and storage capacity of a gas network and transfer them to the electricity sector. The operation of P2G plants is a function of the electricity network's conditions, and in particular of the presence of RES over-generation, but also of the availability of the gas network to receive SNG without violating the operating pressure limits or the state of the plant itself. More details about the coordination logic are reported in Section 3.3.2.

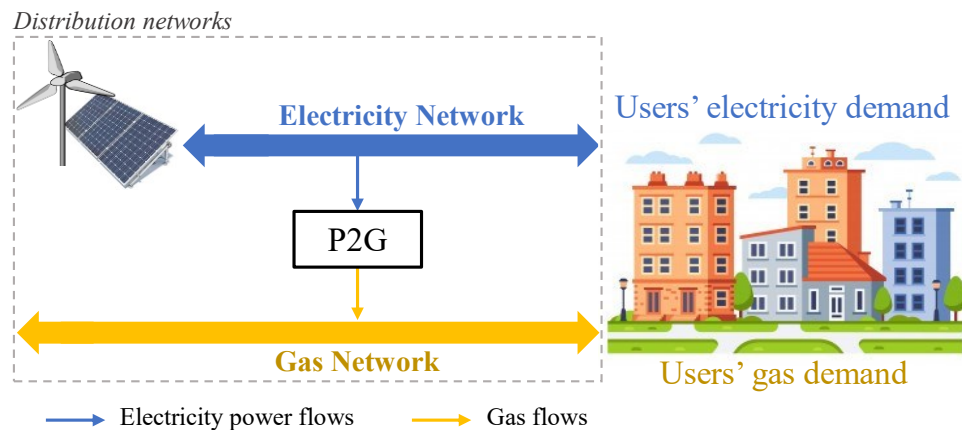


Figure 3-1. Schema of the analyzed multi-energy system.

### 3.2.1 Electricity system

The topology of a sample of the urban distribution system of a city in northern Italy has been used for the electricity network (EN). The network is composed of 43 nodes supplied by three HV/MV transformers (see Figure 3-2). As depicted in Figure 3-2, different RES plants, in particular photovoltaic (PV) and wind turbines (WTs), are spread over the network. The reader may refer back to Chapter 2 for a detailed description of the electricity network model.

The scenario considers the presence of RPF, which may affect both the transmission and the distribution systems. If an RPF exists in only one or two feeders, it is totally or partially redirected to the other ones through the busbar that connects all the feeders. In this case, the transmission system is not affected (or is only affected very slightly) by the consequences of the RPF. Hence the RPF



introduces local issues (for example, the coordination of protection systems) into the distribution system. Conversely, if an RPF exists in all the feeders, it is necessarily injected into the transmission system, thus causing dispatching issues at the transmission system level as well. In this analysis, flexibility assets are used to offer ancillary services to the distribution system and thus to balance the RPFs of each HV/MV transformer in the distribution system.

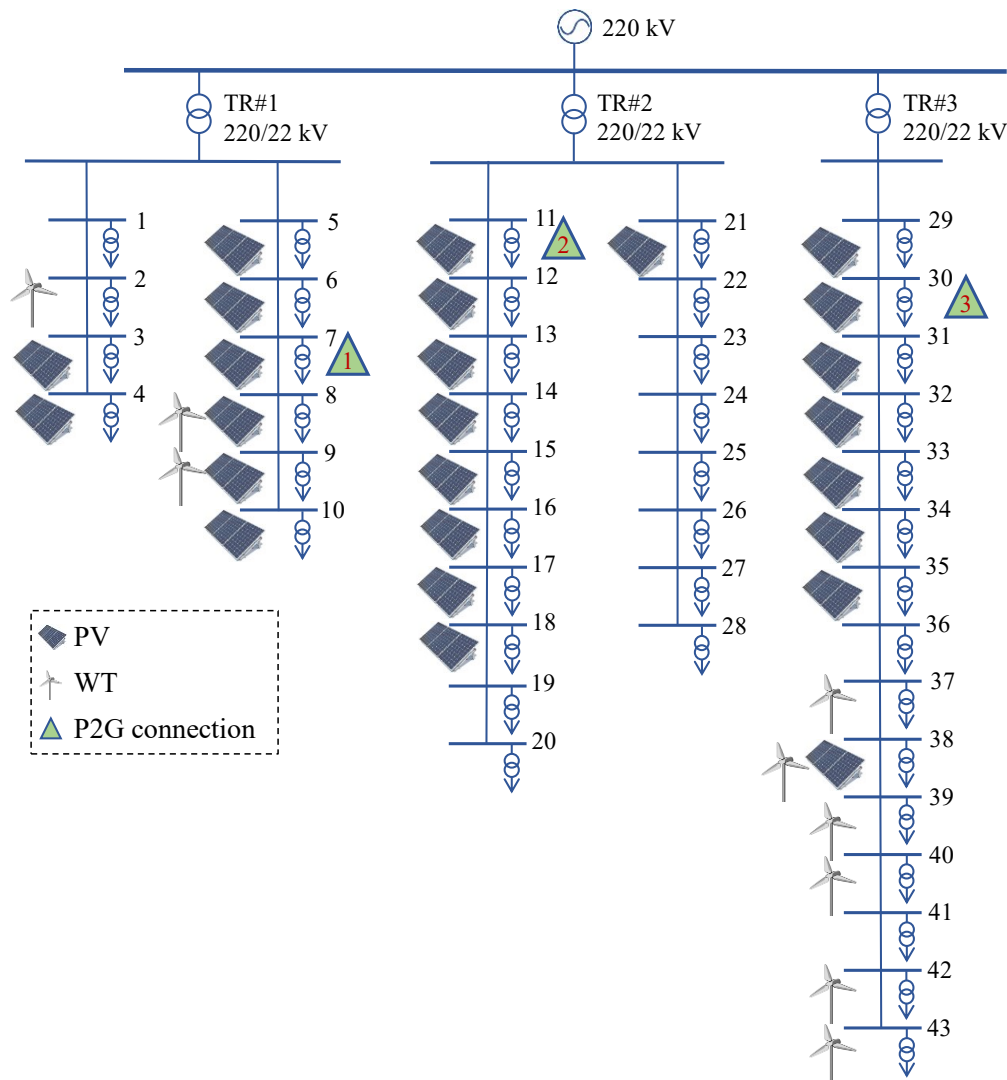


Figure 3-2. Topology of the electricity network.

### 3.2.2 Gas system

The topology of the gas network (GN) (see Figure 3-3) was derived from the one presented in [98]: a medium-pressure distribution network (4th species according to the Italian DM 24/ 11/1984 classification [99]) that covers an urban area of around 29 km<sup>2</sup>. The pressure of a 4th species gas network needs to stay within a range of 1.5 – 5 bar<sub>g</sub>. The gas network is divided into nodes: each withdrawal, injection and junction point is considered as a node. This yields a total

of 70 nodes (see Figure 3-3). The medium-pressure network is connected to a high-pressure network through a city-gate (node 0). At this point the gas is injected from the high-pressure network into the medium-pressure network (the gas cannot flow from the medium-pressure network to the high-pressure network). The gas is supposed to be injected at 4 barg.

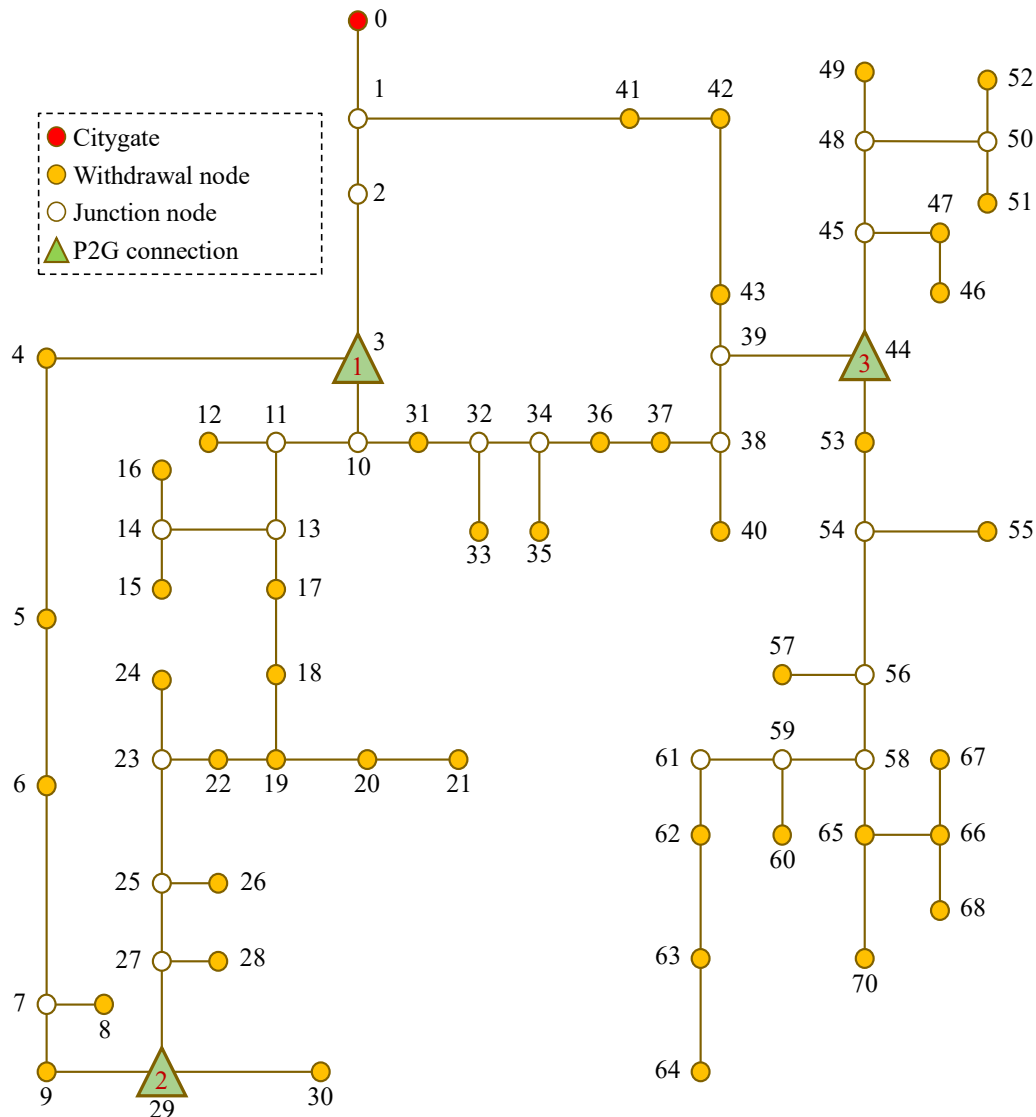


Figure 3-3. Topology of the gas network.

Various gas network models with different levels of complexity are shown in Table 3-1. The main characteristics for evaluating the operation of the gas network with SNG injections were:

- the possibility of considering gas flows in both directions on each pipeline of the network (bi-directional flows); and

- the possibility of considering the pressure increase inside the pipes due to the SNG injection in order to evaluate the linepack effect.

The model used in this study, albeit simplified, took into account both phenomena and demonstrated a very good level of approximation. More information about the gas network model and its validation are reported in Chapter 2.

*Table 3-1. Non-exhaustive overview of gas network literature models characteristics.*

<b>Ref.</b>	<b>Bi-directional flow</b>	<b>Linepack</b>
Sanchez et al. [136]	NO	NO
He et al. [137]	NO	NO
He et al. [138]	YES	NO
Shao et al. [139]	YES	NO
Belderbos et al. [125]	YES	YES
Cavana et al. [98]	YES	YES
This study	YES	YES

### 3.2.3 Power-to-Gas systems

The three P2G plants have the same size and characteristics. Each plant has a Polymer Electrolyte Membrane (PEM) electrolyzer of 1200 kW<sub>e</sub> (in terms of electricity input), and a catalytic methanation reactor of 600 kW<sub>th</sub> (in terms of SNG output). As schematized in Figure 3-4, the PEM electrolyser consumes electricity to produce hydrogen, which is directly fed into an internal hydrogen buffer to be accumulated and used by the methanation unit to produce SNG. In the model configuration, the hydrogen buffer was selected to host up to 92 kg of hydrogen, corresponding to 1024 Sm<sup>3</sup> and, in terms of energy, to 3060 kWh considering the Lower Heating Value (LHV) of hydrogen.

Since the simulation time step is 15 minutes and the PEM can vary its operating setpoint in seconds, the ramp-up and ramp-down constraints have been neglected. The methanation unit has a lower dynamics: the 600 kW<sub>th</sub> methanation unit can increase its hydrogen consumption by about 3.8 kg per hour and decrease it by 46 kg per hour, while sustaining the specified SNG product gas quality without violating the maximum hydrogen content limit (set here to <4%) required. The methanation unit cannot work below 50% of its nominal capacity, without requiring shutdown.

The P2G plant's electricity consumption includes the power consumed by the water splitting to hydrogen and oxygen in the electrolyser stacks, the conversion

losses in the transformer and the rectifier to supply the needed direct power, as well as power needs for the plant (such as electrolyser and methanation unit feed pumps, hydrogen dryers, automation and control system, etc.).

A commercial state-of-the-art PEM electrolyser is capable of supplying output hydrogen at a 30 bar pressure, which is assumed to be the maximum pressure level of the intermediate hydrogen storage. Hence, no hydrogen compressor is assumed to be needed. As schematized in Figure 3-4, the P2G model also calculates the oxygen that is produced during the electrolysis process and the heat recovery in the methanation process. The P2G technical parameters are summarized in Table 3-2, whereas more details about the P2G model are reported in Chapter 2.

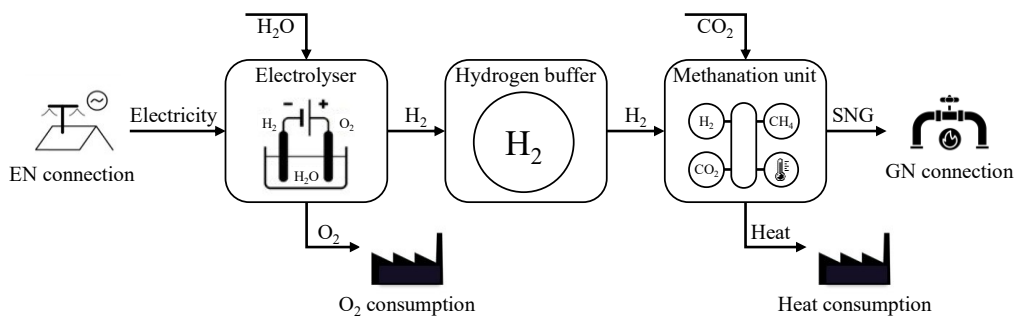


Figure 3-4. Scheme of P2G system.

Table 3-2. Technical parameters of the P2G plants.

Parameter	Unit	Value
Electrolyzer capacity	kW (el. input)	1200
Meth. unit capacity	kW (SNG output)	600
Hydrogen buffer capacity	Sm <sup>3</sup> of H <sub>2</sub>	1024
Meth. unit - minimum load	%	50
Meth. Unit - max ram up	kg (H <sub>2</sub> input)/h	3.8
Meth. unit - max ram down	kg (H <sub>2</sub> input)/h	46

The position of the P2G plants is defined according to the methodology shown in [140]. Each P2G is connected downstream of a different HV/MV transformer. This correspondence allows the RPFs on each transformer to be absorbed by one of the three P2G plants. The connection to the gas network is made in order to distribute the various connections over the network. The P2G connections to the distribution networks are summarized in Table 3-3.

Table 3-3. Network connections to the P2G plants.

	EN node connection	GN node connection
P2G#1	7 (TR#1)	3
P2G#2	11 (TR#2)	29
P2G#3	30 (TR#3)	44

### 3.2.4 Scenario energy demand and production

A critical energy context was chosen to investigate P2G operation. The scenario is characterized by a high number of RES penetrations, which are not equally distributed over the electricity network (i.e., the RES plants are more concentrated downstream of the third HV/MV transformer; see Table 3-4). Moreover, the scenario is assumed to mainly feed residential and tertiary sector users. Thus, the natural gas demand is affected seasonally to a great extent as a result of the high gas demand for building heating purposes during winter. Indeed, the gas consumption during the heating season (01/01-15/4 and 15/10-31/12) is about 10 times higher than during the rest of the year. The electricity user demand capacity, the total RES installation (for each transformer and for the whole network) and the peak gas demand are summarized in Table 3-4. The duration curves of the electricity demand, gas demands and renewable production are shown in Figure 3-5, while Figure 3-6 shows the renewable production and energy demands per month. The demand for electricity is roughly constant throughout the year. RES production increases considerably in the summer months, due to the influence of solar radiation (the renewable production in the summer months is almost double that of the winter months). Thus, the winter season is characterized by a contained excess of RES and a high gas demand. Conversely, in summer, when the highest RES overproductions occur, the natural gas demand is much lower.

Table 3-4. Electricity demand, gas demand and RES installations.

	Installed power [MW]			
	TR#1	TR#2	TR#3	Total
EL demand	3.90	9.30	5.10	12.30
PV	3.90	4.50	6.60	14.30
WT	0.80	0	3.60	4.40
Peak demand [MW]				
Gas demand	23.0			

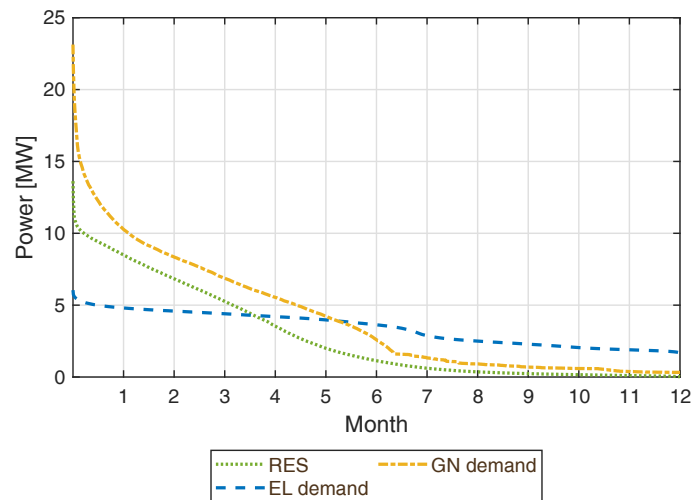


Figure 3-5. Duration curves of RES generation, electricity demand and natural gas.

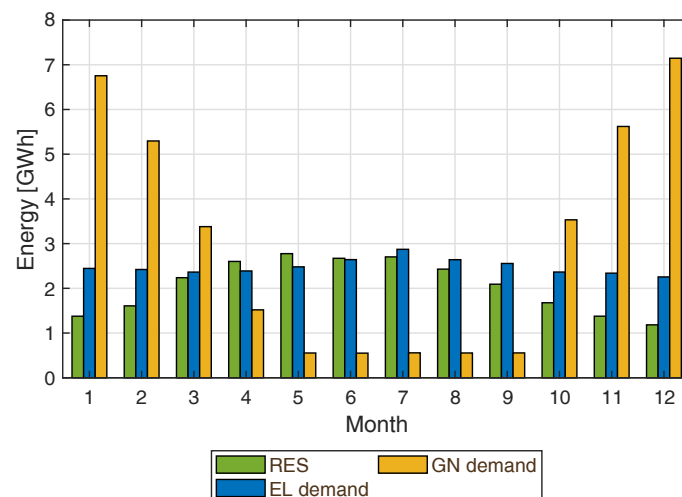


Figure 3-6. Monthly RES generation, monthly electricity and monthly gas demands.

### 3.2.5 Economic analysis

#### Capital and fixed operational expenditure

The cost of P2G shows a decreasing trend that will most probably continue, especially if the P2G plant components are manufactured in standardized sizes and series [141]. Two economic scenarios are considered for this study: the first one refers to the year 2030, whereas the second one pertains to the year 2050. The assumed investment cost and the fixed Operation and Maintenance (O&M) expenditures are shown in Table 3-5. The lifetime of the plant is expected to be 20 years [141], except for the electrolyzer, which needs to be replaced. The replacement cost is assumed to be 35% of the total PEM capital cost, and the replacement takes place with a frequency of once every 5 years [142].

Table 3-5. Specific investment cost, specific fixed O&M cost and lifetime of the components of the P2G plant.

	Unit	Specific investment cost [€/unit]		Specific fixed O&M cost [€/unit]		Lifetime [years]	Ref
		2030	2050	2030	2050		
Electrolyzer	kW <sub>e</sub>	650	400	19.5	8.0	5	[54],[141]–[144]
H <sub>2</sub> buffer	m <sup>3</sup> H <sub>2</sub>	75	50	1.1	0.8	20	[141],[145]
Methanation unit	kW <sub>SNG</sub>	500	300	25.0	9.0	20	[142],[146],[147]

### Variable operational expenditures and revenues

The annual mean cost of the electricity has been considered equal to 60 €/MWh [133]. During periods of RES over-generation, the P2G plants can provide enough flexibility to absorb the energy surplus. In this study, different possible incentive values were considered for the flexibility provided (from 0 €/MWh to 60 €/MWh). It should be noted that the incentives for flexibility generate a reduction in the cost for the purchasing of the over-generation electricity. For instance, with an electricity cost of 60 €/MWh and an incentive for the flexibility of 20 €/MWh, the cost for the consumption of over-generations of renewables is estimated to be 40 €/MWh.

The estimated cost for the CO<sub>2</sub> used for the methanation process is 50 €/t [148]. The cost for the demineralized water has been neglected, as it has a marginal impact on the overall cost [141]. Oxygen and high temperatures are generated as indirect products during P2G operation. It is assumed that these products are valued with a profit of € 70 per ton of oxygen and € 30 per MWh of generated heat. The economic data are summarized in Table 3-6.

Table 3-6. Economic assumptions for the considered P2G.

Parameter	Unit	Value	Ref
Plant lifetime	y	20	[141]
Mean electricity price	€/MWh	60	[133]
Incentives for flexibility	€/MWh	0-60	Our assumption
PEM replacement	% of investment cost	35	[142]
CO <sub>2</sub> specific cost	€/t	50	[148]
O <sub>2</sub> specific revenue	€/t	70	[148],[149]
Heat specific revenue	€/MWh	30	[148]

### Levelized cost of Synthetic Natural Gas

The equations below (3.1-3.5) show how, based on the annual profile, the system's estimated costs and revenues were calculated. Equations (3.1.) and Equations (3.2.) refer to the estimated costs for the purchase of electricity and CO<sub>2</sub>, respectively. The remaining equations refer to the estimated revenues obtainable from heat production (Eq. 3.3), CO<sub>2</sub> production (Eq. 3.4) and the flexibility provided by the system (Eq. 3.5.).

$$Cost_{el,P2G\#i} = c_{el} \sum_{k=1}^K u_{P2G\#i}(k) \cdot \tau \quad (3.1)$$

$$Cost_{CO_2,P2G\#i} = c_{CO_2} \sum_{k=1}^K CO_{2P2G\#i}(k) \quad (3.2)$$

$$Rev_{heat,P2G\#i} = r_{Heat} \sum_{k=1}^K \Phi_{P2G\#i}(k) \cdot \tau \quad (3.3)$$

$$Rev_{O_2,P2G\#i} = r_{O_2} \sum_{k=1}^K O_{2P2G\#i}(k) \quad (3.4)$$

$$Rev_{flex,P2G\#i} = r_{flex} \sum_{k=1}^K [u_{P2G\#i}(k) - u_{P2G\#i}^0(k)] \cdot \tau \quad (3.5)$$

Where:

- $Cost_{el,P2G\#i}$  [€] represents the annual expenses for the electricity consumption of the  $i$ -th P2G plant;
- $c_{el}$  [€/MWh] is the annual average price of electricity;
- $u_{P2G\#i}(k)$  [MW<sub>e</sub>] is the electricity consumption of the  $i$ -th P2G plant at time step  $k$ ;
- $\tau$  [h] is the duration of the time steps;
- $Cost_{CO_2,P2G\#i}$  [€] is the annual cost for the purchasing of the CO<sub>2</sub> consumed by the  $i$ -th P2G plant;
- $c_{CO_2}$  [€/t] is the CO<sub>2</sub> price;
- $CO_{2P2G\#i}(k)$  [t] is the CO<sub>2</sub> consumption of the  $i$ -th P2G plant at time step  $k$ ;
- $Rev_{heat,P2G\#i}$  [€] indicates the annual revenues for the heat production of the  $i$ -th P2G plant,
- $r_{heat}$  [€/MWh] is the specific revenue generated by the heat production;
- $\Phi_{P2G\#i}(k)$  [MW] is the heat production of the  $i$ -th P2G plant at time step  $k$ ;
- $Rev_{O_2,P2G\#i}$  [€] indicates the annual revenues generated by the O<sub>2</sub> production of the  $i$ -th P2G plant,



- $r_{O_2}$  [€/t] is the specific revenue for the  $O_2$  production;
- $O_{2,P2G\#i}(k)$  [t] is the  $O_2$  production of the  $i$ -th P2G plant at time step  $k$ ;
- $Rev_{flex,P2G\#i}$  represents the annual revenues generated by the flexibility provided by the  $i$ -th P2G plant;
- $r_{flex}$ , represents the incentive for the provided flexibility;
- $u_{P2G\#i}^0(k)$  [MW] is the baseload of the  $i$ -th P2G plant at time step  $k$ .

The P2G systems are evaluated from an economic point of view by calculating the levelized cost of SNG ( $LC_{SNG}$ ).  $LC_{SNG}$  is the breakeven selling price of the produced SNG, which is calculated over the plant's lifetime. The latter corresponds to the lifetime of the methanation unit (20 years). It is worth noting that during the time period considered, there are expenses for the replacement of the electrolyser which has a shorter lifetime. The  $LC_{SNG}$  for the  $i$ -th P2G plant ( $LC_{SNG,P2G\#i}$ ) is calculated as [150]:

$$LC_{SNG,P2G\#i} = \frac{CAPEX_{P2G\#i} + \sum_{y=0}^{LT_{P2G\#i}} \frac{-CF_{P2G\#i}}{(1+DR)^y}}{\sum_{y=0}^{LT_{P2G\#i}} \frac{E_{SNG}}{(1+DR)^y}} \quad (3.6)$$

$$CF_{P2G\#i} = Rev_{heat,P2G\#i} + Rev_{O_2,P2G\#i} + Rev_{flex,P2G\#i} - OPEX_{P2G\#i} - Cost_{el,P2G\#i} - Cost_{CO_2,P2G\#i} - Cost_{rep,P2G\#i} \quad (3.7)$$

where:

- $LT_{P2G\#i}$  [years] is the lifetime of the  $i$ -th P2G plant;
- $CAPEX_{P2G\#i}$  [€] is the capital expenditure for all the components of the  $i$ -th P2G plant (considered only at year 0);
- $CF_{P2G\#i}$  [€] is the annual cash flow of the  $i$ -th P2G plant;
- $DR$  [-] is the discount rate, assumed to be equal to 7% [150];
- $E_{SNG}$  [MWh] is the total amount of SNG energy produced yearly;
- $OPEX_{P2G\#i}$  [€] is the fixed annual operational expenditure for all the components of the  $i$ -th P2G plant;
- $Cost_{rep,P2G\#i}$  [€] is the cost of the replacement of the stack of the electrolyzer (for years 5, 10 and 15).

The  $LC_{SNG}$  calculation was performed with the assumption that the annual energy and economic flows resulting from the simulation would repeat throughout the plant's lifetime

### 3.3 Mathematical approach and solution strategy

#### 3.3.1 Co-simulation architecture

In this case study, the co-simulation loop involves five modules:

- the electricity network (EN) module;
- the gas network (GN) module;
- the P2G module;
- the controller;
- the time-synchronizer (Time-Sync).

Detailed models are used both for the modeling of the energy networks (electricity and gas) and for the modeling of the P2G plants (see Table 3-7). These models take into account the internal dynamics (energy and mass flows) that occur in the three components of the scenario (the details on the models are given in Chapter 2).

Table 3-7. Models involved in the co-simulation loop.

Model	Case study 1
Controller	X
Time-Sync	X
Electricity network (detailed)	X
Electricity network (simplified)	
Gas network (detailed)	X
Gas network (simplified)	
DH network and CP2H	
P2G (detailed)	X
P2G (simplified)	
Building and LP2H	
Electric battery	

The co-simulation process is coordinated by the Time-Sync module, which orchestrates all the messages exchanged during the simulation. Each message that is sent between the different modules passes through the Time-Sync and is sent to the receiving module at the appropriate time.

All the messages exchanged during each time step are summarized in Figure 3-7. At each time step of the simulation, Time-Sync sends to the control module the electricity network node's balance and the assets' flexibility, which are both calculated in the previous time step  $k - 1$  (*message 1*). When the control module simulation ends, the Time-Sync receives the P2G setpoints (*message 2*) and it triggers the P2G module simulation, sending it the input data for time step  $k$  (*message 3*), which consists of the setpoints, defined by the control module, and the

GN constraints, defined in the previous step by the GN module. The P2G output, *message 4*, contains the P2G units' flexibility, which will be sent in the next time step (i.e.,  $k + 1$ ) to the control module, the P2G electric power consumptions forwarded to the electricity network module and the P2G SNG productions, forwarded to the GN module. The input of the GN module (*message 5*) contains the SNG productions. The GN module's output (*message 6*) contains the gas flows and the pressure evolution of the network, as well as the SNG injection constraints for the next step. The electricity network module receives as input the P2G electricity consumptions. The output of the EN network module contains the electricity consumptions and generations for each node of the network (*message 7*) that will be used by the control module in order to define the P2G setpoint for the next step (i.e.,  $k + 1$ ).

Annual simulations are performed with a discretization of 15 minutes, resulting in a total of 35040 time steps.

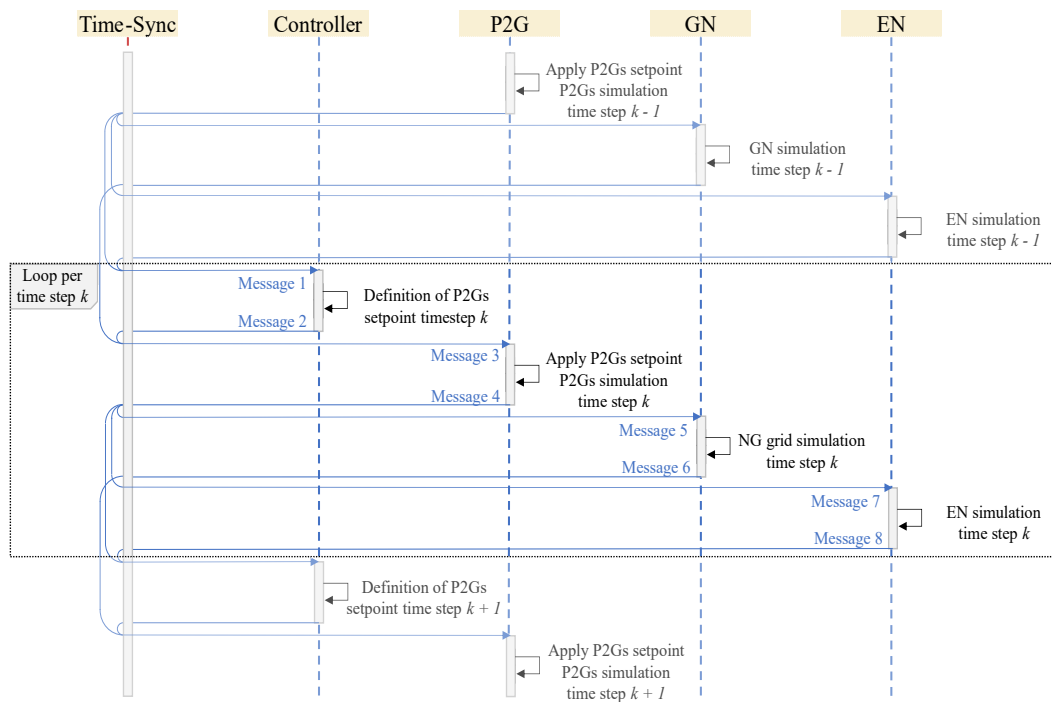


Figure 3-7. Sequence of interactions among co-simulation modules.

### 3.3.2 Simulation control algorithm

In the analyzed scenario each P2G plant is connected downstream of a different transformer. For this reason, the operation of each P2G affects only the portion of the network to which it is connected.

The control algorithm of the  $i$ -th electrolyzer is defined in Figure 3-8.

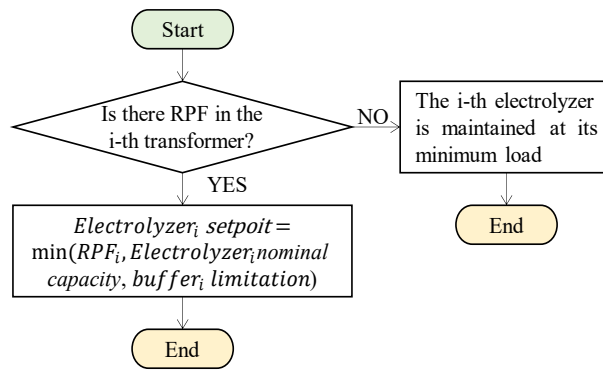


Figure 3-8. Control algorithm of the  $i$ -th electrolyzer.

If there is no energy overproduction downstream of the transformer, the electricity consumption of the P2G system is kept at its minimum load; that is, the electricity consumption of the auxiliary components necessary to keep the system in hot standby. The electrolyzer is turned on when an RPF occurs. The upper limit setpoint is determined by considering the nominal power of the plant and the availability of the buffer. If the hydrogen buffer has reached its maximum operating pressure, the electrolyzer cannot operate unless the methanation unit is in operation as well. In this case, it can produce an equal amount of  $H_2$  to the  $H_2$  consumed by the methanation unit, thereby maintaining the pressure of the buffer within its bounds.

Figure 3-9 reports the methanation unit's control logic. If no external restriction occurs, the methanation units are turned on when the hydrogen buffer reaches a pressure of 15 bar. The conversion of  $H_2$  into the SNG process continues until the buffer is emptied. However, during low NG demand periods, the GN injection availability could be a constraint for the operation of the methanation unit. If the SNG injection is limited, the use of plants that are in the up and running mode is prioritized (even though the plants that are not in operation have accumulated more hydrogen). If the GN does not allow operation of all the up and running units, the units with lower amounts of stored hydrogen are set to stand-by condition. The units in the stand-by condition are only turned on if the up and running units have already reached their maximum load (a limit that is defined by the maximum capacity of the plant and its ramp constraint) and only if the GN allows more SNG to be injected.

It should be noted that, in the case of SNG injection limitations, the various P2G plants should be coordinated to optimize the multi-energy system as a whole. Indeed, even though the different P2G systems operate on different portions of the electricity network (such as in the scenario where each plant is downstream of a different transformer), coordination that takes into account the constraint of the common resource is necessary when the systems involve the use of a common flexibility resource (in this case the gas network). In order to maximize the overall benefits, it is necessary to favor the resources that can lead to the greatest benefits

for the overall system. For example, the use of the units already in operation is prioritized in low GN flexibility conditions, in order to limit the overall number of shutdowns. In the same way, if several systems are in the same state (i.e., all off or all on), the use of the system that has stored the greatest amount of hydrogen inside the buffer is favored in order to increase the continuous operation of the systems as much as possible and, at the same time, increase the availability of use of electrolyzers.

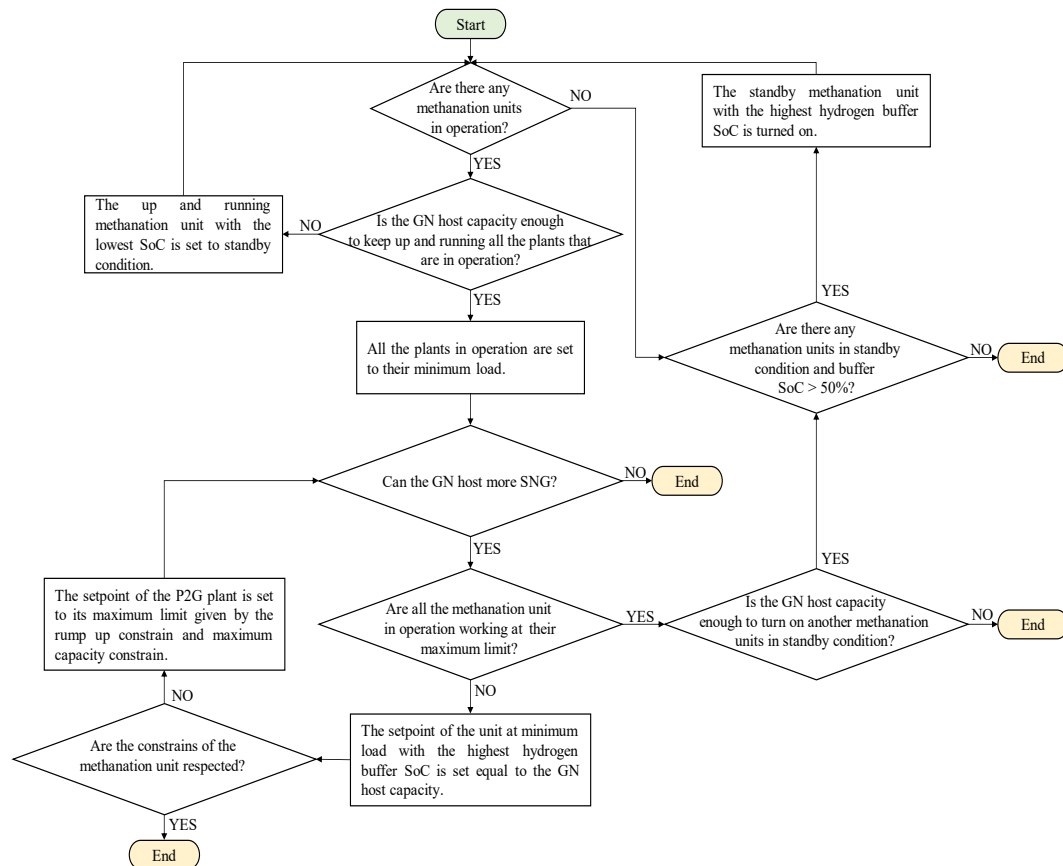


Figure 3-9. Control algorithm of the methanation units<sup>2</sup>.

## 3.4 Results and discussion

### 3.4.1 Energy impact of Power-to-Gas on the electricity and gas networks in winter and summer seasons

The simulations of the scenario were performed over the whole year with a discretization time of 15 minutes. The figures in this section show the energy flows in the electricity and gas networks. For reasons of clarity, it was decided to show

<sup>2</sup> The control algorithm of the methanation units is part of the P2G detailed model described in Chapter 2. For reasons of clarity, this figure is also reported in this section.

some characteristic days in the figures: under opposite conditions in winter and in summer.

Figure 3-10 reports the energy flow for the HV/MV transformers of the electricity network for a typical winter day. The renewable energy production causes over-generation in all the HV/MV transformers. Transformer #3 is the one that is affected by the highest RES overproduction (see Table 3-8). Thanks to the fast response of the PEM electrolyzer, the P2G loads follow the RES surplus and absorb about 85% of it during the whole heating season.

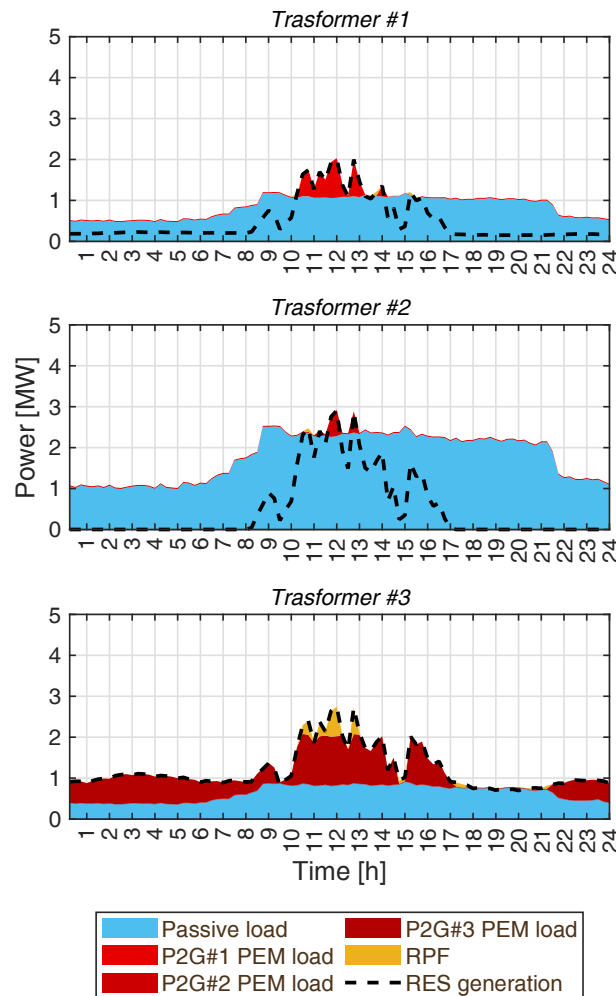


Figure 3-10. Balance of transformers of the electricity network in winter.

When the RES surplus is higher than the PEM capacity (1.2 MW), the electricity excess can no longer be absorbed, and this causes an RPF of the transformer (see the yellow area in Figure 3-10). During the heating season, the gas network can absorb all the produced SNG, without violating any operational constraints for the P2G plants. Under these conditions, the storage capacity of the network is not used (i.e., the SNG injected into the network is not accumulated, but consumed directly due to the high gas demand; see Figure 3-11). During the heating season), the SNG injections cover only 4% of the total gas demand (see Table 3-9).

Figure 3-12 reports the evolution of the gas network pressure; it can be noted that the SNG injection does not cause any relevant pressure variation. The figure reports the highest and lowest network pressures for each time step. The highest pressure is found in the most upstream nodes, where the pressure is kept close to the injection pressure of the city-gate (4 bar<sub>g</sub>). The lowest pressure is recorded in the nodes far from the city-gate. In terms of time, the steps with the lowest network pressure correspond to the periods of the highest gas demand.

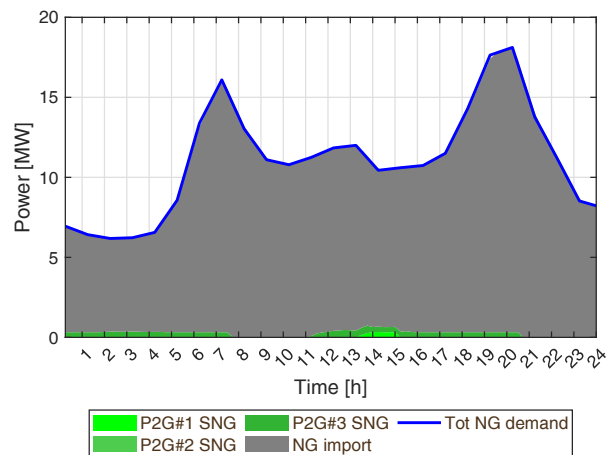


Figure 3-11. Balance of the gas network for the winter

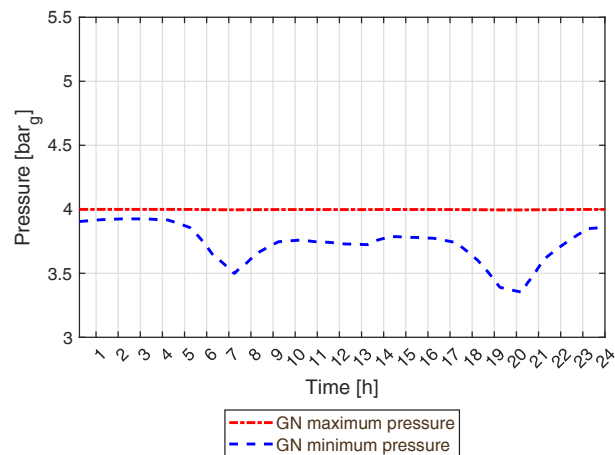


Figure 3-12. Gas network pressure for the winter.

Table 3-8. Results pertaining the electricity network.

	Heating season [GWh]				No heating season [GWh]				Whole year [GWh]			
	TR#1	TR#2	TR#3	Tot	TR#1	TR#2	TR#3	Tot	TR#1	TR#2	TR#3	Tot
El. dem.	3.70	7.80	2.79	14.29	4.12	8.71	2.97	15.80	7.82	16.50	5.76	30.08
RES	2.41	3.23	4.12	9.76	3.90	5.68	5.39	14.97	6.32	8.91	9.51	24.73

Surplus	0.67	0.46	2.04	3.17	1.40	1.08	3.08	5.55	2.07	1.54	5.11	8.72
Abs. surp.	0.62	0.40	1.61	2.63	1.23	0.90	2.07	4.20	1.86	1.30	3.68	6.83
RPF	0.05	0.06	0.43	0.53	0.16	0.18	1.01	1.35	0.21	0.24	1.44	1.88

Table 3-9. Results pertaining the gas network.

	Unit	Heating season	No heat. season	Whole year
NG demand	GWh	31.65	4.37	36.02
NG imported	GWh (%)	30.38 (96%)	2.37 (54%)	32.75 (91%)
SNG	GWh (%)	1.27 (4%)	2.00 (46%)	3.27 (9%)

The demand for electricity increases in summer by about 10%, compared to the heating season, mainly due to the building cooling demand, while the production of RES increases by about 50%, thus creating much more RES over-generation (see Table 3-8). The RES peaks are higher than in winter, thus the RPF on the transformers increases (see the yellow areas in Figure 3-13). About 80% of the energy surplus is absorbed by the P2G plants throughout the whole season. In particular, about 1.35 GWh of RPF is generated during the hot season. that is, 70% of the whole year's RPF. Of these 1.35 GWh, about 75% is generated on transformer #3.

The gas flows inside the network are much lower in the hot season than during the cold season (see Table 3-9 and Figure 3-14<sup>3</sup>). During the hot season, it could happen that the SNG production exceeds the gas demand of the network. When this happens, the SNG could be stored within the gas network volume. The gas network pressure increases, due to the linepack effect (see Figure 3-15). The SNG stored in the gas pipeline can be used later on, when the SNG production alone is not able to cover the network gas demand (see the white areas in Figure 3-14). The gas network can host the SNG production until its pressure is lower than the allowed maximum pressure (5 bar<sub>g</sub>).

<sup>3</sup> In order to make the graph clearer, the y-axis of the figures representing gas flows have different scales.



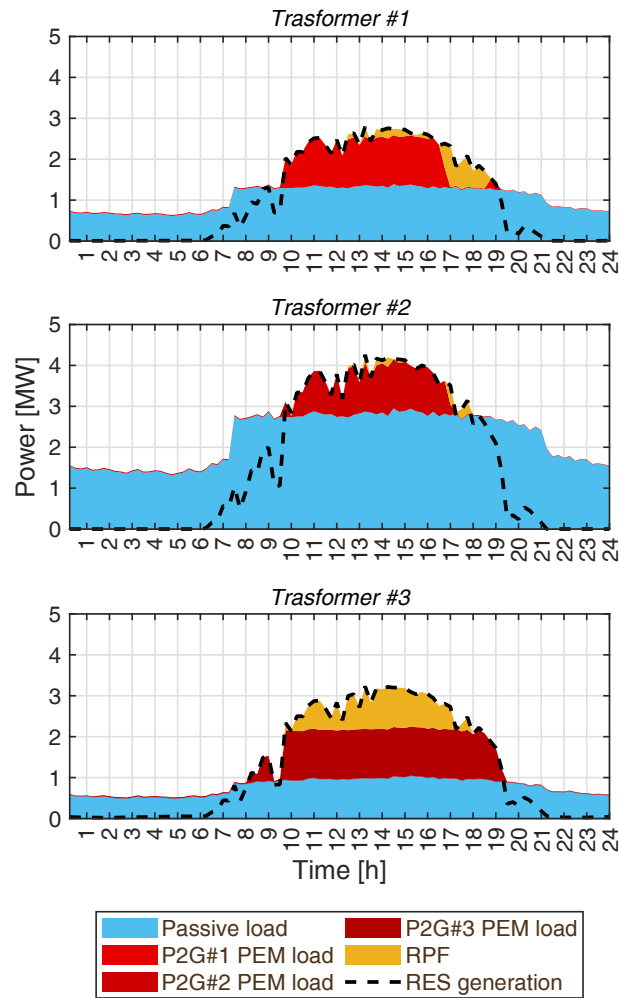


Figure 3-13. Balance of the electricity network transformers for the summer.

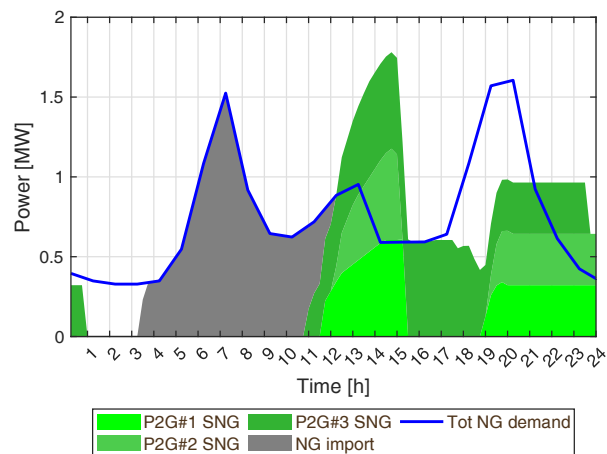


Figure 3-14. Balance of the gas network for the summer.

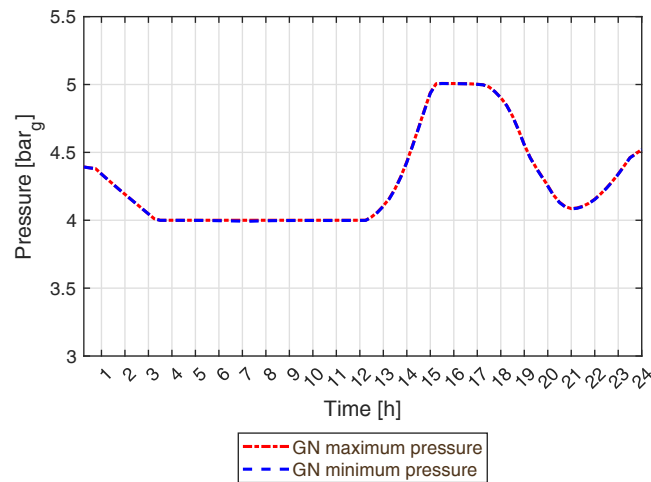


Figure 3-15. Gas network pressure (b) for the summer.

In the case reported, the network pressure reaches its upper constraint at 14:30, at which point control system then limits the production of the methanation unit of P2G#1 and P2G#2 (see Figure 3-16). The control system chooses to maintain the production of P2G#3 as, at that moment, the hydrogen buffer pressure of that plant is the highest of the three (see Figure 3-17). Even though the methanation unit of a plant is in standby, this does not affect the operation of the electrolyzer. For example, the methanation unit of P2G#2 remains in standby from 14:30 to 17:15 (see Figure 3-16); nevertheless, the electrolyzer continues to operate (see Figure 3-13). The produced hydrogen is accumulated inside the buffer, whose pressure therefore increases (see Figure 3-17). Hydrogen can continue to be stored until the pressure limit of the buffer is reached. For example, at 15:45, the pressure of the P2G#1 buffer reaches its limit value and the electrolyzer must therefore limit its load (see Figure 3-13).

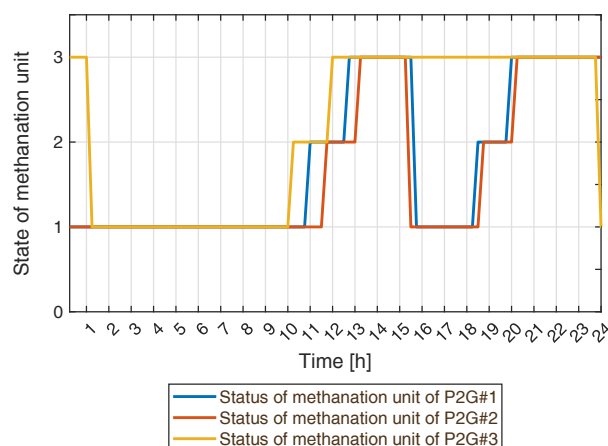


Figure 3-16. Status of the methanation units: 1 hot standby, 2 Reactor balancing phase, 3 up and running.

It is worth noting that, before reaching its maximum pressure limit, the energy stored in the network was about 2.6 MWh (i.e., about 15% of the gas demand on a typical summer day). For this reason, the SNG stored in the gas network in summer is consumed by the network users in the hours after storage. Therefore, the storage capacity of the gas system has proven to be insufficient to be used as seasonal storage. Nevertheless, the storage capacity of the grid has proven to be sufficient for intraday gas storage. In particular, the storage capacity has allowed the flexible operation of P2G power plants to accommodate RES excess production. The importance of the distribution gas grid's storage capacity of the gas network is discussed more in detail in Chapter 4.

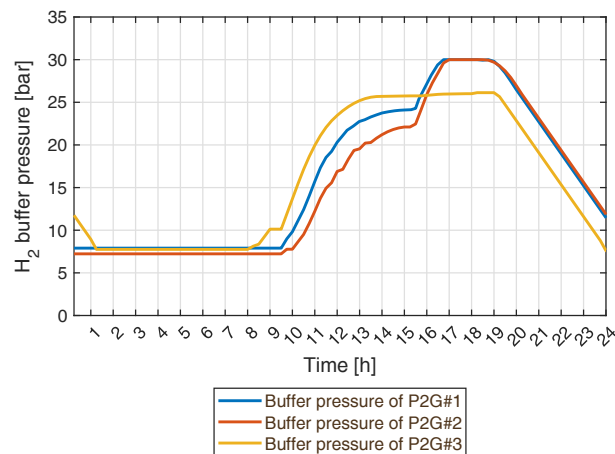


Figure 3-17. Pressure of the hydrogen buffers.

### 3.4.2 Economic results

#### Levelized cost of Synthetic Natural Gas

As previously mentioned, transformer #3 is the one that is affected by the highest RES overproduction. For this reason, P2G#3 is used more than the other two. This plant produces almost 3.5 GWh of SNG throughout the entire year, an amount which is approximately equal to the sum of the productions of the other two plants. Table 3-10 reports the production and consumption of the three plants: the higher the plant utilization is, the higher the production of SNG and of the indirect products (i.e., high temperature heat and oxygen). Considering the economic assumptions to be equal, the higher the utilization of P2G is, the lower the  $LC_{SNG}$  (see Table 3-11). The  $LC_{SNG}$  of P2G#3 is around 50-70% lower than the  $LC_{SNG}$  of P2G#2 (the least used plant).

The scenario has been simulated under different economic assumptions: different cost scenarios, referring to years 2030 and 2050, and different flexibility provision incentives.

Table 3-10. P2G results.

Unit	Heating season				No heating season				Whole year				
	P2G#1	P2G#2	P2G#3	Tot	P2G#1	P2G#2	P2G#3	Tot	P2G#1	P2G#2	P2G#3	Tot	
El. cons	GWh	0.72	0.50	1.69	2.90	1.32	0.98	2.14	4.44	2.03	1.48	3.83	7.34
SNG	GWh	0.29	0.19	0.79	1.27	0.58	0.40	1.02	2.01	0.87	0.59	1.81	3.27
CO <sub>2</sub>	t	59.8	38.5	159.4	257.6	119.4	84.7	204.7	408.8	179.2	123.2	364.1	666.5
Heat	GWh	0.09	0.06	0.23	0.37	0.17	0.12	0.30	0.59	0.26	0.18	0.53	0.96
O <sub>2</sub>	t	89.4	57.6	235.7	382.7	178.5	127.6	303.0	609.1	267.9	185.2	538.7	991.8

Table 3-11. Levelized cost of SNG.

Flexibility provision incentives [€/MWh]	Levelized Cost of SNG (LC <sub>SNG</sub> ) [€/MWh]					
	2030			2050		
	P2G#1	P2G#2	P2G#3	P2G#1	P2G#2	P2G#3
0	299	394	193	230	293	160
10	277	371	173	208	269	140
20	255	348	153	185	246	119
30	232	325	132	163	223	99
40	210	301	111	141	199	78
50	188	278	91	119	176	58
60	166	255	70	97	153	37

The investment cost of the units that compose a P2G plant has been hypothesized to decrease by 2050, compared to 2030: a 25% cost reduction for the electrolyzer, a 10% reduction for the hydrogen buffer and a 33% reduction for the methanation reactor. This reduction leads to a reduction in LC<sub>SNG</sub>, which decreases by 25-47%, depending on the specific case.

Even if greater incentives for flexibility were offered (such as to bring the total cost for the use of the over-generations of RES to 0 €/MWh), LC<sub>SNG</sub> would be higher than the typical cost of fossil natural gas. In 2020, the average price of NG in the European Union was 35 €/MWh [151]. Its average cost from January to June 2022 was around 100 €/MWh [152]. However, such a high cost is atypical, as it is a consequence of the particular international situation caused by the invasion of Ukraine by Russia. The Snam and Terna report [32] predicted that the cost of NG would stabilize at a value slightly higher than the pre-war one. The report estimated a cost of 45 €/MWh for the years 2030 and 2040. However, even if the cost of the NG were 100 €/MWh, further incentives would be very much needed for this technology to be economically competitive.

The results demonstrate that  $LC_{SNG}$  depends to a great extent on both the economic assumptions and on the plant operation. The results yielded by this research are in line with those of previous literature (see Figure 3-18).

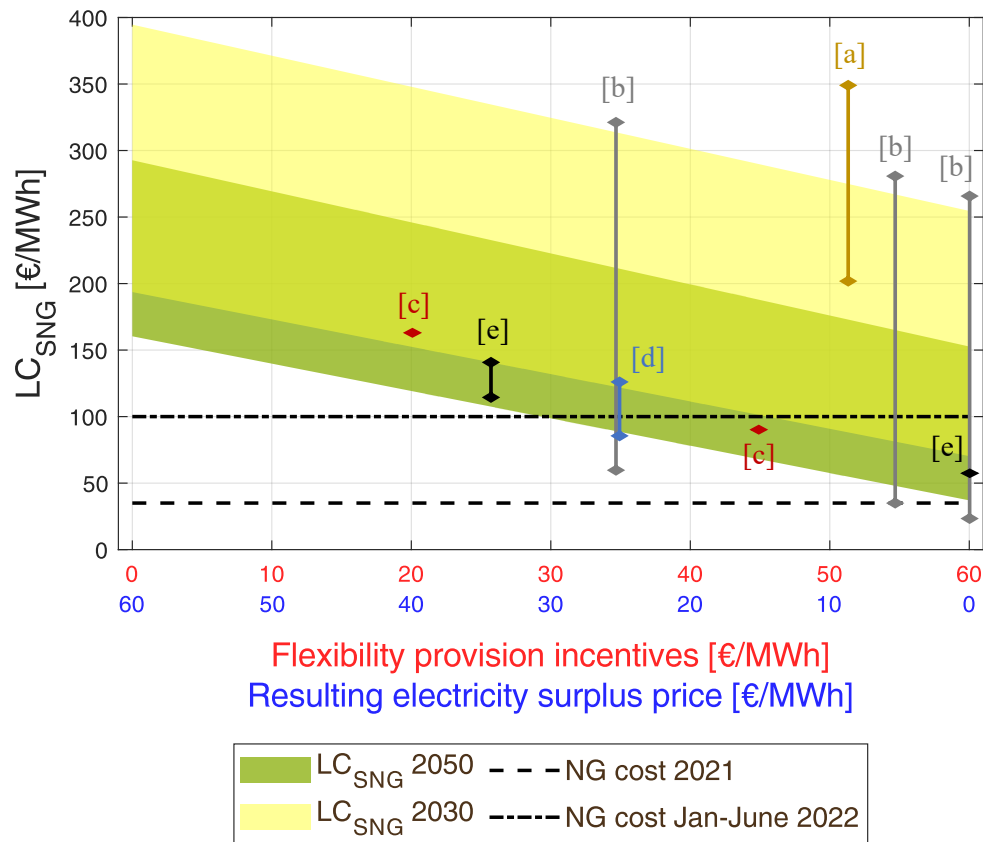


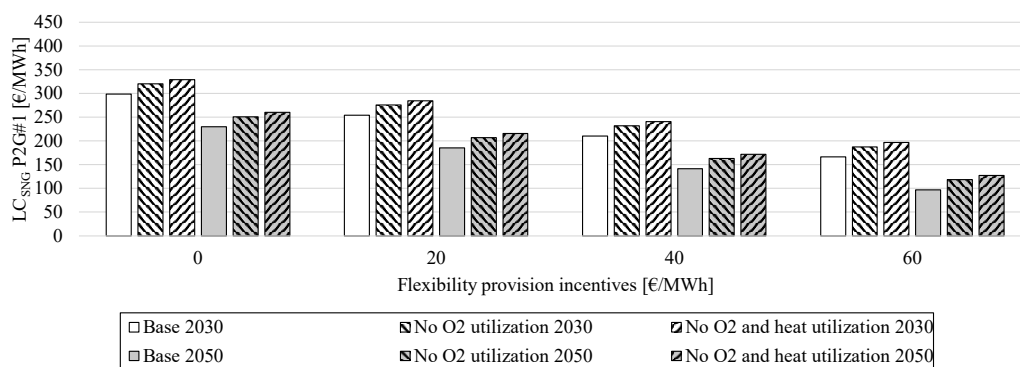
Figure 3-18. Levelized cost of SNG as a function of the flexibility provision price and the resulting electricity surplus price considering the investment cost for year 2030 (yellow area) and 2050 (green area). The figure also reports the values of the levelized cost of SNG reported in other publications: a [133], b [141], c [150], d [153], and e [154].

The assumptions made in study [133] are similar to those made in this case study: a 2050 scenario and a surplus electricity price of 8.71 €/MWh. The cost of SNG for a plant of the size of approximately 1 MW<sub>e</sub> results in the 200 to 350 €/MWh range. The analysis in [141] considers the cost of SNG for a 10 MW<sub>e</sub> plant, assuming a cost of electricity of 0 to 25 €/MWh. Depending on the specific configuration, the SNG cost is envisioned to vary from 42 €/MWh to 313 €/MWh in the 2030 scenario, and from 19 €/MWh to 170 €/MWh in the 2050 scenario. In [150], for a 10 MW<sub>e</sub> P2G plant with investment costs that refer to 2015 and an electricity cost of 40 €/MWh,  $LC_{SNG}$  was around 170 €/MWh. Considering a 2030 scenario with an electricity cost equal to 60 €/MWh,  $LC_{SNG}$  is 180 €/MWh, and  $LC_{SNG}$  will be around 95 €/MWh in 2050 (given an electricity price of 15 €/MWh). In [153], it was concluded that  $LC_{SNG}$  will be in the 92 to 113 €/MWh range in 2050, given an electricity cost of 25 €/MWh. In [154], it is reported that the SNG

cost of a 10 MWe P2G plant would have been 55 €/MWh in 2020, considering a zero cost for electricity, and from 107 to 143 for an electricity price of 35 €/MWh. Considering the same electricity price, but for a 2030 scenario, the SNG cost will drop to 89-121 €/MWh and to 81-103 €/MWh in 2050.

### Economic impact of the utilization of the heat and oxygen

The generation of oxygen and heat in a P2G plant is due to electrolysis and methanation thermochemical processes and they therefore represent by-products of the plant. As shown in Table 3-6, a remuneration of 30 €/MWh has been assumed for the produced high temperature heat and a remuneration of 70 €/t for the produced oxygen. The recovered heat can be sold for industrial use or even injected into the district heating network, if one exists [52], while oxygen could be sold for oxy-combustion in power plants or for medical care [155]. Vandewalle et al. [149] calculated that the valorization of produced oxygen could lead to a reduction in the SNG cost of as much as 20 €/MWh. This result is in line with what has been obtained in this study. In particular, the exploitation of produced oxygen leads to a reduction of 21 €/MWh in  $LC_{SNG}$  for P2G#1 and P2G#3 and of 22 €/MWh for P2G#2. When the revenues from the heat recovery are also considered, a further cost reduction of SNG of around 9 €/MWh is obtained for all the plants. Considering the overall cost of the SNG, this cost reduction is not negligible; in the scenario analyzed, the heat and oxygen remuneration allowed  $LC_{SNG}$  to be reduced by a minimum of 7% (in the P2G#2 case for the year 2030, considering no incentives for the provided flexibility) and a maximum of 44% (in the P2G#3 case for the year 2050, an incentive for the provided flexibility of 60 €/MWh). Importantly, an average decrease attested at 17% when considering all the cases (see Figure 3-19). Exploiting all the possible economic gains of the plant is of pivotal importance since, as it emerged in this analysis, the utilization of P2G technologies may lead to economic profitability problems.



(a)

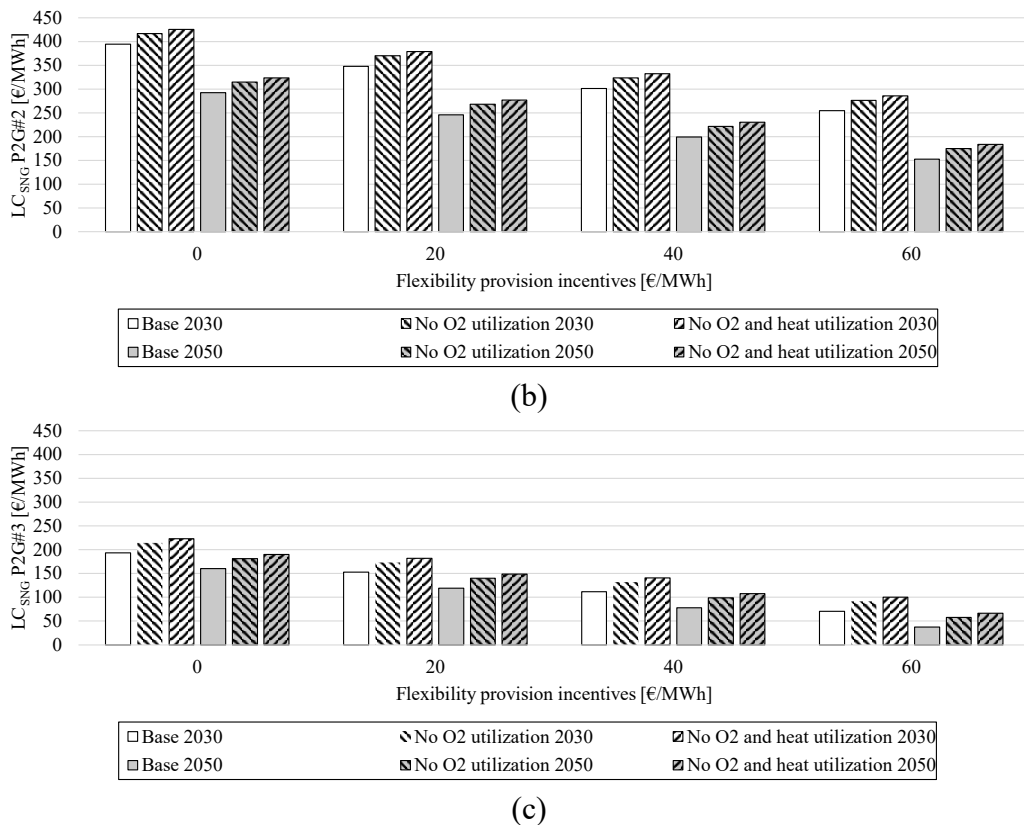


Figure 3-19. Impact of oxygen and heat utilization for P2G#1 (a), P2G#2 (b) and P2G#3 (c).

### 3.5 Conclusions

A high penetration of non-dispatchable distributed generation may introduce issues and lead to challenges concerning the distribution systems. This study analyzed how Power-to-Gas (P2G) plants could be used to optimize the utilization of the overproduction of Renewable Energy Sources (RES). The conclusion of this study can be summarized as follows:

- Thanks to the high flexibility of electrolyzer units, P2G plants can be effectively used to absorb the over-generation of renewable energy and thus alleviate the reverse power flow at the HV/MV transformers.
- The natural gas demand during the heating season is sufficiently high to allow Synthetic Natural Gas (SNG) injection into the gas distribution network without any kind of restriction. However, the P2G production in this season covers less than 5% of the gas demand. In the analyzed scenario, where the P2G plants are only used to absorb the overproduction of RES, the SNG production is not enough to decarbonize the gas sector.
- A low gas demand season may be critical for the utilization of P2G plants. In these periods, the SNG injection needs to be regulated to avoid over pressures in the gas network. This mainly happens in summer, when there is no demand for gas for heating. In this season, the RES production is higher, and thus the criticality of the scenario increases. In these conditions,

---

the P2G systems should be coordinated with each other to limit simultaneous gas injections. In such a context, different energy conversion systems, which share the same destination sink (in this case the gas network), need to cooperate with each other to optimize the utilization of the sink and maximize the benefits of the entire multi-energy system.

- If the SNG production is not consumed directly (as it happens during low gas demand periods), the gas distribution network can be used for gas storage purposes. When the SNG production is higher than the gas demand, the overproduction of SNG can be hosted inside the network until the pressure constraint is respected (linepack effect). It is well known that the linepack effect can also be used for seasonal storage purposes in gas transmission networks. The lower pressure range of the distribution network (compared to the transmission one) does not allow seasonal storage in a medium pressure network but only intraday storage. Nevertheless, the distribution network linepack effect leads to greater flexibility in the use of the methanation units: SNG is accumulated within the gas network in the most critical periods of low gas demand and is then consumed in the following hours, thus allowing a more constant operation of the methanation units to be achieved.
- Even though the low gas demand may be a constraint for methanation units in some cases, it has a limited impact on the electricity side. Indeed, the hydrogen buffer of P2G plants allows the decoupling of the methanation unit and electrolyzer. The RES overproduction is absorbed by the electrolyzer and the produced hydrogen can be accumulated in the buffer. Subsequently, at the appropriate time, it is converted into SNG by the methanation unit and injected into the gas network.
- The levelized cost of SNG ( $LC_{SNG}$ ) varies from 37 to 394 €/MWh, depending on the different assumptions and configurations.
- The cost of the units of the P2G plants for the year 2030 have been forecasted to decrease (a 25% cost reduction for the electrolyzer, a 10% reduction for the hydrogen buffer and a 33% reduction for the methanation reactor). This cost reduction is reflected on the  $LC_{SNG}$ , which on average decreases by 30%, depending on the different configurations and assumptions.
- The incentives for the flexibility provided are hypothesized to vary from 0 to 60 €/MWh and this also impacts  $LC_{SNG}$ : the higher the incentives is, the lower the  $LC_{SNG}$ . Even when considering the maximum incentive, the  $LC_{SNG}$  can be very high, especially if the plant is used to absorb small amounts of RES overproduction. Additional incentives are needed to make green SNG competitive with respects to natural gas.
- The same scenario was simulated considering the possible revenues from  $O_2$  and the heat produced by the P2G plants. Results showed that the



exploitation of these indirect productions allows  $LC_{SNG}$  to be reduced by around 30 €/MWh, which on average corresponds to 17% of the total  $LC_{SNG}$ . It would therefore be important to take into consideration the possible incomes of these byproducts as the resulting gains may not be negligible.

- The electricity network analyzed in this case study is composed of several feeders and several HV/MV transformers. This topology made it possible to consider the case of local renewable over-generation within the distribution system and to draw general considerations. Although all the plants are connected to the same electric distribution network, the location of the P2G plant has a considerable impact on the plant's performance. It turned out to be of pivotal importance to place the P2G plants downstream the transformers most affected by RES overproduction to solve the local problems. The location of the P2G plant showed to have an important impact on  $LC_{SNG}$ : a better placement of the P2G plant allows a greater production of SNG, leading to a reduction of the SNG production costs.
- In the analyzed scenario, the only flexible resources considered were the P2G plants. This made it possible to analyze the pros and cons of the utilization of this specific technology. The presence of other flexible resources, such as electric batteries, would increase the flexibility of the multi-energy system by potentially compensating the limitation of the P2G plants' flexibility. However, the use of other sources of flexibility could reduce the use of P2G plants as flexibility providers, leading to a lower production of SNG, with a consequent increase of  $LC_{SNG}$ .
- The gas network analyzed in this thesis, was a typical medium pressure distribution network of the Italian gas system. Greater flexibility could be obtained if the P2G plants were connected to a larger gas network, such as a transmission network, or if there were the possibility of accumulating the SNG in a dedicated storage located along the network. Nonetheless, the flexibility offered by the distribution network alone resulted to be enough to accommodate a large part of the RES over-generations in the form of SNG.

## **Chapter 4**

# **Case-study 2 – Power-to-Gas plants in gas and electricity distribution network system: a comparison between modeling approaches**

Chapter 4 exploits the module's plug and play co-simulation tool capability. To carry out this study, different modules were alternatively connected on the platform. Thanks to the flexibility enabled by the co-simulation, the replacement of the modules was possible without changing the simulator's structure. The study presents a methodological analysis on the impact of different simulation approaches when Power-to-Gas is installed at the distribution system level. Critical operation conditions can easily arise at the distribution level, in both electrical and gas infrastructures. Consequently, it is of extremely important to select the most appropriate modeling approaches for both Power-to-Gas plant and electricity and gas distribution grids, so that the potential flexibility that Power-to-Gas plants can offer is neither under- or overestimated. The aim of this study is to understand the impact of different modeling approaches, in order to determine whether, and under which conditions, they could be acceptable. Results demonstrated that it is important to take into account the electric distribution network's topology, as the performance of Power-to-Gas plants could be affected by their placement in the network. The accuracy of the gas network and the Power-to-Gas plant models also plays an important role. In conditions of low gas consumption, it is necessary to take into account the gas flows and the linepack potentials of the gas network, as well as the interactions between Power-to-Gas plant components, in order not to underestimate the flexibility of the entire system.

## 4.1 Introduction

### 4.1.1 Scientific contribution

This study is a continuation of the analysis presented in Chapter 3, in which the interactions between an electricity grid, Power-to-Gas (P2G) plants and a gas network were analyzed through the use of detailed models that were able to fully consider the possible interactions among all the elements. However, that simulation approach may lead to an increase in the computation time, and to the problem of accessing data that the owners may not be willing to disclose.

The aim of this study is to present a methodological analysis capable of highlighting the pros and cons of different simulation approaches. In fact, depending on the main modeling approaches presented in the previous literature, one of the components that characterizes the multi-energy scenario is usually modeled in detail, while simplified models may be used for the other components. Table 4-1 shows that none of the studies previously mentioned in the introduction of Chapter 3 about P2G in distribution systems analyzed the dynamics that take place between all three of the main components of a system, i.e., the gas network, the electricity network and the P2G plants. On the basis of these issues, this study aims to investigate what are the effects of previous literature's most common simplifications, and to highlight whether, and in what cases, these simplifications could be acceptable.

The modeling aspects analyzed in this study are summarized below:

- *The impact of including or neglecting the electricity distribution network topology on the results.*

This aspect is closely related with the aim of the study. In terms of power and energy capacity, the determination of the potential flexible resources that can be installed over a wide area is not greatly affected when a simplified version of High Voltage (HV) is considered, as in [120], where the model only considers the equivalent capacity for different sub-regions, or in [52], where the potential of some flexible technologies was studied at a metropolitan level. However, I would argue that if the aim of a study is to both establish the impact of the distributed resources on the distribution system *and* the most effective location for the flexibility resources, the network topology has to be factored in, otherwise aspects like the impact on *local over-generation* and network operation indicators cannot be fully understood.

- *The impact of gas network pressure dynamics.*

It is worth noting that the gas demand, when a high-pressure gas network is considered, is normally high enough to absorb the Synthetic Natural Gas (SNG) generated by the surplus of renewables [125], [156]. Several studies did not

consider any constraint that might affect the injection of gas into the gas network [34], [52], [120]. However, if the P2G plant is connected to a medium pressure distribution grid, the demand for natural gas might be very low, especially in the summer season; this might create a hurdle for SNG injection. Hence, using a detailed gas network model, which considers both the gas flow and the pressure in the pipes, allows the *linepack* effect to be analyzed. The pipeline volume could therefore be used as a vessel to store natural gas inside the network itself. This intrinsic flexibility would allow a possible temporal mismatch between the injected and withdrawn gas to be identified and analyzed. Indeed, if neglected, such a temporal mismatch could lead to an underestimation of the SNG production of P2G plants, especially in the case of a low gas demand. In a multi energy-system scenario, whenever a P2G scenario is simulated, it is important that this flexibility is recognized in order to avoid underestimating the P2G flexibility potential [54].

- *The interaction between the internal units of a P2G plant: the electrolyzer, the hydrogen buffer and the methanation unit.*

In several papers (e.g., [123], [127], [134], [156], [157]), the energy conversion process of a P2G plant was simplified by only taking into consideration the overall process efficiency, that is without considering the separate processes or the interactions between the internal components. As pointed out in [125], this kind of approximation might lead to an underestimation of the flexibility of a P2G unit. In fact, if all the components are considered as single units, the electrolyzer, whose load should vary in order to offer flexibility to the electricity network, is limited by the operations of the methanation unit, which in turn is bounded by the constraints of the gas network. Conversely, when the three components are considered separately, the operation of the electrolyzer results to be more flexible, as the hydrogen is not directly absorbed by the methanation unit and is instead accumulated in the buffer.

Table 4-1. Overview of previous studies on P2G in a distribution network scenario and the modeling assumptions.

Ref.	EN model		GN model		P2G model	
	Grid topology	Notes	Pressure dynamic	Notes	Sub-components	Notes
Dalmau et al. 2015 [129]	YES	• Load flow analysis	NO	• A GN model was not included	NO	• Only P2H <sub>2</sub>
Mendoza et al. 2015 [130]	YES	• Load flow analysis	NO	• A GN model was not included	NO	• Only P2H <sub>2</sub>
Esterman et al. 2016 [128]	NO	• Load and generation balance	-	• No model details	-	• No model details were supplied
Khani et al. 2018 [134]	YES	• Load flow analysis	YES	• Gas flows calculated as a function of the nodal pressure	NO	• Entire process efficiency
Robinius et al. 2018 [126]	YES	• Load flow analysis (Gauss-Seidel method)	NO	• A GN model was not included	NO	• Only P2H <sub>2</sub>
El-Taweel et al. 2019 [127]	YES	• Load flow analysis	YES	• Gas flows calculated as a function of the nodal pressure	NO	• Entire process efficiency
Salomone et al. 2019 [133]	NO	• Load and generation balance	NO	• A GN model was not included	YES	• Electrolyzer, H <sub>2</sub> storage and methanation unit models
Mazza et al. 2019 [131]	YES	• Load flow analysis (Backward Forward Sweep method)	YES	• Gas flows calculated as a function of the nodal pressure	NO	• Only P2H <sub>2</sub>
Diaz-Londono et al. 2020 [135]	YES	• Load flow analysis (Backward Forward Sweep method)	NO	• A GN model was not included	NO	• Entire process efficiency
Mazza et al. 2020 [34]	YES	• Load flow analysis (Backward Forward Sweep method)	NO	• A GN model was not included	YES	• Electrolyzer, H <sub>2</sub> storage and methanation unit models
Weiss et al. 2021 [102]	NO	• Load and generation balance	NO	• A GN model was not included	YES	• Electrolyzer and methanation unit models
Cavana et al. 2021 [132]	YES	• Load flow analysis (Backward Forward Sweep method)	YES	• Gas flows calculated as a function of the nodal pressure	NO	• Only P2H <sub>2</sub>
Chapter 3	YES	• Load flow analysis (Backward Forward Sweep method)	YES	• Gas flows calculated as a function of the nodal pressure	YES	• Electrolyzer, H <sub>2</sub> storage and methanation unit models
<b>This chapter</b>	Comparison between the Backward-Forward-Sweep model approach and a load and generation balance approach		Comparison between an approach that takes into account the dynamics of network pressure and an approach that simplifies this aspect		Comparison between an approach that considers the subcomponents of P2G and an approach that only considers the efficiency of the P2G energy conversion	

## 4.2 The multi-energy system scenario

The scenario used for the analysis of this case study is the one presented in Chapter 3 in which the P2G technology was analyzed as a flexible solution, thanks to the coupling of the electricity and gas sectors (see Figure 4-1). The scenario is composed of a medium voltage distribution network electricity connected to the high voltage network by means of three High Voltage / Medium Voltage (HV/MV) transformers and a medium pressure distribution gas network. The two energy networks are connected through three P2G systems connected downstream of each HV/MV transformer. The scenario is assumed to cover the residential and tertiary sector electricity and gas users. Since the gas demand is mainly for domestic purposes and building heat, the gas consumption is highly seasonal-dependent; the gas demand during the coldest months is almost ten times higher than in summer, due to building heating. The scenario is characterized by a high number of installed Renewable Energy Sources (RES) plants (photovoltaic plant, PV, and wind turbines, WT), which are connected to the electricity distribution grid. The high RES penetration leads to local over-generations that create Reverse Power Flow (RPF) on the HV/MV transformers. The RES plants are not equally distributed in the network. More specifically, the part of the network downstream of the transformer 3 is the one that is most subjected to local RES over-generation (about 60% of the total over-generation takes place in this part of the network). The P2G flexibility is exploited to absorb RES over-generations and mitigate the RPF on the electricity network's transformers. The scenario has been simulated for one year, with a time discretization of 15 minutes. For more details on the scenario, the reader may back to Chapter 3.

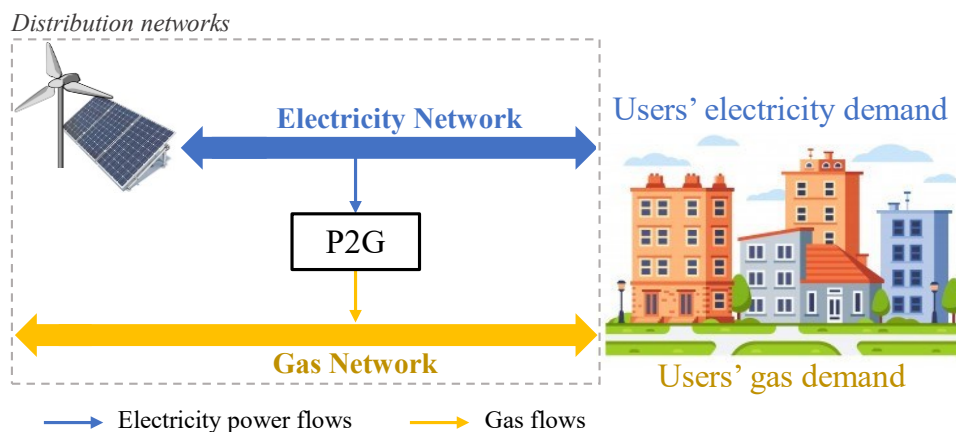


Figure 4-1. Schema of the analyzed multi-energy system.<sup>4</sup>

<sup>4</sup> The scenario analyzed in this chapter is the same as that described in Chapter 3. The scheme of the multi-energy system analyzed is the same as that of Chapter 3. For reasons of clarity, the scheme has also been reported in this chapter.

---

## 4.3 Mathematical approach and solution strategy

### 4.3.1 Analyzed modeling approaches

This section gives the main details of the various models that were used for this study. The various mathematical models can be found in Chapter 2. In order to evaluate the value of modeling, for each component of the multi-energy scenario (electricity network, gas network and P2G), two models were considered, one which takes into account the physics and internal dynamics of the component, and a simplified one which does not. The choice of these models aims to highlight three aspects of the multi-energy scenario:

- i)* the electricity topology and the electricity flows of the network,
  - ii)* the gas flows and pressure inside the gas network
- and
- iii)* the interactions between the sub-components of the P2G plant.

The same scenario was simulated three times; each simulation neglected a specific aspect: *(i)*, *(ii)* or *(iii)*. The various simulations thus obtained were compared with the simulation presented in Chapter 3 (the Reference simulation), in order to identify the effects of various simulation approaches.

#### Electricity network modeling approaches

The detailed model of the electricity network is a multi-nodal steady state model which takes into account the electricity flow in each branch, the voltage in each node and the withdrawals and injections of electricity in each node (see Figure 4-2). The model punctually simulates the generation of RES and the consumption of these resources, by both users and flexible resources (in this case P2G plants). The model therefore allows the local over-generations of RES that can cause RPF in the various transformers of the network to be taken into account.

The simplified electricity network model is a steady state single node model. Instead of simulating the whole electricity network, the electricity network is simplified by considering that all the loads and distributed generation are concentrated in a single node (see Figure 4-3). The different connections to the high voltage network (i.e., the three transformers) are not considered separately, but merged into a single connection point. The model is not able to identify any local RES over-generation that may affect the transformers of the distribution network, but only the total RES over-generation that affects the transmission system. Since it is not possible to identify in which part of the electricity network the overproduction occurs, the excess energy is distributed equally over the three P2G plants.

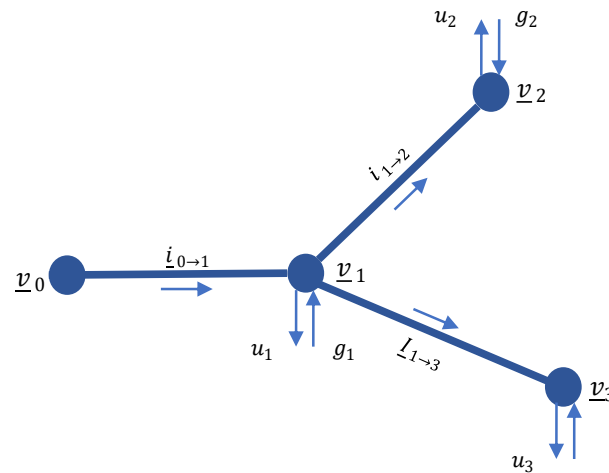


Figure 4-2. Scheme of the electricity network detailed model (multi-nodal model).

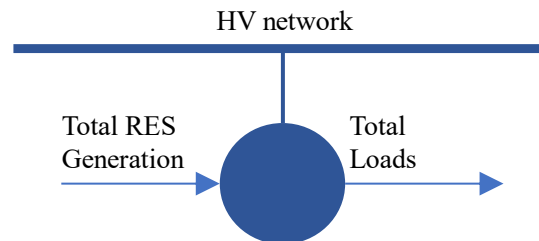


Figure 4-3. Schema of the electricity network simplified model (single node model).

## Gas network modeling approaches

The detailed model of the gas network is a dynamic multi-nodal model, which takes into account the gas flow in each pipe and the pressure in each node of the network (see Figure 4-4). This permit to analyze how the volume of the gas network can be exploited to accumulate the gas inside the network thanks to the linepack effect; storing gas inside the pipes increases the internal pressure of the network, and the accumulation can continue until the network pressure reaches the network operating pressure limit (in this case, 5 barg). If this feature was not taken into account, the injection of SNG into the network would be constrained by the instantaneous demand for gas, whereas, thanks to the physics of this system, the gas network allows a more flexible use of the methanation units.

The simplified gas network does not take into account either the pressure evolution of the network nodes or the gas flow in each network pipe. All the users' gas withdrawals and SNG injections are considered to happen at the same point (see Figure 4-5). If the gas demand is higher than the SNG injection, the difference is taken from the high pressure network. The model cannot take into account the linepack effect: hence, SNG can be injected as long as it does not exceed the gas demand.



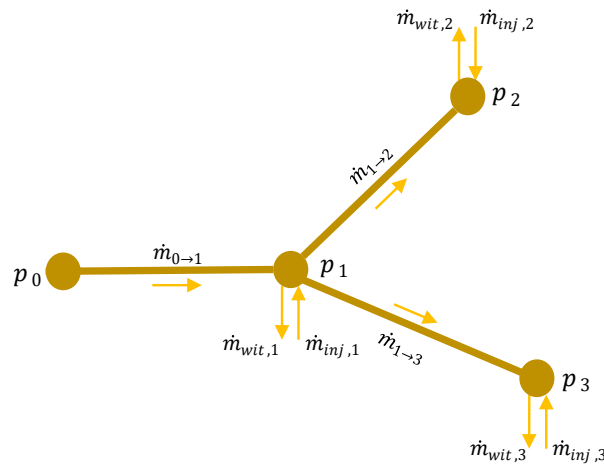


Figure 4-4. Scheme of the gas network detailed model (multi-nodal model).

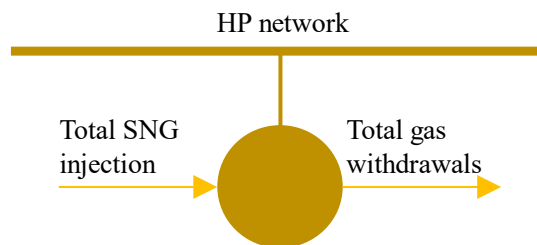


Figure 4-5. Schema of the gas network simplified model (single node model).

## P2G modeling approaches

The detailed model of the P2G plant is a multi-components model which simulates the main component of the P2G plant separately. These components are the Polymer Electrolyte Membrane (PEM) electrolyzer, the hydrogen buffer and the methanation reactor (see Figure 4-6). The hydrogen buffer allows a decoupling to be made between the electrolyzer and the methanation unit. The produced hydrogen is accumulated in the buffer, so that the electrolyzer can work, even though at that moment, the methanation unit does not use the produced hydrogen. Similarly, the methanation unit can use the hydrogen previously produced by the electrolyzer and operate independently.

The model allows the interaction between the plant components to be simulated. The model takes into account the ramp-rate constraints of the methanation unit and the storage capacity of the hydrogen buffer.

The P2G simplified model is a lumped parameters model which does not consider the interaction between the main components of the plant. The entire process is summarized by means of fixed conversion efficiencies (see Figure 4-7). The electricity consumed by the plant is directly converted into SNG, without considering the internal dynamics of the plant, such as the hydrogen accumulation

in the buffer, the methanation unit ramp rates or minimum load constraints. The electricity consumption and SNG generation are thus temporally linked to each other. For the sake of consistency, the energy conversion efficiency (from electricity to SNG,  $\eta_{P2G}$ ) of the simplified model has been set equal to the average efficiencies over the full year, as simulated by the detailed model.

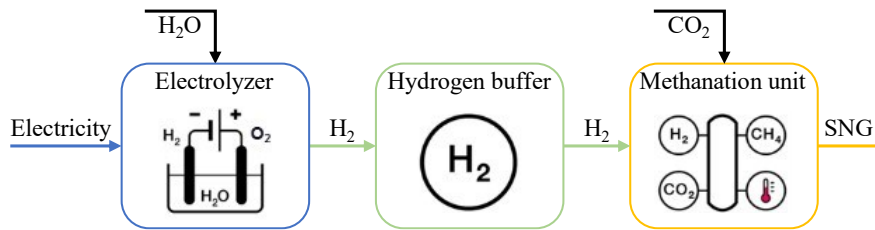


Figure 4-6. Scheme of the detailed P2G model (multi-components model).

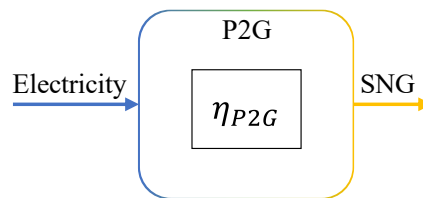


Figure 4-7. Scheme of the P2G simplified model (lumped parameters model).

### 4.3.2 Co-simulation architecture

The simulation of this case study involves five different modules:

- the time-synchronizer (Time-Sync);
- the controller;
- the P2G module;
- the electricity network (EN) module;
- the gas network (GN) module.

The three components of the multi-energy scenario (electricity network, gas network and P2G plants) were simulated both through the use of detailed models and through the use of the simplified models. In this scenario, three different simulations were performed, changing each time the type of model used for the simulation of one of the components (see Table 4-2). Detailed models and simplified models have the same input and output parameters. They can then be connected to the co-simulation loop by laying the same information flows in plug and play fashion. Figure 4-8 shows the flow of information that occurs during the co-simulation process. It should be noted that the information exchanged is the same as that described in Section 3.2. What changes are the modules involved.

Annual simulations were performed with a discretization of 15 minutes, resulting in a total of 35040 time steps.

Table 4-2. Models involved in the co-simulation loop.

Model	Case study 2		
	Simulation 1	Simulation 2	Simulation 3
Controller	X	X	X
Time-Sync	X	X	X
Electricity network (detailed)		X	X
Electricity network (simplified)	X		X
Gas network (detailed)	X		X
Gas network (simplified)		X	
DH network and CP2H			
P2G (detailed)	X	X	
P2G (simplified)			X
Building and LP2H			
Electric battery			

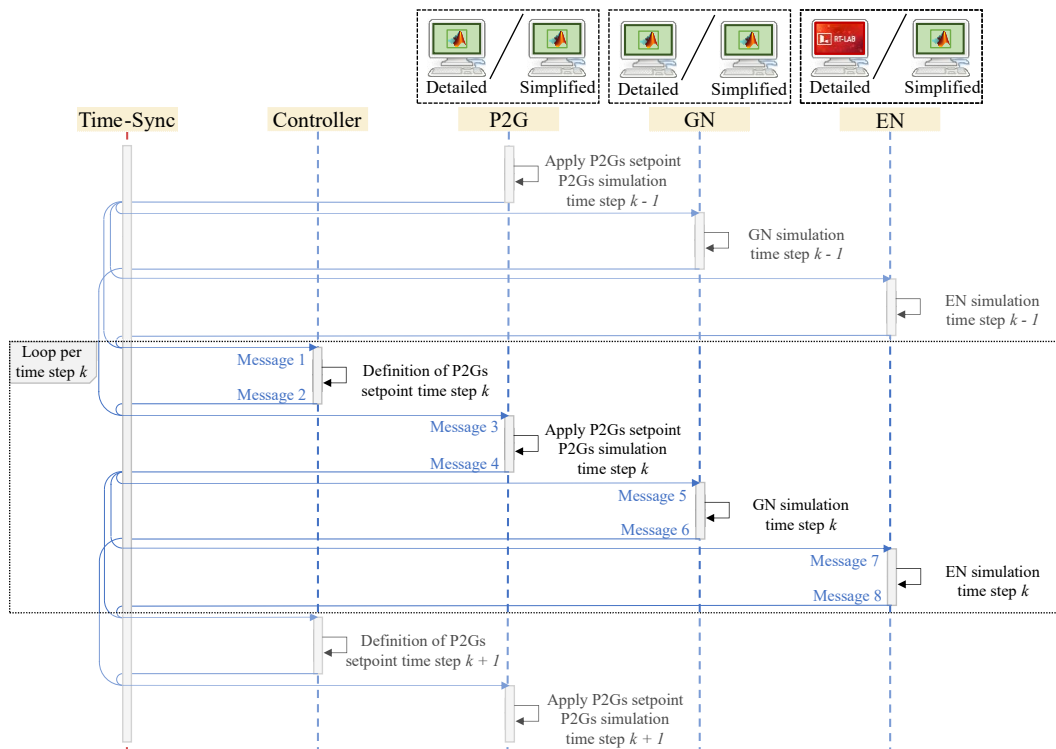


Figure 4-8. Sequence of interactions among co-simulation modules (with detailed and simplified models).

## 4.4 Results and discussion

This section shows the results of the simulations obtained with the various models. The first simulation, the Reference simulation, was performed using the detailed models of all three components of the multi-energy scenario. The results of this simulation were presented in Chapter 3. Subsequently, three other simulations were made, neglecting each time a different aspect of the modeling. The results of the various simulations were then compared with the Reference simulation. Table 4-3 summarizes the simulations performed and the models used.

Table 4-3. List of simulations.

	EN model	GN model	P2G model
Reference simulation	Detailed	Detailed	Detailed
EN simplified simulation	<i>Simplified</i>	Detailed	Detailed
GN simplified simulation	Detailed	<i>Simplified</i>	Detailed
P2G simplified simulation	Detailed	Detailed	<i>Simplified</i>

### 4.4.1 Value of electricity network modeling

The electricity network simplified model does not consider the different HV/MV connection points. Even though the overall network is balanced, in terms of energy generation and consumption, the optimum operation condition may not have been reached, due to a local load/generation mismatch. For example, Figure 4-9 compares the energy balance of the whole electricity network in the Reference simulation versus the one simulated with the simplified electricity network for a typical winter day. The EN simplified simulation underestimates RPF; the P2G plants in EN simplified simulation appear to be able to absorb all the RES over-generation, while the RES over-generations in the Reference simulation are not totally absorbed, thus causing RPF (see the orange area in Figure 4-9a). Moreover, it seems that P2G#3 is activated in the Reference simulation, even when there is no need to actively absorb over-generation (i.e., during the night-time).

However, if the energy balance is computed at each HV/MV transformer level, local unbalances appear (see Figure 4-10)<sup>5</sup>.

<sup>5</sup> In order to evaluate the local unbalances in the EN simplified simulation (which does not consider the HV/MV transformers), the reference model of the electricity network was run with P2G electricity load profiles obtained from the EN simplified simulation.

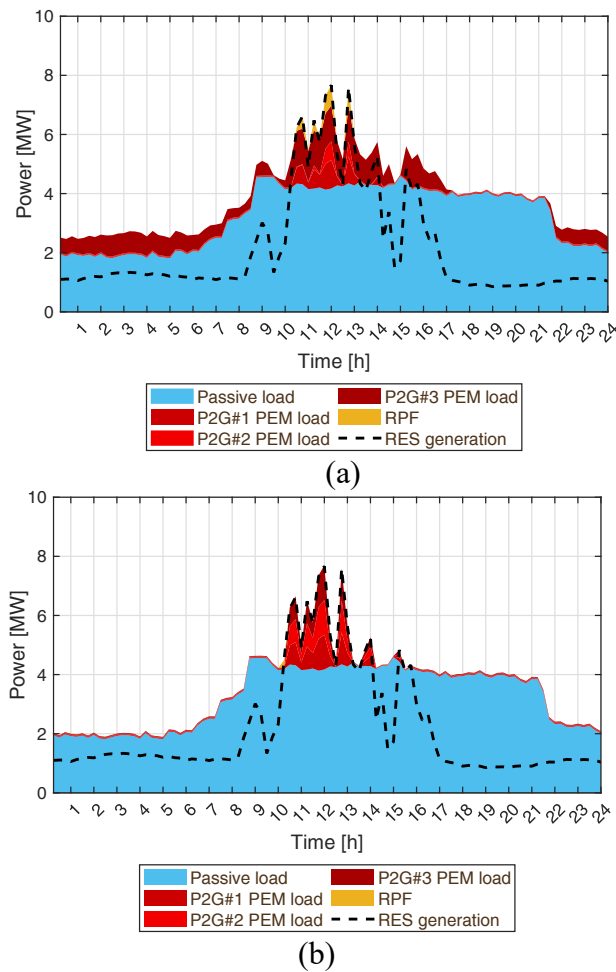


Figure 4-9. Electricity balance referring to the whole grid (winter day): (a) Reference simulation and (b) EN simplified simulation.

Since the simplified model is not able to define where over-generation occurs, the activation of the P2G plants has not been properly coordinated. It could happen that a P2G is sometimes activated, even though there is no need to absorb local unbalances (see the balance of TR#2 in Figure 4-10) and that some local RES over-generations are not detected by the simplified model (see the balance of TR#3 in Figure 4-10). For these reasons, the optimal coordination of various P2G plants cannot be achieved and transformers are not used appropriately. P2G#3 results to be used about 40% less frequently than in the Reference simulation, whereas P2G#2 is used about 50% more (see Table 4-4). It can be noted that, in the EN simplified simulation, the P2G load (i.e., the sum of the electricity consumption of all three plants) is around 10% lower than in the Reference simulation. This also affects the total SNG production of the plants, which leads to an underestimation of the injection of SNG into the gas network (see Table 4-5). This is due to the underestimation of the local RPF, whose sum results to be higher than the one that is seen by the transmission system. It is important to point out, that the more different the local electricity imbalances are, the more marked are the difference between the two models. In fact, the generation disparity within the network is

greater in the winter months; in this period, about 65% of the over-generation takes place in the network portion derived from TR#3. Furthermore, the difference in the use of P2G plants is about 20% (see Table 4-6). Unlike in the winter months, the local grid mismatches are more homogeneous in the summer months, and the difference between the two modeling approaches is reduced to about 5%.

The RES over-generation, calculated by the simplified model (without considering the losses due to the Joule effect), corresponds to the network unbalance that affects the transmission system. Thus, even though the simplified model does not allow an optimum dispatchment of the P2G plant utilization or the evaluation of the best P2G plant network connection, it could be used for a high level qualitative evaluation of P2G flexibility potential for transmission system balancing purposes (as shown in [52] and [133]).

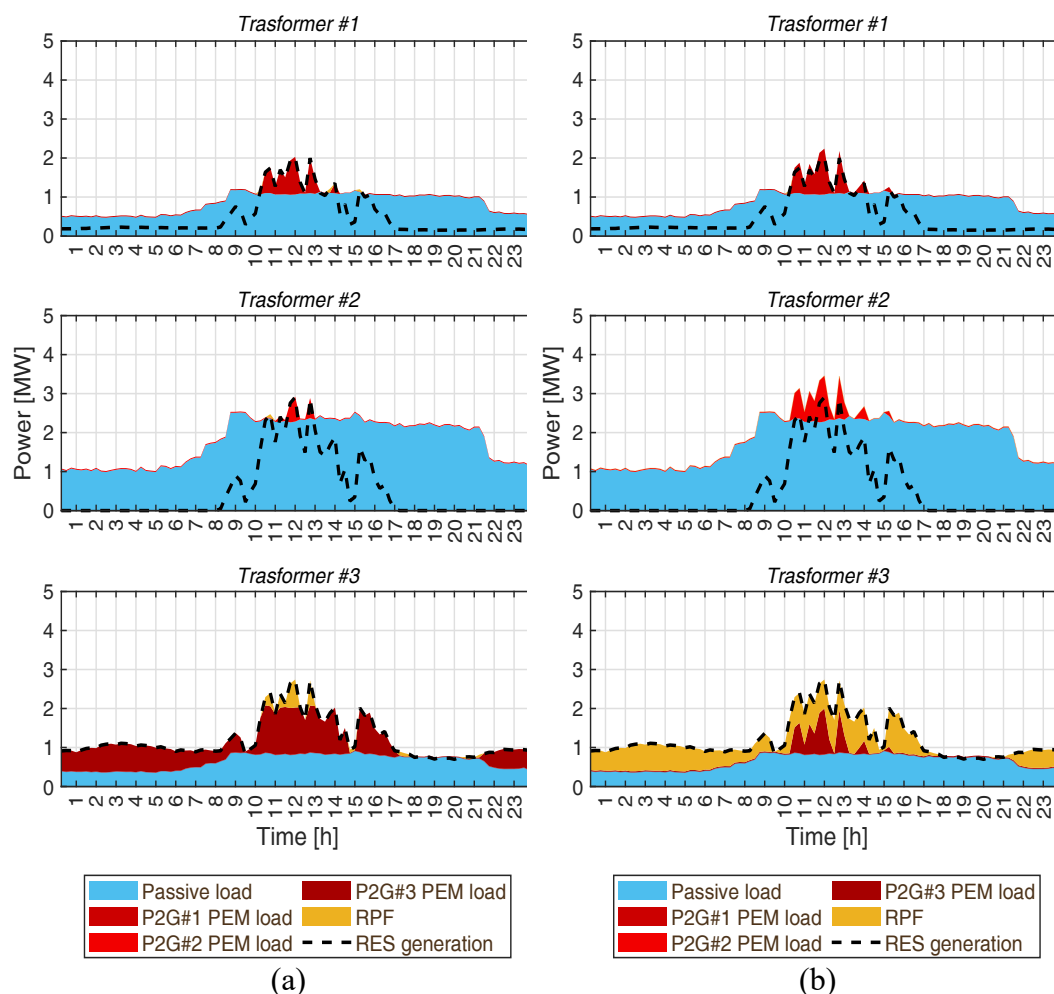


Figure 4-10. Electricity balance on HV/MV transformers (winter day): (a) Reference simulation and (b) EN simplified simulation.

Table 4-4. P2G plant results.

	Heating season [GWh]				Non-heating season [GWh]				Whole year [GWh]			
	P2G#1	P2G#2	P2G#3	Tot	P2G#1	P2G#2	P2G#3	Tot	P2G#1	P2G#2	P2G#3	Tot
<i>Reference simulation</i>												
El. cons	0.72	0.50	1.69	2.90	1.32	0.98	2.14	4.44	2.03	1.48	3.83	7.34
SNG	0.29	0.19	0.79	1.27	0.58	0.40	1.02	2.01	0.87	0.59	1.81	3.27
<i>EN simplified simulation</i>												
El. cons	0.80	0.80	0.80	2.40	1.44	1.43	1.40	4.26	2.23	2.23	2.20	6.66
SNG	0.33	0.33	0.33	1.00	0.64	0.64	0.62	1.91	0.98	0.97	0.96	2.90
<i>GN simplified simulation</i>												
El. cons	0.71	0.50	1.68	2.90	0.85	0.81	1.56	3.23	1.57	1.31	3.25	6.12
SNG	0.29	0.19	0.79	1.27	0.35	0.34	0.72	1.42	0.64	0.53	1.51	2.68
<i>P2G simplified simulation</i>												
El. cons	0.72	0.50	1.70	2.92	1.04	0.76	1.97	3.77	1.76	1.26	3.67	6.69
SNG	0.30	0.19	0.78	1.27	0.46	0.32	0.91	1.69	0.76	0.52	1.69	2.96

Table 4-5. Gas network results.

	Heating season [GWh]	Non-heating season [GWh]	Whole year [GWh]
<i>Reference simulation</i>			
Gas demand	31.65	4.37	36.02
Imported Gas	30.38	2.37	32.75
Imported Gas	1.27	2.00	3.27
<i>EN simplified simulation</i>			
Gas demand	31.65	4.37	36.02
Imported Gas	30.65	2.47	33.12
SNG	1.00	1.91	2.90
<i>GN simplified simulation</i>			
Gas demand	31.65	4.37	36.02
Imported Gas	30.38	2.96	33.34
SNG	1.27	1.42	2.68
<i>P2G simplified simulation</i>			
Gas demand	31.65	4.37	36.02
Imported Gas	30.38	2.68	33.06
SNG	1.27	1.69	2.96

Table 4-6. Electricity network results.

	Heating season [GWh]				Non-heating season [GWh]				Whole year [GWh]			
	TR#1	TR#2	TR#3	Tot	TR#1	TR#2	TR#3	Tot	TR#1	TR#2	TR#3	Tot
<i>Reference simulation</i>												
EL demand	3.70	7.80	2.79	14.29	4.12	8.71	2.97	15.80	7.82	16.50	5.76	30.08
RES	2.41	3.23	4.12	9.76	3.90	5.68	5.39	14.97	6.32	8.91	9.51	24.73
Surplus	0.67	0.46	2.04	3.17	1.40	1.08	3.08	5.55	2.07	1.54	5.11	8.72
Absorbed surplus	0.62	0.40	1.61	2.63	1.23	0.90	2.07	4.20	1.86	1.30	3.68	6.83
RPF	0.05	0.06	0.43	0.53	0.16	0.18	1.01	1.35	0.21	0.24	1.44	1.88
<i>EN simplified simulation</i>												
EL demand	-	-	-	14.29	-	-	-	15.80	-	-	-	30.08
RES	-	-	-	9.76	-	-	-	14.97	-	-	-	24.73
Surplus	-	-	-	2.45	-	-	-	5.09	-	-	-	7.54
Absorbed surplus	-	-	-	1.98	-	-	-	3.80	-	-	-	5.78
RPF	-	-	-	0.46	-	-	-	1.29	-	-	-	1.76
<i>GN simplified simulation</i>												
EL demand	3.70	7.80	2.79	14.29	4.12	8.71	2.97	15.80	7.82	16.50	5.76	30.08
RES	2.41	3.23	4.12	9.76	3.90	5.68	5.39	14.97	6.32	8.91	9.51	24.73
Surplus	0.67	0.46	2.04	3.17	1.40	1.08	3.08	5.55	2.07	1.54	5.11	8.72
Absorbed surplus	0.62	0.40	1.61	2.63	0.77	0.73	1.49	2.98	1.39	1.13	3.10	5.61
RPF	0.05	0.06	0.43	0.54	0.63	0.35	1.59	2.57	0.68	0.41	2.02	3.10
<i>P2G simplified simulation</i>												
EL demand	3.65	7.74	2.74	14.13	4.07	8.66	2.91	15.64	7.72	16.40	5.65	29.77
RES	2.41	3.23	4.12	9.76	3.90	5.68	5.39	14.97	6.32	8.91	9.51	24.73
Surplus	0.68	0.47	2.06	3.21	1.42	1.09	3.10	5.61	2.10	1.56	5.17	8.82
Absorbed surplus	0.64	0.41	1.65	2.70	0.98	0.68	1.92	3.58	1.61	1.10	3.57	6.28
RPF	0.04	0.06	0.42	0.51	0.44	0.41	1.18	2.03	0.48	0.46	1.60	2.55



## 4.4.2 Value of gas network modeling

Unlike the detailed model, the simplified model does not take into account the pressure or gas flows in the gas network. Nevertheless, whenever only the heating season is considered, the results obtained with the simplified model are almost the same as those of the Reference simulation (see Table 4-4, Table 4-5, Table 4-6). In these conditions, the production of SNG covers only 4% of users' gas demand (see Table 4-5) and, at any time step, the production of SNG is considerably lower than the users' gas demand (see Figure 4-11). All the injected SNG is directly consumed by the users and this behavior is clearly simulated by both models.

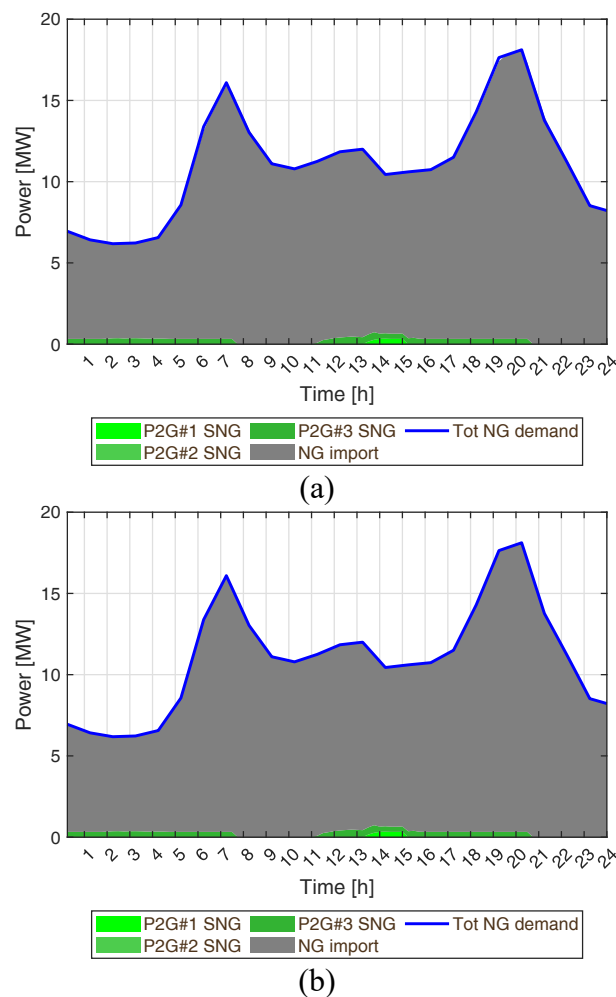


Figure 4-11. Gas network balance (winter day): (a) Reference simulation and (b) simplified GN simulation.

The demand for gas is highly seasonal, due to the use of gas to heat buildings. In the scenario analyzed, the gas demand during the hot season is about 10 times lower than in the winter season. In summer, the SNG production could exceed users' gas demand (see Figure 4-12a). When this happens, the produced SNG could be stored by exploiting the gas network's volume, thanks to the linepack effect. The accumulation of gas increases the pressure in the network (see the red curve in

Figure 4-12a). When the maximum operating pressure in the network is reached, the SNG injection must be reduced (in the case reported in Figure 4-12a, the pressure reaches a level of 5 bar<sub>g</sub> at 15:15 and the P2G#1 and P2G#2 methanation units block their SNG injection to let the network lie within its operation pressure range). The accumulated SNG is used in the following hours to meet the gas demand (see the white areas in Figure 4-12a). When this happens, the gas stored inside the network decreases, as does the network pressure. The gas network simplified model does not allow the network linepack to be taken into account: SNG injection is limited in order to always be lower than the network gas demand (see Figure 4-12b). Therefore, ignoring the intrinsic flexibility of the gas network limits the use of methane gas units, and, in the hot season, leads to underestimating the SNG production by about 30% (see Table 4-5).

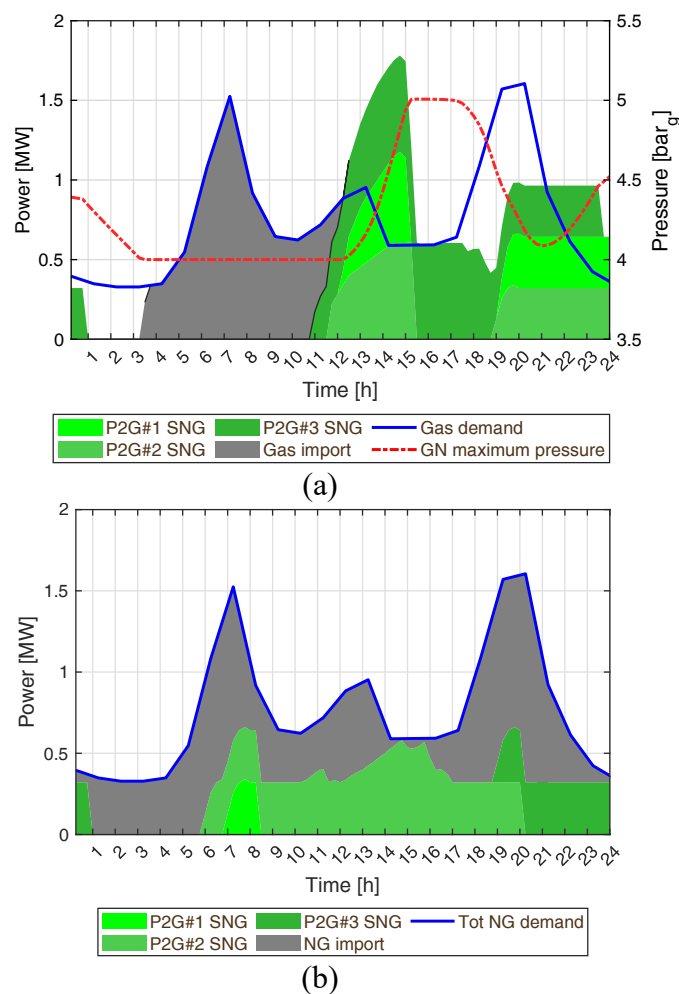


Figure 4-12. Gas network's balance and pressure (summer day): (a) Reference simulation and (b) simplified GN simulation.

The limitation of the methanation units also affects the functioning of the electrolyzers: if the methanation units are unable to consume the hydrogen accumulated in the buffers, once the saturation of the hydrogen buffers is reached, the electrolyzers have to block their production of hydrogen and, consequently, they

are no longer able to offer flexibility to the electricity grid. The underestimation of the flexibility of the gas network, induced as a result of the use of the simplified model, not only affects the gas network, but also the electricity network. In fact, the electrolyzers result to be less flexible, and to cause an overestimation of almost 190% of the RPF generated by the HV/MV transformers during the hot season (see Table 4-6 and Figure 4-13).

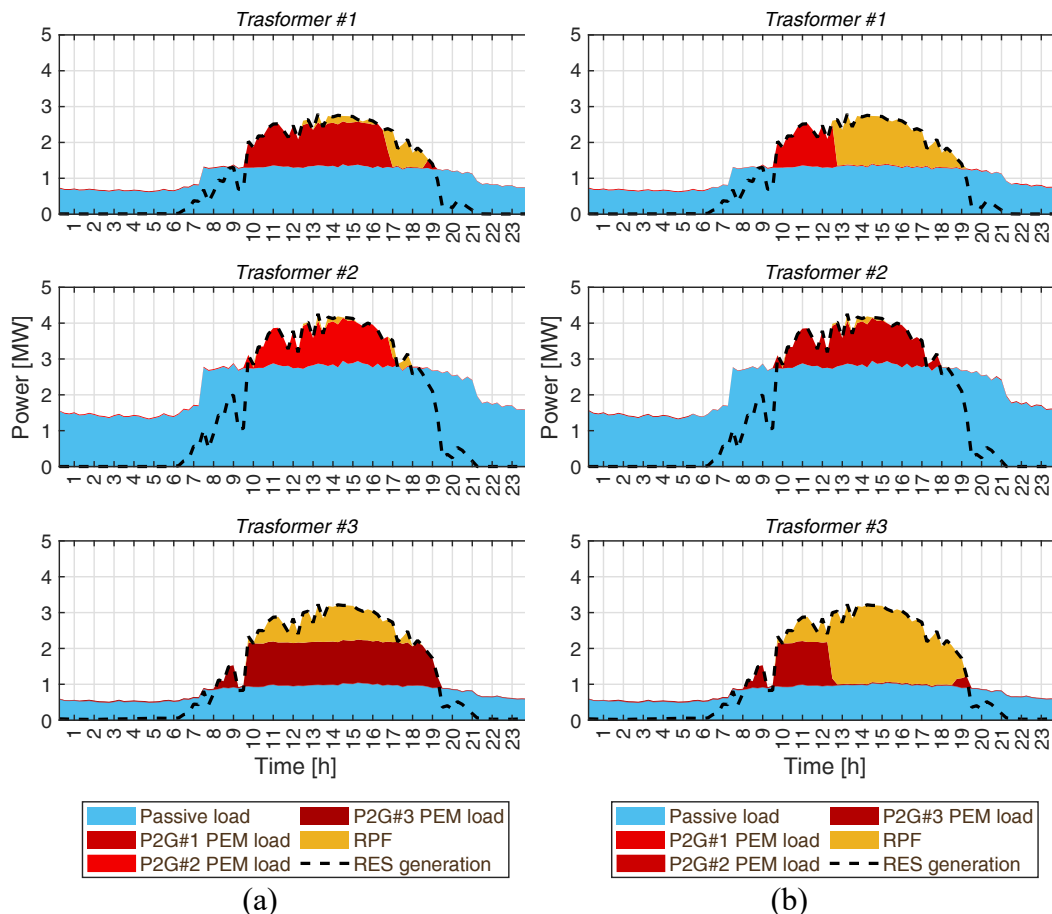


Figure 4-13. HV/MV transformers' balance (summer day): (a) Reference simulation and (b) simplified GN simulation.

#### 4.4.3 Value of P2G modeling

The P2G simplified model neglects the presence of the hydrogen buffer. In such a simulation, the electricity energy is considered to be directly converted into SNG, without any possibility of storing hydrogen. Hence, the SNG production starts earlier than in the Reference simulation. Whenever the P2G reference model is used, the methanation units are only turned on when the hydrogen buffers have reached a predetermined state of charge (see Figure 4-14). Figure 4-14 shows that the production of SNG in the simplified P2G simulation is less uniform than in the Reference simulation, as the former model does not consider the ramp up and ramp down constraints of the plant. Consequently, the SNG production follows the much faster characteristic variation of the electrolyzers. Apart from this misalignment,

the use of this simplification during the heating season, when there is a high gas demand, does not substantially change the simulation results (see Table 4-4, Table 4-5, Table 4-6). The small differences that can be seen in Table 4-4, which are lower than 4%, are mainly due to the fact that the reference model takes into account the change in energy conversion efficiency for different working conditions, whereas the simplified model considers a constant average efficiency.

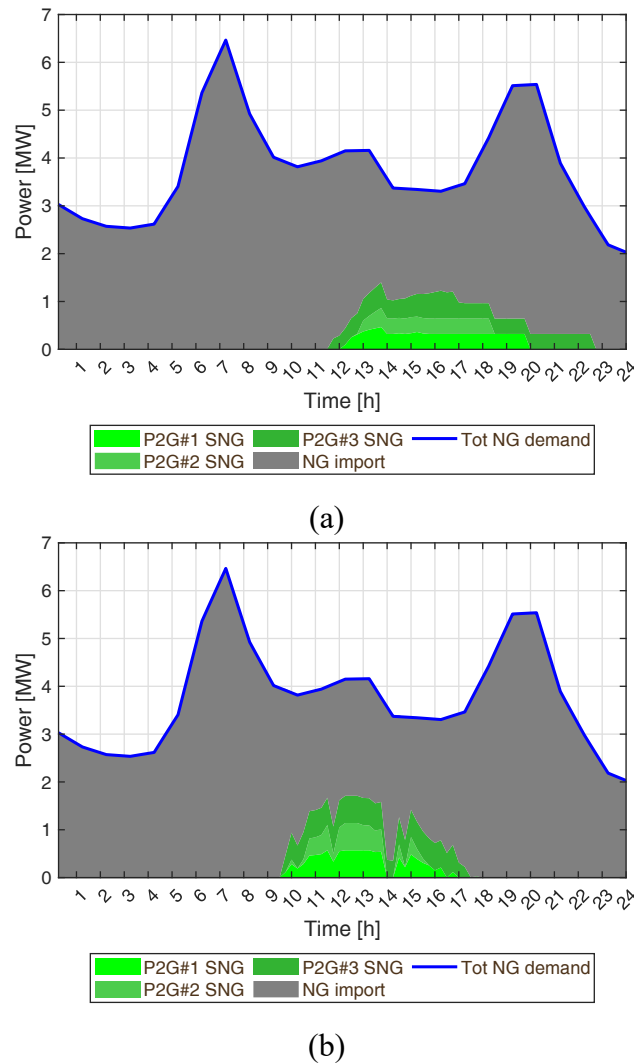


Figure 4-14. Gas network balance (Mid-season day): (a) Reference simulation and (b) simplified P2G simulation.

However, in the summer season, due to the low gas demand, the gas network becomes less flexible, as it can accept a smaller quantity of SNG. In this case, neglecting the flexibility given by the decoupling of the methanation units from the electrolyzers affects the results of the simulation. In fact, when the gas network reaches the maximum allowed pressure, the electrolyzers could continue to work by accumulating the hydrogen produced inside the buffer. In the case of simplified P2G, though, when the pressure in the gas network reaches its maximum limit at

12:45 (see Figure 4-15), the electrolyzers must also limit their loads (see Figure 4-16).

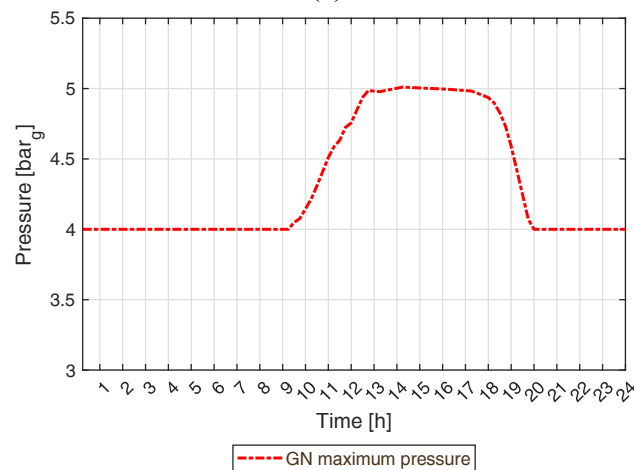
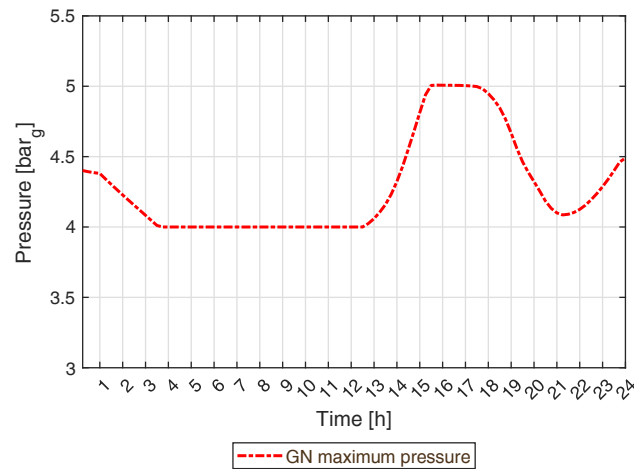


Figure 4-15. Gas network pressure (summer day): (a) Reference simulation and (b) simplified P2G simulation.

It should be noted that, even in the Reference simulation, the electrolyzer may be affected by restrictions (see P2G#1 in Figure 4-16a): this may happen when the hydrogen buffer reaches its maximum SoC, and the hydrogen production needs to be reduced to prevent an overpressure being created in the buffer. Nevertheless, without considering the hydrogen buffer, the P2G plants have less flexibility, which leads to the P2G potential being underestimated during the low gas demand period (i.e., in the summer season), and the use of P2G plants being underestimated by about 10%, which is also reflected by an equal underestimation of the SNG injection in the gas network. Moreover, the RPF on the electricity network is overestimated by about 150% (see Table 4-4, Table 4-6, Table 4-5).

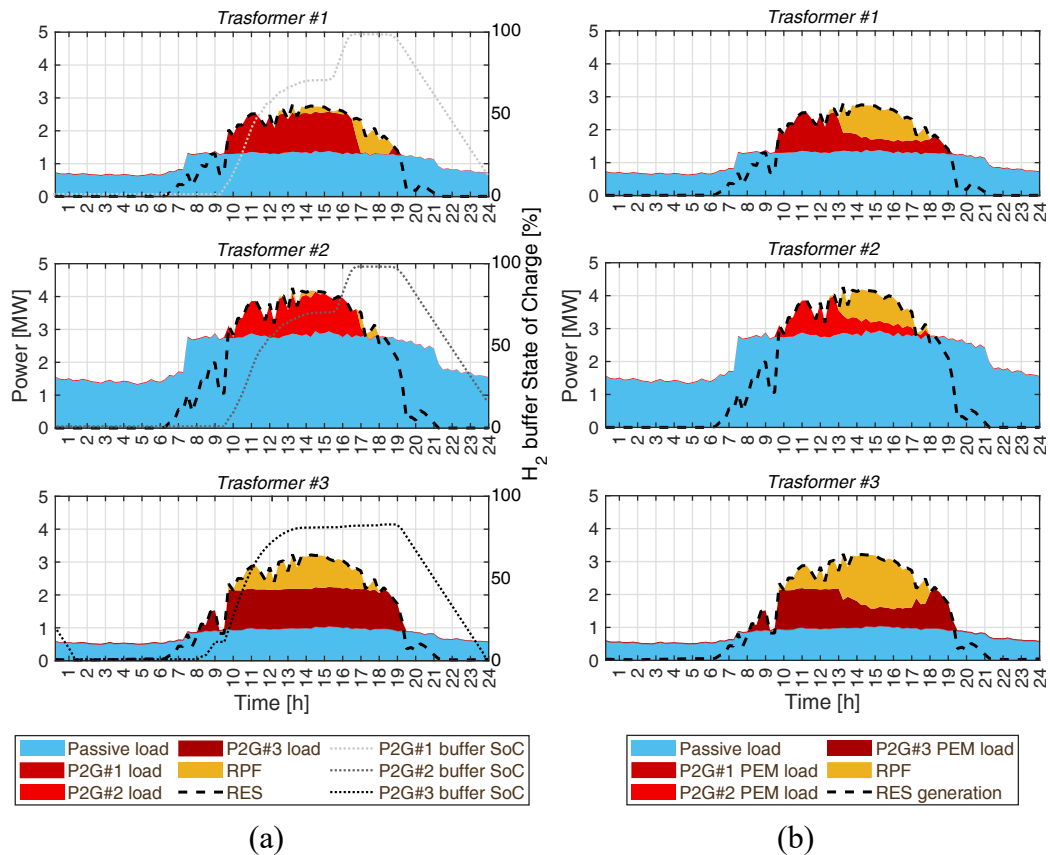


Figure 4-16. HV/MV transformers' balance and hydrogen buffer's SoC: (a) Reference simulation and (b) simplified P2G simulation.

## 4.5 Conclusions

This case study discusses the use of Power-to-Gas (P2G) technology to balance Renewable Energy Sources (RES) production at the distribution level. The study presents a methodological analysis on the impact of different simulation approaches for this type of multi-energy scenarios. Critical conditions for the operation of P2G at the distribution level can in fact easily arise: the choice of the most appropriate modeling approaches is necessary, in order to correctly simulate the dynamics between the various components of the multi-energy system (the electricity network, the gas network and P2G plants) and avoid overestimating or underestimating the potential flexibility of this solution.

The results obtained using detailed models of the three components have been compared with those obtained by simulating scenarios in which different modeling aspects had been neglected. Three different simulations were carried out. In each simulation, one of the following aspects was neglected: *i*) the topology of the electricity distribution network and, consequently, the local power flows that occur within it, *ii*) the topology of the gas network, the gas flows and the evolution of the network pressure and *iii*) the intermediate energy conversion processes and storage lying in P2G plants between electricity and Synthetic Natural Gas (SNG).

---

The main conclusions that can be drawn from these analyses can be summarized as follows:

*i) Electricity distribution system modeling*

Taking into account the topology of the electricity network makes it possible to evaluate in which area of the electricity network the over-generations of renewable energy occur. Hence, it allows one to choose the most appropriate resources to use, i.e., those closest to the electricity unbalances. The use of an electricity network model allows both the dispatching of flexible resources to be optimized and the best connection nodes for these resources to be evaluated.

- It is essential to consider electricity distribution network power flows, if flexible resources are used to optimize the distribution network. Local RES over-generations can only be highlighted by taking into account the distribution network topology. It is useful to analyze these phenomena, because they can create Reverse Power Flow (RPF) on HV/MV transformers, thus leading to problems for the operation of the distribution system. Local over-generations of renewables can be mitigated, thanks to distributed flexible resources; if these local imbalances are not detected, the potential benefit of using flexible distributed resources is underestimated.
- The single node representation of the electricity system cannot detect local overproductions. Nevertheless, it may be employed to evaluate whether it would be useful to offer the flexibility resources for the operation of the transmission system.

*ii) Gas network modeling*

Simulating the dynamics of the gas network makes it possible to more precisely evaluate the flexibility offered by this infrastructure, because linepack effect permits that the volume of the gas network be used to store the production of SNG. This storage is possible as long as the pressure in the network remains within the allowable pressure range. Hence, by allowing the gas demand to be decoupled from the SNG production, the gas network acts like a gas storage device.

- The gas network flexibility could be relatively low in low gas demand periods. Indeed, under certain conditions, the gas withdrawal can be lower than the SNG injection. When this happens, the gas network can reach saturation. In these cases, the SNG injections should be limited. Under these conditions, it is possible to evaluate the linepack potential and, consequently, the gas network's flexibility, by considering the gas flows and the network pressure evolution. Since all the components in a multi-energy system scenario are closely connected, an underestimation of the gas network flexibility implies a lower flexibility of the connected P2G plants, which in

turn leads to an underestimation of their utilization and also affects the operation of the electricity network (measured as residual RPF).

- The gas demand in a high gas demand scenario is normally much higher than for SNG injections. Such a high gas withdrawal makes the gas network flexibility higher, because the injected SNG may be absorbed directly by the user, without causing network saturation problems. In these cases, the linepack flexibility of the network may be neglected without affecting the simulation results.

### *iii) P2G plant modeling*

A detailed model of a P2G plant allows all the processes that take place in a P2G plant to be simulated. This makes it possible to consider the decoupling between the methanation unit and the electrolyzer. The electrolyzer can therefore work even when, due to external restrictions, the methanation unit cannot operate. Taking these factors into account allows the flexibility of these plants to be properly estimated.

- On the one hand, in low gas demand periods, when the flexibility of the gas network is lower, the utilization of P2G plants may be constrained, because no SNG injection is allowed. In these circumstances, neglecting the interactions between the various components of the P2G system leads to an underestimation of the P2G flexibility and, therefore, an underestimation of both the possible SNG production and the services that these resources can offer to the electricity system.
- On the other hand, in high gas demand periods, the flexibility offered by the gas network is high enough to compensate for the underestimation of the P2G plant flexibility. In these conditions, the utilization of a simplified model that does not simulate the entire electricity-hydrogen-SNG chain in the P2G plant allows the energy flows within the multi-energy system, in which P2G plants are used to offer flexibility to the electricity network, to be evaluated with a good level of approximation.



## **Chapter 5**

### **Case-study 3 – Techno-economic analysis of centralized Power-to-Heat plants in a district heating and electricity distribution network system**

Chapter 5 analyzes the centralized Power-to-Heat energy conversion process carried out by heat pumps connected to a district heating network. Centralized Power-to-Heat plants are used to provide heat to a district heating and, at the same time, to provide flexibility to the electricity grid. The storage of energy within the district heating sector, in the form of heat, enables a flexible use of centralized Power-to-Heat plants. This flexibility can be exploited to absorb the local over-generation of renewable energy sources in the distribution system, which could cause problems in balancing electricity generation and consumption. Three different configurations were analyzed, based on three possible connection points of the centralized Power-to-Heat systems with the electricity network. The energy flows between the electricity and thermal sectors enabled by the centralized Power-to-Heat technology were analyzed. The installation of centralized Power-to-Heat systems was also evaluated from an economic point of view by calculating the Net Present Value and the Simple Pay Back time of the investment cost. The results showed that, thanks to their high heat production efficiency, the plants are always advantageous, even when their flexibility is not exploited. The flexible use of these systems allows the centralized Power-to-Heat plants to shift their electric loads in periods of renewable over-generation, with significant benefits from an economic point of view.

## 5.1 Introduction

### 5.1.1 State of the art

The term centralized Power-to-Heat (CP2H) refers to large-scale technologies that convert electricity into heat. In case study 3, the Power-to-Heat energy conversion process is obtained by means of geothermal heat pumps. CP2H systems are used in district heating (DH) to increase the water temperature to a maximum temperature of about 100°C [158]. Their thermal power ranges between some kW<sub>th</sub> to more than 10 MW<sub>th</sub>. Air [160], groundwater [161], river/lake/seawater [162], drinking water [163] and waste heat [164] are among the sources that can be used to feed heat pumps in DH networks. In 2017, the analysis reported in [165] showed that 149 units larger than 1 MW<sub>th</sub> were connected to DH networks in Europe (for a total of 1580 MWh<sub>th</sub> heat produced), and that the technical level of the heat pumps currently available for DH installation is advanced enough to allow an even larger diffusion. In order to obtain high performance heat pumps, it is necessary to exploit heat that is available at low or close to ambient temperatures. In [164], the availability of eight types of heat sources was analyzed: low-temperature industrial excess heat, supermarkets, waste-water, drinking and usage water, groundwater, river, lake, and sea water. The analysis showed that potential sources exist almost everywhere in DH areas and that sea water, when available, represents an important opportunity. Various works in the literature have dealt with installing heat pumps in DH networks, which can also provide important economic benefits. An heat pump connected to a DH was analyzed in [166], considering air, seawater or groundwater as the evaporating sources. The economic benefit was shown to range from €2500 to €6800 per house, depending on the choice of the evaporating source, economic lifetime and discount rate.

Ommen et al. [167] compared the performances of five possible heat pump configurations in Combined Heat and Power (CHP) driven DH systems, considering different network temperatures, production technologies and fuels. The analysis clearly showed that a change in the supply temperature has a more significant effect on power production than the modification of the supply temperature, and that a configuration that increases the source temperature up to the supply temperature is a convenient choice. The best option for heat pumps at the CHP level is to increase the return temperature, which results in the lowest operation cost. As far as the connection of heat pumps is concerned, a study on the installation of heat pumps with a high temperature and a large sized DH was conducted in [168]. Results showed that connecting heat pumps to distribution networks provided a larger Coefficient of Performance (COP) than a transmission network, and that a large number of full-load heat pumps could be reached (3500-4000 instead of 2500-3000).

As discussed in [169], the classic way of controlling CP2H plants in DH systems is to balance the heat production and demand. In addition, it is possible to

exploit the flexibility of these plants to reduce production costs and/or environmental impacts by providing ancillary services and assistance in the integration of Renewable Energy Sources (RES) [169]. Most of the previous research analyzed the advantages of exploiting the flexibility of CP2H plants at the regional or national level. The available heat sources for use in CP2H systems in Denmark were mapped in [164]. The authors reported that the use of centralized heat pump systems can benefit from the use of electricity during periods of high RES generation. The potential of CP2H plants in the Baltic countries was analyzed in [170]. Results showed that the CP2H plant took advantage of the available high renewable production. Another study, set in the North-Eastern part of the United States, analyzed several solutions enabled by CP2H technologies in order to take advantage of the electricity surpluses that occurred at the national level [171]. The authors of [172] investigated how the utilization of CP2H in DH could increase the RES market value of Northern European Countries. The flexibility enabled by coupling the DH and electricity sector by means of CP2H and a combined heat and power system was investigated for a future Italian scenario in [173]. The impact of different tax designs on the flexibility enabled by CP2H systems combined with centralized thermal storage was studied for the Danish system in [174]. Still in the Danish context, the role of electricity grid tariff schemes for the flexible operation of CP2H plants connected to the DH was investigated in [175].

### 5.1.2 Scientific contribution

To the best of my knowledge, no previous study has investigated the potentials that of CP2H systems at a local level have to balance the over-generations of RES at the distribution system level. In order to fill this gap, case study 3 analyzes how CP2H systems could be inserted into a distribution context as a flexible connection point between the electricity and DH sectors. CP2H systems are used for sector coupling for two functionalities: high efficiency heat production in a DH system and to provide flexibility and absorb local RES over-generation.

A scenario based on real data from the electricity network and the district heating network of the city of Turin (in the north-west of Italy) was considered for this study. Although the scenario is based on the energy system of this specific city, results and conclusions could be generalizable to other cities served by high temperature networks. Three distinct configurations with different connection points within the electricity distribution system were analyzed. This allowed our research group to enquire into how a different connection point of the distributed resources could affect the performance of the plants. Moreover, two different control strategies were applied: in the first one, the DH heat flows were optimized by maximizing the use of the heat produced by the CP2H systems; in the second control strategy, in addition to providing heat to the DH, the CP2H systems were used to provide flexibility to the electricity sector. This distributed flexible resource was evaluated from a technical and an economic point of view. Indeed, this study

analyzed the energy flows between electricity and the DH sector enabled by the CP2H technology, as well as the economic profitability of these plants.

## 5.2 Scenario description and techno-economic parameters

A multi-energy system, consisting of DH Sub-Networks (SN) and a medium voltage (MV) distribution Electricity network (EN), is here analyzed, in order to establish the benefits of coupling the electricity and district heating sectors at the distribution level (see Figure 5-1). The CP2H plant absorbs the EN electricity and injects heat into the DH. The CP2H plants preheat the return flows of the district heating network, thus decreasing the heat load required by the central system that feeds the district heating. The CP2H systems can operate flexibly, thanks to the presence of Thermal Energy Storages (TES) installed at the district heating sub-network level. Moreover, the CP2H systems can store the energy taken from the electricity network inside the thermal storages in the form of heat, which can subsequently be used to satisfy the thermal demand of the DH. This scenario has been simulated for one year, with a time resolution of 15 minutes.

The mathematical models used for the simulation of the DH network electricity network and for the CP2H systems are described in Chapter 2.

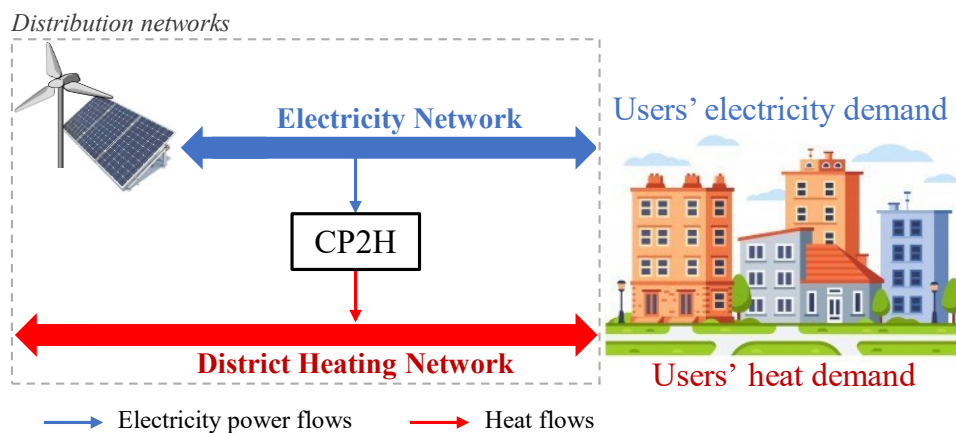


Figure 5-1. Schema of the analyzed multi-energy system.

### 5.2.1 District heating system

The case study presented in this chapter is based on the Turin DH, which is linked to more than 5000 buildings (about 60 million m<sup>3</sup>). This makes it the largest DH in Italy and one of the largest in Europe. The network is supplied by two CHP gas plants and storage systems, located in different areas of the city. The Turin DH network consists of two interconnected parts: a transport network, which includes large diameter pipes (usually larger than 200 mm) that link the thermal plants to the distribution networks, and 182 distribution networks that connect the transport

network to a group of buildings located in the same area of the city. In this case study the DH distribution networks are analyzed. The water is currently supplied to buildings at a constant temperature of about 115°C, while the return temperature is between 65°C and 45°C. Sensible water Thermal Energy Storages (TES) have been adopted in the Turin network for peak shaving purposes, especially the morning peaks. In the considered application, the adoption of TES increases the thermal mass of the system. This provides a significant benefit, since it increases the potential of DH to act as a source of flexibility for the electricity network. In this study, three new distribution networks were analyzed, which were hypothesized to have the same thermal characteristics (see Figure 5-2). This methodological choice was made in order to evaluate the effects on the thermal sector of different CP2H system configurations. More specifically, it was investigated how a different connection point of the CP2H plant with the electricity network could modify the performance of the thermal sector and, at the same time, how the same flexible resource could be more or less advantageous for the electricity sector, depending on the specific connection point with the electricity distribution network. The reader may refer back to Chapter 2 for the description of the gas network model.

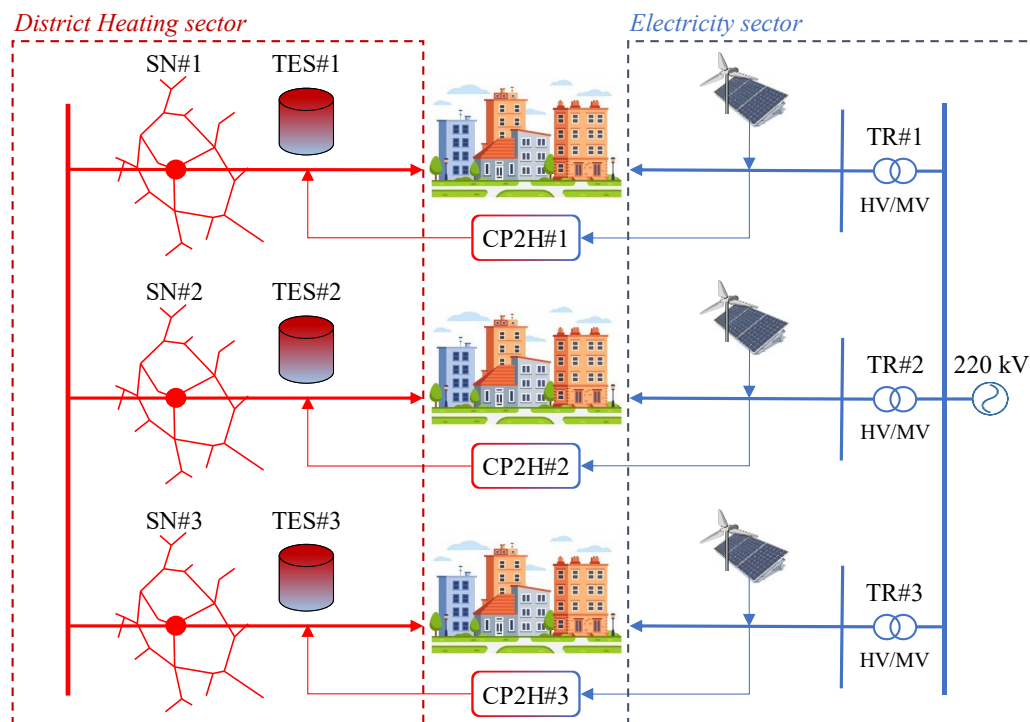


Figure 5-2. Multi-energy system scenario.

## 5.2.2 Electricity system

The distribution electricity network (EN) is part of the MV system of the city of Turin. The network is connected to the high voltage (HV) system via three HV/MV transformers (TR). The EN is characterized by a high penetration of RES.

When the RES production exceeds the electricity demand of the network, the over-generations cause Reverse Power Flow (RPF) in the HV/MV transformers. The loads and RES plants are not uniformly distributed within the electricity network (see Figure 5-3). Most of the RES systems are installed downstream of TR#2 and TR#3. About half of the electricity network users are connected to the part of the network powered by TR#2. TR#3 is the part of the network that is most subject to over-generations of renewables: 70% of RES over-generations occurs downstream of TR#3, 21% downstream of TR#1, and 9% downstream of TR#2. The reader may refer back to Chapter 2 for a detailed description of the electricity network model.

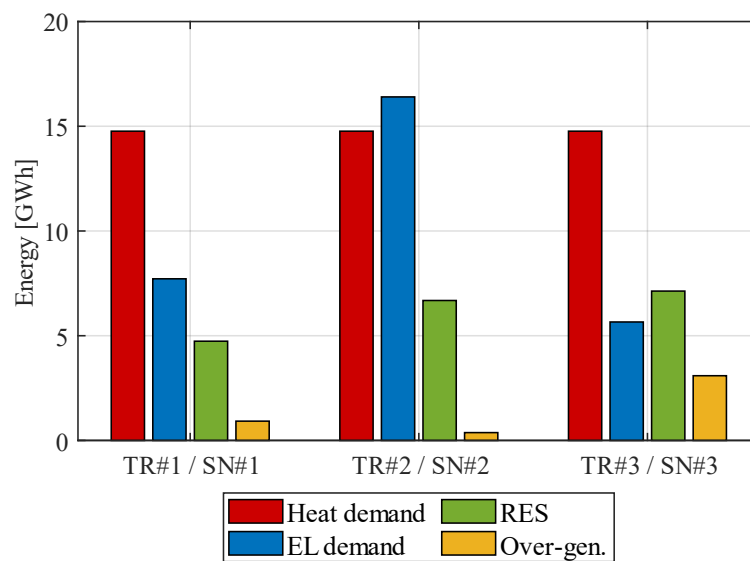


Figure 5-3. Yearly heat demand, electricity (EL) demand, RES generation and RES over-generation (Over-gen.).

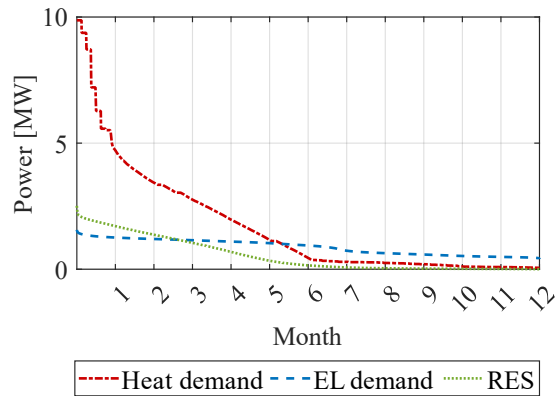
### 5.2.3 Centralized Power-to-Heat systems

The electricity and the district heating sector are connected through three CP2H plants. Each CP2H plant is connected downstream of one of the three EN transformers and connects a different DH Sub-Networks (for the sake of simplicity, the TRs, the CP2H systems, the SNs and the TES have been enumerated as shown in Figure 5-2). Each CP2H is assumed to have a nominal thermal power of 2.5 MW<sub>th</sub>. The reader may refer back to Chapter 2 for a detailed description of the CP2H model.

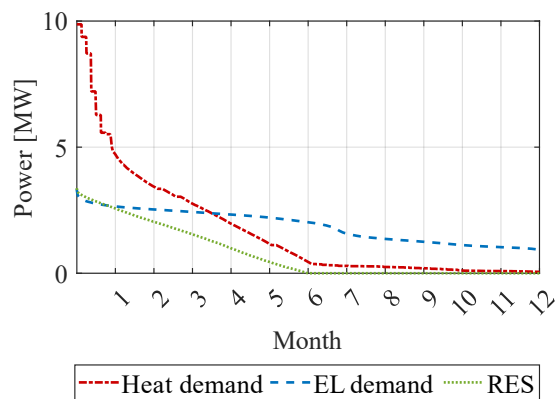
### 5.2.4 Scenario energy demand and production

This configuration makes it possible to analyze CP2H systems in the three considered positions of the electricity network, which have very different local characteristics: medium local RES over-generation (CP2H#1), low local RES over-generation (CP2H#2) and high local RES over-generation (CP2H#3). The three DH sub-networks to which the CP2H plants are connected and the three CP2H plants

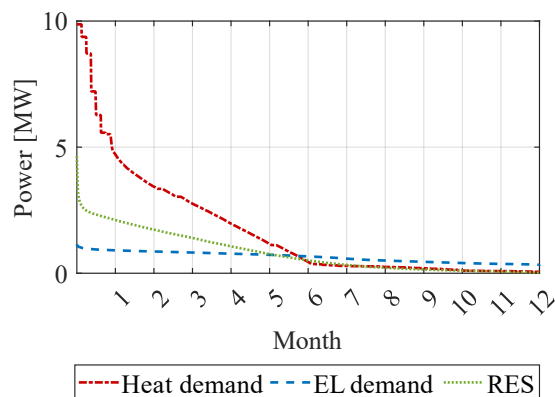
were chosen with the same characteristics to emphasize the effect that the connection point of the CP2H plants has on the EN (see Table 5-1). Each SN feeds the thermal demand of an equal volume of buildings. Consequently, the three subnets have an equal heat demand profile (see Figure 5-4). In this way, the three configurations only differ as far as the connection point with the EN is concerned. The choice of analyzing a scenario with three different plants, three transformers and three DH subnets was made to make results more generalizable: a scenario with multi plants and different possible configurations.



(a)



(b)



(c)

Figure 5-4. Duration curve of heat demand, electricity (EL) demand and RES generation. TR#1 and DH SN#1 (a), TR#2 and DH SN#2 (b), TR#3 and DH SN#3 (c).

Table 5-1. Multi-energy system parameters.

	Unit	TR#1 / CP2H#1 / SN#1	TR#2 / CP2H#2 / SN#2	TR#3 / CP2H#3 / SN#3
Electricity users	MW <sub>e</sub>	5.10	9.30	3.90
PV	MW <sub>e</sub>	2.90	4.50	3.30
WT	MW <sub>e</sub>	0.60	0	2.70
CP2H installed capacity	MW <sub>th</sub>	2.50	2.50	2.50
TES volume	m <sup>3</sup>	250	250	250
Heated volume	m <sup>3</sup>	250,000	250,000	250,000

## 5.2.5 Economic analysis

### Energy costs and incentives for flexibility

The average price of the electricity consumed by the CP2H plants was estimated to be 60 €/MWh. The heat generated by the plants was estimated to be worth 45 €/MWh. Indeed, the heat injected into the DH represents a source of revenues, as it brings about a reduction in the central CHP usage, thus reducing the associated costs. Until now, the flexibility offered at the distribution level has not been regulated. For this reason, a sensitivity analysis was performed: by varying the value of incentives from 0 to 60 €/MWh, the impact of these incentives on the cash flow of CP2H plants has been investigated.

The energy costs and the incentives for the provided flexibility are summarized in Table 5-2.

Table 5-2. Flexibility incentives and energy costs

Parameter	Unit	Value
Electricity cost	€/MWh	60
Heat cost	€/MWh	45
Incentives for flexibility	€/MWh	0 – 60

### CP2H plant cost assumption

The investment cost includes the heat pump purchase cost and the excavation/installation costs for the sink construction. Indications of the total cost



of various kinds of existing large scale heat pump projects are reported in [176]. An investment cost of 700-1100 €/kW<sub>th</sub> is indicated for the specific case of a groundwater heat pump. According to [177], the investment cost for a large scale CP2H plant will decrease by 10% in 2030 and by 16-20% in 2050, as a result of a scale effect. Indeed, even though the use of large heat pump plants connected to the DH is still not particularly widespread, the penetration of this technology is expected to increase, with a consequent reduction in the production cost of the components. In this study, we considered an investment cost of 770 €/kW<sub>th</sub>. Following [174], the fixed operational and maintenance (O&M) costs were estimated to be 2 €/kW<sub>th</sub>/year and the plant's lifetime to be 25 years (see Table 5-3).

Table 5-3. CP2H plant cost assumptions.

Parameter	Unit	Value
Specific investment cost	€/kW <sub>th</sub>	770 [176]
Specific fixed O&M cost	€/kW <sub>th</sub> /year	2 [174]
Lifetime	years	25 [174]

### Simple Payback and Net Present Value

The economic flows of P2H plants are assessed on the basis of the electricity consumed, the heat produced, and the flexibility provided, which are calculated as follows:

$$Cost_{el,CP2H\#i} = c_{el} \sum_{k=1}^K u_{CP2H\#i}(k) \cdot \tau \quad (5.1)$$

$$Rev_{heat,CP2H\#i} = r_{heat} \sum_{k=1}^K \Phi_{CP2H\#i}(k) \cdot \tau \quad (5.2)$$

$$Rev_{flex,CP2H\#i} = r_{flex} \sum_{k=1}^K \left( u_{CP2H\#i}(k) - u_{CP2H\#i}^0(k) \right) \cdot \tau \quad (5.3)$$

where:

- $Cost_{el,CP2H\#i}$  [€] represents the annual expenses for the electricity consumption of the  $i$ -th CP2H plant;
- $c_{el}$  [€/MWh] is the annual average electricity price;
- $\tau$  [h] is the duration of the time step;
- $Rev_{heat,CP2H\#i}$  [€] indicates the annual revenues for the heat production of the  $i$ -th CP2H plant;

- $r_{\text{heat}}$  [€/MWh] is the specific revenue for the heat injected into the DH;
- $Rev_{flex,CP2H\#i}$  [€] represents the annual revenues for the flexibility provided by the  $i$ -th CP2H plant. It should be mentioned that this kind of revenue is not available in the base case as the flexibility of the CP2H plants is not exploited in that simulation;
- $r_{flex}$ , [€/MWh] represents the specific incentives for the provided flexibility. Up until to now, the flexibility provided at the distribution level has not been regulated. In this work, a sensitivity analysis was carried out by varying the price of flexibility from 0 to 60 €/MWh.

The annual cash flows of the  $i$ -th CP2H plant ( $CF_{CP2H\#i}$ ) were determined by considering four factors: the earnings from the production of heat, the earnings from the flexibility provided, the costs for the consumption of electricity, and the fixed operational expenditure ( $OPEX_{CP2H\#i}$  [€]) for the operation and maintenance of the plant:

$$CF_{CP2H\#i} = Rev_{\text{heat},CP2H\#i} + Rev_{flex,CP2H\#i} - Cost_{el,CP2H\#i} - OPEX_{CP2H\#i} \quad (5.4)$$

The CP2H plants were evaluated from an economic point of view by means of the calculation of the NPV and SPB.

$$NPV_{CP2H\#i} = -CAPEX_{CP2H\#i} + \sum_{y=0}^{LT_{CP2H\#i}} \left( \frac{CF_{CP2H\#i}}{(1-DR)^y} \right) \quad (5.5)$$

$$SPB_{CP2H\#i} = \frac{CAPEX_{CP2H\#i}}{CF_{CP2H\#i}} \quad (5.6)$$

Where:

- $LT_{CP2H\#i}$  [years] is the lifetime of the  $i$ -th CP2H plant
- $CAPEX_{CP2H\#i}$  [€] is the capital expenditure for all the components of the  $i$ -th CP2H plant (considered only at year 0);
- $DR$  [-] is the discount rate, which is assumed to be equal to 7%.

## 5.3 Mathematical approach and solution strategy

### 5.3.1 Co-simulation architecture

In this case study the co-simulation loop involved four modules (see Table 5-4):

- the time-synchronizer (Time-Sync);
- the controller;
- the DH and centralized P2H (DH & CP2H) module;

- the electricity network (EN) module.

Table 5-4. Models involved in the co-simulation loop.

Model	Case study 3
Controller	X
Time-Sync	X
Electricity network (detailed)	X
Electricity network (simplified)	
Gas network (detailed)	
Gas network (simplified)	
DH network and CP2H	X
P2G (detailed)	
P2G (simplified)	
Building and LP2H	
Electric battery	

The sequence of interaction of the co-simulation loop is reported in Figure 5-5. The figure shows that all the messages exchanged go through the Time-Sync. The Control module receives as input the CP2H flexibility and the electricity network unbalances calculated in the previous step (*message 1*). The output of the Control module contains the CP2H unit setpoints (*message 2*) sent to the Time-Sync module, which is then forwarded to the DH & CP2H module (*message 3*). The DH & CP2H module performs the simulation (of 1 time step) calculating the heat flows inside the DH network, as well as the electricity consumption and heat production of the CP2H plants and the CP2H flexibility available for the next simulation step (*message 4*). The CP2H flexibility data is stored inside the Time-Sync module and used in the next simulation step as input for the control module, while the electricity consumption of the CP2H units is sent to the electricity network (EN) module (*message 5*). The EN module performs the calculation of the time step and sends in output the network balance (*message 6*) used by the Control module to define the CP2H setpoint in the following time step.

Annual simulations have been performed with a discretization of 15 minutes, resulting in a total of 35040 time steps.

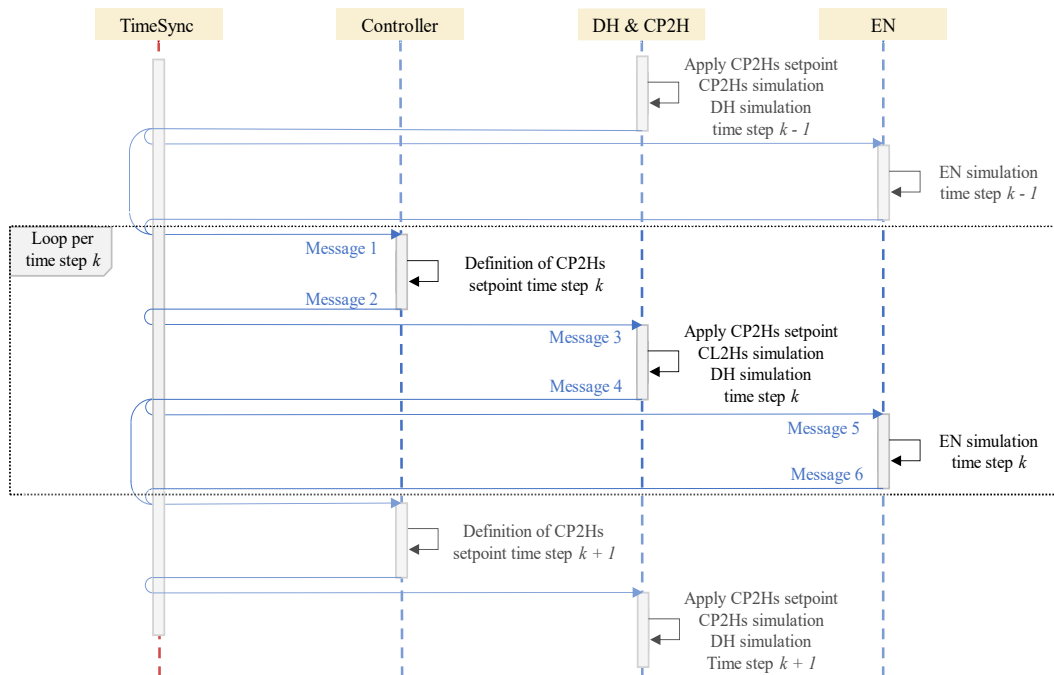


Figure 5-5. Sequence of interactions among co-simulation modules.

### 5.3.2 Simulation control algorithm

In this case study, the CP2H technology is used to supply heat to the DH by converting electricity from the electricity distribution network into heat. In order to maximize the electrification of the heating sector, the CP2H system feeds as much heat as possible into the DH, according to the users' heating needs. During the night (from 0:00 to 5:00), the heat generated by the CP2H is also used to charge the thermal storages. The heat injected into the storages is regulated to charge the storages in a linear manner during the accumulation period. During the day, the CP2H system is turned off to allow the storage to discharge the accumulated heat until the thermal storage is completely empty. In such a situation, the DH heat demand is met entirely by the heat coming from the storages.

To be mentioned that when CP2H is in operation (to charge the storage or to supply heat directly to the SN), it must be supported by high temperature heat from the DH transmission network, due to the limited temperature that CP2H can reach, in order to reach the required operating temperature.

The baseload of the  $i$ -th CP2H at each simulation step ( $k$ ),  $u_{LP2H\#i}^0(k)$ , is defined according to the flow diagram shown in Figure 5-6.

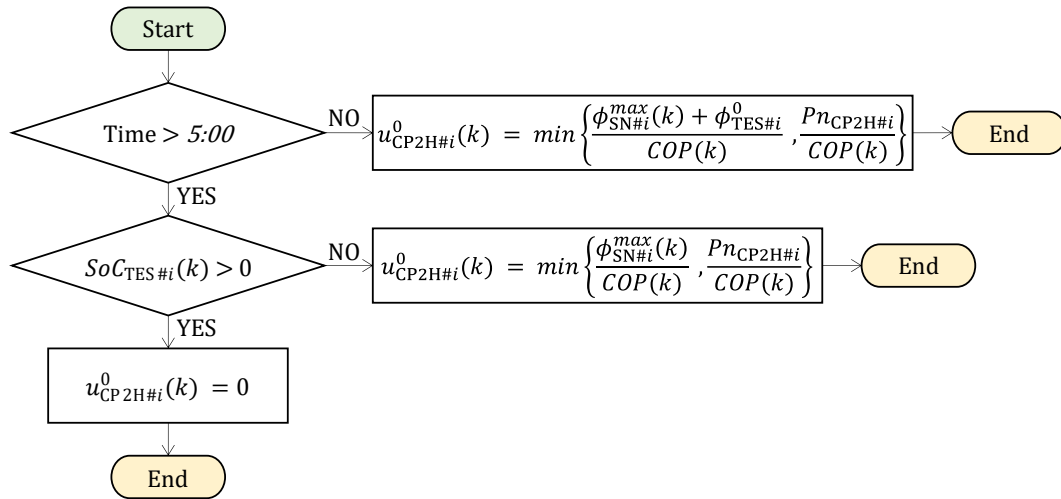


Figure 5-6. The  $i$ -th CP2H baseload control algorithm. Optimization of DH heat flows <sup>6</sup>

Where:

- $\Phi_{SN\#i}^{max}(k)$  [MW] is the maximum heat power that the  $i$ -th CP2H plant can inject into the  $i$ -th SN at step  $k$ ;
- $\Phi_{TES\#i}^0(k)$  [MW] is the heat that the  $i$ -th CP2H must provide to the  $i$ -th TES to store heat during the charging period and linearly reach the maximum charge at the end of the accumulation period;
- $Pn_{CP2H\#i}$  [MW] is the nominal heat power of the  $i$ -th CP2H plant;
- $SoC_{TES\#i}(k)$  [-] is the State of Charge (SoC) of the  $i$ -th TES at step  $k$ ;
- $COP_{CP2H\#i}(k)$  [-] is the COP of the  $i$ -th CP2H at step  $k$ .

Downward flexibility is defined as the maximum allowable downward deviation from the baseload. Since we consider a time interval of 15 minutes, the electricity consumption of the CP2H systems can always be brought to 0. Upward flexibility is defined as the difference between the baseload and the electrical load of the plant when it works to deliver the maximum amount of heat storable in the DH sector.

The mathematical details on calculating upward and downward flexibility are reported in Chapter 2.

In this case study, two different types of control are analyzed, which are referred to as base case and optimized case.

### Base case: without CP2H flexibility exploitation

In the Base case, although the two energy sectors are connected, the synergies enabled by the energy conversion technologies are not exploited. CP2H systems

<sup>6</sup> The control algorithm for the baseload of the CP2H system is part of the CP2H model described in Chapter 2. For reasons of clarity this figure has been reported also in this section.

only operate to satisfy the needs of the thermal sector. At each time step  $k$ , the load of the  $i$ -th CP2H, namely  $u_{CP2H\#i}$  [MW], is always set equal to its baseload  $u_{CP2H\#i}^0$  [MW], defined as stated in the control logic illustrated in Figure 5-6.

$$u_{CP2H\#i}(k) = u_{CP2H\#i}^0(k) \quad (5.7)$$

### Optimized case: with CP2H flexibility exploitation

In the optimized case, the flexibility of the CP2H systems is exploited to control their electricity consumption and optimize the energy flows of the electricity sector. The electrical load of the CP2H plants is shifted as much as possible to match the RES over-generations, and thus reduce the RPF in the network transformers. Figure 5-7 summarizes the logic adopted to control the CP2H plants at the generic time step  $k$ . In the absence of RES over-generation downstream of the  $i$ -th transformer, the electrical load of the  $i$ -th CP2H is kept equal to the baseload. If a transformer in the electricity grid is subject to an RPF, the flexibility of the CP2H plants is exploited to absorb as much of the local RES over-generation as possible. In this condition, the CP2H transforms the RES over-generation in heat that is then used to charge the thermal storages of the district heating.

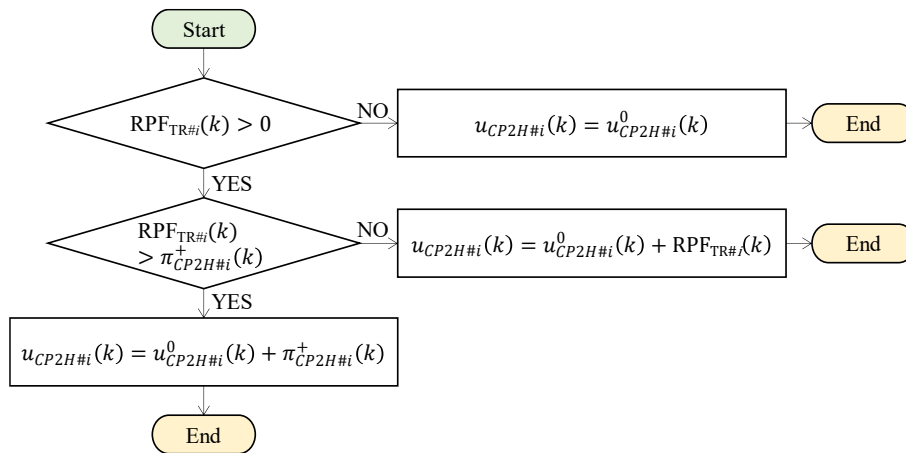


Figure 5-7. Flexibility exploitation control algorithm of the  $i$ -th CP2H unit for RPF absorption.

Where:

- $RPF_{TR\#i}(k)$  [MW] is the RPF on the  $i$ -th TR at step  $k$ ;
- $\pi_{CP2H\#i}^-(k)$  [MW] is the downward flexibility of the  $i$ -th CP2H at step  $k$  (see Chapter 2);
- $\pi_{CP2H\#i}^+(k)$  [MW] is the upward flexibility of the  $i$ -th CP2H at step  $k$  (see Chapter 2).

## 5.4 Results and discussion

### 5.4.1 Energy flows between the electricity and district heating energy sectors

In the Base case, CP2H plants have been controlled to optimize the energy flows in the thermal sector. The energy flows in the electricity sector and the thermal sector of a characteristic day with a high heat demand are shown in Figure 5-8 (details pertaining to mid-February). Since the three DH subnetworks of the scenario have the same characteristics, the heat demand profile is the same for all three subnetworks. The CP2H units are used from 0:00 to 5:00 to charge the thermal storage (light green area). Because of the limited temperature that can be reached (90°C), the CP2H plants alone are not able to charge the thermal storage, whose accumulation temperature is 118°C. The storage charge is therefore supported by the heat coming from the transmission DH network (called Central Heat: CH in the figures - light gray area). The storage is loaded linearly at night until it reaches the maximum charge at 5:00. In the following hours, the accumulated heat is used to cover the peak of the morning heat demand (orange area). The heat accumulated in the storage, being at a high temperature, is able to satisfy the thermal demand of the network, without needing to take additional heat from the DH transmission network. Once the storage is empty (SoC = 0), the CP2H plants are again put into operation to supply as much heat as possible to the DH network. The CP2H plants are used to preheat the return flows of the thermal utilities of the network, thus reducing the heat load required by the central heat power plant. The central plant supplies heat to the return flows, preheated by the CP2H plants, up to the operating working temperature of the DH. The heat from the central system is highlighted in dark gray in the figures.

Figure 5-8b shows the electricity flows that occur downstream of the electricity network's transformers. The dashed line shows the RES production within the network; it can be seen that TR#3 is the transformer that is affected the most by over-generation. The flexibility of the CP2H plants is not exploited to absorb RES generation in the Base case. The load of the CP2H systems is distributed during the day to satisfy the needs of the thermal sector (red area).

Figure 5-9 shows the heat and electricity energy flows for the same day in the optimized case in which the flexibility of the CP2H plants is exploited. In the middle of the day (12-15 for SN#1 and SN2, 10-15 for SN#3), the CP2H systems are used to store heat inside the thermal storages (see Figure 5-9a). The daytime charge of the thermal storage is regulated on the basis of RES over-generations.

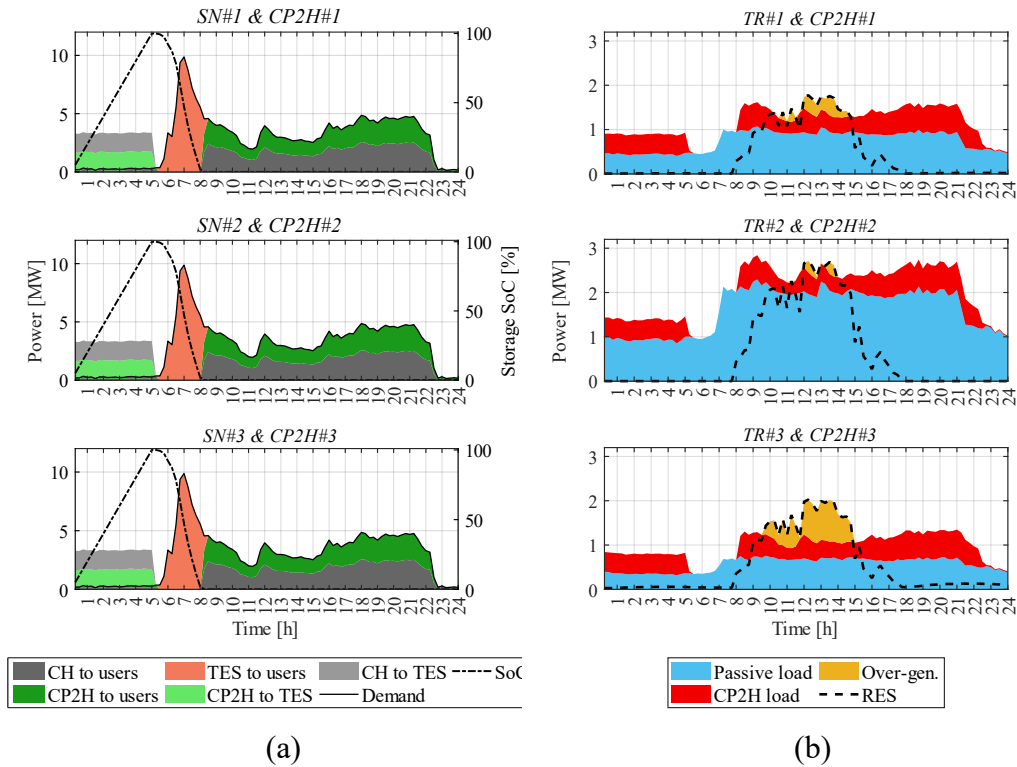


Figure 5-8. Energy flows in each DH subnetwork (a) and in each transformer (b). Base case. Details of a day with a high DH heat demand (February).

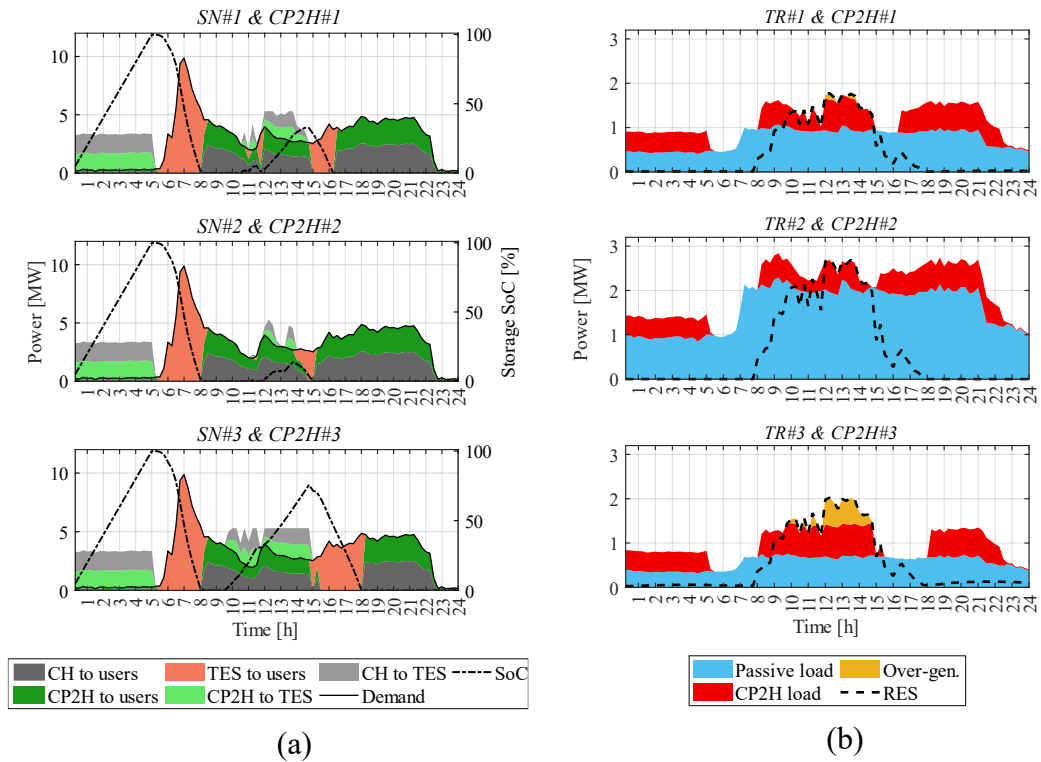


Figure 5-9. Energy flows in each DH subnetwork (a) and in each transformer (b). Optimized case. Details of a day with a high DH heat demand (February).



Figure 5-9b shows the electric power flows that occur in the three electrical network transformers. In the optimized case, the electrical load of the CP2H plants is controlled to follow the RES over-generation and mitigate the RPF that adversely affects the network TRs. The overproduction in TR#1 and TR#2 is completely absorbed, while the over-generation in TR#3 is not completely absorbed, thus leaving a residual RPF. CP2H#3 cannot absorb all the over-generation of RES, as it has already reached its nominal capacity load. In the period immediately following the over-generation of RES, the thermal demand of the users is completely covered by the storage heat; see, for example, the orange area for SN#3 from 15:00 to 18:00. From the electrical network point of view, the loads of the CP2H units are shifted to match the local RES production of the network. For example, the electricity consumption of CP2H#3, which would have been from 15:00 to 18:00 (see Figure 5-8b), is anticipated and redistributed in a controlled manner during the RES peak (see Figure 5-9b).

Figure 5-10 and Figure 5-11 show the energy flows for a characteristic day with a low heat demand (end of September) for the base case and the optimized case, respectively. The heat demand is much lower than that in the winter period (see Figure 5-10a). Nonetheless, the morning peak demand remains almost constant. In this period of the day, the water inside the network, which is at a low temperature due to the limited energy flows at night, must be brought back to the operating temperature of the network, with a consequent significant heat demand. The morning peak is covered again using the heat accumulated during the night. In the Base case, the CP2H load is more concentrated at night for the storage charge, and during the evening, when user's heat demand is higher. The electricity consumption profile of the CP2H plants is therefore out of phase with the RES generation, whose peak production occurs in the central hours of the day (see Figure 5-10b). The flexible use of CP2H plants makes it possible to shift part of the electricity consumption to the RES over-generation hours (see Figure 5-11b). The energy over-generation that afflicts TR#1 and TR#2 is completely absorbed on the considered day, while only a part of the over-generation in TR#3 is absorbed. The absorption of the RES over-generation on TR#3 is blocked at 13:00, as the thermal storage has reached its maximum state of charge and is no longer able to accumulate energy. The reader may note that the heat accumulated in TES#1 and TES#3 is not completely released to the DH during the day (the SoC of the two storage units is greater than 0 at the end of the day, see Figure 5-11a). The heat that remains accumulated in the storage at the end of the day is used the following day. Even for the day before the one represented in Figure 5-11, TES#1 and TES#3 are not completely discharged at the end of the day. In fact, as can be seen in Figure 5-11a, the SoC of the two storages at 0:00 is greater than 0. The heat accumulated in the previous day is used to decrease the energy consumption used for night storage charging; the night energy consumption (thermal and electrical) in Figure 5-10 should be compared with that in Figure 5-11.

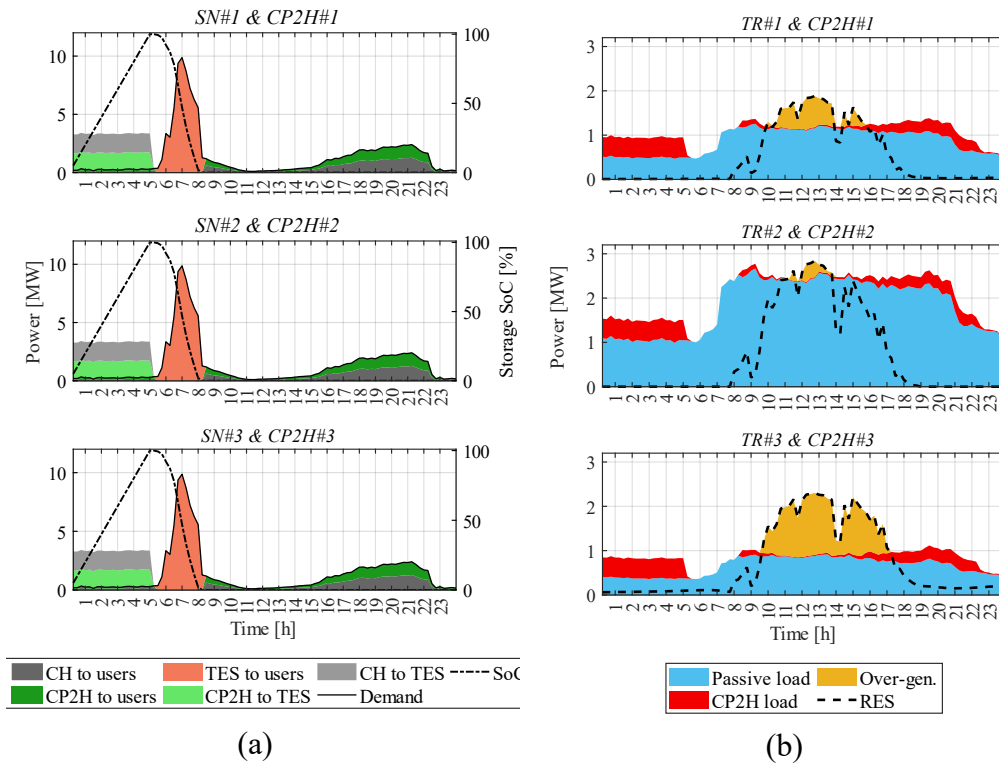


Figure 5-10. Energy flows in each DH subnetwork (a) and in each transformer (b). Base case. Details of a day with a low DH heat demand (September).

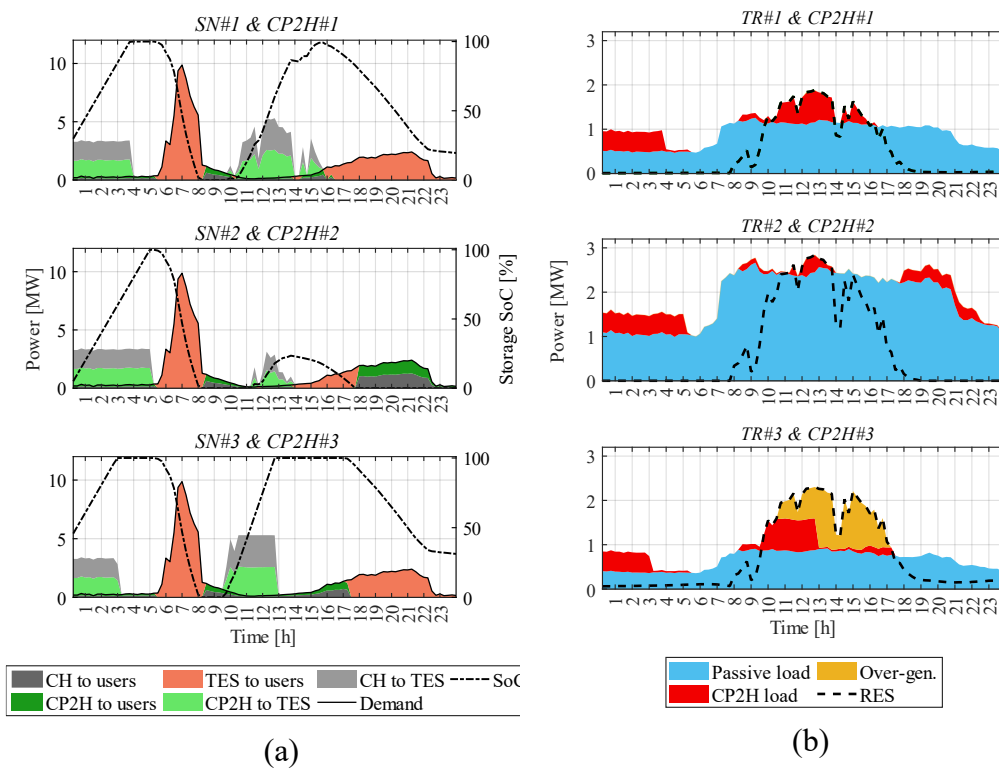


Figure 5-11. Energy flows in each DH subnetwork (a) and in each transformer (b). Optimized case. Details of a day with a low DH heat demand (September).

Table 5-5 reports the annual energy flows of the three DH subnetworks considered in the base case for the optimized case. The table shows:

- the total heat demand of each thermal SN;
- the heat supplied to the users produced directly by the central heat system;
- the heat of the CP2H used directly to provide heat to the users;
- the heat that the central system and the CP2Hs accumulate in the TES;
- the total heat that is absorbed and then released by the TES plants.

As mentioned above, the three thermal subnetworks in the Base case behave in the same way, as they have the same characteristics. A total of 33% of the heat supplied to users is supplied directly by the CH plant, 29% is supplied directly by the HPs, and the remaining 38% comes from thermal storage. In turn, 53% of the heat accumulated in the thermal storage comes from the DH central heating system and the remaining 47% from the CP2Hs.

*Table 5-5. Annual energy flows of the district heating network.*

	Unit	SN#1		SN#2		SN#3	
		Base Case	Opt. Case	Base Case	Opt. Case	Base Case	Opt. Case
Heat demand	GWh <sub>th</sub>	14.77	14.77	14.77	14.77	14.77	14.77
CH to user	GWh <sub>th</sub>	4.83	3.96	4.83	4.30	4.83	3.88
CP2H to user	GWh <sub>th</sub>	4.31	3.53	4.31	3.84	4.31	3.46
CH to TES	GWh <sub>th</sub>	2.97	3.84	2.97	3.50	2.97	3.93
CP2H to TES	GWh <sub>th</sub>	2.65	3.43	2.65	3.13	2.65	3.50
TES heat	GWh <sub>th</sub>	5.62	7.27	5.62	6.63	5.62	7.43

The possibility of decoupling the heat demand from the production enabled by thermal storage is exploited in the optimized case. The heat accumulated in the storage, which is produced by the centralized heat plant and the CP2H plants, increases. Conversely the heat that is supplied directly to the users (i.e., without first passing through the storage), which comes from the thermal power plant and the CP2H system decreases. It is important to point out that the total heat coming from the thermal power plant (CH to users + CH to TES) and the total heat produced by CP2H (CP2H to users + CP2H to TES) remain unchanged, compared to the Base case. The flexible use of the CP2H system, in fact, does not change the amount of energy required. Instead, it brings about a production time-shift, which is made possible by the passage of energy through the storage systems. The greater the exploitation of the flexibility of the CP2H systems, the greater the use of the storage systems. In the analyzed scenario, SN#3 is the one that is most exploited to offer flexibility. As a result of the flexible use of storage, the thermal energy that is accumulated annually in TES#3 increases by 32%, compared to the Base case. As

for TES#1 and TES#2, even though their energy flexibility is exploited to a lesser extent, they show an increase of accumulated energy of 29% and 19%, respectively.

Thanks to the exploitation of flexibility, the CP2H load is shifted to the RES production hours. Table 5-6 shows that the quantity of RES consumed by the network increases and the imported energy (i.e., withdrawn from the HV system) decreases. The greater the surplus is, the more the electricity load can be shifted and, in turn, the lower the electricity withdrawn from the transmission system. Thanks to the flexible use of CP2H plants, it is possible to absorb 1.37 GWh of RES over-generation (about 40% of the total over-production of the entire grid). The amount of energy taken from the HV system decreases by the same amount, as the over-generation RES decreases. In fact, the total load of the CP2H plants is not modified, and is only shifted from the periods of low RES production to the periods of high RES production.

The part of the network downstream of TR#3 is the one with the greatest over-generation of RES (see Table 5-6). Consequently, the amount of over-generation that has been absorbed by CP2H in this part of the network is also the greatest: 0.67 GWh<sub>e</sub>, calculated as the over-generations in the base case minus the over-generations in the optimized case. The over-generations absorbed by TR#1 and TR#2 are instead 0.48 GWh<sub>e</sub> and 0.22 GWh<sub>e</sub> respectively. Despite the fact that a greater over-generation of RES in absolute terms is mirrored/accompanied by a greater amount of over-generation absorbable by flexible units, the effect is the opposite in percentage terms: thanks to CP2H units, it is possible to absorb 65% of the over-generations that affect TR#1, 73% of those that affect TR#2 and only 26% of those that affect TR#3. In fact, the flexibility of CP2H is limited by two constraints: the CP2H nominal load and the state of charge of the storage system. The greater the required flexibility is, the more frequent are the periods during which the unit works at nominal load, thereby limiting the ability to absorb more over-generations of RES. Moreover, when a greater flexibility and greater amount of energy to inject into the storage are required, there is an increase in the periods during which the CP2H plant cannot provide flexibility, as the storage has reached the maximum state of charge.

*Table 5-6. Annual energy flows of the electricity network.*

	Unit	TR#1		TR#2		TR#3	
		Base Case	Opt. Case	Base Case	Opt. Case	Base Case	Opt. Case
El. demand	GWh <sub>e</sub>	7.72	7.72	16.40	16.40	5.65	5.65
CP2H load	GWh <sub>e</sub>	2.00	2.00	2.00	2.00	2.00	2.00
El. withdrawn	GWh <sub>e</sub>	5.72	5.24	12.02	11.80	3.05	2.38
RES consumption	GWh <sub>e</sub>	4.00	4.48	6.38	6.60	4.60	5.27
RES over-gen.	GWh <sub>e</sub>	0.74	0.26	0.30	0.08	2.53	1.86

## 5.4.2 Economic results

The CP2H plants were evaluated from an economic point of view through a sensitivity analysis that considered incentives for flexibility as a variation parameter. The sensitivity analysis was performed without changing the design parameters of the scenario. In addition, the control of the CP2H devices optimizes the energy flows of the system. For these reasons, variations in incentives do not change the energy flows of the scenario. Table 5-7 shows the electricity consumption, production and annual flexibility provided by the three CP2H plants for both the base and optimized cases. The total production of heat and the total electrical consumption of the three units is the same. Since all three DH subnetworks have the same characteristics, the quantity of heat that their CP2Hs can provide and, consequently, their electricity consumptions are the same.

The optimized use of the flexible units allows the load of the units to be shifted over time and enables flexibility of the plants, without altering their annual energy production or consumption. The plant located downstream of TR#3 is the one that provides the greatest amount of flexibility. The other two plants are located in less advantageous positions, and hence they are less frequently used to offer flexibility. The exploitation of flexibility affects the economic flows of the plants: the greater the flexibility provided by the plant is, the greater are the revenues for the related incentives.

In the hypothesis of 0 incentives (value of incentives = 0 €/MWh), the economic revenues are exclusively derived from the production of heat (equal for all the plants). Under this hypothesis, all three plants are subjected to the same economic flows, which correspond to the economic flows of the base case, in which flexibility is not exploited. The NPV of all the plants is €670,000 with an SPB of 10.2 years (see Figure 5-12a and Figure 5-12b).

The economic benefits derived from the flexible use of the CP2H facilities can be appreciated when flexibility incentives have values higher than 0. The greater the incentives are, the greater is the economic profitability of these plants (i.e., their NPVs) when their flexibility is exploited. On the other hand, the variation of the incentive parameter in the base case does not change the economic flows, since the provided flexibility is always zero (see Figure 5-12a).

As mentioned above, the sensitivity analysis to the variation of the incentives for flexibility was performed keeping the other parameters constant. Combining equations 5.3, 5.4 and 5.5, the positive linear relationship between incentive values and NPV can be fully appreciated. Instead, an inverse linear relationship can be found between incentive values and SPB by combining the equations 5.3, 5.4 and 5.6. That is, as the incentives increase, the NPV increases linearly while the SPB decreases linearly.

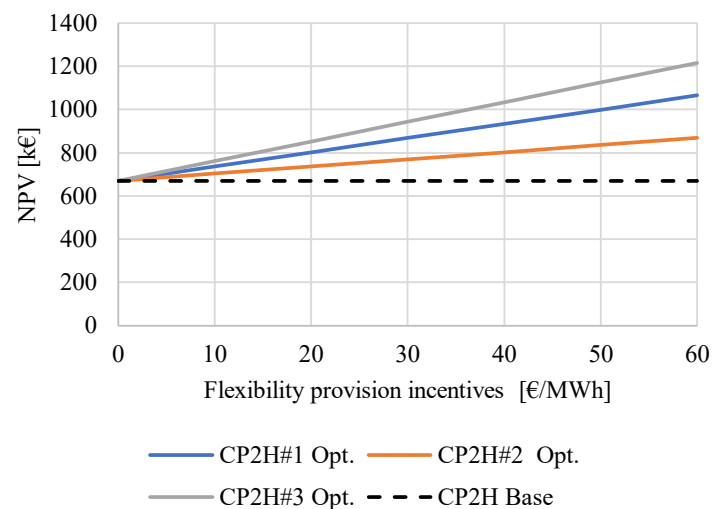
From an economic point of view, the best results are those pertaining to CP2H#3. In the most optimistic hypothesis on the value of incentives (60 €/MWh), the exploitation of flexibility allows the NPV of CP2H#3 to increase by 82% and

the SPB to decrease by 18%. The exploitation of flexibility also allows the other two plants to improve their economic flows, even though to a lesser extent. In the most favorable incentive conditions, compared to the base case, the NPV of plants 1 and 2 increases by 59% and 30% respectively, and the SPB decreases by 13% and 7%.

It should be pointed out that the installation of a CP2H system is always convenient, even when flexibility is not exploited. The gains that can be derived from the production of heat compensate for electricity and investment costs. Nevertheless, economic profitability increases significantly if the flexibility of the plants is exploited. In this case, the placement of the CP2H plant within the electricity network plays a significant role. In order to maximize the economic revenues, the CP2H plant should be located close to the local RES over-generations. In fact, the greater the over-generations that the plant can absorb are, the greater the flexibility that the plant can provide, with a consequent increase in the revenues for the related incentives. In the analyzed scenario, the NPV of CP2H#3, the one that is better located (i.e., closer to the local RES over-generations), is as much as 40% higher than the NPV of CP2H#2.

Table 5-7. Annual energy flows of CP2H.

	Unit	TR#1		TR#2		TR#3	
		Base Case	Opt. Case	Base Case	Opt. Case	Base Case	Opt. Case
CP2H load	GWh <sub>e</sub>	2.00	2.00	2.00	2.00	2.00	2.00
CP2H flexibility	GWh <sub>e</sub>	0.00	0.48	0.00	0.22	0.00	0.70
CP2H heat	GWh <sub>th</sub>	6.96	6.96	6.96	6.96	6.96	6.96



(a)

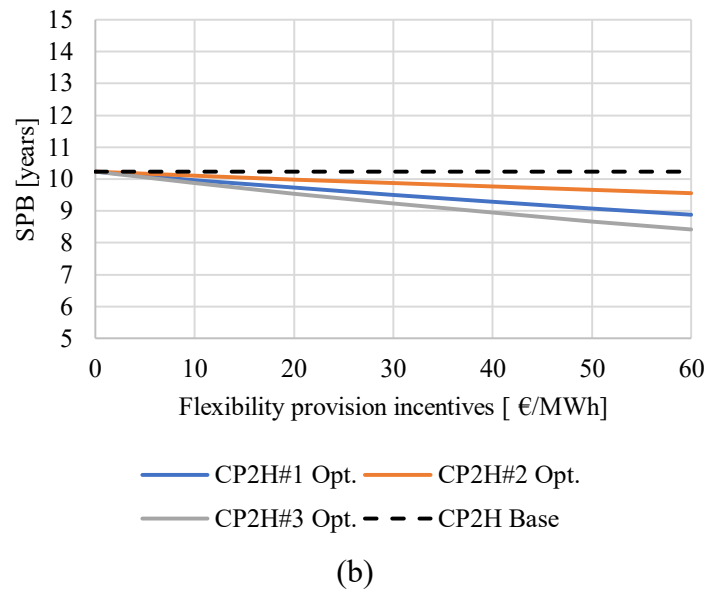


Figure 5-12. Net Present Value (a) and Simple Pay Back (b) of the three CP2H plants for the base case and for the optimized case.

## 5.5 Conclusions

This case study investigated the concept of using district heating (DH) connected centralized Power-to-Heat (CP2H) systems to provide heat to the DH sector and to provide flexibility to the electrical sector. A case study, based on data from the DH and electricity network of the city of Turin, was analyzed. In the considered scenario, three CP2H plants were connected to the distribution network in three different points. The energy flows between the electricity and DH sectors, made possible by the CP2H energy conversion technology, were analyzed. The CP2H flexibility was exploited to absorb the Renewable Energy Sources (RES) over-generations. The main conclusions can be summarized as follows:

- The CP2H energy conversion technology makes it possible to connect the electricity and heating sectors. This allows new synergies between the two energy sectors to emerge and increases the flexibility of the multi-energy system. Three benefits arise from using CP2H systems: *a)* the use of heat pump plants represents an efficient solution for the production of heat, *b)* these plants can be powered directly by renewable sources, thus allowing the production of heat with a low environmental impact, and *c)* the CP2H energy conversion technology makes it possible to transfer the flexibility of the district heating sector to the electricity sector.
- In the analyzed scenario, the heat produced by the CP2H plants could cover about 50% of the DH heat demand. However, the heat demand cannot be completely satisfied by CP2H systems, due to the limited output temperature this technology reaches (a heat pump capable of reaching 90°C

was considered in this study). However, the current Turin district heating network works at a temperature of about 115°C. For this reason, the heat generated by heat pumps should always be integrated by heat generated at high temperatures to reach the working temperature of the network.

- The flexibility enabled by CP2H plants was used to absorb the over-generation of Renewable Energy Sources (RES) that occurred at the distribution level, which could cause Reverse Power Flow (RPF) problems in HV/MV transformers. The CP2H plants allowed the RES over-generations to be reduced by 40% over the whole year.
- Thanks to the high efficiency of heat production, CP2H systems proved to be advantageous from an economic point of view. Even in the most disadvantageous analyzed case, i.e., without any economic incentive for providing flexibility, the investment cost of building a CP2H plant was found to be economically positive, with a Simple Payback (SPB) of approximately 10.2 years.
- The exploitation of CP2H flexibility allows the economic profitability of the plant to be increased. In the most favorable analyzed case (i.e., the one that assumed higher incentives for the offered flexibility), the use of flexibility made it possible to increase the Net Present Value (NPV) of the plant by about 82% and to reduce the SPB by about 20%.
- Although all the analyzed CP2H units were connected to the same electricity distribution network, the location of the flexibility units had considerable impact on the CP2H plants' performance. In order to maximize the economic profitability of the plant, it would be necessary to place the CP2H plant downstream of the transformer that is affected the most by RES over-generation. In the analyzed scenario, the optimal positioning of CP2H within the electricity network yielded a 40% increase in profitability.



# Chapter 6

## Case-study 4 – Techno-economic analysis of localized Power-to-Heat plants in an energy community

Chapter 6 analyzes the flexibility enabled by the localized Power-to-Heat energy conversion technology applied in an Energy Community context. The mass and thermal inertia of buildings is exploited to flexibly modulate the use of localized Power-to-Heat technologies. This allows the flexibility of the thermal sector to be used within the electricity sector, according to the Virtual Energy Storage principle. The flexibility enabled by Virtual Energy Storage was used to optimize the self-consumption of an Energy Community. This solution was evaluated from a technical and an economic point of view, and then compared with the more traditional solution of electrical storage systems. Finally, a sensitivity analysis was performed. The analysis analyzed the variations of the Renewable Energy Sources penetration, in order to evaluate the impact of the flexibility of the two flexible solutions in different Renewable Energy Sources penetration scenarios. Results showed that the exploitation of Virtual Energy Storage flexibility allows the self-consumption of an Energy Community to be increased significantly, thus also leading to a benefit from an economic point of view. The electric battery solution enables a higher level of flexibility. However, as a result of the high investment cost, this solution does not result to be economically profitable. It has also been found that the higher the Renewable Energy Sources penetration is, the greater are the energy and economic benefits that a flexible asset may have on an Energy Community.

### 6.1 Introduction

#### 6.1.1 State of the art

The Renewable Energy Directive n.2001/2018 (RED II) [178] and Internal Electricity Market Directive n.944/2019 [179], of the European Community introduced the entity of the Energy Community (EC) to incentivize the consumption of different types of renewable energy. Energy Communities are groups of Renewable Energy Sources (RES) self-consumers that act collectively to produce,

---

share and directly consume clean electricity. The members of an EC may be private users, small and medium-sized enterprises or local authorities. All the EC members must have electricity supply contracts and must be connected to the same low voltage network. An EC must be equipped with one or more renewable production plants, the most common types being photovoltaic, wind and biomass plants. Members must use the existing electricity grid to exchange the self-produced electricity [180]. The installation and use of renewable sources is promoted through incentives for the production of energy and for its self-consumption. The goal of such communities is to promote sustainable and resilient territories by favoring the penetration of RES at local level.

In this context, flexible distributed resources can be used to increase the self-consumption of local renewable energy sources. This chapter analyzes how the localized Power-to-Heat (LP2H) technology can be used to provide flexibility and improve EC energy flows. Indeed, stand-alone electric heating devices (i.e., LP2H systems), such as heat pumps, allow exploiting the inherent flexibility of building heating [56]. Thanks to the thermal inertia of the building mass, the electrical load of LP2H systems can be changed with a certain degree of flexibility. Indeed, the temperature of the building can be changed within a predetermined range without affecting the internal thermal comfort. In this way, the load of the LP2H devices could be controlled to follow the RES production. As described in Section 6.5.1, from the electricity sector point of view, this flexible load could be equated with pure electrical storage, according to the principle known as Virtual Energy Storage (VES) [181].

The energy flexibility of buildings, via LP2H devices, has gained momentum in recent years. In [182], the authors developed a VES model based on a building space equivalent thermal model and used it to calculate the optimal schedule for VES operation. A building based VES model was presented in [183]; the VES was coupled with an economic dispatching model of a hybrid microgrid, in order to effectively reduce daily operating costs. In [184], the authors analyzed the thermal storage capacity that is intrinsically present in a building mass by considering an apartment-block building and a single family house. Their results demonstrated that low energy buildings are particularly suitable for providing flexibility, as such buildings have a large heat capacity. The authors of [185] investigated the performance of an LP2H device and PV panels under different electricity pricing strategies. A smart controller activated the flexible LP2H as a function of the day ahead electricity price so as to reduce overloading of the electricity network and, at the same time, to reduce the LP2H operation cost. In [186], the authors investigated how the flexibility enabled by LP2H, which is used for air conditioning in Singapore, could be exploited to provide ancillary services for the electricity sector. In [187], the flexibility of these systems was analyzed by defining a flexibility parameter composed of the different characteristics of the thermo-physical properties and LP2H systems of a building. In [188], the authors studied, through a

sensitivity analysis, how the building envelope, the weather conditions and users' behavior affected VES flexibility.

For the sake of completeness, it should also be mentioned that numerous articles (e.g. in [189], [190], [191]) dealt with the flexibility of LP2H coupled with dedicated thermal storage systems. This solution allows the flexibility of LP2H systems to be exploited, with less effect on the internal thermal comfort. Nevertheless, the strength of the VES approach is that it is not necessary to install new components to activate this flexibility, except for the monitoring and control system devices (see also [184]). VES flexibility is in fact enabled only by the building heating system and by the thermal mass of the building. In light of that, only the use of the thermal mass of buildings for heat storage is considered in this case study. The use of additional thermal storage systems is beyond the scope of this work.

### **6.1.2 Scientific contribution**

The energy system analyzed in this work is a Multi-Energy System (MES) that encompasses the electricity sector and the heat demand sector of buildings connected through LP2H technologies. This allows the building thermal mass to be used as VES units, thereby enabling the internal flexibility of the building's heating sector. VES enabled flexibility has been compared with the flexibility offered by a centralized Electric Battery (EB). The flexibility of these two technologies is here analyzed in the context of energy communities. The flexible use of both technologies makes it possible to modulate the consumption of electricity at the local level and improve the match between the generation and consumption of energy. This in turn leads to an increase in the self-consumption of renewable energy produced by the energy community and, consequently, an increase in earnings for dedicated incentives. The energy flows of the energy community were assessed on an annual basis. VES and EB solutions were compared, from an energy point of view, by calculating the self-sufficiency and self-consumption of the EC, and from an economic point of view, by calculating the cash flows of the energy community on an annual basis and the Net Present Value (NPV).

## **6.2 Scenario description and techno-economic parameters**

The EC was analyzed from an MES point of view. The MES encompassed the electricity sector and the heating sector. Three different EC configurations were considered:

- The Base case (BC), where the electricity and heating sectors were connected through LP2H distributed systems. In this scenario, the LP2H

systems were not flexibly controlled to offer flexibility. Hence, the LP2H systems of this case-study constituted a non-flexible load. See Figure 6-1a.

- The VES case. From the point of view of the technologies installed within the EC, the VES case was the same as the Base case. However, the LP2H systems are here controlled to enable VES flexibility that was used to optimize the energy flows of the EC. See Figure 6-1b.
- The EB case, where a centralized electrical storage system was connected to the photovoltaic plant. The electrical battery allowed the energy produced by the PV plant to be absorbed and released flexibly, according to the EC needs. As in the Base case, VES flexibility was not exploited in this case, and the electricity consumption of the LP2H systems constituted a non-flexible load (See Figure 6-1c).

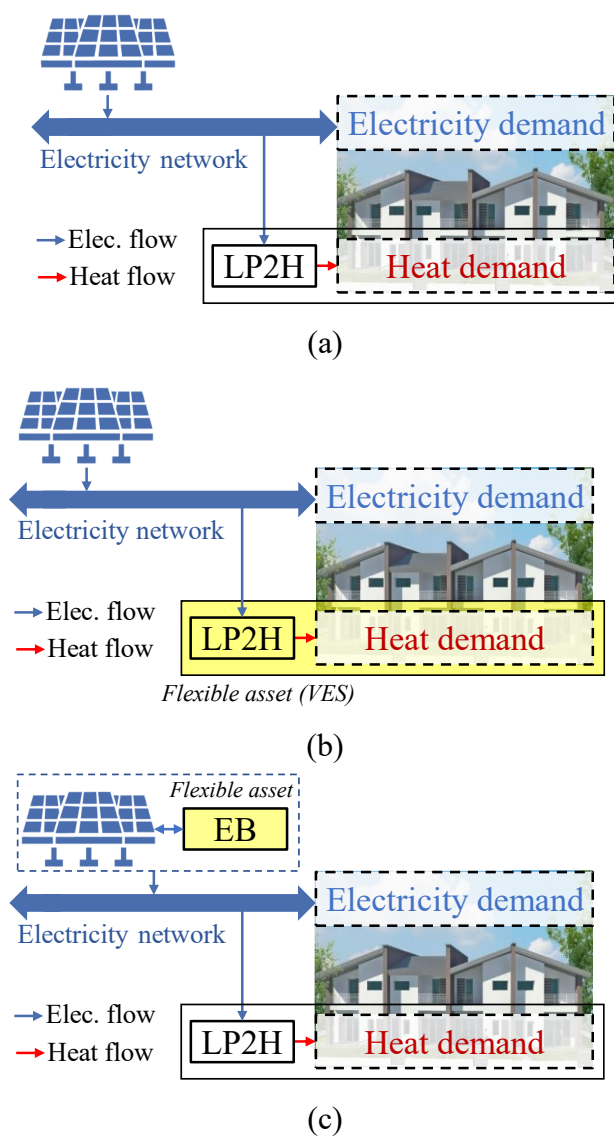


Figure 6-1. Schema of the analyzed multi-energy systems: Base case (a), VES case (b) and EB case (c). The flexibility assets have been highlighted in yellow.

Compared to the Base and the VES cases, the EB case required an additional investment cost due to the installation and maintenance of the electric battery.

The three cases were simulated separately for a whole year with a temporal discretization of 15 minutes.

### 6.2.1 Type of buildings and localized Power-to-Heat systems

As described in Chapter 2, the VES model was created on the basis of real data from buildings in of St. Julien-Mont-Denis, a municipality located at about 600 m above sea level in the Western Alps, near the border between Italy and France. In order to estimate the heat demand of the buildings and photovoltaic production, the climatic and solar radiation data used for the simulation of the scenario were also taken from the same site as the pilot plant. It was assumed that the EC consisted of 50 single-family terraced villas. All the buildings were assumed to have identical characteristics. Each unit had an area of 100 square meters. It was assumed that the dwellings were all new generation energy class A dwellings, according to the European Directive 2010/31/EU classification [192]. Hence, their annual consumption was estimated to be between 15 and 30 kWh/m<sup>2</sup> per year. All the EC users were considered to be equipped with ground source heat pump heating systems (i.e., LP2H systems). Each LP2H device had a nominal electric power of 3 kW. Thanks to the thermal insulation of the buildings and the not too high outside temperature, the buildings did not require cooling, not even in the summer months. In fact, the outside temperature can drop below 15°C, even in the summer months, due to the Alpine climate (see Figure 6-2). It was assumed that LP2H systems would be used only for heating purposes.

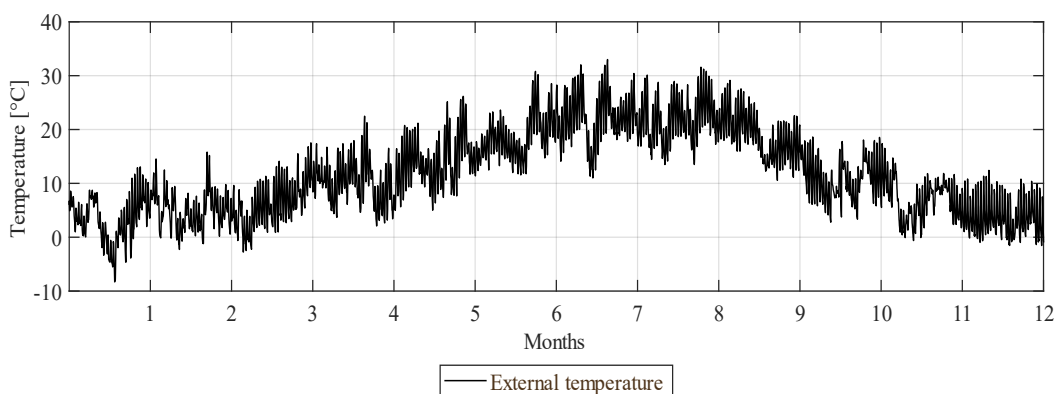


Figure 6-2. Annual profile of the external temperature [193].

### 6.2.2 Scenario energy demand, energy production and storage capacity

The buildings' heat demand and the resulting electricity consumption were calculated as a function of the climatic profiles by means of the VES model

described in Chapter 2. The electricity consumption of the LP2H devices is reported in Figure 6-3. The electricity consumption of the users, excluding the electricity consumption of the LP2H devices, was estimated through a characteristic profile of electricity consumption for residential users (e.g., the electric load represented the electrical consumption of household appliances, lighting, etc.; see Figure 6-4.). Henceforth, we will refer to this electrical consumption with the term “passive load”: unlike the electrical consumption of the LP2H devices, the passive load is here considered as a non-flexible electrical load. The energy community is hypothesized to have a photovoltaic plant.

In order to highlight the impact of flexibility on the EC under different conditions of renewable energy penetration, a sensitivity analysis was performed on the variation of the installed capacity of the PV system. 60 kW was the estimated maximum capacity of the PV system. A larger PV plant was considered, because, given its high cost, a system of this size would be unrealistic for the analyzed EC. A nominal capacity of 40 kW has been chosen as a starting value for the sensitivity analysis. The annual production profile of the plant is shown in Figure 6-5. The results of a sensitivity analysis, performed on the variation of the installed photovoltaic power in order to consider different levels of RES penetration, are presented in Sections 6.5.3 and 6.5.4.

In the scenario with the electric battery, it is assumed that the energy community is equipped with a centralized lithium-ion electrical storage system directly connected to the PV plant. The energy flows of the EC are influenced not only by the capacity of the PV plant, but also by the storage capacity. However, the VES storage capacity is constrained by the number of buildings in the energy community. The storage capacity of the electric battery, instead, can be modified without these kinds of restrictions. However, in order to compare the flexibility of the two flexible solutions under equal conditions, the electric battery capacity has been chosen in order to be as close as possible to the VES storage capacity (see Section 6.5.2). According to this approach, the electric battery capacity is assumed to have a storage capacity of 115 kWh. For the sake of completeness, in Section 6.5.4, a sensitivity analysis on the variation of the capacity of the electric battery is also reported.

The scenario’s parameters are summarized in Table 6-1. Figure 6-6 reports the load duration curve of PV generation, LP2H electricity consumption and passive load.

*Table 6-1. Scenario parameters.*

<b>Parameter</b>	<b>Unit</b>	<b>Value</b>
Number of residential users	-	50
PV installed power	kW	40
EB capacity	kWh	115

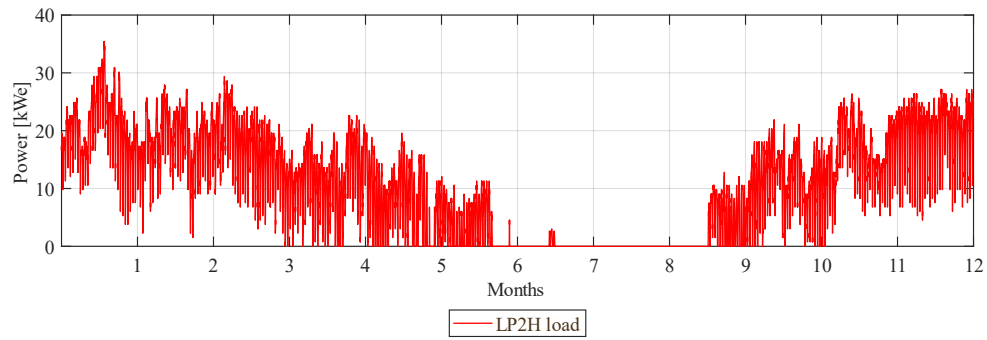


Figure 6-3. Annual profile of LP2H devices' electricity consumption.

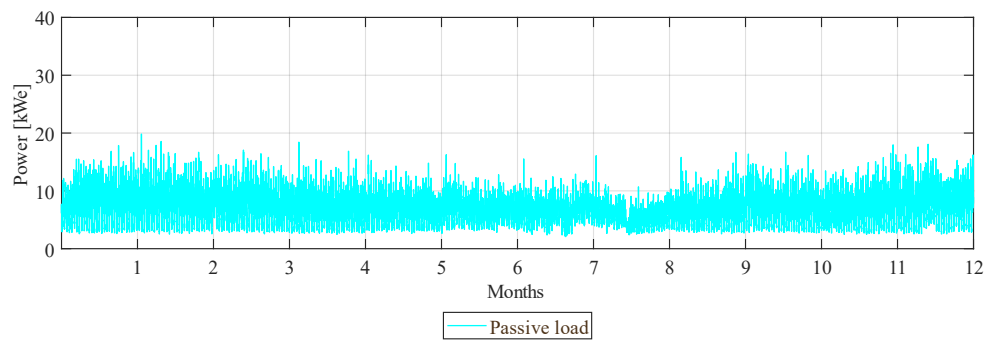


Figure 6-4. Annual profile of the passive electricity load.

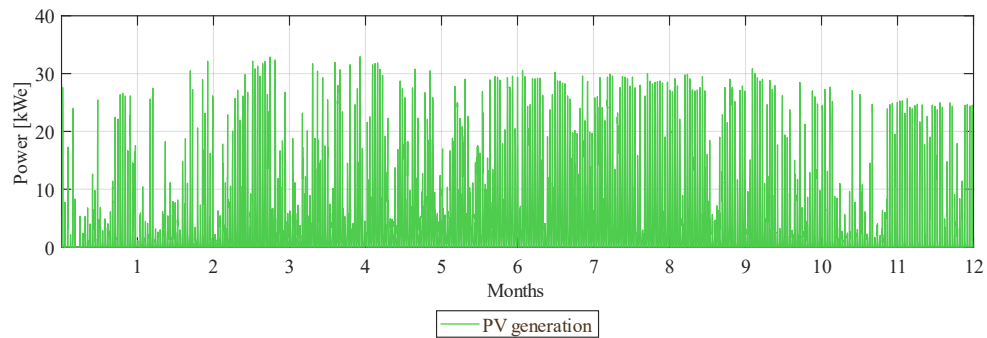


Figure 6-5. Annual profile of the PV production [193].

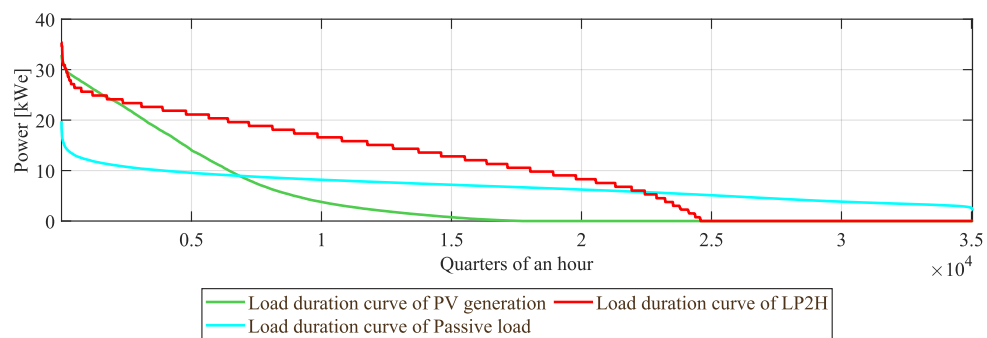


Figure 6-6. Load duration curve of PV generation, LP2H electricity consumption and passive load.

## 6.3 Economic analysis

### 6.3.1 Flexible assets cost assumptions

As previously concluded in different studies [184],[185],[188],[194], one of the main advantages of exploiting the flexibility that is derived from the thermal mass of a building is that this flexible solution is enabled by components, namely, the thermal mass of the buildings and the heating system device, both of which were already available for each building and hence required no additional expenditure. In order to control the LP2H devices in a flexible manner, it is necessary to have a suitable control of the heating system, which needs to be equipped with smart meters and dedicated software to manage the heating of a building. However, as also concluded in [184] and [194], in new residential buildings (such as those analyzed in this case study), the heating system is connected to a building's management system. In this case is therefore sufficient to reprogram the management software to flexibly control the LP2H systems, with no need to invest in new components.

In [195], the authors collected several reports on the evolution of the cost of lithium-ion stationary batteries ([196],[197],[198],[199],[200]). They concluded that the investment cost for lithium-ion batteries is still very uncertain. Considering the studies analyzed in that report, the total investment cost of lithium-ion battery storage plants<sup>7</sup>, was estimated to cover a wide possible cost range, between 850 and 100 €/kWh. For this study, we decided to consider an optimistic value of 300 €/kWh. According to [120], [201], the EB O&M is assumed to be equal to 1% of capital expenditure (CAPEX) each year and the EB's lifetime is 10 years [202]. The cost to replace the battery after 10 years is estimated to be 200 €/kWh. The EB cost assumptions are summarized in Table 6-2.

*Table 6-2. The main economic parameters of the electric battery plant.*

<b>Parameter</b>	<b>Unit</b>	<b>Value</b>
Inv. cost for EB	€/kWh	300
O&M EB	% Inv. cost /year	1
EB replacement time	years	10
EB replacement cost	€/kWh	200

<sup>7</sup> The investment includes the battery pack, the balance of system, power conversion system, the energy management system and the construction.



### 6.3.2 Energy Community costs and incentives

According to the Italian law 8/2020 [203],[204], the electricity fed into the grid by the energy community is remunerated by 50 €/MWh. The Italian legislation introduced incentives to encourage the self-consumption of energy. An EC receives € 110 for each self-consumed MWh as an incentive for the self-consumption, plus an additional incentive of € 8 for each self-consumed MWh to compensate the users' charge for the electricity transport and distribution (since, in the case of self-consumed energy, the costs that the network operator must incur for the transport and distribution of energy are reduced). The expenditure for the energy withdrawn from the network is calculated considering a mean cost of 220 €/MWh [180], [185]. The evaluation of the EC's energy flows (the electricity consumption, the electricity fed into the grid and the self-consumed electricity) takes place on an hourly basis [203],[204].

All the possible electricity flows of the analyzed scenario are summarized in Figure 6-7. The PV plant is connected directly to the grid. In the periods in which the EC consumes the energy produced by the PV plant (green arrow), the community sells energy to the grid at a price of €50/MWh, buys energy from the grid at a mean price of €220/MWh and, since that energy is self-consumed, receives incentives of €110 plus €8/MWh. If the PV electricity injected into the grid is not consumed by the EC users (red arrow), the electricity production is remunerated at €50/MWh. In the EB case, the electrical storage is directly connected to the PV system. When the storage absorbs the PV energy, the energy flow does not pass from the grid (purple arrow) and there are therefore neither costs nor incentives. When the battery releases energy to feed the consumption of the EC (yellow arrow), the energy is sold on the grid and purchased by the EC, with the associated incentives for electricity production and self-consumption.

*Table 6-3. Economic parameters.*

<b>Parameter</b>	<b>Unit</b>	<b>Value</b>
Electricity price	€/MWh	220
Electricity sold to the grid	€/MWh	50
Incentives for self-consumption	€/MWh	110
Compensation for unused charges for electricity transport and distribution	€/MWh	8
Incentive lifetime	years	20

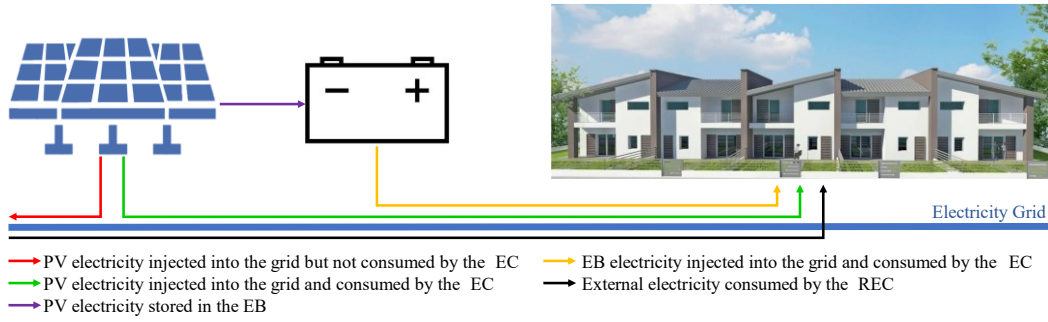


Figure 6-7. Electricity flows in the energy community.

### 6.3.3 Net Present Value

The economic flows of the energy community are assessed on the basis of the electricity consumed, the electricity injection and the flexibility provided, which are calculated as follows:

$$Cost_{el} = c_{el} \cdot \sum_{k=1}^K u_{pass}(k) + u_{LP2H}(k) \quad (6.1)$$

$$Rev_{inj} = r_{inj} \cdot \sum_{k=1}^K g_{PV}(k) + g_{EB}(k) - u_{EB}(k) \quad (6.2)$$

$$Rev_{sc} = \begin{cases} r_{sc} \cdot \sum_{k=1}^K u_{pass}(k) + u_{LP2H}(k), & \text{if } u_{pass}(k) + u_{LP2H}(k) > g_{PV}(k) + g_{EB}(k) \\ r_{sc} \cdot \sum_{k=1}^K g_{PV}(k) + g_{EB}(k), & \text{otherwise} \end{cases} \quad (6.3)$$

where:

- $Cost_{el}$  represents the annual expenses for electricity withdrawn from the grid;
- $c_{el}$  is the annual average electricity price;
- $u_{pass}(k)$  is the load of the passive load at time step  $k$ ;
- $u_{LP2H}(k)$  is the load of the LP2H devices at time step  $k$ ;
- $r_{inj}$  is the specific revenues for the electricity sold to the grid;
- $Rev_{inj}$  indicates the annual revenues for the electricity sold to the grid;
- $g_{PV}(k)$  is the electricity generation of the PV plant at time step  $k$ ;
- $u_{EB}(k)$  is the electric battery electricity absorption at time step  $k$ .
- $g_{EB}(k)$  is the electricity released by electric battery at time step  $k$ ;
- $Rev_{sc}$  indicates the annual revenues deriving from self-consumption incentives;

- $r_{sc}$  represents the specific revenues for self-consumption incentives, which is equal to incentives for the self-consumed electricity, plus the compensation for unused charges for electricity transport and distribution.

The annual cash flow ( $CF$ ) of the energy community is composed by the revenues for the energy injection in the grid ( $Rev_{inj}$ ) plus the revenues for self-consumption incentives ( $Rev_{sc}$ ) minus the costs for energy withdrawn from the grid ( $Cost_{el}$ ) minus the fixed operation cost for the operation and maintenance of the electric battery ( $OPEX_{EB}$ ), which was considered only in the scenario with the electric battery:

$$CF = Rev_{inj} + Rev_{sc} - Cost_{el} - OPEX_{EB} \quad (6.4)$$

The fixed operation and maintenance cost of the LP2H is a sunk cost; the members of the energy community would have to pay the maintenance cost of the heating system, even if they had not decided to establish an energy community. For this reason, the fixed operation and maintenance cost of the LP2H devices was not considered in the economic analysis.

To evaluate and compare the two flexible technologies from an economic point of view, we compared the annual cash flows of the energy community for the conditions without installing a flexibility system (i.e., the BC) with the cash flows that occur when using VES and EB flexibility (i.e., the VES and EB cases respectively).

Specifically, the gains resulting from the use of the VES solution were calculated as the difference in the annual cash flows obtained thanks to the VES solution minus the cash flows calculated for the base scenario (i.e., the BC solution). Similarly, the economic benefits of the EB solution were assessed as the difference between the economic flows that would be generated by the use of the electric battery (i.e., those of the EB scenario) and the cash flows calculated for the base scenario. According to this approach, the annual incomes from the installation of the flexible equipment ( $INC_{VES}$ ,  $INC_{EB}$ ) can be defined as follows:

$$INC_{VES} = CF_{VES} - CF_{BC} \quad (6.5)$$

$$INC_{EB} = CF_{EB} - CF_{BC} \quad (6.6)$$

Based on the incomes from the installation of the flexible technology, the Net Present Value (NPV) of the two solutions ( $NPV_{VES}$  and  $NPV_{EB}$  respectively) can be calculated. The calculation considers a time horizon equal to the years for which the incentives are granted ( $LT_{EC} = 20$  years) and assumes both that the EC has the same energy demand each year and that the PV system produces the same amount of energy. In the EB case, the costs related to the electric battery system must also be considered. These costs include: initial capital expenditure, ( $CAPEX_{EB}$ ), which

occurs only at year 0, and the battery replacement cost ( $REP_{EB}$ ), which occurs only at year 10.

$$NPV_{VES} = \sum_{y=0}^{LT_{EC}} \left( \frac{INC_{VES}}{(1-DR)^y} \right) \quad (6.7)$$

$$NPV_{EB} = -CAPEX_{EB} - \frac{REP_{EB}}{(1-DR)^{10}} + \sum_{y=0}^{LT_{EC}} \left( \frac{INC_{EB}}{(1-DR)^y} \right) \quad (6.8)$$

where  $DR$  is the discount rate assumed to be equal to 5% [180].

## 6.4 Mathematical approach and solution strategy

### 6.4.1 Co-simulation architecture

The electrical network is simulated by the electricity network simplified model. All users are connected to the same MV node. Indeed, as pointed out by [180]'s authors, the users of the EC must be connected to the same low voltage network (i.e., connected to the same medium voltage node). The detailed model is able to simulate the energy flows between the various medium voltage nodes. Since the scenario consists of a single medium voltage node, the use of the detailed model could not add value to the simulation. The electrical network could be simulated with a more detailed model that also takes into account the topology of the low voltage network, but this is beyond the interest of this study.

The LP2H systems and the heat demand of the buildings are simulated by the LP2H model. The electric battery plant is simulated by the EB module.

The modules involved in the co-simulation are listed below (see Table 6-4):

- the time-synchronizer (Time-Sync);
- the controller;
- the electricity network (EN) module;
- the building and localized P2H (LP2H) module;
- the electric battery module (used only for the simulation of the EB case).

Figure 6-8 provides a holistic view of the information exchange architecture and the sequence of interactions of the co-simulation modules for the simulation scenarios Base and VES (the two scenarios involved the same modules and thus have the same co-simulation architecture). As for the other case studies, all the messages exchanged are collected and dispatched by the Time-Sync module. The control system receives as input the LP2H flexibility and the electricity network unbalance calculated in the previous step (*message 1*). The control module output

contains the LP2H electric setpoints<sup>8</sup> (*message 2*), which is sent to the Time-Sync module and subsequently forwarded to the LP2H module (*message 3*). The output LP2H module (*message 4*) contains the electricity consumption of the LP2H units, which is sent to the electricity network (EN) module (*message 5*), and the LP2H flexibility for the next step, which is sent to the control module in the next step of the simulation. The EN module receives the LP2H electricity consumption and calculates the load and generation balance of the network. The output of the EN module (*message 6*) contains the network unbalance used in the following simulation step by the control module, in order to define the new LP2H electric setpoint. Annual simulations are performed with a discretization of 15 minutes, resulting in a total of 35040 time steps.

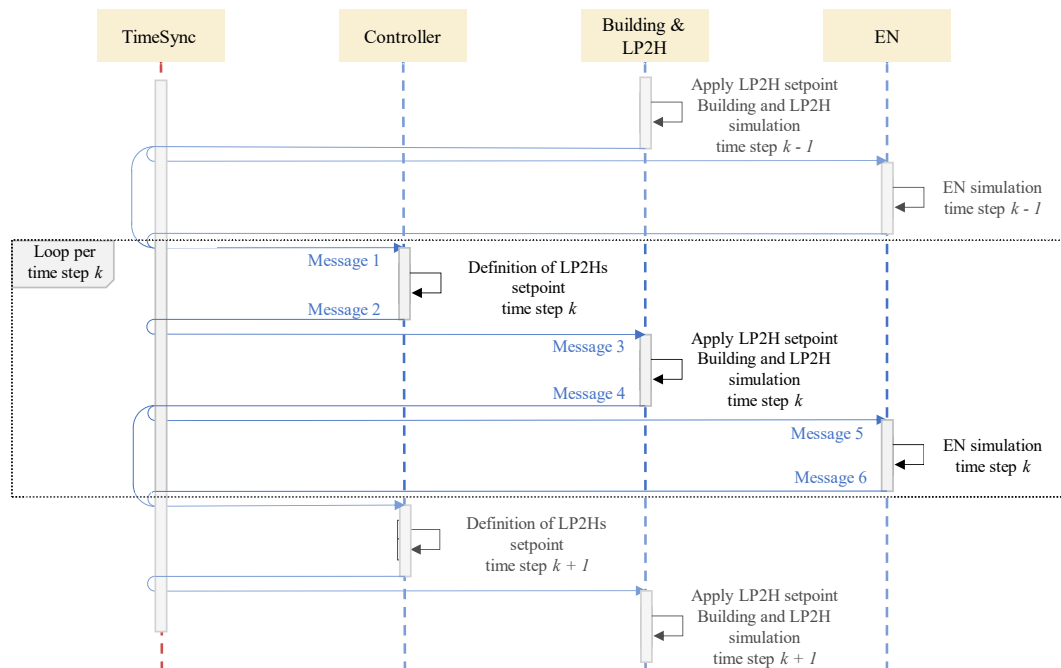


Figure 6-8. Sequence of interactions among co-simulation modules (VES case).

In the EB scenario, the EB module is added in the co-simulation loop (see Figure 6-9). The control module receives, in addition to the balance of the electricity network and the flexibility of the LP2H systems, the flexibility of the system's EB. Based on these values (contained in *message 1*), the control module defines both the setpoints of the LP2H systems<sup>9</sup> and the setpoint of the EB system. These data are contained in *message 2* and are then sent to the Time-Sync. The Time-Sync extracts the setpoint values and sends them: firstly, to the LP2H module (*message 3*) and then, when the simulation of the LP2H module ends (i.e., when the Time-

<sup>8</sup> The reader may note that in the Base case, the flexibility of these systems is not exploited. Hence, the control module sets the setpoints of LP2H units always equal to their baseline value.

<sup>9</sup> The reader may note that in EB case, the flexibility of these systems is not exploited. Hence, the control module sets the setpoints of LP2H units always equal to their baseline value.



---

## 6.4.2 Simulation control algorithms

### Base case

Neither the VES nor the EB flexibility is used in the Base scenario. The LP2H units work to always maintain the internal temperature at 20.5°C. Hence, the LP2H exclusively depends on the external temperature and on the needs of the buildings.

### VES case

VES flexibility is exploited in the VES scenario. If the RES generation is lower than the total network load, the LP2H systems work to maintain the building temperature at the base temperature (20.5°C). When the RES generation exceeds the network's electricity consumption, the LP2H devices increase their consumption to absorb the over-generation of RES. The VES units can absorb the RES over-generation until the internal temperature of the buildings reaches the limit temperature of 23°C. These boundaries are derived from the thermal comfort analysis that were carried out in the pilot plant.

It is important to point out that the building model used for this study (described in Chapter 2) does not allow a change in the baseline setpoint temperature during the heating season. However, the main purpose of the building model is to simulate the heat storage capacity of the thermal mass of the building. This capacity mainly depends on the temperature variation with respect to the baseline temperature, and *not* on the baseline temperature itself. To give a concrete example, the energy that can be stored in the thermal mass of a building by increasing the temperature from 20.5°C to 23°C is very close to the energy that could be stored in the same building by changing the temperature from 19°C to 21.5°C. For this reason, the heat storage capacity of the building can still be simulated with a good approximation, even if the set temperature is kept constant throughout the heating period.

### EB case

In the EB scenario, it is assumed that the EB is purchased. In this case, instead of exploiting the flexibility of the VES, the over-generation of RES is stored in the batteries. When the period of over-production ends, the batteries release the stored energy to satisfy the EC electricity demand. The LP2H devices operate as passive loads, as in the Base case.

## 6.5 Results and discussion

### 6.5.1 The Virtual Energy Storage effect

Figure 6-10a shows the energy flows of the energy community (EC) in the Base case. The simulation was done over the whole year, to show the effects of the control of the LP2H devices on the energy flows of the EC it was chosen to show a

characteristic day: the chosen day is April 20. The blue area is the passive electricity consumption of the EC; the green area is the electricity load of the LP2H systems. The black dotted curve is the renewable energy produced by the EC. Part of the RES energy is consumed by the EC and the remainder (i.e., the RES over-generation, see the yellow area) is sold to the grid, but is not remunerated as self-consumption. The electricity consumption of the LP2H systems is controlled to keep the internal temperature of the buildings at 20.5°C. In Figure 6-10a, it can be seen that the electricity consumption of the LP2H systems decreases during the renewable production peak until it reaches zero. This occurs because solar radiation, in addition to powering the PV systems, raises the temperature, and the heat requirement of the buildings therefore decreases.

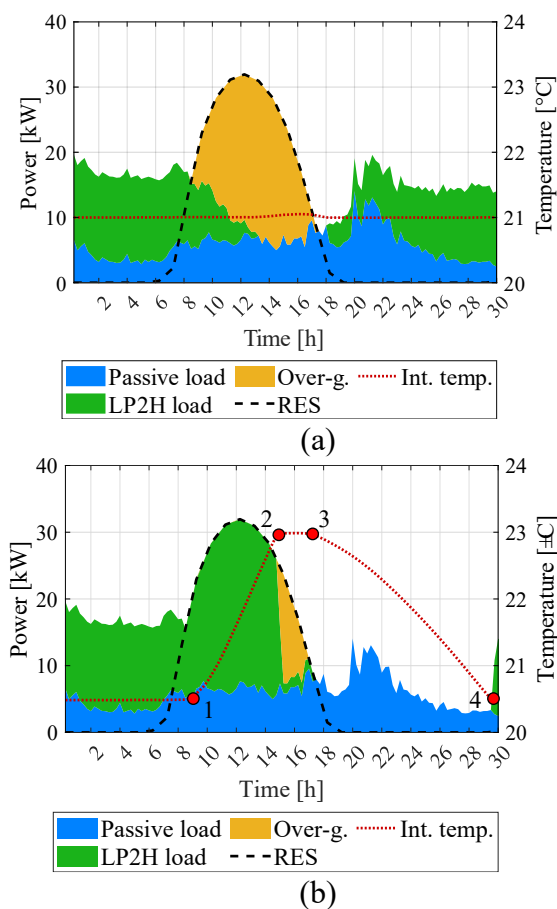


Figure 6-10. Energy community's electricity balance: base case (a) versus LP2H optimized load case (b). Details pertaining to 20<sup>th</sup> April.

The energy flows for the case of a flexible use of LP2H systems (i.e., the VES case) are shown in Figure 6-10b. The EC electricity load coincides with that of the BC scenario up to 9:00 (point 1 in Figure 6-10b). Before this point, the RES generation does not exceed the EC electricity consumption. Beyond this point, the controller modulates the LP2H consumption in order to absorb the renewable over-generation as much as possible. The over-generated RES is completely absorbed up to point 2: the over-generation is converted into thermal energy by the LP2H



systems and stored inside the thermal mass of the buildings. When this happens, the internal temperature of the buildings increase. At point 2, the internal temperature of the buildings reaches 23°C, which is the maximum thermal comfort limit. Once this limit is reached, the surplus energy can no longer be stored inside the buildings. From point 1 to point 3, the LP2H plant operates to maintain the internal temperature at the upper limit of 23°C. When the RES over-generation ends (point 3), the LP2H systems are switched off; it is no longer necessary to heat the buildings as, thanks to the preheating of the previous hours, the internal temperature of the buildings is high enough to maintain thermal comfort. The internal temperature decreases due to the thermal losses of the buildings and, when it reaches 20.5°C, the LP2H systems are switched on again to keep the internal temperature at this temperature level (point 4).

It should be noted that, thanks to the flexible use of these systems, it is possible to shift part of the electricity consumption of the energy community in periods of renewable over-generation, thus allowing the RES self-consumption to be improved.

By comparing the energy flows of the Base case with those of the case in which the consumption of the LP2H devices is controlled to maximize self-consumption (VES case), it can be seen that the effect of the flexible use of LP2H systems causes a shift in the electrical loads (see Figure 6-11). The controlled increase and decrease of the electricity load can be equated with the effect of an electric accumulator. This interpretation of the energy flows is called the Virtual Energy Storage (VES) approach. When LP2H systems are required to consume more than in the Base case, it is interpreted as an accumulation of electricity energy inside the VES. It can be noted that, if compared to that of the baseline, the electrical consumption of the energy community decreases between point 3 and point 4 in Figure 6-10b. This is a release of electricity from the “virtual” batteries, whose accumulated energy is used to cover part of the electricity demand. In this case, the use of the term "virtual" is evident: there is no actual release of electricity. Nonetheless, the overall effect is the same: part of the electricity demand is covered.

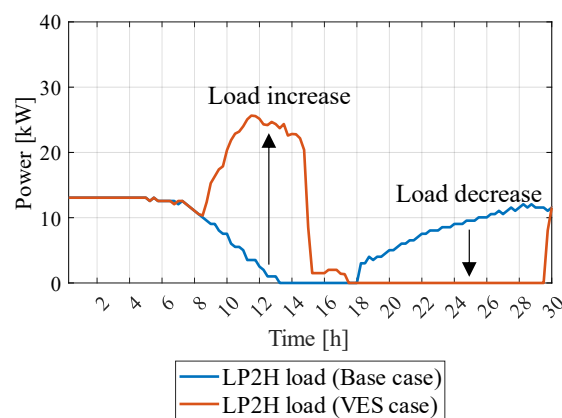


Figure 6-11. LP2H electricity load in Base case and VES case.

Figure 6-12a highlights the electricity virtually accumulated and released by VES. It can be seen that the stored energy is higher than the released one (see Figure 6-12b). This difference is due to the fact that, when energy is accumulated in the VES, the thermal difference between the internal and external temperature of the buildings increases, thus increasing the heat losses. In the VES analogy, this difference corresponds to a non-unitary virtual storage efficiency.

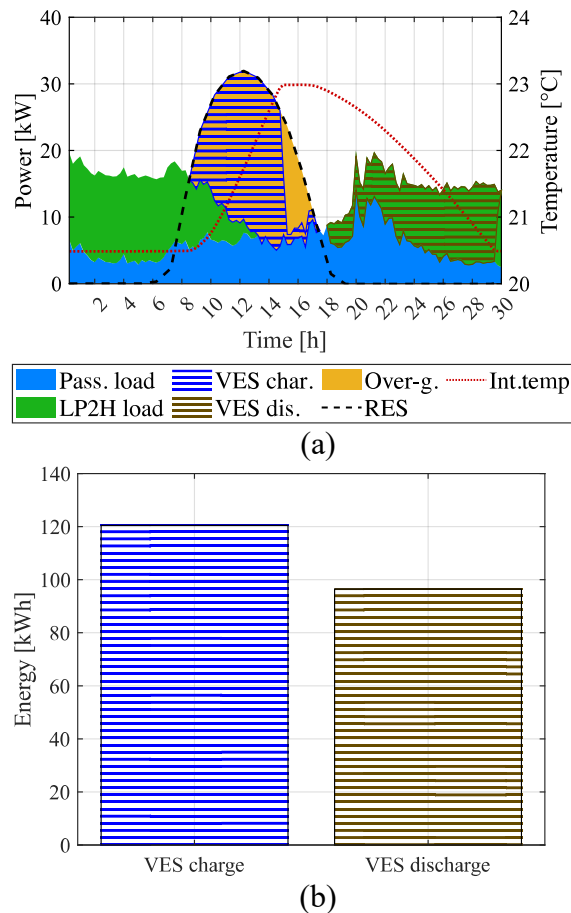


Figure 6-12. The Virtual Energy Storage (VES) effect (a). VES electricity charge and discharge (b). Details pertaining to 20<sup>th</sup> April.

## 6.5.2 Virtual Energy Storage versus electric batteries

This section compares the energy flows obtain in the VES scenario with those of EB scenario. Figure 6-13a shows the electricity flows of the energy community for the case of the installation of an EB. The electricity consumption of the LP2H systems is the same as that of the Base case (see Figure 6-10a). The flexibility of electric batteries is used when the renewable production exceeds the community's electricity demand: excess energy is accumulated inside the battery and released in the hours following the peak. The EB is not able to completely absorb the RES over-generation for the represented day. The EB can absorb energy until its SoC reaches its maximum level. When this happens, the RES surplus is injected into the electricity grid. It can be seen that the electric battery releases the stored energy

faster than the VES. In fact, contrary to what happens in the VES case, the energy accumulated inside the batteries can be used to cover both the passive load (blue area) and the load of the LP2H units (see Figure 6-13a). Conversely, the energy virtually accumulated inside the VES cannot be used to satisfy the passive load (see Figure 6-12a). The two flexibility solutions are able to absorb roughly the same amount of energy before reaching saturation (see Figure 6-12b and Figure 6-13b). The EB storage capacity was in fact chosen to match the storage capacity of the VES in order to compare the flexibility of the two technological solutions.

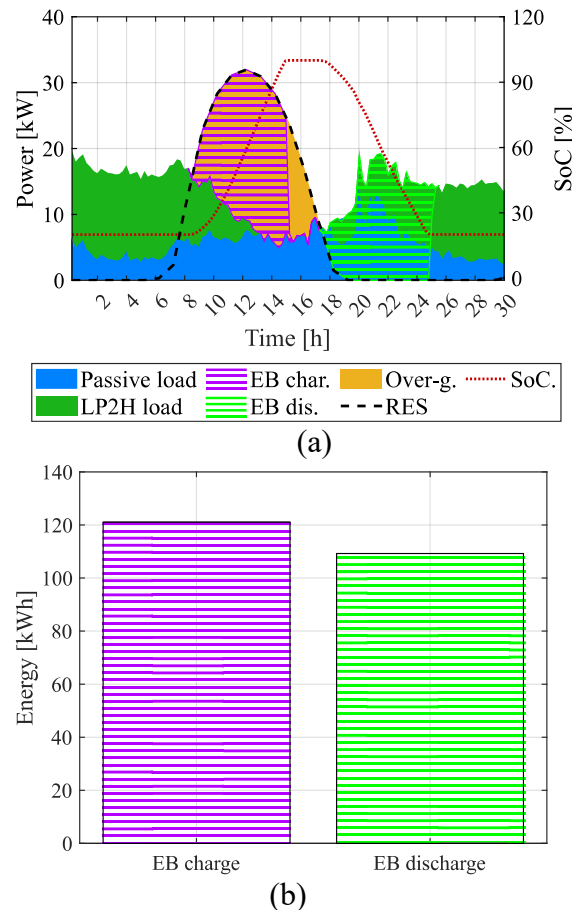


Figure 6-13. Electricity balance of the energy community for the EB case (a). EB electricity charge and discharge (b). Details pertaining to 20<sup>th</sup> April.

Figure 6-14 and Figure 6-15 show the energy flows in winter, in the mid-season and in summer for the VES and EB cases, respectively. The flexibility offered by the two technologies is very similar for the winter and mid-season: both solutions allow the absorption of the overproduction of electricity, thus increasing the EC self-consumption. On the other hand, VES is unable to offer flexibility in the summer period. In fact, when buildings do not require heating, it is not possible to shift the electrical load of the LP2H systems and therefore exploit the VES flexibility. Conversely, EB is not affected by this constraint and its flexibility can always be used.

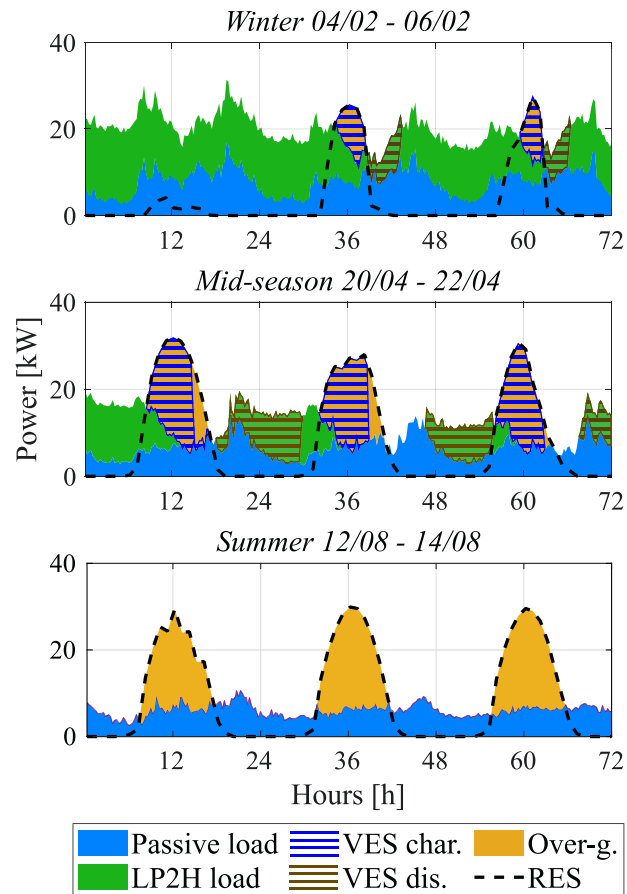


Figure 6-14. Electricity balance of the energy community for different seasons: VES case.

The energy absorbed and released by the two technologies for all the days of the year is represented in Figure 6-16 to better compare the two solutions. The figure groups the energy accumulated and released as a function of the average daily temperature in those days in which flexibility was used: for example, the sum of all the energy absorbed and released in all the days of the year in which the average daily temperature was in the 7.5 – 10°C range is shown in the "7.5 – 10" interval. It can be noted that, as long as the average daily external temperature is below 15°C, both solutions can offer flexibility. In general, the electric battery is able to accumulate energy more efficiently and continuously than the VES solution. As can be seen from the data summarized in Table 6-5, the higher the average external temperature is, the higher is the RES over-generation. This positive relation is due to the fact that on the coldest winter days, the solar radiation is lower and, at the same time, the electricity needs of the EC increase due to the higher electricity consumption of the LP2H devices. On days when the average outside temperature is below 15°C, the flexibility offered by the two technologies is very similar. Under these conditions, both flexible solutions can almost completely absorb the over-generations of RES (see Table 6-5). On days when the average outside temperature is higher, the flexibility of the VES is drastically reduced due to the shutdown of

the heating systems. As previously mentioned, the days with the highest external temperature are those with the highest RES over-generation. In these conditions, the daily RES over-generations saturate the storage capacity of the electric battery: on days when the external temperature exceeds  $22.5^{\circ}\text{C}$ , the electric battery is able to store less than 60% of the over-generations of RES.

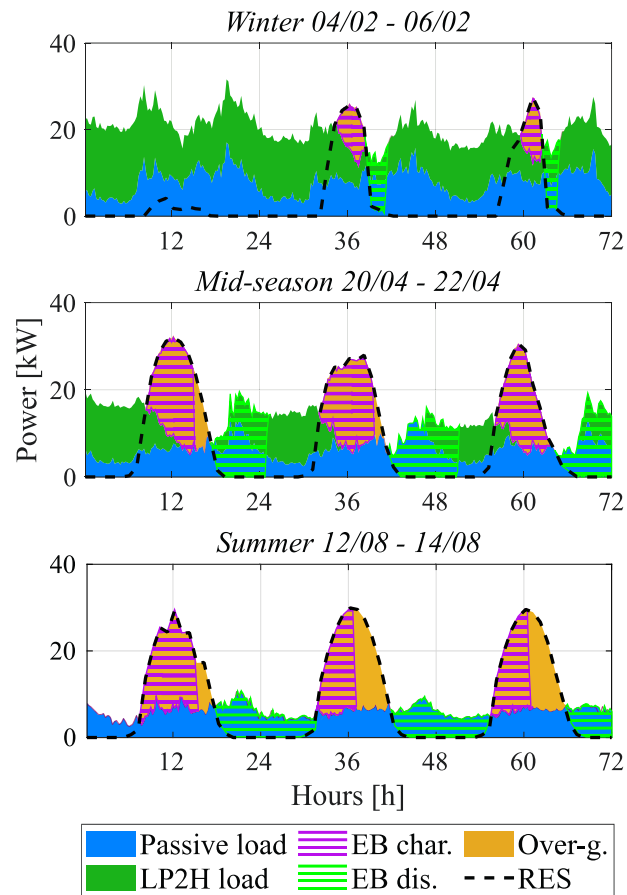


Figure 6-15. Electricity balance of the energy community for different seasons: EB case.

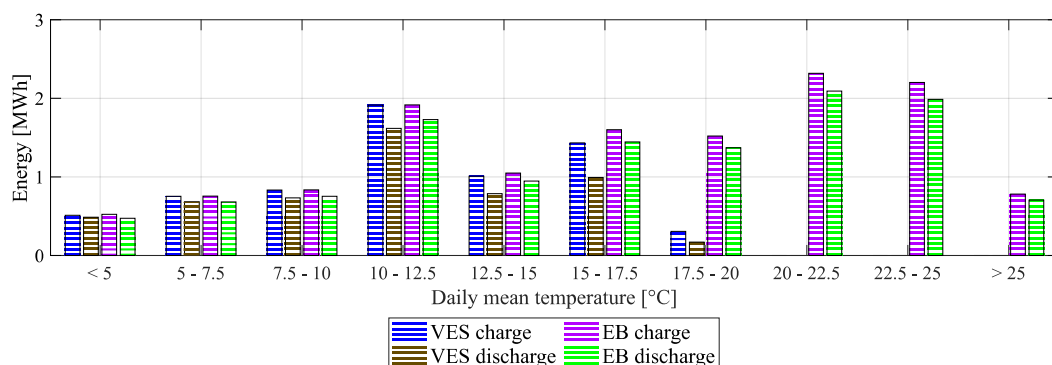


Figure 6-16. Energy accumulated and released by VES and EB throughout the year divided by the average daily temperature.

Table 6-5. RES over-generation and over-generation absorption as a function of the external temperature.

Mean external temperature [°C]	Number of days [-]	RES over-gen. [kWh]	Mean daily RES over-gen [kWh/day]	RES absorbed by VES [%]	RES absorbed by EB [%]
< 5	81	524	6.5	100	100
5 – 7.5	49	756	15.4	100	100
7.5 – 10	35	835	23.9	100	100
10 – 12.5	46	1967	42.8	96	97
12.5 – 15	29	1113	38.4	91	94
15 – 17.5	34	1610	47.3	89	100
17.5 – 20	18	1778	98.8	17	84
20 – 22.5	35	2801	80.0	0	83
22.5 – 25	28	3707	132.4	0	58
> 25	10	1400	140.0	0	56

### 6.5.3 Self-consumption and Self-sufficiency: sensitivity analysis of the RES penetration

This section shows the annual energy flows of the various cases (BC, VES and EB).

Table 6-6 shows the energy flows exchanged between the energy community and the electricity grid on an annual basis: the electricity injected into the grid, the self-consumed electricity and the electricity withdrawn from the grid. The RES electricity fed into the grid in the VES case is the same as that in the Base case, as the LP2H systems do not interact with the PV plant. On the other hand, the EB is directly connected to the photovoltaic systems. When the flexibility of the EB is exploited, the RES energy is not directly injected into the electricity grid, but it is first accumulated inside the battery and, when the EC needs it, fed into the grid. The non-unitary efficiency of the battery leads to a loss of energy during storage, and the quantity of energy fed into the grid therefore decreases.

The energy consumption of the EB case is the same as that of the Base case, as the electric battery use does not change the EC's electricity demand. In the case of VES, however, there is a slight increase in electricity consumption. The flexible use of the LP2H systems causes a non-optimized management of the building heating, which in turn leads to an increase in the building's heat losses and, consequently, in the electricity consumption of the heating systems.

Table 6-6. Annual energy flow of the energy community for the three cases (BC, VES and EB) as a function of different RES penetration scenarios.

RES [kW]	Electricity injection [MWh]			Electricity self-consumed [MWh]			Electricity withdrawn [MWh]		
	Base Case	VES Case	EB Case	Base Case	VES Case	EB Case	Base Case	VES Case	EB Case
20	20.28	20.28	19.92	16.72	17.72	19.92	121.47	121.62	121.47
30	30.42	30.42	29.53	21.07	24.53	29.20	121.47	122.05	121.47
40	40.56	40.56	39.25	24.07	30.83	36.18	121.47	122.76	121.47
50	50.71	50.71	49.05	26.30	36.13	41.53	121.47	123.38	121.47
60	60.85	60.85	58.92	28.09	40.58	45.78	121.47	123.94	121.47

However, the worsening of these two parameters is much lower than the improvement obtained for the self-consumed energy parameter. The VES enabled flexibility allows the self-consumed energy to increase by between 6% and 42%. The greater the RES penetration is, the greater is the percentage increase in self-consumed energy (in the scenario with 40 kW of PV the increase is almost 27%). An even more significant increase, between 19 and 63%, is obtained in the EB case (in the intermediate case with 40 kW, it is about 50%). The flexibility offered by the electric battery has a greater impact since, unlike the VES flexibility, it has fewer utilization constraints. Nevertheless, the impact of VES flexibility on the energy flows is still relevant.

Figure 6-17a and Figure 6-17b report the EC's self-sufficiency and self-consumption, respectively, calculated over the entire year. In the scenario with 40 kW of PV, the use of the VES flexibility increases self-sufficiency by 5 percentage points and self-consumption by 17 percentage points, if compared to the Base case. In the same scenario, the use of EB brings about an increase in self-sufficiency and self-consumption of 10 and 33 percentage points, respectively.

As the RES penetration increases, the endogenous energy production of the EC increases, and so does its self-sufficiency. However, the increase in RES penetration causes an increase in over-generated energy, which makes the EC self-consumption decrease. It can be seen that the greater the penetration of renewable energy is, the greater the benefits brought about by the two flexible solutions. In the scenario in which the greatest improvements of the self-consumption and self-sufficiency parameters occurred (the scenario with 60 kW of PV), almost 38% of self-sufficiency is reached, as a result of the use of the electric battery flexibility. This represents an increase of 15 percentage points, compared to the Base case. It is possible, through the use of the VES flexibility, to reach approximately 33% of self-sufficiency: 10 percentage points greater than in the Base case. Compared to

the Base case, the self-consumption increases by 32 percentage points in the EB case, and by 21 percentage points in the VES case.

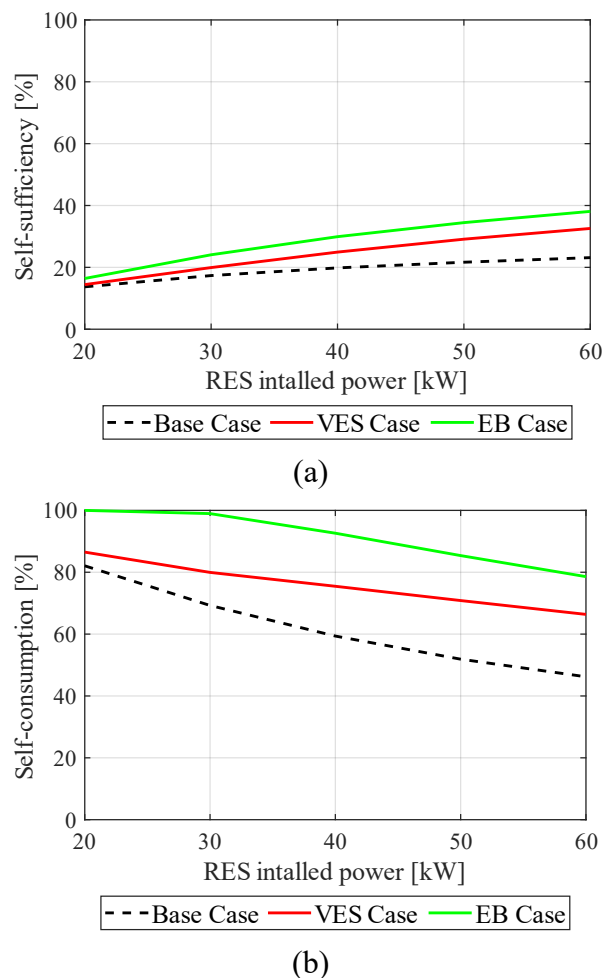


Figure 6-17. Self-sufficiency (a) and self-consumption (b) of the energy community as a function of the RES installed power.

Finally, it can be noted that for low levels of renewable penetration (PV nominal power lower than 30 kW), the EB solution allows all the RES production to be absorbed and almost 100% of self-consumption to be reached. Instead, it is never possible to reach this value with the VES solution. In general, both solutions improve the energy flows of the energy community, but the EB system achieves better self-sufficiency and better self-consumption values.

## 6.5.4 Economic results

### Sensitivity analysis on RES penetration

The annual cash flows for the three different RES penetration scenarios are reported in Table 6-7. As mentioned in the previous section, the use of flexible resources could slightly increase the electricity consumption of the EC and slightly decrease the amount of PV energy fed into the grid slightly. Consequently, the

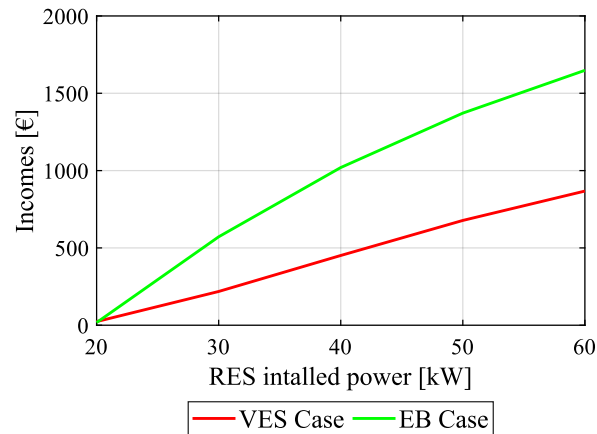


electricity consumption cost could increase slightly and the earnings for the energy fed into the grid could decrease. Moreover, in the EB case the installation of the centralized EB leads to an increase in the operating and maintenance costs. However, the use of flexible resources significantly increases the income from incentives for self-consumption. In the scenario with 40 kW of PV power, the revenues from self-consumption incentives in the VES case are about 30% more than in the Base case. In the EB case, the self-consumption revenues are almost twice as much as those of the Base case. The higher the RES penetration is, the more does the self-consumption revenue percentage increase, thanks to the flexible assets.

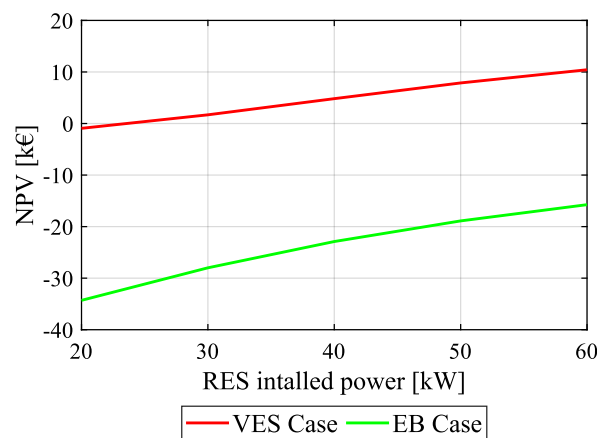
Figure 6-18a shows the total annual incomes for the two VES and EB cases defined in Eq. 6.5 and Eq. 6.6, respectively. Both solutions allow the energy community to improve its annual incomes. The economic benefits of using flexible assets increase as function of renewable penetration. The EB enables greater flexibility and, consequently, the annual gains obtainable with such a solution are greater than those obtainable with the VES flexibility asset. However, when calculating the NPV of the two solutions, it can be seen that the increase in economic revenues resulting from self-consumption of the EC are not sufficient to compensate for the high investment cost necessary for the purchase of the electric battery (this solution has a negative NPV; see Figure 6-18b). Indeed, although the annual earnings are lower than in the EB case, the VES solution resulted to be economically more viable, as yields a positive NPV. The increase in the revenues for self-consumption as the PV penetration increases is also reflected in the NPV: for both solutions, the greater the PV penetration is, the greater is the NPV.

*Table 6-7. Annual cash flows of the energy community for the three cases (BC, VES and EB) under/as a function of different RES penetration scenarios.*

RES [kW]	Electricity injection revenues [€]			Total incentive revenues [€]			Withdrawn electricity expenditure [€]			Fixed O&M expenditure [€]		
	BC	VES	EB	BC	VES	EB	BC	VES	EB	BC	VES	EB
20	1,014	1,014	996	1,973	2,091	2,351	26,723	26,756	26,723	0	0	345
30	1,521	1,521	1,477	2,486	2,895	3,446	26,723	26,851	26,723	0	0	345
40	2,028	2,028	1,963	2,840	3,638	4,270	26,723	27,007	26,723	0	0	345
50	2,536	2,536	2,453	3,103	4,263	4,901	26,723	27,144	26,723	0	0	345
60	3,043	3,043	2,946	3,315	4,788	5,402	26,723	27,267	26,723	0	0	345



(a)



(b)

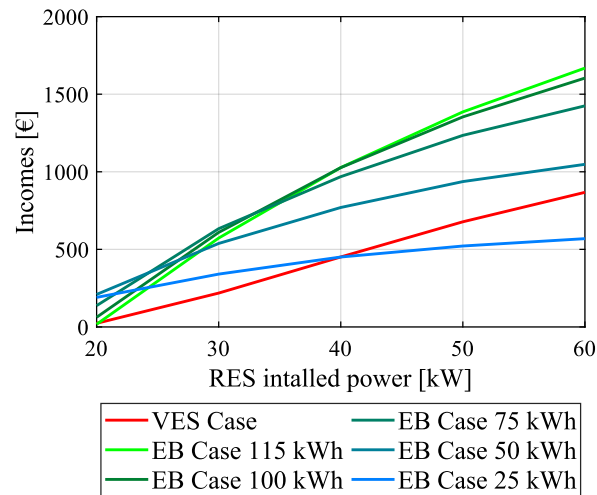
Figure 6-18. Energy community incomes derived from the use of flexible assets as a function of RES penetration (a). Flexible assets Net Present Value as a function of RES penetration (b).

### Sensitivity analysis on EB capacity

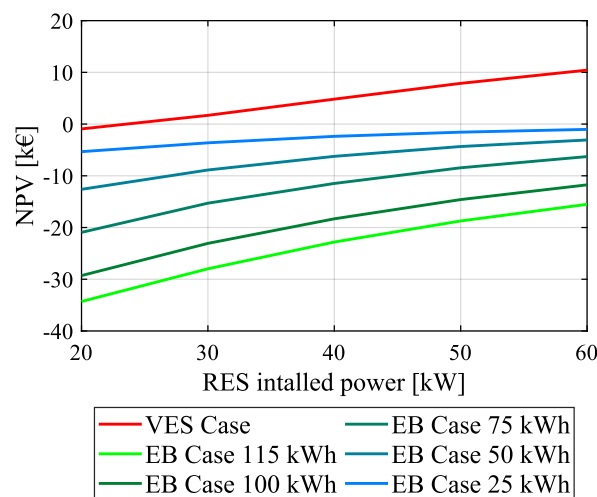
In the previous section, it was seen that the increase in revenues for self-consumption incentives are not sufficient to balance the investment cost for a 115 kWh electric battery. In this section, a sensitivity analysis is performed on the variation of EB storage capacity. Another four new scenarios with a lower battery storage capacity have been considered: 25 kWh, 50 kWh, 75 kWh and 100 kWh (see Figure 6-19).

It can be noted that by decreasing the capacity of the electric battery, the annual incomes for the energy community decrease (see Figure 6-19a). This is because lower battery capacity involves a lower level of self-consumption for the EC and, consequently, the corresponding revenues decrease. However, a lower capacity of the electric battery leads to a lower investment cost, which has a positive effect on the NPV: the lower the installed capacity of the electric battery, the higher the NPV (see Figure 6-19b). Nevertheless, it can be observed that the NPV always remains negative for all the considered cases. It is important to point out that that it would

be technically possible to have a greater r EB storage capacity, which would lead to better flexibility and an associated increase in REC self-consumption. However, the economic benefits derived from a higher level of self-consumption would not counterbalance the increase in the investment cost and would lead to a consequent further deterioration of the NPV parameter.



(a)



(b)

Figure 6-19. Energy community incomes derived from the use as a function of RES penetration and EB capacity (a). Net Present Value as a function of RES penetration and EB capacity (b).

## 6.6 Conclusions

The European Union has recently introduced Energy Community (EC) entities in order to promote the use of Renewable Energy Sources (RES) and promote their consumption at the local level. In this context, flexible assets can be used to optimize the self-consumption of an EC. This study analyzed the energy flows of an EC through the Multi-Energy System approach: (LP2H) conversion technologies allow the electricity sector and the thermal sector to be connected.

LP2H systems can offer flexibility, as they can exploit the thermal inertia of buildings, according to the principle of Virtual Energy Storage (VES). The flexibility enabled by VES, used to optimize the self-consumption of an EC, was compared, from a technical and economic point of view, with that provided by a centralized electrical battery (EB) system.

The LP2H energy conversion technology allows the intrinsic flexibility of the heating sector to be transposed to the electricity one. This flexibility makes it possible to move part of the electrical loads necessary to heat buildings over time. In the VES approach, when the load of the LP2H systems is forcibly increased, electric energy is *virtually* accumulated (hence the name *Virtual Energy Storage*). When this happens, the LP2H system exploits the thermal mass of the building to accumulate heat. In the hours immediately following storage, it is not necessary to use the LP2H systems, as the temperature is kept within the comfort range by means of a buildings' thermal inertia. In the VES analogy, the decrease in the electricity consumption is equated with a release of the electric energy previously accumulated in the VES.

The main conclusions that can be drawn from this analysis can be summarized as follows:

- During the heating season, the flexibility enabled by VES is very similar to that of an electric battery system. However, when the heating systems are not in operation, due to the warm outside temperature, the flexibility of VES cannot be exploited. In these conditions, an accumulation of thermal energy inside the building could cause a violation of its thermal comfort conditions. Conversely, electric batteries are not affected by these constraints and can be used each and every day of the year. In general, the flexibility enabled by an electric battery on an annual basis is greater than that made available by the VES solution. Therefore, from an energy point of view, the benefits brought about by the installation of an EB are greater than those derived from the activation of VES flexibility.
- In the scenario analyzed, considering a 40 kW photovoltaic system, the energy community would reach a self-sufficiency level of 20% and a self-consumption of 59%, without the use of any flexible assets. Enabling VES flexibility would allow both of these parameters to improve. In particular, the VES solution would allow the energy community to improve its self-sufficiency and self-consumption by 5 17 percentage points, respectively. Instead, in the case of the use of a centralized electric battery, self-sufficiency would increase by 10 percentage points, compared to the Base case, and self-consumption would increase by 33 percentage points.
- The two flexible solutions (VES and EB) were analyzed in different scenarios by varying the PV installed power. The higher the penetration of renewable energy is, the greater are the benefits brought about by the two flexible solutions. The improvement in the self-sufficiency and self-

consumption parameters resulting from the use of flexible VES and EB technologies increases as the renewable penetration increases.

- Both technologies make it possible to increase the EC self-consumption of the renewable energy community to a great extent, with a consequent increase in revenues for the related incentives. The EB solution allows higher levels of self-consumption to be reached than the VES solution. This translates into higher economic. However, the gains deriving from the increase in self-consumption of the energy community are not sufficient to compensate for the high investment cost of the electric battery. On the contrary, the VES solution, although less performing from an energy point of view, is economically convenient thanks to the low investment cost required for the activation of this flexible asset. The higher the RES penetration is, the higher is the NPV of the VES solution.

# Chapter 7

## Conclusions

### 7.1 General conclusions

The European decarbonization goals will lead to an increase in distributed renewable generation. The use of renewable sources is essential to mitigate the effects of climate change. Nonetheless, to achieve this type of goal, it is necessary to review the design of the current energy system. The current electrical system is structured with a vertical architecture with few centralized production plants, whose generation is flexibly regulated according to the energy demand. With the increase in distributed energy generation, a new horizontal architecture is emerging, in which small plants inject energy into the system, which is consumed locally. Production from renewable sources is however characterized by a high volatility and intermittency. For this reason, it is necessary to introduce new forms of flexibility at the local level, in order to ensure the match between energy production and demand.

The optimal solution can only be achieved if the energy system is analyzed as a whole, through a comprehensive approach that considers all the various energy sectors (e.g., the electricity sector, the thermal sector and the gas sector). Currently, the various energy sectors are managed mostly independently, without exploiting the possible synergies that may emerge from their coupling. By using energy conversion technologies, it is possible to connect different energy sectors and significantly increase the flexibility of the energy system as a whole.

In the past decades, scientific research has analyzed the various energy sectors independently, which mirrors how energy infrastructures have been managed. Only recently, the analysis of multi-energy systems gained more attention. However, the study of these systems inherently requires a holistic approach that spans across different energy sectors and conversion technologies. This thesis analyzed multi-energy systems by taking the above-mentioned holistic approach: a co-simulation platform was built, in which the physically separate modules of the system

exchanged input and output data. The main advantage of this approach was that in the co-simulation architecture, each component of the multi-energy system was developed in a separate module. In this way, a developer expert in a given component of the system could develop a specific detailed model, without having to directly interact with the modeling of the other multi-energy system components. Thanks to this platform, it was possible to analyze different multi-energy scenarios in collaboration with different research groups, each expert in a specific energy sector.

The scenarios analyzed in this thesis concerned three different energy conversion technologies:

- a) Power-to-Gas plants for the production of Synthetic Natural Gas;
- b) large scale Power-to-Heat plants for the production of heat in a district heating network;
- c) small scale Power-to-Heat for the direct production of heat inside buildings.

The Power-to-Gas technology made it possible to transfer the flexibility of the gas sector within the electricity sector, while the Power-to-Heat technology made it possible to integrate into the electricity sector the flexibility of the centralized heating sector (i.e., of the district heating sector) and of the localized sector (i.e., of buildings not connected to district heating). In this thesis, it was analyzed how the flexibility enabled by these energy conversion technologies could be exploited to optimize the dispatch of distributed renewable resources.

The Power-to-Gas technology was found to be the one with the highest level of flexibility, thanks to the high usability of Synthetic Natural Gas and the storage capacity of the gas network. However, due to the relatively low conversion efficiency and the high investment costs related to the construction of these types of plants, the Synthetic Natural Gas produced from renewable sources is nowadays not able to compete with the cheaper fossil fuel natural gas. Due to its low efficiency and high costs, the Power-to-Gas technology does not appear to be a viable solution for the decarbonization of the gas sector. Nevertheless, given the need to cut fossil fuels, the use of this technology, as well as the other Power-to-fuel solutions, will be pivotal for the decarbonization of some sectors that are difficult to electrify (such as heavy transport, naval transport and aviation).

The use of the Power-to-Heat energy conversion technology within the district heating sector proved to be an efficient solution. The benefits of this technology are twofold. Firstly, it allows the district heating sector to be electrified. Secondly, it allows the intrinsic flexibility of the district heating sector to be used within the electricity sector. However, unlike the gas network, whose storage capacity can be very high, the district heating network was found to be less flexible. In the summer months, when the heat demand is much lower than in winter, the flexible use of Power-to-Heat plants can be hindered by the constraints deriving from the limited heat demand of the district heating network. Nevertheless, the high conversion

efficiency of this technology makes this solution economically convenient, even when their flexibility is not exploited. Furthermore, the flexible utilization of these plants can bring significant economic benefits.

The last technology analyzed was the small-scale Power-to-Heat directly installed inside buildings. Given the decarbonization policies, in the future, the heating systems of many buildings will be based on Power-to-Heat technologies (for example with heat pumps). This allows the thermal flexibility of buildings to be exploited in the electrical sector. In this thesis, it was analyzed how the flexibility of this solution could be exploited in an energy community context to optimize the self-consumption of renewable energy. The analysis found out that weather conditions affect the flexibility of this solution: when the heating system is not in operation, this solution cannot be used to provide flexibility. However, the low investment costs required to activate this flexible resource make this technology an interesting solution to improve energy and economic flows in energy community scenarios.

## 7.2 Outlook

As previously mentioned in the general conclusions, one of the strengths of the work of this thesis lies in the tool's co-simulation approach. In the co-simulation architecture, each module is physically separate from the others. The integration between the various modules takes place by managing the input and output data that the different modules exchange. Thanks to these features, the co-simulation platform can be easily modified. The possible future developments of the research presented in this thesis are therefore manifold and can be summarized as follows:

- *Improvement / modification of existing models*

Each module of the co-simulation platform, being physically separate from the others, can be easily modified or replaced in a plug and play way. Some of the models used in this thesis were made for the simulations of some specific cases. For example, the gas network model developed assumed that the chemical composition of the gas was homogeneous along the network. For this reason, the model could not be used to analyze the injection of hydrogen into the gas network. The model could be improved, or replaced with another model, in order to take these dynamics into account and be able to analyze the injection of hydrogen into the gas network.

The control module could also be modified without changing the co-simulation architecture. In principle, it would be possible to change both the objective function of the optimization and the optimization method used. The control algorithm implemented in the work of this thesis was developed for the control of flexible assets, in order to increase the match between renewable energy production and electricity consumption. This algorithm could be modified in



order to control the setpoints of flexible assets according to other criteria, such as the cost of energy. In addition, the current control algorithm optimized the setpoints of flexible assets with a time horizon of only one step. This algorithm could be improved by introducing new optimization techniques that use a longer time horizon. For instance, a rolling horizon approach, in which the next step is optimized, would also permit to consider the probable evolution of future steps.

- *Connection of new modules*

By modifying the co-simulation architecture, i.e., by modifying the dispatching of the input/output data exchanged between the various modules, it would be possible to integrate new modules into the co-simulation loop. In this way, technologies that were not included in the work of this thesis could be considered. For instance, demand response technologies, flexible cooling in buildings and other energy storage systems, such as pump hydro storage. In addition, it would be possible to integrate new energy sectors and infrastructures, such as the hydrogen sector (injection into the network, storage and use), the district cooling and the electric mobility sector.

- *Hardware in the loop*

The messages that are exchanged during the co-simulation can be redirected to any device. According to this idea, it would be possible to integrate a real plant into the co-simulation platform. The data coming from a real component, collected through specific smart meters could be used by the platform as input for the other software models. Likewise, the simulated data from the platform could be used to control the real device.

With this approach, it would be possible to test how a certain real component could be inserted within a hypothetical multi-energy scenario. This type of simulation, in which a physical component is interacted with a mathematical model that simulates the scenario in which the physical component interacts, is known in the literature as hardware-in-the-loop approach.

- *Co-simulation with other simulation tools*

The co-simulation methodology can also be used by other multi-energy systems simulation platforms. During the last months of my PhD, I collaborated with Professor Henrik Lund of the University of Aalborg (Denmark). The research group of Professor Lund has created a software for the analysis of multi-energy systems: EnergyPLAN. This tool is one of the most used tools for academic studies on multi-energy systems. The goal of the collaboration is to enable the EnergyPLAN software to co-simulation. Co-simulation, in fact, would increase the possible uses of the simulator, thanks to its ability to integrate external models.

## 7.3 Publications

The work of this thesis has led to the publication of the scientific articles listed below. In particular, the mathematical models described in Chapter 2 have been presented in papers 2, 4, 6, 7, 8, 9. The multi-energy system modeling methodology reported in Chapter 2 was published in Papers 3 and 10. The case study presented in Chapter 3 has been published in Paper 6. The results of Chapter 4 has been used for the publication of Paper 7. The analysis presented in Chapter 5 have been published in Paper 8. Finally, the case study analyzed in Chapter 6 have been reported in Paper 9.

### Journal papers

1. Badami M, Bruno JC, Coronas A, **Fambri G**. Analysis of different combined cycles and working fluids for LNG exergy recovery during regasification. *Energy*. 2018;159:373-84.
2. Badami M, **Fambri G**. Optimising energy flows and synergies between energy networks. *Energy*. 2019;15;173:400-12.
3. Badami M, **Fambri G**, Mancò S, Martino M, Damousis IG, Agtzidis D, Tzovaras D. A Decision Support System Tool to Manage the Flexibility in Renewable Energy-Based Power Systems. *Energies*. 2019;13(1):153.
4. **Fambri G**, Badami M, Tsagkrasoulis D, Katsiki V, Giannakis G, Papanikolaou A. Demand Flexibility Enabled by Virtual Energy Storage to Improve Renewable Energy Penetration. *Energies*. 2020;13(19), 5128.
5. Auer H, Patt A, del Granado PC, Peiró LT, **Fambri G**. Modelling climate neutrality for the European Green Deal. *Energy*. 2022;239:122249.
6. **Fambri G**, Diaz-Londono C, Mazza A, Badami M, Sihvonen T, Weiss R. Techno-economic analysis of Power-to-Gas plants in a gas and electricity distribution network system with high renewable energy penetration. *Applied Energy*. 2022;312:118743.
7. **Fambri G**, Diaz-Londono C, Mazza A, Badami M, Sihvonen T, Weiss R. Power-to-Gas in gas and electricity distribution systems: a comparison between modeling approaches. *Journal of Energy Storage*. 2022;55:105454.

### Journal papers that are currently under review:

8. **Fambri G**, Badami M, Tsagkrasoulis D. Flexibility of Virtual Energy Storage based on buildings thermal inertia in Energy Communities: a techno-economic

analysis and comparison with Electric Batteries solution. Under review in *Journal of Energy Storage*.

9. **Fambri G**, Guelpa E, Mazza A, Verda V, Badami M. Power-to-Heat plants in district heating and electricity distribution systems: a techno-economic analysis. Under review in *Energy Conversion and Management*.

### Conference papers

10. Badami M, **Fambri G**, Martino M, Papanikolaou A. ICT optimization tool for RES integration in combined energy networks. In INTELEC 2018 International Telecommunications Energy Conference, IEEE, Turin Oct 7th-11th 2018, Proceedings 2019.
11. Mazza A, Badami M, **Fambri G**, Diaz C, Fantino M, Mirtaheri H, Bertone F. Integration of power to gas and power to heat systems into the electricity grid by the mean of flexibility service for the aggregators. In EfS 2019 4th Energy for Sustainability International Conference, Turin July 24th-26th 2019.
12. Diaz-Londono C, **Fambri G**, Mazza A, Badami M, Bompard E. A Real-Time Based Platform for Integrating Power-to-Gas in Electrical Distribution Grids. In 2020 55th International Universities Power Engineering Conference (UPEC) 2020 Sep 1 (pp. 1-6). IEEE

# References

- [1] Intergovernmental Panel on Climate Change IPCC. AR6 Climate Change 2021: The Physical Science Basis. 2021. Available online at: <https://www.ipcc.ch/report/ar6/wg1/>.
- [2] IPCC - The Intergovernmental Panel on Climate Change IPCC. AR 5 Climate Change 2014: Synthesis report. 2014. Available online at: <https://www.ipcc.ch/report/ar5/syr/>.
- [3] Singh MS, Kuang Z, Maloney ED, Hannah WM, Wolding BO. Increasing potential for intense tropical and subtropical thunderstorms under global warming. *Proceedings of the National Academy of Sciences*. 2017;114(44):11657-62. <https://doi.org/10.1073/pnas.1707603114>.
- [4] Fowler HJ, Lenderink G, Prein AF, Westra S, Allan RP, Ban N, Barbero R, Berg P, Blenkinsop S, Do HX, Guerreiro S. Anthropogenic intensification of short-duration rainfall extremes. *Nature Reviews Earth & Environment*. 2021;2(2):107-22. <https://doi.org/10.1038/s43017-020-00128-6>.
- [5] Chen CT, Lui HK, Hsieh CH, Yanagi T, Kosugi N, Ishii M, Gong GC. Deep oceans may acidify faster than anticipated due to global warming. *Nature Climate Change*. 2017;7(12):890-4. <https://doi.org/10.1038/s41558-017-0003-y>.
- [6] Wigley TM. The Paris warming targets: emissions requirements and sea level consequences. *Climatic Change*. 2018;147(1):31-45. <https://doi.org/10.1007/s10584-017-2119-5>.
- [7] Ding Y, Zhang S, Zhao L, Li Z, Kang S. Global warming weakening the inherent stability of glaciers and permafrost. *Science bulletin*. 2019;64(4):245-53. <https://doi.org/10.1016/j.scib.2018.12.028>.
- [8] Pattyn F, Ritz C, Hanna E, Asay-Davis X, DeConto R, Durand G, Favier L, Fettweis X, Goelzer H, Golledge NR, Kuipers Munneke P. The Greenland and Antarctic ice sheets under 1.5 C global warming. *Nature climate change*. 2018;8(12):1053-61. <https://doi.org/10.1038/s41558-018-0305-8>.
- [9] Hoffmann AA, Rymer PD, Byrne M, Ruthrof KX, Whinam J, McGeoch

- M, Bergstrom DM, Guerin GR, Sparrow B, Joseph L, Hill SJ. Impacts of recent climate change on terrestrial flora and fauna: Some emerging Australian examples. *Austral Ecology*. 2019;44(1):3-27. <https://doi.org/10.1111/aec.12674>.
- [10] Desmet K, Rossi-Hansberg E. On the spatial economic impact of global warming. *Journal of Urban Economics*. 2015;88:16-37. <https://doi.org/10.1016/j.jue.2015.04.004>.
- [11] Carleton TA, Hsiang SM. Social and economic impacts of climate. *Science*. 2016;353(6304):aad9837. <https://doi.org/10.1126/science.aad9837>.
- [12] Diffenbaugh NS, Burke M. Global warming has increased global economic inequality. *Proceedings of the National Academy of Sciences*. 2019;116(20):9808-13. <https://doi.org/10.1073/pnas.1816020116>.
- [13] United Nations Framework Convention on Climate Change UNFCCC website. Available online at: <https://unfccc.int/>.
- [14] UNFCCC. Kyoto Protocol to the United Nations Framework Convention on Climate Change. 1997. Available online at: [http://unfccc.int/kyoto\\_protocol/items/1678.php](http://unfccc.int/kyoto_protocol/items/1678.php).
- [15] UNFCCC. Report of the Conference of the Parties on its fifteenth session, held in Copenhagen from 7 to 19 December 2009. Available online at: <https://unfccc.int/sites/default/files/resource/docs/2009/cop15/eng/11a01.pdf>.
- [16] UNFCCC. The Paris agreement. Available online at: <https://unfccc.int/process-and-meetings/the-paris-agreement/the-paris-agreement>.
- [17] European Commission. Energy roadmap 2050. 2012. Available online at: [https://ec.europa.eu/energy/sites/ener/files/documents/2012\\_energy\\_road\\_map\\_2050\\_en\\_0.pdf](https://ec.europa.eu/energy/sites/ener/files/documents/2012_energy_road_map_2050_en_0.pdf).
- [18] European Commission. Clean energy for all Europeans. 2019. Available online at: [https://energy.ec.europa.eu/topics/energy-strategy/clean-energy-all-europeans-package\\_en](https://energy.ec.europa.eu/topics/energy-strategy/clean-energy-all-europeans-package_en).
- [19] European Commission. Resolution of 14 March 2019 on climate change - a European strategic long-term vision for a prosperous, modern, competitive and climate neutral economy in accordance with the Paris Agreement (2019/2582(RSP)). 2019. Official Journal of the European Union. Available online at: [https://oeil.secure.europarl.europa.eu/oeil/popups/ficheprocedure.do?lang=en&reference=2019/2582\(RSP\)](https://oeil.secure.europarl.europa.eu/oeil/popups/ficheprocedure.do?lang=en&reference=2019/2582(RSP)).
- [20] European Commission. Communication from the commission to the European parliament, the council, the European economic and social

- committee of the regions. Stepping up Europe's 2030 climate ambition. 2020. Available online at: <https://eur-lex.europa.eu/legal-content/EN/TXT/?uri=CELEX%3A52020DC0562>.
- [21] European Commission. Communication from the commission to the European parliament, the council, the European economic and social committee of the regions. 'Fit for 55': delivering the EU's 2030 Climate Target on the way to climate neutrality. 2021. Available online at: <https://eur-lex.europa.eu/legal-content/EN/TXT/?uri=CELEX%3A52021DC0550>.
- [22] U.S. Environmental Protection Agency EPA. Sources of Greenhouse Gas Emissions. Available online at: <https://www.epa.gov/ghgemissions/sources-greenhouse-gas-emissions>.
- [23] European Environmental Agency EEA. Greenhouse gas emission intensity of electricity generation in Europe. Available online at: <https://www.eea.europa.eu/data-and-maps/indicators/overview-of-the-electricity-production-3/assessment-1>.
- [24] International Energy Agency IEA. Evolution of renewable compared to fossil fuel production in OECD Europe, 2010-2020. Available online at: <https://www.iea.org/data-and-statistics/charts/evolution-of-renewable-compared-to-fossil-fuel-production-in-oecd-europe-2010-2020>.
- [25] International Renewable Energy Agency IRENA. Renewable power generation costs in 2019. 2020. Available online at: <https://www.irena.org/publications/2020/Jun/Renewable-Power-Costs-in-2019>.
- [26] Our World in Data. Electricity Mix. Available online at: <https://ourworldindata.org/electricity-mix>.
- [27] Eurostat. Where does our energy come from? Available online at: <https://ec.europa.eu/eurostat/cache/infographs/energy/bloc-2a.html>.
- [28] Hydropower in Europe. Hydropower Energy. Available online at: <https://hydropower-europe.eu/about-hydropower-europe/hydropower-energy/>.
- [29] Jäger-Waldau A, Kougias I, Taylor N, Thiel C. How photovoltaics can contribute to GHG emission reductions of 55% in the EU by 2030. Renewable and Sustainable Energy Reviews. 2020;126:109836. <https://doi.org/10.1016/j.rser.2020.109836>.
- [30] Wind Europe. Wind energy in Europe, Scenarios for 2030. Available online at: <https://windeurope.org/about-wind/reports/wind-energy-in-europe-scenarios-for-2030/>.
- [31] Lichtenegger G, Rentizelas AA, Trivyza N, Siegl S. Offshore and onshore wind turbine blade waste material forecast at a regional level in Europe

- until 2050. Waste Management. 2020;106:120-31. <https://doi.org/10.1016/j.wasman.2020.03.018>.
- [32] Snam, Terna. Documento di Descrizione degli Scenari 2022. 2022. Available online at: [https://download.terna.it/terna/Documento\\_Descrizione\\_Scenari\\_2022\\_da74044f6ee28d.pdf](https://download.terna.it/terna/Documento_Descrizione_Scenari_2022_da74044f6ee28d.pdf).
- [33] North American Electric Reliability Corporation NERC. Understanding the Grid. 2013. Available online at: <https://www.nerc.com/AboutNERC/Documents/Understanding%20the%20Grid%20AUG13.pdf>.
- [34] Mazza A, Salomone F, Arrigo F, Bensaid S, Bompard E, Chicco G. Impact of Power-to-Gas on distribution systems with large renewable energy penetration. Energy Conversion and Management: X. 2020;7:100053. <https://doi.org/10.1016/j.ecmx.2020.100053>.
- [35] Bertsch J, Growitsch C, Lorenczik S, Nagl S. Flexibility in Europe's power sector-An additional requirement or an automatic complement? Energy Economics. 2016;53:118–31. <https://doi.org/10.1016/j.eneco.2014.10.022>.
- [36] Schermeyer H, Vergara C, Fichtner W. Renewable energy curtailment: A case study on today's and tomorrow's congestion management. Energy Policy. 2018;112:427-36. <https://doi.org/10.1016/j.enpol.2017.10.037>.
- [37] CEDEC, Eurogas, GEODE. Flexibility in the Energy Transition: A Toolbox for Gas DSOs. 2016. Available online at: [https://eurogas.org/media\\_centre/reports-flexibility-for-the-energy-transition-a-toolbox-for-electricity-and-gas-dsos/](https://eurogas.org/media_centre/reports-flexibility-for-the-energy-transition-a-toolbox-for-electricity-and-gas-dsos/).
- [38] Council of the European Union EP. Regulation (EU) 2019/943 of the European Parliament and of the Council of 5 June 2019 on the internal market for electricity. vol. 62. 2019. Available online: <https://eur-lex.europa.eu/legal-content/EN/TXT/PDF/?uri=CELEX:32019R0943&from=EN>.
- [39] The SmartNet Consortium. TSO-DSO Coordination for Acquiring Ancillary Services From Distribution Grids. 2019. Available online: <http://smartnet-project.eu/wp-content/uploads/2019/05/SmartNet-Booklet.pdf>.
- [40] Li N, Uckun C, Constantinescu EM, Birge JR, Hedman KW, Botterud A. Flexible Operation of Batteries in Power System Scheduling with Renewable Energy. IEEE Transactions on Sustainable Energy. 2016;7:685–96. <https://doi.org/10.1109/TSTE.2015.2497470>.
- [41] Simão M, Ramos HM. Hybrid pumped hydro storage energy solutions towards wind and PV integration: Improvement on flexibility, reliability

- and energy costs. *Water*. 2020;12. <https://doi.org/10.3390/w12092457>.
- [42] Amoli NA, Meliopoulos APS. Operational flexibility enhancement in power systems with high penetration of wind power using compressed air energy storage. 2015 Clemson Univ. Power Syst. Conf. PSC 2015, Clemson, SC, USA: IEEE; 2015. <https://doi.org/10.1109/PSC.2015.7101694>.
- [43] Lund H, Østergaard PA, Connolly D, Ridjan I, Mathiesen BV, Hvelplund F, et al. Energy storage and smart energy systems. *International Journal of Sustainable Energy Planning and Management*. 2016;11:3–14. <https://doi.org/10.5278/ijsepm.2016.11.2>.
- [44] Chicco G, Riaz S, Mazza A, Mancarella P. Flexibility from Distributed Multienergy Systems. *Proceedings of the IEEE*. 2020;108:1496–517. <https://doi.org/10.1109/JPROC.2020.2986378>.
- [45] Mathiesen B V, Lund H, Connolly D, Wenzel H, Ostergaard PA, Möller B, et al. Smart Energy Systems for coherent 100% renewable energy and transport solutions. *Applied Energy*. 2015;145:139–54. <https://doi.org/10.1016/j.apenergy.2015.01.075>.
- [46] Mancarella P. Smart multi-energy grids: concepts, benefits and challenges. In 2012 IEEE Power and Energy Society General Meeting 2012 Jul 22 (pp. 1-2). IEEE. <https://doi.org/10.1109/PESGM.2012.6345120>.
- [47] Mancarella P. MES (multi-energy systems): An overview of concepts and evaluation models. *Energy*. 2014;65:1-7. <https://doi.org/10.1016/j.energy.2013.10.041>.
- [48] Corsetti E, Riaz S, Riello M, Mancarella P. Modelling and deploying multi-energy flexibility: The energy lattice framework. *Advances in Applied Energy*. 2021;2:100030. <https://doi.org/10.1016/j.adapen.2021.100030>.
- [49] Mi J, Khodayar ME. Operation of natural gas and electricity networks with line pack. *Journal of Modern Power Systems and Clean Energy*. 2019;7(5):1056-70. <https://doi.org/10.1007/s40565-019-0547-0>.
- [50] Zheng J, Zhou Z, Zhao J, Wang J. Integrated heat and power dispatch truly utilizing thermal inertia of district heating network for wind power integration. *Applied energy*. 2018;211:865-74. <https://doi.org/10.1016/j.apenergy.2017.11.080>.
- [51] Verbeke S, Audenaert A. Thermal inertia in buildings: A review of impacts across climate and building use. *Renewable and sustainable energy reviews*. 2018;82:2300-18. <https://doi.org/10.1016/j.rser.2017.08.083>.
- [52] Badami M, Fambri G. Optimising energy flows and synergies between energy networks. *Energy*. 2019;173:400–12. <https://doi.org/10.1016/j.energy.2019.02.007>.



- 
- [53] Blanco H, Nijs W, Ruf J, Faaij A. Potential of Power-to-Methane in the EU energy transition to a low carbon system using cost optimization. *Applied Energy*. 2018;232:323–40. <https://doi.org/10.1016/j.apenergy.2018.08.027>.
- [54] Quarton CJ, Samsatli S. Power-to-gas for injection into the gas grid: What can we learn from real-life projects, economic assessments and systems modelling? *Renewable and sustainable energy reviews*. 2018;98:302–16. <https://doi.org/10.1016/j.rser.2018.09.007>.
- [55] Thomaßen G, Kavvadias K, Navarro JP. The decarbonisation of the EU heating sector through electrification: A parametric analysis. *Energy Policy*. 2021;148:111929. <https://doi.org/10.1016/j.enpol.2020.111929>.
- [56] Fambri G, Badami M, Tsagkrasoulis D, Katsiki V, Giannakis G, Papanikolaou A. Demand flexibility enabled by virtual energy storage to improve renewable energy penetration. *Energies*. 2020;13(19):5128. <https://www.mdpi.com/1996-1073/13/19/5128>.
- [57] De Luca G, Ballarini I, Paragamyran A, Pellegrino A, Corrado V. On the improvement of indoor environmental quality, energy performance and costs for a commercial nearly zero-energy building. *Science and Technology for the Built Environment*. 2021;27(8):1056-74. <https://doi.org/10.1080/23744731.2021.1940275>.
- [58] Reynders G, Diriken J, Saelens D. Generic characterization method for energy flexibility: Applied to structural thermal storage in residential buildings. *Appl energy*. 2017;198:192-202. <https://doi.org/10.1016/j.apenergy.2017.04.061>.
- [59] Hu G, Chen C, Lu HT, Wu Y, Liu C, Tao L, Men Y, He G, Li KG. A review of technical advances, barriers, and solutions in the Power to Hydrogen (P2H) roadmap. *Engineering*. 2020;6(12):1364-80. <https://doi.org/10.1016/j.eng.2020.04.016>.
- [60] Maroufmashat A, Fowler M. Transition of future energy system infrastructure; through power-to-gas pathways. *Energies*. 2017;10(8):1089. <https://doi.org/10.3390/en10081089>.
- [61] Schmidt O, Gambhir A, Staffell I, Hawkes A, Nelson J, Few S. Future cost and performance of water electrolysis: An expert elicitation study. *International journal of hydrogen energy*. 2017;42(52):30470-92. <https://doi.org/10.1016/j.ijhydene.2017.10.045>.
- [62] Marocco P, Ferrero D, Lanzini A, Santarelli M. Optimal design of stand-alone solutions based on RES+ hydrogen storage feeding off-grid communities. *Energy Conversion and Management*. 2021;238:114147. <https://doi.org/10.1016/j.enconman.2021.114147>.
- [63] Marocco P, Ferrero D, Martelli E, Santarelli M, Lanzini A. An MILP
-

- approach for the optimal design of renewable battery-hydrogen energy systems for off-grid insular communities. *Energy Conversion and Management*. 2021;245:114564. <https://doi.org/10.1016/j.enconman.2021.114564>.
- [64] Dawood F, Shafiullah GM, Anda M. Stand-alone microgrid with 100% renewable energy: A case study with hybrid solar PV-battery-hydrogen. *Sustainability*. 2020;12(5):2047. <https://doi.org/10.3390/su12052047>.
- [65] Marchese M, Giglio E, Santarelli M, Lanzini A. Energy performance of Power-to-Liquid applications integrating biogas upgrading, reverse water gas shift, solid oxide electrolysis and Fischer-Tropsch technologies. *Energy Conversion and Management: X*. 2020;6:100041. <https://doi.org/10.1016/j.ecmx.2020.100041>.
- [66] Chen H, Song J, Zhao J. Synergies between power and hydrogen carriers using fuel-cell hybrid electrical vehicle and power-to-gas storage as new coupling points. *Energy Conversion and Management*. 2021;246:114670. <https://doi.org/10.1016/j.enconman.2021.114670>.
- [67] Oliveira AM, Beswick RR, Yan Y. A green hydrogen economy for a renewable energy society. *Current Opinion in Chemical Engineering*. 2021;33:100701. <https://doi.org/10.1016/j.coche.2021.100701>.
- [68] Field RA, Derwent RG. Global warming consequences of replacing natural gas with hydrogen in the domestic energy sectors of future low-carbon economies in the United Kingdom and the United States of America. *International Journal of Hydrogen Energy*. 2021;46(58):30190-203. <https://doi.org/10.1016/j.ijhydene.2021.06.120>.
- [69] Lu HT, Li W, Miandoab ES, Kanehashi S, Hu G. The opportunity of membrane technology for hydrogen purification in the power to hydrogen (P2H) roadmap: A review. *Frontiers of Chemical Science and Engineering*. 2021;15(3):464-82. <https://doi.org/10.1007/s11705-020-1983-0>.
- [70] Zhao B, Li S, Gao D, Xu L, Zhang Y. Research on intelligent prediction of hydrogen pipeline leakage fire based on Finite Ridgelet neural network. *International Journal of Hydrogen Energy*. 2022;47(55):23316-23. <https://doi.org/10.1016/j.ijhydene.2022.05.124>.
- [71] Wu X, Zhang H, Yang M, Jia W, Qiu Y, Lan L. From the perspective of new technology of blending hydrogen into natural gas pipelines transmission: mechanism, experimental study, and suggestions for further work of hydrogen embrittlement in high-strength pipeline steels. *International Journal of Hydrogen Energy*. 2022;47(12):8071-90. <https://doi.org/10.1016/j.ijhydene.2021.12.108>.
- [72] Korkmaz P, Schmid D, Fahl U. Incorporating uncertainties towards a sustainable European energy system: A stochastic approach for

- decarbonization paths focusing on the transport sector. *Energy Strategy Reviews*. 2021;38:100707. <https://doi.org/10.1016/j.esr.2021.100707>.
- [73] García-Villalobos J, Zamora I, San Martín JI, Asensio FJ, Aperribay V. Plug-in electric vehicles in electric distribution networks: A review of smart charging approaches. *Renewable and Sustainable Energy Reviews*. 2014;38:717-31. <https://doi.org/10.1016/j.rser.2014.07.040>.
- [74] Deilami S, Masoum AS, Moses PS, Masoum MA. Real-time coordination of plug-in electric vehicle charging in smart grids to minimize power losses and improve voltage profile. *IEEE Transactions on Smart Grid*. 2011;2(3):456-67. <https://doi.org/10.1109/TSG.2011.2159816>.
- [75] Li C, Zhang L, Ou Z, Wang Q, Zhou D, Ma J. Robust model of electric vehicle charging station location considering renewable energy and storage equipment. *Energy*. 2022;238:121713. <https://doi.org/10.1016/j.energy.2021.121713>.
- [76] Babrowski S, Heinrichs H, Jochem P, Fichtner W. Load shift potential of electric vehicles in Europe. *journal of power sources*. 2014;255:283-93. <https://doi.org/10.1016/j.jpowsour.2014.01.019>.
- [77] Diaz-Londono C, Colangelo L, Ruiz F, Patino D, Novara C, Chicco G. Optimal strategy to exploit the flexibility of an electric vehicle charging station. *Energies*. 2019;12(20):3834. <https://doi.org/10.3390/en12203834>.
- [78] Wulff N, Miorelli F, Gils HC, Jochem P. Vehicle Energy Consumption in Python (VencoPy): Presenting and Demonstrating an Open-Source Tool to Calculate Electric Vehicle Charging Flexibility. *Energies*. 2021;14(14):4349. <https://doi.org/10.3390/en14144349>.
- [79] Borba BS, Szklo A, Schaeffer R. Plug-in hybrid electric vehicles as a way to maximize the integration of variable renewable energy in power systems: The case of wind generation in northeastern Brazil. *Energy*. 2012;37(1):469-81. <https://doi.org/10.1016/j.energy.2011.11.008>.
- [80] Boström T, Babar B, Hansen JB, Good C. The pure PV-EV energy system—A conceptual study of a nationwide energy system based solely on photovoltaics and electric vehicles. *Smart Energy*. 2021;1:100001. <https://doi.org/10.1016/j.segy.2021.100001>.
- [81] Giordano F, Ciocia A, Di Leo P, Spertino F, Tenconi A, Vaschetto S. Self-consumption improvement for a nanogrid with photovoltaic and vehicle-to-home technologies. In 2018 IEEE International Conference on Environment and Electrical Engineering and 2018 IEEE Industrial and Commercial Power Systems Europe (EEEIC/I&CPS Europe) 2018. (pp. 1-6). IEEE. <https://doi.org/10.1109/EEEIC.2018.8493708>.
- [82] Shamami MS, Alam MS, Ahmad F, Shariff SM, AlSaidan I, Rafat Y, Asghar MJ. Artificial intelligence-based performance optimization of

- electric vehicle-to-home (V2H) energy management system. *SAE International Journal of Sustainable Transportation, Energy, Environment, & Policy*. 2020;1(13-01-02-0007):115-25. <https://doi.org/10.4271/13-01-02-0007>.
- [83] Wenzel G, Negrete-Pincetic M, Olivares DE, MacDonald J, Callaway DS. Real-time charging strategies for an electric vehicle aggregator to provide ancillary services. *IEEE Transactions on Smart Grid*. 2017;9(5):5141-51. <https://doi.org/10.1109/TSG.2017.2681961>.
- [84] Khemakhem S, Rekik M, Krichen L. A flexible control strategy of plug-in electric vehicles operating in seven modes for smoothing load power curves in smart grid. *Energy*. 2017;118:197-208. <https://doi.org/10.1016/j.energy.2016.12.039>.
- [85] Stinner S, Huchtemann K, Müller D. Quantifying the operational flexibility of building energy systems with thermal energy storages. *Applied Energy*. 2016;181:140-54. <https://doi.org/10.1016/j.apenergy.2016.08.055>.
- [86] De Coninck R, Helsen L. Quantification of flexibility in buildings by cost curves—Methodology and application. *Applied Energy*. 2016;162:653-65. <https://doi.org/10.1016/j.apenergy.2015.10.114>.
- [87] Feuerriegel S, Neumann D. Integration scenarios of Demand Response into electricity markets: Load shifting, financial savings and policy implications. *Energy Policy*. 2016;96:231-40. <https://doi.org/10.1016/j.enpol.2016.05.050>.
- [88] Li H, Tang Z, Liu Z, Zhi C. Evaluating flexibility and wearability of flexible energy storage devices. *Joule*. 2019;3(3):613-9. <https://doi.org/10.1016/j.joule.2019.01.013>.
- [89] Teng Y, Wang Z, Li Y, Ma Q, Hui Q, Li S. Multi-energy storage system model based on electricity heat and hydrogen coordinated optimization for power grid flexibility. *CSEE Journal of Power and Energy Systems*. 2019;5(2):266-74. <https://doi.org/10.17775/CSEEJPES.2019.00190>.
- [90] Kubik ML, Coker PJ, Barlow JF. Increasing thermal plant flexibility in a high renewables power system. *Applied Energy*. 2015;154:102-11. <https://doi.org/10.1016/j.apenergy.2015.04.063>.
- [91] Jacobsen HK, Schröder ST. Curtailment of renewable generation: Economic optimality and incentives. *Energy Policy*. 2012;49:663-75. <https://doi.org/10.1016/j.enpol.2012.07.004>.
- [92] Brandstätter C, Brunekreeft G, Jahnke K. How to deal with negative power price spikes?—Flexible voluntary curtailment agreements for large-scale integration of wind. *Energy Policy*. 2011;39(6):3732-40. <https://doi.org/10.1016/j.enpol.2011.03.082>.

- 
- [93] Ulbig A, Andersson G. Analyzing operational flexibility of electric power systems. *International Journal of Electrical Power & Energy Systems*. 2015;72:155-64. <https://doi.org/10.1016/j.ijepes.2015.02.028>.
- [94] Heussen K, Koch S, Ulbig A, Andersson G. Unified system-level modeling of intermittent renewable energy sources and energy storage for power system operation. *IEEE Systems Journal*. 2011;6(1):140-51. <https://doi.org/10.1109/JSYST.2011.2163020>.
- [95] Shirmohammadi D, Hong HW, Semlyen A, Luo GX. A compensation-based power flow method for weakly meshed distribution and transmission networks. *IEEE Transactions on power systems*. 1988;3(2):753-62. <https://ieeexplore.ieee.org/document/192932>.
- [96] Badami M, Bompard E, Diaz-Londono C, Fambri G, Mazza A, Verda V. Deliverable D3.6 PLANET simulation model generator and integration to the distribution grid simulation suite. PLANET 2020. Available online: <https://www.h2020-planet.eu/deliverables>.
- [97] SNAM. Codice di rete SNAM rete gas. (report in Italian) 2012. Available online: [https://www.snam.it/export/sites/snam-rp/repository-srg/file/Codice\\_di\\_rete/05\\_Archivio\\_CdR/2012/33.Codice\\_di\\_Rete\\_Rev\\_XXXIII.pdf](https://www.snam.it/export/sites/snam-rp/repository-srg/file/Codice_di_rete/05_Archivio_CdR/2012/33.Codice_di_Rete_Rev_XXXIII.pdf).
- [98] Cavana M, Leone P. Biogas blending into the gas grid of a small municipality for the decarbonization of the heating sector. *Biomass and Bioenergy*. 2019;127:105295. <https://doi.org/10.1016/j.biombioe.2019.105295>.
- [99] Italian Ministry of the Interior. Norme di sicurezza antincendio per il trasporto, la distribuzione, l'accumulo e l'utilizzazione del gas naturale con densità non superiore a 0,8. 1984.
- [100] Guelpa E, Sciacovelli A, Verda V. Thermo-fluid dynamic model of large district heating networks for the analysis of primary energy savings. *Energy* 2019;184:34–44. <https://doi.org/10.1016/j.energy.2017.07.177>.
- [101] Fischer D, Kaufmann F, Selinger-Lutz O, Voglstätter C. Power-to-gas in a smart city context—Influence of network restrictions and possible solutions using on-site storage and model predictive controls. *International Journal of Hydrogen Energy*. 2018;43(20):9483-94. <https://doi.org/10.1016/j.ijhydene.2018.04.034>.
- [102] Weiss R, Saastamoinen H, Ikäheimo J, Abdurafikov R, Sihvonen T, Shemeikka J. Decarbonised District Heat, Electricity and Synthetic Renewable Gas in Wind- and Solar-based Energy Systems. *Journal of Sustainable Development of Energy, Water and Environment Systems*. 2021;9(2):1080340. <https://doi.org/10.13044/j.sdewes.d8.0340>.
- [103] Savolainen J, Kannari L, Pennanen J, Tähtinen M, Sihvonen T, Pasonen

- R, Weiss R. Operation of a PtG plant under power scheduling. In 10<sup>th</sup> International Renewable Energy Storage. IRES 2016. Düsseldorf, Germany, 2016.
- [104] Sihvonen T, Savolainen J, Tähtinen M. Modelling and simulation of ptg plant start-ups and shutdowns. 9th EUROSIM Congress on Modelling and Simulation, EUROSIM 2016, The 57th SIMS Conference on Simulation and Modelling SIMS 2016. Linköping University Electronic Press; 2018. <http://dx.doi.org/10.3384/ecp17142>.
- [105] Eero S, Kaj J, Markku H, Olli T, Jorma K, Kari P. The APROS software for process simulation and model development. VTT Technical Research Centre of Finland; 1989.
- [106] Wilson ZT, Sahinidis NV. The ALAMO approach to machine learning. *Computers & Chemical Engineering*. 2017 Nov 2;106:785-95. <https://doi.org/10.1016/j.compchemeng.2017.02.010>.
- [107] Badami M, Verda V, Mazza A, Fambri G, Weiss R, Savolainen J, et al. Deliverable D2.5 Power-to-Gas process / system models. PLANET 2020. Available online: <https://www.h2020-planet.eu/deliverables>.
- [108] Makris S, Nikolopoulos D, Ververidis C, Katsiki V, Badami M, Fambri G, Granroth-Wilding H, Hussam S, Soppela O, Kakardakos N, Kakardakos T, Rontogianni E, Samara A. Deliverable D3.3 PLANET P2H-enabled human-centric VES module. PLANET 2019. Available online: <https://www.h2020-planet.eu/deliverables>.
- [109] Gracia L, Casero P, Bourasseau C, Chabert A. Use of hydrogen in off-grid locations, a techno-economic assessment. *Energies*. 2018;11(11):3141. <https://doi.org/10.3390/en11113141>.
- [110] Bottaccioli L, Patti E, Macii E, Acquaviva A. Distributed Infrastructure for Multi-Energy-Systems Modelling and Co-simulation in Urban Districts. In Proceedings of the 7th International Conference on Smart Cities and Green ICT Systems (SMARTGREENS), Funchal, Portugal, 16–18 March 2018.
- [111] Schiera DS, Barbierato L, Lanzini A, Borchiellini R, Pons E, Bompard E, Patti E, Macii E, Bottaccioli L. A Distributed Multimodel Platform to Cosimulate Multienergy Systems in Smart Buildings. *IEEE Transactions on Industry Applications*. 2021;57(5):4428-40. <https://doi.org/10.1109/TIA.2021.3094497>.
- [112] Hatledal LI, Styve A, Hovland G, Zhang H. A language and platform independent co-simulation framework based on the functional mock-up interface. *IEEE Access*. 2019;7:109328-39. <https://doi.org/10.1109/ACCESS.2019.2933275>.
- [113] Badami M, Fambri G, Mancò S, Martino M, Damousis IG, Agtzidis D,

- Tzovaras D. A decision support system tool to manage the flexibility in renewable energy-based power systems. *Energies*. 2020;13(1):153. <https://doi.org/10.3390/en13010153>.
- [114] Liberatore V, Al-Hammouri A. Smart grid communication and co-simulation. *IEEE 2011 EnergyTech*. 2011;1-5. <https://doi.org/10.1109/EnergyTech.2011.5948542>.
- [115] Mets K, Ojea JA, Develder C. Combining power and communication network simulation for cost-effective smart grid analysis. *IEEE Communications Surveys & Tutorials*. 2014;16(3):1771-96. <https://doi.org/10.1109/SURV.2014.021414.00116>.
- [116] Steinbrink C, Blank-Babazadeh M, El-Ama A, Holly S, Lüers B, Nebel-Wenner M, Ramírez Acosta RP, Raub T, Schwarz JS, Stark S, Nieße A. Cpes testing with mosaik: Co-simulation planning, execution and analysis. *Applied Sciences*. 2019;9(5):923. <https://doi.org/10.3390/app9050923>.
- [117] Schiera DS, Barbierato L, Lanzini A, Borchellini R, Pons E, Bompard E, Patti E, Macii E, Bottaccioli L. A distributed multimodel platform to cosimulate multienergy systems in smart buildings. *IEEE Transactions on Industry Applications*. 2021;57(5):4428-40. <https://doi.org/10.1109/TIA.2021.3094497>.
- [118] Barbierato L, Estebarsari A, Bottaccioli L, Macii E, Patti E. A distributed multimodel co-simulation platform to assess general purpose services in smart grids. *IEEE Transactions on Industry Applications*. 2020;56(5):5613-24. <https://doi.org/10.1109/TIA.2020.3010481>.
- [119] De Souza E, Ardakanian O, Nikolaidis I. A co-simulation platform for evaluating cyber security and control applications in the smart grid. In *ICC 2020-2020 IEEE International Conference on Communications (ICC) 2020* (pp. 1-7). IEEE. <https://doi.org/10.1109/ICC40277.2020.9149212>.
- [120] Kötter E, Schneider L, Sehnke F, Ohnmeiss K, Schröer R. The future electric power system: Impact of Power-to-Gas by interacting with other renewable energy components. *Journal of Energy Storage*. 2016;5:113–9. <https://doi.org/10.1016/j.est.2015.11.012>.
- [121] Weiss R, Savolainen J, Peltoniemi P, Inkeri E. Optimal scheduling of a P2G plant in dynamic power, heat and gas markets. 10<sup>th</sup> Int. Renew. Energy Storage. Conf. IRES 2016, Düsseldorf, Germany: EUROSOLAR; 2016.
- [122] Weiss R, Kannari L, Pennanen J, Sihvonen T, Savolainen J. Optimal Co-Production of Market Based Power Grid Support and Renewable Fuels or Chemicals. 2016 AICHe Annual Meeting: Sustainable Engineering Forum, San Francisco, CA, USA: AICHe; 2016.
- [123] Xi Y, Fang J, Chen Z, Zeng Q, Lund H. Optimal coordination of flexible

- resources in the gas-heat-electricity integrated energy system. *Energy*. 2021;223:119729. <https://doi.org/10.1016/j.energy.2020.119729>.
- [124] Ikäheimo J, Weiss R, Kiviluoma J, Pursiheimo E, Lindroos TJ. Impact of power-to-gas on the cost and design of the future low-carbon urban energy system. *Applied Energy*. 2022; 305: 117713. <https://doi.org/10.1016/j.apenergy.2021.117713>.
- [125] Belderbos A, Valkaert T, Bruninx K, Delarue E, D'haeseleer W. Facilitating renewables and power-to-gas via integrated electrical power-gas system scheduling. *Applied Energy* 2020;275:115082. <https://doi.org/10.1016/j.apenergy.2020.115082>.
- [126] Robinius M, Raje T, Nykamp S, Rott T, Müller M, Grube T, et al. Power-to-Gas: Electrolyzers as an alternative to network expansion – An example from a distribution system operator. *Applied Energy* 2018;210:182–97. <https://doi.org/10.1016/j.apenergy.2017.10.117>.
- [127] El-Taweel NA, Khani H, Farag HEZ. Voltage regulation in active power distribution systems integrated with natural gas grids using distributed electric and gas energy resources. *International Journal of Electrical Power & Energy Systems*. 2019;106:561–71. <https://doi.org/10.1016/j.ijepes.2018.10.037>.
- [128] Estermann T, Newborough M, Sterner M. Power-to-gas systems for absorbing excess solar power in electricity distribution networks. *International Journal of Hydrogen Energy*. 2016;41:13950–9. <https://doi.org/10.1016/j.ijhydene.2016.05.278>.
- [129] Dalmau AR, Perez DM, Diaz De Cerio Mendaza I, Pillai JR. Decentralized voltage control coordination of on-load tap changer transformers, distributed generation units and flexible loads. In 2015 IEEE Innovative Smart Grid Technologies-Asia (ISGT ASIA), IEEE; 2016. <https://doi.org/10.1109/ISGT-Asia.2015.7386966>.
- [130] Diaz De Cerio Mendaza I, Bhattarai BP, Kouzelis K, Pillai JR, Bak-Jensen B, Jensen A. Optimal sizing and placement of power-to-gas systems in future active distribution networks. In 2015 IEEE Innovative Smart Grid Technologies-Asia (ISGT ASIA), IEEE; 2016. <https://doi.org/10.1109/ISGT-Asia.2015.7387053>.
- [131] Mazza A, Cavana M, Medina EL, Chicco G, Leone P. Creation of representative gas distribution networks for multi-vector energy system studies. In 2019 IEEE International Conference on Environment and Electrical Engineering and 2019 IEEE Industrial and Commercial Power Systems Europe (EEEIC/I&CPS Europe). IEEE. 2019;1-6. <https://doi.org/10.1109/EEEIC.2019.8783701>.
- [132] Cavana M, Mazza A, Chicco G, Leone P. Electrical and gas networks coupling through hydrogen blending under increasing distributed



- photovoltaic generation. *Applied Energy*. 2021;290:116764. <https://doi.org/10.1016/j.apenergy.2021.116764>.
- [133] Salomone F, Giglio E, Ferrero D, Santarelli M, Pirone R, Bensaïd S. Techno-economic modelling of a Power-to-Gas system based on SOEC electrolysis and CO<sub>2</sub> methanation in a RES-based electric grid. *Chemical Engineering Journal*. 2019;377:120233. <https://doi.org/10.1016/j.cej.2018.10.170>.
- [134] Khani H, El-Taweel N, Farag HEZ. Real-time optimal management of reverse power flow in integrated power and gas distribution grids under large renewable power penetration. *IET Generation, Transmission & Distribution*. 2018;12:2325–31. <https://doi.org/10.1049/iet-gtd.2017.1513>.
- [135] Diaz-Londono C, Fambri G, Mazza A, Badami M, Bompard E. A Real-Time Based Platform for Integrating Power-to-Gas in Electrical Distribution Grids. In 2020 55<sup>th</sup> International Universities Power Engineering Conference (UPEC 2020). IEEE. 2020;1–6. <https://doi.org/10.1109/UPEC49904.2020.9209803>.
- [136] Borraz-Sánchez C, Bent R, Backhaus S, Hijazi H, Hentenryck PV. Convex relaxations for gas expansion planning. *INFORMS Journal on Computing* 2016;28(4):645-56. <https://doi.org/10.1287/ijoc.2016.0697>.
- [137] He Y, Shahidehpour M, Li Z, Guo C, Zhu B. Robust constrained operation of integrated electricity-natural gas system considering distributed natural gas storage. *IEEE Transactions on Sustainable Energy* 2017;9(3):1061-71. <https://doi.org/10.1109/TSTE.2017.2764004>.
- [138] He L, Lu Z, Zhang J, Geng L, Zhao H, Li X. Low-carbon economic dispatch for electricity and natural gas systems considering carbon capture systems and power-to-gas. *Applied Energy* 2018;224:357–70. <https://doi.org/10.1016/j.apenergy.2018.04.119>.
- [139] Shao C, Wang X, Shahidehpour M, Wang X, Wang B. An MILP-based optimal power flow in multicarrier energy systems. *IEEE Transactions on Sustainable Energy* 2016;27;8(1):239-48. <https://doi.org/10.1109/TSTE.2016.2595486>.
- [140] Mazza A, Chicco G. Losses Allocated to the Nodes of a Radial Distribution System with Distributed Energy Resources – A Simple and Effective Indicator. In 2019 International Conference on Smart Energy Systems and Technologies (SEST), Porto, Portugal: IEEE; 2019. <https://doi.org/10.1109/SEST.2019.8849127>.
- [141] Gorre J, Ortloff F, van Leeuwen C. Production costs for synthetic methane in 2030 and 2050 of an optimized Power-to-Gas plant with intermediate hydrogen storage. *Applied Energy* 2019;253:113594. <https://doi.org/10.1016/j.apenergy.2019.113594>.

- 
- [142] Marocco P, Ferrero D, Gandiglio M, Ortiz MM, Sundseth K, Lanzini A, et al. A study of the techno-economic feasibility of H<sub>2</sub>-based energy storage systems in remote areas. *Energy Conversion and Management*. 2020;211:112768. <https://doi.org/10.1016/j.enconman.2020.112768>.
- [143] Kanellopoulos K, Blanco Reano H. The potential role of H<sub>2</sub> production in a sustainable future power system - An analysis with METIS of a decarbonised system powered by renewables in 2050. European Commission 2019. <https://doi.org/10.2760/540707>.
- [144] Buttler A, Splietho H. Current status of water electrolysis for energy storage, grid balancing and sector coupling via power-to-gas and power-to-liquids: A review. *Renewable and Sustainable Energy Reviews*. 2018;82:2440–54. <https://doi.org/10.1016/j.rser.2017.09.003>.
- [145] Gorre J, Ruoss F, Karjunen H, Scha J, Tynjälä T. Cost benefits of optimizing hydrogen storage and methanation capacities for Power-to-Gas plants in dynamic operation. *Applied Energy* 2020;257:113967. <https://doi.org/10.1016/j.apenergy.2019.113967>.
- [146] Böhm H, Zauner A, Goers S, Tichler R, Kroon P. Deliverable D7.5 Innovative large-scale energy storage technologies and Power-to-Gas concepts after optimization - Report on experience curves and economies of scale. STORE&GO 2020. Available online: <https://www.storeandgo.info/publications/deliverables/>.
- [147] Zauner A, Böhm H, Rosenfeld DC, Tichler R. Deliverable D7.7 Innovative large-scale energy storage technologies and Power-to-Gas concepts after optimization - Analysis on future technology options and on techno-economic optimization. STORE&GO 2020. Available online: <https://www.storeandgo.info/publications/deliverables/>.
- [148] Breyer C, Tsupari E, Tikka V, Vainikka P. Power-to-Gas as an Emerging Profitable Business through Creating an Integrated Value Chain. In: *Energy Procedia*, editor. 9th Int. Renew. Energy Storage Conf. IRES 2015, vol. 73, Düsseldorf, Germany: Elsevier B.V.; 2015, p. 182–9. <https://doi.org/10.1016/j.egypro.2015.07.668>.
- [149] Vandewalle J, Bruninx K, D W. Effects of large-scale power to gas conversion on the power, gas and carbon sectors and their interactions. *Energy Conversion and Management*. 2015;94:28–39. <https://doi.org/10.1016/j.enconman.2015.01.038>.
- [150] ENEA Consulting. The potential of Power-to-Gas: Technology review and economic potential assessment. vol. 33. 2016. Available online: <https://www.enea-consulting.com/static/3663dbb115f833de23e4c94c8fa399ec/enea-the-potential-of-power-to-gas.pdf>.
- [151] Eurostat. Gas prices for non-household consumers - bi-annual data (from

- 2007 onwards). 2021. Available online: [https://appsso.eurostat.ec.europa.eu/nui/show.do?dataset=nrg\\_pc\\_203&lang=en](https://appsso.eurostat.ec.europa.eu/nui/show.do?dataset=nrg_pc_203&lang=en).
- [152] Gestore dei mercati energetici. 2022. Available online: <https://www.mercatoelettrico.org/It/Statistiche/Gas/StatMGP-GAS.aspx>.
- [153] E&E consultant, HESPUL, Solagro. Etude portant sur l'hydrogène et la méthanation comme procédé de valorisation de l'électricité excédentaire. (Report in French) 2014. Available online: [https://www.ademe.fr/sites/default/files/assets/documents/etude\\_powerto\\_gas\\_ademe-grdf-grtgaz.pdf](https://www.ademe.fr/sites/default/files/assets/documents/etude_powerto_gas_ademe-grdf-grtgaz.pdf).
- [154] McDonagh S, O'Shea R, Wall DM, Deane JP, Murphy JD. Modelling of a power-to-gas system to predict the levelised cost of energy of an advanced renewable gaseous transport fuel. *Applied Energy*. 2018;215:444–56. <https://doi.org/10.1016/j.apenergy.2018.02.019>.
- [155] Götz M, Lefebvre J, Mörs F, Koch AM, Graf F, Bajohr S, Reimert R, Kolb T. Renewable Power-to-Gas: A technological and economic review. *Renewable Energy*. 2016;85:1371–90. <https://doi.org/10.1016/j.renene.2015.07.066>.
- [156] Clegg S, Mancarella P. Integrated modeling and assessment of the operational impact of power-to-gas (P2G) on electrical and gas transmission networks. *IEEE Transactions on Sustainable Energy*. 2015;6(4):1234-44. <https://doi.org/10.1109/TSTE.2015.2424885>.
- [157] Clegg S, Mancarella P. Storing renewables in the gas network: modelling of power-to-gas seasonal storage flexibility in low-carbon power systems. *IET Generation, Transmission & Distribution*. 2016;10(3):566-75. <https://doi.org/10.1049/iet-gtd.2015.0439>.
- [158] Sayegh MA, Jadwiszczak P, Axcell BP, Niemierka E, Bryś K, Jouhara H. Heat pump placement, connection and operational modes in European district heating. *Energy and Buildings*. 2018;166:122–44. <https://doi.org/10.1016/j.enbuild.2018.02.006>.
- [159] Arpagaus C, Bless F, Uhlmann M, Schiffmann J, Bertsch SS. High temperature heat pumps: Market overview, state of the art, research status, refrigerants, and application potentials. *Energy*. 2018;152:985–1010. <https://doi.org/10.1016/J.ENERGY.2018.03.166>.
- [160] Wu W, Shi W, Li X, Wang B. Air source absorption heat pump in district heating: Applicability analysis and improvement options. *Energy Conversion and Management*. 2015;96:197–207. <https://doi.org/10.1016/j.enconman.2015.02.068>.
- [161] Sciacovelli A, Guelpa E, Verda V. Multi-scale modeling of the environmental impact and energy performance of open-loop groundwater

- 
- heat pumps in urban areas. *Applied Thermal Engineering*. 2014;71. <https://doi.org/10.1016/j.applthermaleng.2013.11.028>.
- [162] Hiawen S, Tingyu W, Xin J, Zhiyong R, Haiyang Y, Duanmu L. Energy Efficiency Enhancement Potential of the Heat Pump Unit in a Seawater Source Heat Pump District Heating System. *Procedia Engineering*. 2016;146:134–8. <https://doi.org/10.1016/j.proeng.2016.06.363>.
- [163] De Pasquale AM, Giostri A, Romano MC, Chiesa P, Demeco T, Tani S. District heating by drinking water heat pump: Modelling and energy analysis of a case study in the city of Milan. *Energy*. 2017;118:246–63. <https://doi.org/10.1016/j.energy.2016.12.014>.
- [164] Lund R, Persson U. Mapping of potential heat sources for heat pumps for district heating in Denmark. *Energy*. 2016;110:129–38. <https://doi.org/10.1016/j.energy.2015.12.127>.
- [165] David A, Mathiesen BV, Averfalk H, Werner S, Lund H. Heat Roadmap Europe: Large-scale electric heat pumps in district heating systems. *Energies*. 2017;10:1–18. <https://doi.org/10.3390/en10040578>.
- [166] Østergaard PA, Andersen AN. Economic feasibility of booster heat pumps in heat pump-based district heating systems. *Energy*. 2018;155:921–9. <https://doi.org/10.1016/j.energy.2018.05.076>.
- [167] Ommen T, Markussen WB, Elmegaard B. Heat pumps in combined heat and power systems. *Energy*. 2014;76:989–1000. <https://doi.org/10.1016/j.energy.2014.09.016>.
- [168] Bach B, Werling J, Ommen T, Münster M, Morales JM, Elmegaard B. Integration of large-scale heat pumps in the district heating systems of Greater Copenhagen. *Energy*. 2016;107:321–34. <https://doi.org/10.1016/j.energy.2016.04.029>.
- [169] Vandermeulen A, van der Heijde B, Helsen L. Controlling district heating and cooling networks to unlock flexibility: A review. *Energy*. 2018;151:103–15. <https://doi.org/10.1016/j.energy.2018.03.034>.
- [170] Lauka D, Gusca J, Blumberga D. Heat pumps integration trends in district heating networks of the Baltic States. *Procedia Computer Science*. 2015;52:835–42. <https://doi.org/10.1016/j.procs.2015.05.140>.
- [171] Pensini A, Rasmussen CN, Kempton W. Economic analysis of using excess renewable electricity to displace heating fuels. *Applied Energy*. 2014;131:530–43. <https://doi.org/10.1016/j.apenergy.2014.04.111>.
- [172] Kirkerud JG, Bolkesjø TF, Trømborg E. Power-to-heat as a flexibility measure for integration of renewable energy. *Energy*. 2017;128:776–84. <https://doi.org/10.1016/j.energy.2017.03.153>.
-

- 
- [173] Magni C, Quoilin S, Arteconi A. Evaluating the Potential Contribution of District Heating to the Flexibility of the Future Italian Power System. *Energies*. 2022;15(2):584. <https://doi.org/10.3390/en15020584>.
- [174] Østergaard PA, Andersen AN. Variable taxes promoting district heating heat pump flexibility. *Energy*. 2021;221:119839. <https://doi.org/10.1016/j.energy.2021.119839>.
- [175] Johannsen RM, Arberg E, Sorknæs P. Incentivising flexible power-to-heat operation in district heating by redesigning electricity grid tariffs. *Smart Energy*. 2021;2:100013. <https://doi.org/10.1016/j.segy.2021.100013>.
- [176] Pieper H, Ommen T, Buhler F, Lava Paaske B, Elmegaard B, Brix Markussen W. Allocation of investment costs for large-scale heat pumps supplying district heating. *Energy Procedia* 2018;147:358–67. <https://doi.org/10.1016/j.egypro.2018.07.104>.
- [177] Danish Energy Agency. Technology Data for Industrial Process Heat. 2020. Available online at: <https://ens.dk/en/our-services/projections-and-models/technology-data/technology-data-industrial-process-heat>
- [178] European Commission. Directive (EU) 2018/2001 of the European Parliament and of the Council of 11 December 2018 on the promotion of the use of energy from renewable sources. Renewable Energy Directive n.2001/2018. Available online at: [https://eur-lex.europa.eu/legal-content/EN/TXT/?uri=uriserv:OJ.L\\_.2018.328.01.0082.01.ENG&toc=OJ:L:2018:328:TOC](https://eur-lex.europa.eu/legal-content/EN/TXT/?uri=uriserv:OJ.L_.2018.328.01.0082.01.ENG&toc=OJ:L:2018:328:TOC).
- [179] European Commission. Directive (EU) 2019/944 of the European Parliament and of the Council of 5 June 2019 on common rules for the internal market for electricity and amending Directive. Available online at: <https://eur-lex.europa.eu/legal-content/EN/TXT/?uri=CELEX%3A32019L0944>.
- [180] Todeschi V, Marocco P, Mutani G, Lanzini A, Santarelli M. Towards Energy Self-consumption and Self-sufficiency in Urban Energy Communities. *International Journal of Heat and Technology*. 2021;39:1-1. <https://doi.org/10.18280/ijht.390101>.
- [181] Xie K, Hui H, Ding Y. Review of modeling and control strategy of thermostatically controlled loads for virtual energy storage system. *Protection and Control of Modern Power Systems*. 2019;4(1):1-3. <https://doi.org/10.1186/s41601-019-0135-3>.
- [182] Jin X, Wang X, Mu Y, Jia H, Xu X, Qi Y, Yu X, Qi F. Optimal scheduling approach for a combined cooling, heating and power building microgrid considering virtual storage system. In 2016 IEEE Power and Energy Society General Meeting (PESGM), Tianjin, China. 2016 (pp. 1-5). IEEE. <https://doi.org/10.1109/PESGM.2016.7741879>.
-

- 
- [183] Jin X, Mu Y, Jia H, Wu J, Jiang T, Yu X. Dynamic economic dispatch of a hybrid energy microgrid considering building based virtual energy storage system. *Applied Energy*. 2017;194:386-98. <https://doi.org/10.1016/j.apenergy.2016.07.080>.
- [184] Foteinaki K, Li R, Heller A, Rode C. Heating system energy flexibility of low-energy residential buildings. *Energy and Buildings*. 2018;180:95-108. <https://doi.org/10.1016/j.enbuild.2018.09.030>.
- [185] Romero Rodríguez L, Ramos JS, Domínguez SÁ, Eicker U. Contributions of heat pumps to demand response: A case study of a plus-energy dwelling. *Applied Energy*. 2018;214:191-204. <https://doi.org/10.1016/j.apenergy.2018.01.086>.
- [186] Utama C, Troitzsch S, Thakur J. Demand-side flexibility and demand-side bidding for flexible loads in air-conditioned buildings. *Appl Energy*, 2021;285:116418. <https://doi.org/10.1016/j.apenergy.2020.116418>.
- [187] Arteconi A, Mugnini A, Polonara F. Energy flexible buildings: A methodology for rating the flexibility performance of buildings with electric heating and cooling systems. *Appl Energy*. 2019;251:113387. <https://doi.org/10.1016/j.apenergy.2019.113387>.
- [188] Vivian J, Chiodarelli U, Emmi G, Zarrella A. A sensitivity analysis on the heating and cooling energy flexibility of residential buildings. *Sustainable Cities and Society*. 2020;52:101815. <https://doi.org/10.1016/j.scs.2019.101815>.
- [189] Lizana J, Friedrich D, Renaldi R, Chacartegui R. Energy flexible building through smart demand-side management and latent heat storage. *Applied Energy*. 2018;230:471-85. <https://doi.org/10.1016/j.apenergy.2018.08.065>.
- [190] Finck C, Li R, Kramer R, Zeiler W. Quantifying demand flexibility of power-to-heat and thermal energy storage in the control of building heating systems. *Applied Energy*. 2018;209:409-25. <https://doi.org/10.1016/j.apenergy.2017.11.036>.
- [191] Balint A, Kazmi H. Determinants of energy flexibility in residential hot water systems. *Energy and Buildings*. 2019;188:286-96. <https://doi.org/10.1016/j.enbuild.2019.02.016>.
- [192] European Parliament, EPBD Recast e Energy Performance of Buildings Directive. Directive 2010/31/EU of the European Parliament and of the Council of the European Union, European Parliament, 2010.
- [193] European Commission. Photovoltaic Geographical Information System (PVGIS) portal. Available online at: [https://re.jrc.ec.europa.eu/pvg\\_tools/it/#PVP](https://re.jrc.ec.europa.eu/pvg_tools/it/#PVP).
- [194] Psimopoulos E, Bee E, Widén J, Bales C. Techno-economic analysis of
-

- control algorithms for an exhaust air heat pump system for detached houses coupled to a photovoltaic system. *Applied Energy*. 2019;249:355-67. <https://doi.org/10.1016/j.apenergy.2019.04.080>.
- [195] Tsiropoulos I, Tarvydas D, Lebedeva N. Li-ion batteries for mobility and stationary storage applications. Publications Office of the European Union. 2018. <http://dx.doi.org/10.2760/87175>.
- [196] Schmidt O, Hawkes A, Gambhir A, Staffell I. The future cost of electrical energy storage based on experience rates. *Nature Energy*. 2017;2(8):1-8. <https://doi.org/10.1038/nenergy.2017.110>.
- [197] Hocking M, Kan J, Young P, Terry C, Begleiter D. Lithium 101 F.I.T.T. for investors Welcome to the Lithium-ion Age. Deutsche Bank Market Research. 2016; ISBN: 1055100898643, pp: 1-179. <http://www.belmontresources.com/LithiumReport.pdf>.
- [198] Frankel BD, Kane S, Tryggstad C. The new rules of competition in energy storage. McKinsey & Company. 2018. Available online at: <https://www.mckinsey.com/industries/electric-power-and-natural-gas/our-insights/the-new-rules-of-competition-in-energy-storage>.
- [199] Eller A, Gauntlett D. Energy storage trends and opportunities in emerging markets. Navigant Consulting Inc.: Boulder, CO, USA. 2017. Available online at: <https://www.esmap.org/sites/default/files/esmap-files/7151-IFC-EnergyStorage-report.pdf>.
- [200] IRENA. Electricity storage and renewables: Costs and markets to 2030. IRENA. 2018. Available online at: <https://www.irena.org/publications/2017/Oct/Electricity-storage-and-renewables-costs-and-markets#RestrictedModal>.
- [201] Sadiqa A, Gulagi A, Breyer C. Energy transition roadmap towards 100% renewable energy and role of storage technologies for Pakistan by 2050. *Energy*. 2018;147:518-33. <https://doi.org/10.1016/j.energy.2018.01.027>.
- [202] Marocco P, Ferrero D, Gandiglio M, Ortiz MM, Sundseth K, Lanzini A, Santarelli M. A study of the techno-economic feasibility of H<sub>2</sub>-based energy storage systems in remote areas. *Energy Conversion and Management*. 2020;211:112768. <https://doi.org/10.1016/j.enconman.2020.112768>.
- [203] RSE. Gli schemi di Autoconsumo Collettivo e le Comunità dell'Energia. Available online at: <https://cdn.qualenergia.it/wp-content/uploads/2020/10/Schemi-di-Autoconsumo-Collettivo-e-Comunita-dell-Energia.pdf>.
- [204] Ministero dello sviluppo economico. Individuazione della tariffa incentivante per la remunerazione degli impianti a fonti rinnovabili inseriti nelle configurazioni sperimentali di autoconsumo collettivo e comunità

energetiche rinnovabili. Gazzetta Ufficiale della Repubblica Italiana.  
Availabe online at:  
<https://www.gazzettaufficiale.it/eli/id/2020/11/16/20A06224/sg>.